Schweizerische Eidgenossenschaft
Confédération suisse
Confederazione Svizzera
Confederaziun svizra

Eidgenössisches Departement für Umwelt, Verkehr, Energie und Kommunikation UVEK
Département fédéral de l'environnement, des transports, de l'énergie et de la communication DETEC
Dipartimento federale dell'ambiente, dei trasporti, dell'energia e delle comunicazioni DATEC

Bundesamt für Strassen
Office fédéral des routes
Ufficio federale delle Strade

Partial safety factors recalibration for actions and resistances for new and existing bridges

Réévaluation des facteurs partiels pour les actions et les résistances des ouvrages d'art nouveaux et existants

Neubewertung der Teilsicherheitsbeiwerte für Einwirkungen und Widerstände von neuen und bestehend Brücken

École Polytechnique Fédérale de Lausanne,
Structural Concrete Laboratory
Resilient Steel Structures Laboratory

Prof. Aurelio Muttoni
Prof. Alain Nussbaumer
Dr Xhemsi Malja
Dr João T. Simões
Dr Qianhui Yu
Colin Vaccari

Forschungsprojekt BGT_20_02B_01 auf Antrag der AG BGT (Arbeitsgruppe Brücken, Geotechnik und Tunnel)

May 2025 **1782**

Schweizerische Eidgenossenschaft
Confédération suisse
Confederazione Svizzera
Confederaziun svizra

Eidgenössisches Departement für Umwelt, Verkehr, Energie und Kommunikation UVEK
Département fédéral de l'environnement, des transports, de l'énergie et de la communication DETEC
Dipartimento federale dell'ambiente, dei trasporti, dell'energia e delle comunicazioni DATEC

Bundesamt für Strassen
Office fédéral des routes
Ufficio federale delle Strade

Partial safety factors recalibration for actions and resistances for new and existing bridges

Réévaluation des facteurs partiels pour les actions et les résistances des ouvrages d'art nouveaux et existants

Neubewertung der Teilsicherheitsbeiwerte für Einwirkungen und Widerstände von neuen und bestehend Brücken

École Polytechnique Fédérale de Lausanne,
Structural Concrete Laboratory
Resilient Steel Structures Laboratory

Prof. Aurelio Muttoni
Prof. Alain Nussbaumer
Dr Xhemsi Malja
Dr João T. Simões
Dr Qianhui Yu
Colin Vaccari

Forschungsprojekt BGT_20_02B_01 auf Antrag der AG BGT (Arbeitsgruppe Brücken, Geotechnik und Tunnel)

May 2025 **1782**

Impressum

Forschungsstelle und Projektteam

Projektleitung
Prof. Aurelio Muttoni

Mitglieder
Prof. Alain Nussbaumer
Dr Xhemsi Malja
Dr João T. Simões
Dr Qianhui Yu
Colin Vaccari

Begleitkommission

Präsident
Dr Hans-Rudolf Ganz

Mitglieder
Ehrfried Kölz
Dr Pascal Kronenberg
Thierry Meystre
Prof. Andreas Taras
Dr Rudolf Vogt

Antragsteller

Arbeitsgruppe Brücke, Geotechnik und Tunnel (AG BGT)

Bezugsquelle

Das Dokument kann kostenlos von http://www.mobilityplatform.ch heruntergeladen werden.

Table of contents

Zusammenfassung

Nach der Methode der Teilsicherheitsbeiwerte, die Mitte des letzten Jahrhunderts in die Bemessungsregeln für Betonbauwerke eingeführt wurde, wird die Tragsicherheit durch die Durchführung von Grenzzustandsnachweisen unter Verwendung von Bemessungswerten gewährleistet, die mit Teilsicherheitsbeiwerten berechnet werden. In den letzten Jahren wurden Anstrengungen unternommen, um einen Standardrahmen für die Wahrscheinlichkeitsmodellierung zu schaffen. Die Quellen der Unsicherheiten, die von den einzelnen Teilsicherheitsbeiwerten abgedeckt werden, sind jedoch immer noch Gegenstand von Diskussionen in der wissenschaftlichen Gemeinschaft, da sie in den Regelwerken und den zugehörigen Hintergrunddokumenten nicht klar definiert sind. Darüber hinaus werden die statistischen Verteilungen der grundlegenden Zufallsvariablen nach dem besten Kenntnisstand zu einem bestimmten Zeitpunkt angenommen. Wenn sich das Wissen weiterentwickelt, der technologische Fortschritt voranschreitet und mehr Daten zur Verfügung stehen, sollten diese statistischen Daten aktualisiert werden und entweder zu einer Bestätigung oder zu einer Aktualisierung der Teilsicherheitsbeiwerte führen. Die Tatsache, dass einige der Teilsicherheitsbeiwerte keine solide wissenschaftliche Grundlage haben, könnte zu unzureichenden Sicherheitsniveaus in verschiedenen Szenarien (Art der Tragwerke, Versagensarten, Materialien usw.) oder in einigen Fällen auch zu übermässig teuren Tragwerken führen. Darüber hinaus ist eine angemessene Kenntnis der grundlegenden Zufallsvariablen, die von jedem Teilsicherheitsbeiwert abgedeckt werden, von grundlegender Bedeutung für eine bessere Entscheidungsfindung im Umgang mit bestehenden Tragwerken. Um sichere und wirtschaftlichere Bauwerke zu bemessen, besteht das Ziel dieses Berichts darin, die wichtigsten Ungewissheiten zu klären, die von jedem Teilsicherheitsbeiwert abgedeckt werden, und die Teilsicherheitsbeiwerte bei Bedarf auf der Grundlage aktualisierter statistischer Verteilungen zu aktualisieren. Zu diesem Zweck ist anzumerken, dass es im Rahmen des Partial Safety Factor (PSF) Formats nicht korrekt ist, sich auf einen einzelnen PSF zu beziehen; stattdessen muss man konsequent einen Satz von PSF betrachten. Tatsächlich muss zusätzlich zur Variabilität jeder Zufallsvariablen das Ausmass, in dem diese Grössen zur Grenzzustandsfunktion beitragen, die den sicheren Tragwerksbereich vom unsicheren trennt, berücksichtigt werden. Bei der Methode der Zuverlässigkeitsanalyse erster Ordnung (FORM), wird dieser Beitrag beispielsweise durch die Sensitivitätsfaktoren dargestellt, die die partielle Ableitung der Grenzzustandsfunktion nach der untersuchten Variablen darstellen. In diesem Rahmen und da sich dieser Bericht hauptsächlich auf Strassenbrücken konzentriert, werden Anstrengungen unternommen, um die Unsicherheiten sowohl auf der Widerstands- als auch auf der Einwirkungsseite zu quantifizieren. Neben dem Eigengewicht der Tragkonstruktion werden auch die Variabilitäten der Verkehrslast und des Belagsgewichts untersucht.

Teilsicherheitsbeiwerte für Betontragwerke

Es werden verschiedene Unsicherheitsquellen untersucht, die den Widerstand von Stahlbetonbauteilen und die entsprechenden Teilsicherheitsbeiwerte beeinflussen. Zu diesem Zweck werden neue statistische Daten gesammelt und ausgewertet. Für die Bewertung der Teilsicherheitsbeiwerte wird der einfache, aber rigorose Ansatz der Empfindlichkeitsexponentenanalyse verwendet. Dieser Ansatz entspricht insbesondere der Durchführung einer Taylor-Erweiterung erster Ordnung der Widerstandsfunktion im logarithmischen Raum der grundlegenden Zufallsvariablen, die den Widerstand beeinflussen. Der Empfindlichkeitsexponent stellt die lokale partielle Ableitung des logarithmischen Widerstands in Bezug auf jede Variable dar (unter der Annahme einer -Lognormalverteilung). Einer der Vorteile dieser Berechnungsmethode besteht darin, dass die Empfindlichkeitsexponenten einheitenlos sind und direkt mit der Unsicherheit durch den Einfluss einer bestimmten Basisvariablen auf das Widerstandsmodell verknüpft werden können. Darüber hinaus kann die Gründlichkeit der

Empfindlichkeitsexponentenanalyse unter Berücksichtigung der Einheiten der einzelnen Widerstandsvariablen leicht überprüft werden.

Um die Teilsicherheitsbeiwerte auf der Widerstandsseite zu kalibrieren, ohne die Variabilität auf der Einwirkungsseite zu berücksichtigen, besteht eine übliche Annahme darin, jede Komponente separat zu betrachten, indem ein fester Empfindlichkeitsfaktor der Zuverlässigkeitsmethode erster Ordnung (FORM) für die Widerstands- (*R*) und die Einwirkungsseite (*E)* angenommen wird. In diesem Fall werden die Empfindlichkeitsfaktoren mit α_E = -0,7 und α_R = 0,8 angenommen. Diese Werte sind in EN 1990:2023 und dem fib Model Code 2010 angegeben und sind im Allgemeinen konservativ und berücksichtigen eine grosse Anzahl von Szenarien.

Auf der Grundlage der obigen Annahme wird der Ansatz der Empfindlichkeitsexponentenanalyse für fünf gängige Widerstandsmodelle für Betontragwerke verwendet (Zugnormalkraft, Drucknormalkraft, Biegung, Querkraft mit Querkraftbewehrung, Durchstanzen). Die Ergebnisse zeigen, dass die Exponenten, die den verschiedenen geometrischen und Material Parametern zugeordnet sind, von einem Fall zum anderen variieren, was darauf hinweist, dass die massgeblichen Unsicherheiten entsprechend variieren. Die Ergebnisse dieser Analysen zeigen, dass der Ansatz der Materialbeiwerte (γ_S und γ_C) auf eine breite Palette typischer Widerstandsmodelle angewandt werden kann (Zug- und Drucknormalkraft, Biegung, Querkraft bei Vorhandensein einer ausreichenden Querkraftbewehrung; bei denen das Material und die geometrischen Unsicherheiten massgebend sind), während der Ansatz des Widerstandsbeiwerts (γ_V) für andere spezifische Widerstandsmodelle (Querkraft ohne Querkraftbewehrung und Durchstanzen; bei denen die geometrischen und die Modellunsicherheiten massgebend sind) besser geeignet ist.

Das Modell für den Biegewiderstand von Stahlbetonträgern wird als Referenz für die Kalibrierung des Teilfaktors für die Streckgrenze der Stahlbewehrung verwendet. Für die Kalibrierung des Teilfaktors für die Betondruckfestigkeit wird das Modell für den Widerstand von Stützen mit reiner Drucknormalkraft verwendet. Beide Widerstandsmodelle werden in der Praxis häufig verwendet und stellen Fälle dar, bei denen die Materialfestigkeitsvariablen einen dominierenden Einfluss haben und relativ hohe Modellunsicherheiten aufweisen.

Für die Stahlstreckgrenze wird der Teilsicherheitsbeiwert γ_S = 1,15 bestätigt, der die Material-, Modell- und Geometrieunsicherheiten abdeckt. Dieser Ansatz kann jedoch zu unsicheren Nachweisen für Platten mit einer statischen Höhe von weniger als 200 mm führen und für höhere Bauteile zu konservativ sein. Es wird gezeigt, dass ein konstantes Sicherheitsniveau und eine wirtschaftlichere Bemessung erreicht werden können, wenn Bemessungswerte für die statische Höhe (zur expliziten Abdeckung der geometrischen Unsicherheit) zusammen mit einem reduzierten Teilfaktor γ_S angenommen werden.

Auch für die Betondruckfestigkeit wird der aktuelle Teilsicherheitsbeiwert γ_C = 1,50 bestätigt. Dieser Wert beinhaltet nicht nur die Material-, Geometrie- und Modellunsicherheiten, sondern auch solche, die sich auf die Herstellung, den Transport, das Giessen und die Nachbehandlung von Beton beziehen.

Trotz der Tatsache, dass die aktuellen Werte von γ_S und γ_C bestätigt werden, bietet die durchgeführte Forschung neben der Möglichkeit, die Teilfaktoren zu reduzieren, wenn der Bemessungswert der statischen Höhe verwendet wird, auch nützliche Informationen für mehrere praktische Fälle:

- Für die Anpassung von Teilsicherheitsbeiwerten für (i) eine verbesserte Qualitätskontrolle und (ii) falls Messwerte von Abmessungen und die Betondruckfestigkeit f_{ck} nach EN 13791 zur Beurteilung von bestehenden Bauwerken zur Verfügung stehen.
- Klärung des Unterschieds zwischen der Betonfestigkeit von Prüfkörpern und der Betonfestigkeit in situ.

- Berechnung von γ_C und γ_S für verschiedene Werte des Ziel-Zuverlässigkeitsindex (anders als 3,8).
- Für die Kalibrierung des Sicherheitsformats verfeinerter nichtlinearer Finite-Elemente-Analysen ist es wichtig, dass bei diesen Ansätzen sämtliche Material- und Geometrieunsicherheiten ebenso konsistent behandelt werden wie bei der Verwendung konventioneller Modelle. Zu diesem Zweck werden die statistischen Daten (Variationskoeffizient und Bias-Faktor) für Material- und Geometriewerte dargelegt, die zur Begründung der Beiwerten γ_C = 1,50 und γ_S = 1,15 angenommen wurden.

Für den Teilwiderstandsbeiwert γ_V für den Durchstanzwiderstand und den Querkraftwiderstand von Elementen ohne Querkraftbewehrung wird, wenn die geometrischen Unsicherheiten durch den Teilsicherheitsbeiwert abgedeckt werden, γ_V = 1,40 vorgeschlagen. Es wird jedoch festgestellt, dass ein konstanter Wert von γ_V = 1,40 zu einer unsicheren Bemessung von Platten mit einer statischen Höhe von weniger als 200 mm führen kann und für dickere Platten zu konservativ sein kann. Schliesslich wird gezeigt, dass ein konstanteres Sicherheitsniveau erreicht wird, wenn der Bemessungswert der statischen Höhe mit einem niedrigeren Wert des Teilfaktors γ_V kombiniert wird.

Die meisten Ergebnisse dieser Arbeit wurden in der zweiten Generation der europäischen Norm für die Bemessung von Betonbauwerken (Eurocode 2 von 2023) und dem zugehörigen Hintergrunddokument umgesetzt, so dass sie implizit in die zukünftigen Versionen der Schweizer Norm für Betonbauwerke übernommen werden.

Modellunsicherheiten bei der Schnittkraft- und Tragfähigkeitsberechnung in statisch unbestimmten Tragwerken

Diese Arbeit konzentriert sich auf die Unsicherheiten bei der Berechnung der Schnittkräfte und der Tragfähigkeit von Stahlbeton- und Verbundkonstruktionen (Stahl-Beton). Für die Bemessung und Beurteilung von Tragwerken ist es üblich, die Schnittkräfte mit den Querschnittswiderständen zu vergleichen. Während die Modellunsicherheiten auf der Widerstandsseite wie oben beschrieben umfassend untersucht wurden, ist die Modellunsicherheit bei der Berechnung von Schnittkräften in statisch unbestimmten Tragwerken noch nicht ausreichend untersucht worden. Insbesondere wird die Modellunsicherheit bei Schnittkräfte- und Tragfähigkeitsberechnungen unter Berücksichtigung verschiedener mechanischer Modelle und Versagensarten untersucht. Um eine ausreichende Menge an Daten zu sammeln und statistische Analysen durchzuführen, wird das experimentelle Verhalten statisch unbestimmter Systeme mit einer einfachen und effektiven Technik ermittelt, die es ermöglicht, in der Literatur verfügbare experimentelle Ergebnisse zu verwenden.

Im Vergleich zu verfeinerten Modellen führt ein linear-elastisches Modell mit ungerissener Querschnittssteifigkeit zu einem grösseren Variationskoeffizient (CoV) der Modellunsicherheit bei der Tragfähigkeitsberechnung; einem grösseren CoV entsprechen jedoch grössere Mittelwerte, was zu einer ähnlichen Schwanzverteilung und damit zu einer ähnlichen Sicherheitsmarge wie bei verfeinerten Ansätzen (d. h. nichtlinearen Modellen) führt. Bei linearen, elastischen, ungerissenen Modellen kann auch beobachtet werden, dass eine Überdimensionierung einer oder mehrerer Komponenten eines statisch unbestimmten Systems den CoV der Modellunsicherheit bei der Berechnung der Schnittkräfte beeinflusst. Bei verfeinerten Berechnungsmodellen ist bei der Tragfähigkeitsberechnung ein geringerer CoV der Modellunsicherheit zu beobachten, während dies bei der Berechnung der Schnittkräfte in Abhängigkeit vom Überbemessungsgrad der Teilelemente nicht immer der Fall ist.

Bei Stahlbetonelementen ohne Duktilitätsanforderungen, führt die Anwendung der Plastizitätstheorie (starr-plastische Betrachtung) zu einem sehr grossen CoV und potenziell unsicheren Ergebnissen. Die Begrenzung der Verformungskapazität oder der Nachweis, dass die Anforderungen an die Duktilität erfüllt sind, verringert den CoV erheblich. Die Versagensart beeinflusst die Modellunsicherheit bei der Tragfähigkeitsberechnung, nicht aber die Modellunsicherheit bei der Berechnung der Schnittkräfte. Ein grösserer CoV für die Tragfähigkeitsberechnung wird für spröde Systeme unabhängig vom Berechnungsmodell beobachtet.

Bei Stahl-Beton-Verbundkonstruktionen ist die Modellunsicherheit bei der Tragfähigkeitsberechnung bei Verwendung eines linear elastischen Modells ähnlich wie bei Stahlbetonkonstruktionen. Auch die Querschnittsklasse, die mit dem Versagensmodus zusammenhängt, beeinflusst die Modellunsicherheit bei der Tragfähigkeitsberechnung unabhängig von der durchgeführten Analyse, wie bei Stahlbetonstrukturen beobachtet. Schliesslich wird eine Verringerung des CoV durch die Begrenzung der Verformungskapazität bei der Verwendung von plastischen Modellen beobachtet. Zusätzlich zum zusammengesetzten System aus zwei Trägern, werden diese Ergebnisse für Verbundkonstruktionen durch die Untersuchung eines kontinuierlichen Systems bestätigt, das aus den experimentellen Last-Verformungsbeziehungen der einfachen Balken zusammengesetzt wird. Insgesamt kann auf der Grundlage der Ergebnisse für zusammengesetzte Zweibalkensysteme davon ausgegangen werden, dass die Unsicherheiten bei der Berechnung der Tragfähigkeit und folglich der Schnittkräfte ähnlich sind wie bei Stahlbetonkonstruktionen.

Anhand von parametrischen Analysen und untersuchten Fallstudien liegt der Teilsicherheitsbeiwert γ_{Sd}, der die Unsicherheiten im Zusammenhang mit den Berechnungen der Schnittkräfte abdeckt und implizit in den Teilsicherheitsbeiwerten γ_G und γ_Q auf der Einwirkungsseite implementiert ist, zwischen 1,05 und 1,15. Es ist wichtig darauf hinzuweisen, dass der Beiwert γ_{Sd} die Unsicherheiten im Zusammenhang mit Systemänderungen während des Baus oder der strukturellen Modellierung komplexer Tragwerke nicht berücksichtigt. Diese zusätzlichen Unsicherheiten sollten genauer untersucht werden und hängen wesentlich von der Komplexität der Tragkonstruktion, der Konstruktionsmethode, den verwendeten Werkzeugen und der Erfahrung des Ingenieurs ab.

Rekalibrierung der Teilsicherheitsbeiwerte für ständige Lasten

Die Kalibrierung des Teilsicherheitsbeiwerts wird im Allgemeinen durchgeführt, um ein annehmbares Sicherheitsniveau für ein breites Spektrum von Szenarien zu gewährleisten, und jeder Teilsicherheitsbeiwert deckt genau definierte Unsicherheiten ab, die mit der Variabilität einer oder mehrerer grundlegender Zufallsvariablen, wie Geometrie, Materialfestigkeiten und Nachweismodelle, zusammenhängen. Obwohl die statistischen Verteilungen der grundlegenden Zufallsvariablen nach bestem Wissen und Gewissen zu einem bestimmten Zeitpunkt angenommen werden, sollten diese Verteilungen mit zunehmendem Wissensstand, technologischem Fortschritt und mehr verfügbaren Daten aktualisiert werden, was zu einer Bestätigung oder Aktualisierung der Teilsicherheitsbeiwerte führt. Auf dieser Grundlage werden zur Aktualisierung der Teilsicherheitsbeiwerte für das strukturelle und nichtstrukturelle Eigengewicht die statistischen Verteilungen anhand von Daten aktualisiert, die auf dem Schweizer Strassennetz gesammelt und von Institutionen und privaten Unternehmen zur Verfügung gestellt wurden. Auch die Variabilität der Verkehrslasten wird auf der Grundlage von Messungen des Gewichts in Bewegung (WIM) quantifiziert, die während mehr als 20 Jahren an mehreren Standorten (~15 Stationen) in der Schweiz durchgeführt wurden. Auf der Grundlage der aktualisierten statistischen Verteilungen werden parametrische Analysen durchgeführt, um die Empfindlichkeit der Teilsicherheitsbeiwerte zu untersuchen und ihren Wert zu schätzen.

Die Variabilität des Eigengewichts von Stahlbetonbauteilen wird im Allgemeinen durch geometrische und Raumgewichtsschwankungen verursacht. Durch die Verwendung von Toleranzen als Standardabweichung der geometrischen Parameter und der in der Literatur verfügbaren statistischen Verteilungen scheinen die geometrischen Schwankungen bei grossen Bauteilen weniger bedeutend zu sein. Der CoV für das strukturelle Eigengewicht von Stahlbetonbauteilen liegt im Allgemeinen zwischen 3 und 6%.

Messungen an mehreren bestehenden Brücken im Schweizer Strassennetz zeigen, dass die Variabilität der Belagsdicke einer Strassenbrücke im Allgemeinen durch bereits vorhandene Verformungen und die Brückengeometrie beeinflusst wird. In den untersuchten Fällen ist die mittlere Belagsdicke zwischen 1,2 und 1,5 mal grösser als der Nominalwert. In einigen Fällen ist die gemessene Belagsdicke mehr als das Doppelte des Nennwerts was darauf hindeutet, dass der Nennwert der Belagsdicke während einer Erneuerung erhöht wurde. Der Variationskoeffizient der gesamten Belagsdicke liegt zwischen 10 und 20% und damit deutlich über dem Wert für das strukturelle Eigengewicht, was die in anderen Ländern veröffentlichten Werte bestätigt.

Aus diesen Gründen werden zwei Teilsicherheitsbeiwerte vorgeschlagen, nämlich γ_{G1} für strukturelles und γ_{G2} für nichtstrukturelles Eigengewicht. Während die Teilsicherheitsbeiwerte für die Materialfestigkeiten unabhängig von den anderen Unsicherheiten kalibriert wurden (um bei Bedarf eine einfache Anpassung zu ermöglichen), wurden die beiden Teilsicherheitsbeiwerte für ständige Einwirkungen unter Berücksichtigung aller Unsicherheiten kalibriert, um eine zuverlässigere Bewertung für alle potenziell massgebenden Kombinationen zu ermöglichen.

In diesem Zusammenhang werden die Variabilitäten der Materialfestigkeit anhand von in der Schweiz erhobenen Daten aktualisiert. Die Verteilungen stimmen im Allgemeinen mit den in Abschnitt 1 angegebenen Werten überein. Allerdings sind der CoV und der Bias-Faktor der Betonfestigkeit für die analysierten Daten grösser als die in der internationalen Literatur gefundenen Daten. Diese überhöhte Festigkeit ist wahrscheinlich darauf zurückzuführen, dass die Hersteller den Zementgehalt erhöht haben, um die Kriterien der Dauerhaftigkeit und Verarbeitbarkeit zu erfüllen.

Die Variabilität der Verkehrslast für die wöchentlichen Maximalereignisse liegt zwischen 10 und 18%. Die Extrapolation von 50-Jahres-Maxima-Verteilungen hängt wesentlich von der Genauigkeit der Schwanzanpassung der wöchentlichen Ausgangsverteilung ab. Die Berücksichtigung von Lognormal- und Gumbel-Extrem-Maxima-Verteilungen für die Schwanzanpassung der Ausgangsverteilung führt zu einem CoV der Verkehrslastvariabilität zwischen 6 und 10%.

Nach den parametrischen Zuverlässigkeitsanalysen liegt der erforderliche Wert von γ_{G1} für das Eigengewicht, um den Zielwert des Zuverlässigkeitsindex $\beta_{tgt,50y} = 3{,}8$ zu erreichen, zwischen 1,1 und 1,2, während γ_{G2} für andere ständige Einwirkungen zwischen 1,3 und 1,8 liegt, wenn der Nennwert der Belagsdicke als Referenzwert betrachtet wird. Zuverlässigkeitsanalysen, die an ausgewählten Fallstudien mit verschiedenen Versagensarten durchgeführt wurden, bestätigen, dass $\gamma_{G1} = 1{,}2$ und $\gamma_{G2} = 1{,}5$ im Allgemeinen zu ausreichend sicheren Ergebnissen für den Entwurf neuer und die Bewertung bestehender Bauwerke führen. In Bezug auf den Referenzwert der Belagsdicke ist, wie in Eurocode 1 empfohlen, eine Erhöhung um 20% des Nennwerts gerechtfertigt. Zuverlässigkeitsanalysen, die an ausgewählten Fallstudien mit verschiedenen Versagensarten durchgeführt wurden, bestätigen, dass $\gamma_{G1} = 1{,}2$ und $\gamma_{G2} = 1{,}5$ für das strukturelle bzw. nicht-strukturelle Eigengewicht zu ausreichend sicheren Ergebnissen in Bezug auf die aktuellen Werte und in absoluten Zahlen führen.

Systemänderungen während der Konstruktion und erhebliche Unterschiede zwischen der Modellierung komplexer Strukturen und dem tatsächlichen Verhalten werden in den oben beschriebenen Teilsicherheitsbeiwerten auf der Lastseite nicht berücksichtigt. Wenn es für das Tragwerkssystem relevant ist, sollte es je nach seiner Komplexität und insbesondere

im Fall von massgeblichen spröden Versagensarten, wenn das Verhalten nicht durch konstruktiven Massnahmen verbessert werden kann, in einer angemessen konservativen Weise modelliert und die Ergebnisse entsprechend interpretiert werden.

Zusammenfassung der vorgeschlagenen Teilsicherheitsbeiwerten

Auf der Grundlage der in diesem Bericht beschriebenen Untersuchungen werden für einen Zielwert des Zuverlässigkeitsindex $\beta_{tgt,50}$ = 3,8 (CC2) die folgenden Teilsicherheitsbeiwerte für ständige und vorübergehende Bemessungssituationen vorgeschlagen.

- Für den Bewehrungsstahl:
  - wenn die Prüfung mit Nennwerten der geometrischen Abmessungen durchgeführt wird, wird der Wert γ_S = 1,15 bestätigt
  - wenn der Nachweis auf der Grundlage der Bemessungswerte der statischen Höhe $d_d = d_{nom}$ - 15 mm geführt wird, kann der Teilsicherheitsbeiwert für Bewehrungsstahl auf γ_S = 1,05 reduziert werden.
- Für den Beton:
  - Der Wert γ_C = 1,50 wird bestätigt.
- Für Querkraft in Elementen ohne Querkraftbewehrung und für Durchstanzen nach EN 1992-1-1:2023:
  - wenn der Nachweis mit Nennwerten der geometrischen Abmessungen durchgeführt wird, γ_V = 1,40
  - wird der Nachweis auf der Grundlage von Bemessungswerten der statischen Höhe $d_d = d_{nom}$ - 15 mm geführt, darf der Teilfaktor für Querkraft und Durchstanzen auf γ_V = 1,30 reduziert werden.
- Der Teilsicherheitsbeiwert γ_{Sd}, der die Modellunsicherheiten in der Schnittkraftberechnung abdeckt, liegt in Abhängigkeit von den anderen Unsicherheiten zwischen 1,05 und 1,15. Dieser Beiwert ist implizit in den Teilsicherheitsbeiwerten γ_G und γ_Q berücksichtigt. Letztere können alternativ unter Annahme folgender statistischer Werte der Modellunsicherheit kalibriert werden: Bias-Faktor μ = 1,0 und CoV = 8%. Es ist zu beachten, dass diese Beiwerte und statistischen Werte potenzielle Unsicherheiten im Zusammenhang mit der Modellierung komplexer Tragwerken und/oder dem Einfluss von Systemänderungen bei Tragwerken mit begrenzter Verformungsfähigkeit und begrenzter Möglichkeit zur Umverteilung der internen Kräfte im Grenzzustand der Tragfähigkeit nicht berücksichtigen.
- Für die ständigen Einwirkungen:
  - Da die Unsicherheiten des Eigengewichts der tragenden und der nichttragenden Elemente unterschiedlich sind, empfiehlt es sich, zwei getrennte Teilsicherheitsbeiwerte zu verwenden, nämlich γ_{G1} für tragende und γ_{G2} für nichttragende Elemente.
  - Der Standardwert für das Eigengewicht der Tragkonstruktion ist γ_{G1} = 1,35 wie in der aktuellen SIA 260. γ_{G1} kann auf 1,20 reduziert werden, wenn die Modellierung des Tragwerks durch den Planer hinreichend zuverlässig durchgeführt wird (ausreichende Erfahrung in Bezug auf die Art des Tragwerks / verwendete Software / Einfluss der Modellierung des Tragwerks auf die Ergebnisse auf der Grundlage ähnlicher Berechnungen an ähnlichen Tragwerken) und der Einfluss der Systemänderungen während des Baus hinreichend zuverlässig berücksichtigt wird (verwendete Methode / angenommene Materialparameter / Erfahrung des Planers in Bezug auf den Einfluss der Annahmen auf die Ergebnisse). Die gleiche Reduktion ist auch bei statisch bestimmten Tragwerken zulässig.
  - Es wird der Teilfaktor für das Eigengewicht der nichttragenden Elemente γ_{G2} = 1,50 vorgeschlagen. Für den Fahrbahnbelag von Strassenbrücken sollte zusätzlich zu γ_{G2} = 1,50 die Nenndicke um 20% erhöht werden, wie in EN 1991-1:2023 [138] vorgeschlagen.
- Für die variablen Einwirkungen:
  - Die Bemessungswerte werden auf der Grundlage von Zuverlässigkeitsanalysen abgeleitet (dies ist nicht Gegenstand der vorliegenden Untersuchung, da die

Kalibrierung der Verkehrslasten, einschliesslich der Bemessungswerte, derzeit in anderen Forschungsarbeiten untersucht wird). Die charakteristischen Werte können mit einem nominalen Teilsicherheitsbeiwert γ_Q = 1,50 bestimmt werden.

- Die oben genannten Teilsicherheitsbeiwerte gelten für die Bemessung neuer Bauwerke und für die Bewertung bestehender Bauwerke, wenn die entsprechenden Variablen nicht durch direkte Messungen ermittelt wurden.
- Für die Beurteilung bestehender Bauwerke, bei denen die Abmessungen vor Ort gemessen und/oder die Materialfestigkeiten anhand von Prüfungen an Proben des bestehenden Bauwerks ermittelt wurden, können die Teilsicherheitsbeiwerte anhand des in diesem Bericht beschriebenen Verfahrens und der aus den Messungen abgeleiteten statistischen Werte angepasst werden. Vereinfachend können die folgenden Teilsicherheitsbeiwerte angenommen werden:
  - Für γ_S und γ_C können die in Anhang A (Modifikation von Teilsicherheitsbeiwerten für Baustoffe) von EN 1992-1-1:2023 angegebenen Werte verwendet werden;
  - Für das strukturelle Eigengewicht sollten die oben beschriebenen Werte von γ_{G1} verwendet werden;
  - Für die anderen ständigen Einwirkungen kann γ_{G2} = 1,20 angenommen werden, wenn die Abmessungen an der bestehenden Struktur gemessen werden.

Résumé

Selon la méthode des facteurs partiels, introduite dans les normes de dimensionnement des structures en béton au milieu du siècle dernier, la sécurité structurale est assurée en effectuant des vérifications de l'état limite ultime à l'aide de valeurs de calcul calculées avec des facteurs partiels. Ces dernières années, des efforts ont été faits pour établir un cadre standard de modélisation des probabilités. Toutefois, les sources d'incertitudes couvertes par chaque facteurs partiel font encore l'objet de discussions au sein de la communauté scientifique, car elles ne sont pas clairement définies dans les normes et les documents de référence relatifs. En outre, les distributions statistiques des variables aléatoires de base sont supposées correspondre aux meilleures connaissances à un moment donné. Au fur et à mesure de l'évolution des connaissances, des progrès technologiques et scientifiques ainsi que de la disponibilité des connaissances, ces données statistiques devraient être mises à jour et conduire à une confirmation ou à une mise à jour des facteurs partiels. Le fait que certains facteurs partiels ne reposent pas sur une base scientifique solide peut conduire à des niveaux de sécurité insuffisants dans différents scénarios (type de structures, modes de défaillance, matériaux, etc.) ou, dans certains cas, à des structures excessivement coûteuses (trop sûres). En outre, une connaissance adéquate des variables aléatoires de base couvertes par chaque facteur partiel est fondamentale pour améliorer la prise de décision lorsqu'il s'agit de structures existantes. Ainsi, pour dimensionner des structures sûres et plus économiques, l'objectif de ce rapport est de clarifier les principales incertitudes couvertes par chaque facteur partiel et de les mettre à jour sur la base de distributions statistiques actualisées si nécessaire. À cette fin, il convient de noter que dans le cadre du format des facteurs partiels (PSFF), il n'est pas correct de se référer à un PSF individuel ; au lieu de cela, il faut considérer de manière cohérente un ensemble de PSF. En fait, outre la variabilité de chaque variable aléatoire, il faut tenir compte de la mesure dans laquelle ces quantités contribuent à la fonction d'état limite, qui sépare le domaine structurel sûr de celui qui ne l'est pas. Par exemple, dans la méthode d'analyse de la fiabilité du premier ordre (FORM), cette contribution est représentée par les coefficients de sensibilité, qui sont la dérivée partielle de la fonction d'état limite par rapport à la variable étudiée. Dans ce cadre, et puisque ce rapport se concentre principalement sur les ponts routiers, un effort sera fait pour quantifier les incertitudes à la fois du côté de la résistance et du côté de l'action. Outre le poids propre de la structure, les variabilités de la charge de trafic et de la charge de la chaussée sont étudiées.

Facteurs partiels dans le béton structurel

Différentes sources d'incertitude affectant la résistance des éléments en béton armé et les facteurs partiels correspondants sont étudiées. À cette fin, de nouvelles données statistiques sont collectées et évaluées. L'approche simple mais rigoureuse de l'analyse de sensibilité des exposants est utilisée pour évaluer les facteurs partiels. En particulier, l'approche de l'analyse de sensibilité de l'exposant équivaut à effectuer une expansion de Taylor du premier ordre de la fonction de résistance dans l'espace logarithmique des variables aléatoires de base qui influencent la résistance. L'exposant de sensibilité représente la dérivée partielle locale de la résistance logarithmique par rapport à chaque variable (supposée suivre une distribution log-normale). L'un des avantages de cette méthode de calcul est que les facteurs de sensibilité de l'exposant sont sans dimension et peuvent être directement liés à l'incertitude par l'influence d'une variable de base donnée sur le modèle de résistance. En outre, l'exhaustivité de l'analyse de sensibilité de l'exposant peut être facilement vérifiée en tenant compte des unités de chaque variable de résistance.

Pour calibrer les facteurs partiels du côté de la résistance sans tenir compte de la variabilité du côté de l'action, une hypothèse généralement faite est de considérer chaque composant séparément en supposant un facteur de sensibilité fixe de la méthode de fiabilité du premier ordre (FORM) pour la résistance (*R)* et le côté de l'action (*E)*. Dans ce cas, les facteurs de sensibilité sont supposés respectivement α_E = -0,7 et α_R = 0,8. Ces valeurs sont indiquées

dans la norme EN 1990:2023 et dans le Code modèle *fib* 2010 et sont généralement conservatrices, tenant compte d'un grand nombre de scénarios.

Sur la base de l'hypothèse ci-dessus, l'approche de l'analyse de sensibilité des exposants est utilisée pour cinq modèles de résistance courants pour les structures en béton armé (effort normal de traction, effort normal de compression, flexion, effort tranchant en présence d'armature d'effort tranchant, poinçonnement). Les résultats montrent que les exposants associés aux différents paramètres géométriques et des résistances des matériaux varient d'un cas à l'autre, ce qui indique que les incertitudes déterminantes varient en conséquence. Les résultats de ces analyses montrent que si une approche par facteur partiel de matériau (γ_S et γ_C) peut être appliquée à une large gamme de modèles de résistance typiques (effort normal de traction et compression, flexion, effort tranchant en présence d'une armature d'effort tranchant suffisante ; lorsque les incertitudes concernant les résistances des matériaux et géométriques sont déterminantes), une approche par facteur de résistance (γ_V) est plus appropriée pour d'autres modèles de résistance (effort tranchant sans armature d'effort tranchant et poinçonnement ; lorsque les incertitudes géométriques et celles du modèle sont déterminantes).

Le modèle pour la résistance à la flexion des sections en béton armé est utilisé comme référence pour la calibration du facteur partiel pour la limite d'élasticité de l'armature en acier. Pour la calibration du facteur partiel de la résistance à la compression du béton, le modèle de résistance des colonnes soumises à une effort normal de compression centrée est utilisé. Les deux modèles de résistance sont couramment utilisés dans la pratique et représentent des cas où les variables de résistance des matériaux ont une influence dominante et présentent des incertitudes de modèle relativement élevées.

Pour la limite d'élasticité de l'acier d'armature, le facteur partiel $\gamma_S = 1{,}15$ couvrant les incertitudes liées au matériau, au modèle et à la géométrie est confirmé. Cependant, cette approche peut conduire à des dimensionnements avec un niveau de sécurité insuffisant pour les dalles dont la hauteur utile est inférieure à 200 mm et peut être trop conservatrice pour les éléments plus épais. Il est démontré qu'un niveau de sécurité constant et un dimensionnement plus économique pourraient être obtenus si les valeurs de dimensionnement de la hauteur utile (pour couvrir l'incertitude géométrique explicitement) sont adoptées avec un facteur partiel réduit γ_S.

Pour la résistance à la compression du béton, le facteur partiel actuel $\gamma_C = 1{,}50$ est également confirmé. Cette valeur couvre non seulement les incertitudes liées aux matériaux, à la géométrie et au modèle, mais aussi celles liées à la production, au transport, au bétonnage et à la cure du béton.

Bien que les valeurs actuelles de γ_S et γ_C soient confirmées, la recherche menée, outre la possibilité de réduire les facteurs partiels en cas d'utilisation de la valeur de dimensionnement de la hauteur utile, fournit également des informations utiles pour plusieurs cas pratiques :

- Pour la modification des facteurs partiels pour (i) un niveau plus élevé de contrôle de qualité et (ii) les valeurs mesurées des données géométriques et la résistance à la compression du béton f_{ck} selon EN 13791 à utiliser pour l'évaluation des structures existantes.
- Clarification de la différence entre la résistance du béton mesurée sur des éprouvettes de contrôle et la résistance in situ.
- Calcul de γ_C et γ_S pour différentes valeurs cible de l'indice de fiabilité (autre que 3,8).
- Pour la calibration du format de sécurité des analyses par éléments finis non linéaires: il est important qu'en utilisant ces approches, toutes les incertitudes des matériaux et géométriques soient traitées de la même manière qu'en utilisant des modèles conventionnels. À cette fin, les données statistiques (coefficient de variation et facteurs de biais) pour les valeurs des résistances des matériaux et géométriques qui justifient les facteurs $\gamma_C = 1{,}50$ et $\gamma_S = 1{,}15$ sont présentées.

En ce qui concerne le facteur partiel de résistance γ_V pour le poinçonnement et la résistance à l'effort tranchant des éléments sans armature d'effort tranchant, si les incertitudes géométriques sont couvertes par le facteur partiel de résistance, γ_V = 1,40 est proposé. Cependant, il est observé qu'une valeur constante de γ_V = 1,40 peut conduire à un dimensionnement avec un niveau de sécurité insuffisant pour des dalles avec une hauteur utile inférieure à 200 mm et peut être trop conservatrice pour des éléments plus épais. Finalement, il est démontré qu'un niveau de sécurité plus constant est atteint si la valeur de dimensionnement de la hauteur utile est combinée avec une valeur plus faible du facteur partiel γ_V.

La plupart des résultats de ce travail ont été mis en œuvre dans la deuxième génération de la norme européenne pour le calcul des structures en béton (EN 1992-1-1:2023) et son document de référence, de sorte qu'ils seront adoptés implicitement dans les futures versions de la norme suisse pour les structures en béton.

Incertitudes du modèle dans les effets d'action et le calcul de la charge ultime dans les structures statiquement indéterminées

Ce travail se concentre sur les incertitudes dans le calcul des effets d'action et de la charge ultime des structures en béton armé et des structures mixtes acier-béton. Pour le dimensionnement et l'évaluation des structures, il est courant de comparer les effets d'action avec les résistances sectionnelles. Alors que les incertitudes du modèle du côté de la résistance ont été largement étudiées comme décrit ci-dessus, l'incertitude du modèle dans le calcul des effets d'action dans les systèmes statiquement indéterminés n'a pas encore été correctement étudiée. En particulier, l'incertitude du modèle dans les calculs des effets d'action et de la charge ultime est étudiée en tenant compte de divers modèles mécaniques et modes de défaillance. Pour collecter une quantité suffisante de données et effectuer des analyses statistiques, la réponse expérimentale des systèmes statiquement indéterminés est obtenue en adoptant une technique simple et efficace qui permet d'utiliser les résultats expérimentaux disponibles dans la littérature.

Comparé à des modèles plus raffinés, un modèle élastique linéaire avec une rigidité sectionnelle non fissurée conduit à un plus grand coefficient de variation (CoV) de l'incertitude de modèle dans le calcul de la charge ultime ; cependant, à un plus grand CoV correspondent de plus grandes valeurs de la moyenne, conduisant à une distribution de la queue statistique similaire, donc à une marge de sécurité similaire à celle des approches plus raffinées (comme par exemple les modèles non linéaires). Pour les modèles linéaires élastiques non fissurés, on peut également observer qu'un surdimensionnement d'un ou plusieurs composants d'un système statiquement indéterminé influence le CoV de l'incertitude de modèle dans le calcul des effets de l'action. En ce qui concerne les modèles de calcul plus raffinés, on peut observer un plus faible CoV de l'incertitude de modèle pour le calcul de la charge ultime, alors que ce n'est pas toujours le cas pour le calcul des effets d'action, en fonction du taux de surdimensionnement des éléments.

Pour les structures en béton armé, les modèles basés sur la théorie de la plasticité supposant une capacité de déformation illimitée, s'ils sont exécutés sans exigences de ductilité, conduisent à des CoV très élevés et à des résultats potentiellement dangereux. Limiter la capacité de déformation ou vérifier que les exigences de ductilité sont remplies réduit considérablement le CoV. Le mode de défaillance influence l'incertitude de modèle dans le calcul de la charge ultime, mais pas l'incertitude de modèle dans le calcul des effets de l'action. Un plus grand CoV pour le calcul de la charge ultime est observé pour les systèmes fragiles, indépendamment du modèle de calcul.

Pour les structures mixtes acier-béton, lors de l'utilisation d'un modèle élastique linéaire, l'incertitude de modèle dans le calcul de la charge ultime est similaire à celle obtenue pour les structures en béton armé. De même, la classe de section, qui est liée au mode de

défaillance, influence l'incertitude de modèle dans le calcul de la charge ultime, quelle que soit l'analyse effectuée, comme cela a été observé pour les structures en béton armé. Enfin, une diminution du CoV est observée en limitant la capacité de déformation lors de l'utilisation de modèles plastiques. Outre le système à deux poutres assemblées, ces résultats sont confirmés pour les structures mixtes par l'étude d'un système de poutre continue assemblé à l'aide des réponses expérimentales des poutres simplement appuyées. Globalement, sur la base des résultats obtenus pour les systèmes à deux poutres assemblées, on peut supposer que les incertitudes dans le calcul de la charge ultime et, par conséquent, des effets de l'action sont similaires à celles obtenues pour les structures en béton armé.

Au moyen d'analyses paramétriques et d'études de cas, le facteur partiel γ_{Sd} qui couvre les incertitudes liées aux calculs des effets d'action, et qui est implicitement considéré dans les facteurs partiels γ_G et γ_Q du côté de l'action, se situe entre 1,05 et 1,15. Il est important de noter que ce facteur γ_{Sd} ne tient pas compte des incertitudes liées aux variations du système structurel pendant la construction ou à la modélisation structurelle des structures complexes. Ces incertitudes supplémentaires méritent d'être étudiées plus en détail et dépendent fortement de la complexité de la structure, de la méthode de construction, des outils utilisés et de l'expérience de l’ingénieur.

Recalibration des facteurs partiels pour les charges permanentes

La calibration du facteur partiel est généralement effectuée pour fournir un niveau de sécurité acceptable pour un large éventail de scénarios de dimensionnement et chaque facteur partiel couvre des incertitudes bien définies liées à la variabilité d'une ou plusieurs variables aléatoires de base, telles que la géométrie, la résistance des matériaux et les modèles de calcul. Bien que les distributions statistiques des variables aléatoires de base soient supposées correspondre aux meilleures connaissances à un moment donné, au fur et à mesure que les connaissances augmentent, que le progrès technologique progresse et que davantage de données sont disponibles, ces distributions doivent être mises à jour et conduire à la confirmation ou à l'actualisation des facteurs partiels. Sur cette base, pour mettre à jour les facteurs partiels concernant le poids structurel et non-structurel, les distributions statistiques sont mises à jour en utilisant les données collectées sur le réseau routier suisse et fournies par des institutions et des entreprises privées. De plus, la variabilité des charges de trafic est quantifiée sur la base des mesures de poids en mouvement (WIM) effectuées pendant plus de 20 ans en plusieurs endroits (~15 stations) situés en Suisse. Sur la base des distributions statistiques mises à jour, des analyses paramétriques sont effectuées pour étudier la sensibilité des facteurs partiels et pour estimer leur valeur.

La variabilité du poids propre des éléments en béton armé est généralement due à la variabilité géométrique et à la variabilité du poids spécifique du béton. En utilisant les tolérances comme écart-type des paramètres géométriques et les distributions statistiques disponibles dans la littérature, les variabilités géométriques semblent être moins importantes pour les grands éléments. Le CoV pour le poids propre structurel des éléments en béton armé est généralement compris entre 3 et 6%.

Les mesures effectuées sur plusieurs ponts existants du réseau routier suisse montrent que la variabilité de l'épaisseur de l’enrobé dans un pont routier est généralement influencée par les déformations préexistantes et la géométrie du tablier. Pour les cas analysés, l'épaisseur moyenne de l’enrobé est supérieure à la valeur nominale, la valeur moyenne mesurée étant généralement entre 1,2 et 1,5 fois la valeur nominale. Dans certains cas, la valeur mesurée dépasse même deux fois la valeur nominale, ce qui suggère que la valeur nominale de l'épaisseur de l’enrobé a été augmentée lors du resurfaçage. Le coefficient de variation de l'épaisseur totale de l’enrobé se situe entre 10 et 20 %, ce qui est nettement plus élevé que pour le poids propre structurel et confirme les valeurs publiées dans d'autres pays.

Pour ces raisons, deux facteurs partiels, respectivement γ_{G1} pour le poids structurel et γ_{G2} pour le poids propre non-structurel, sont proposés. Alors que les facteurs partiels pour les matériaux ont été calibrés indépendamment des autres variabilités (pour permettre une simple modification si nécessaire), les deux facteurs partiels pour les actions permanentes ont été calibrés en tenant compte de toutes les variabilités afin de fournir une évaluation plus fiable pour toutes les combinaisons potentiellement déterminantes.

À cet égard, les variabilités de résistance des matériaux sont mises à jour à l'aide des données recueillies en Suisse. Les distributions sont généralement conformes aux valeurs spécifiées dans le premier chapitre. Cependant, le CoV et le facteur de biais de la résistance du béton pour les données analysées sont plus importants que les données trouvées dans la littérature internationale. Cette sur-résistance est probablement attribuable à une augmentation de la teneur en ciment pour répondre aux critères de durabilité et d'ouvrabilité du béton.

La variabilité de la charge de trafic pour les événements hebdomadaires maximaux se situe entre 10 et 18%. L'extrapolation des distributions des maxima sur 50 ans dépend de manière significative de la précision de l'ajustement de la queue de la distribution hebdomadaire de départ. La prise en compte des distributions log-normales et de Gumbel pour l'ajustement de la queue de la distribution de départ conduit à une valeur de référence de la variabilité de la charge de trafic comprise entre 6 et 10%.

Selon les analyses de fiabilité paramétriques, la valeur requise de γ_{G1} pour le poids propre afin d'atteindre la valeur cible de l'indice de fiabilité $\beta_{tgt,50y} = 3,8$ se situe entre 1,1 et 1,2 tandis que γ_{G2} pour les autres actions permanentes se situe entre 1,3 et 1,8 dans le cas où l'épaisseur nominale de l'enrobé est considérée comme valeur de référence. Les analyses de fiabilité effectuées sur des études de cas sélectionnés comprenant divers modes de défaillance confirment que $\gamma_{G1} = 1,2$ et $\gamma_{G2} = 1,5$ conduisent en général à des résultats suffisamment sûrs pour le dimensionnement de nouvelles structures et l'évaluation de structures existantes. En ce qui concerne la valeur de référence de l'épaisseur de l'enrobage, une augmentation de 20 % de la valeur nominale recommandée dans l'EN 1991-1:2023 est justifiée. Les analyses de fiabilité effectuées sur des études de cas sélectionnés comprenant divers modes de défaillance confirment que $\gamma_{G1} = 1,2$ et $\gamma_{G2} = 1,5$, respectivement pour le poids propre structurel et non-structurel, conduisent à des résultats suffisamment sûrs par rapport aux valeurs actuelles et en termes absolus.

Les modifications du système structural au cours de la construction et les différences significatives entre la modélisation de structures complexes et le comportement réel ne sont pas prises en compte dans les facteurs partiels du côté de la charge décrits ci-dessus. Si le système structurel le permet, en fonction de sa complexité et en particulier dans le cas de modes de défaillance fragiles, si le comportement ne peut pas être amélioré par des détails judicieux au cours du processus de dimensionnement, la structure doit être modélisée de manière raisonnablement conservatrice et les résultats doivent être interprétés en conséquence.

Résumé des facteurs partiels proposés

Sur la base des études décrites dans le présent rapport, les facteurs partiels suivants pour les situations de projet durables et transitoires sont proposés pour une valeur cible de l'indice de fiabilité $\beta_{tgt,50} = 3,8$ (CC2).

- Pour l'acier d'armature :
  - si la vérification est effectuée avec les valeurs nominales des dimensions géométriques, la valeur $\gamma_S = 1,15$ est confirmée
  - si la vérification est effectuée sur la base des valeurs de dimensionnement de la hauteur utile $d_d = d_{nom}$ - 15 mm, le facteur partiel pour l'armature peut être réduit à $\gamma_S = 1,05$.
- Pour le béton :

    - La valeur γ_C = 1,50 est confirmée.
- Pour l'acier de construction métallique (structural steel) :
    - La valeur γ_{M1} = 1,05 est confirmée.
- Pour l'effort tranchant dans les dalles sans armature d'effort tranchant et pour le poinçonnement selon EN 1992-1-1:2023 :
    - si la vérification est effectuée avec les valeurs nominales des dimensions géométriques, γ_V = 1,40 ;
    - si la vérification est effectuée sur la base des valeurs de dimensionnement de la hauteur utile $d_d = d_{nom}$ - 15 mm, le facteur partiel pour l'effort tranchant et le poinçonnement peut être réduit à γ_V = 1,30.
- Le facteur partiel γ_{Sd} couvrant les incertitudes de modèle dans le calcul de l'effet d'action se situe entre 1,05 et 1,15 en fonction des autres incertitudes. Ce facteur est implicitement pris en compte dans les facteurs partiels γ_G et γ_Q . Ces derniers peuvent également être calibrés en supposant les valeurs statistiques suivantes de l'incertitude de modèle : facteur de biais μ = 1,0 et CoV = 8%. Il convient de noter que ces coefficients et valeurs statistiques ne tiennent pas compte des incertitudes potentielles liées à la modélisation de structures complexes et/ou de l'influence des changements de système dans le cas de structures ayant une capacité de déformation limitée et une possibilité limitée de redistribuer les efforts à l'état limite ultime.
- Pour les actions permanentes :
    - Étant donné que les incertitudes relatives au poids propre des éléments structuraux et non structuraux sont différentes, il est recommandé d'utiliser deux facteurs partiels distincts, à savoir γ_{G1} pour les éléments structuraux et γ_{G2} pour les éléments non-structuraux.
    - La valeur par défaut du facteur pour le poids propre de la structure est γ_{G1} = 1,35 comme dans la norme SIA 260 actuelle. γ_{G1} peut être réduit à 1,20 si la modélisation de la structure est effectuée par le concepteur de manière suffisamment fiable (expérience suffisante par rapport au type de structure / logiciel utilisé / influence de la modélisation de la structure sur les résultats basés sur des calculs similaires sur des structures similaires) et si l'influence des changements du système pendant la construction est prise en compte de manière suffisamment fiable (méthode utilisée / paramètres des matériaux supposés / expérience du concepteur par rapport à l'influence des suppositions sur les résultats). La même réduction est autorisée dans le cas de structures statiquement déterminées.
    - Le facteur partiel pour le poids propre des éléments non-structuraux γ_{G2} = 1,50 est proposé. Pour les enrobés des ponts routiers, en plus de γ_{G2} = 1,50, l'épaisseur nominale doit être augmentée de 20% conformément à la norme EN 1991-1:2023 [138].
- Pour les actions variables :
    - Les valeurs de dimensionnement sont dérivées sur la base d'analyses de fiabilité (hors du champ de la présente recherche puisque la calibration des charges de trafic, y compris les valeurs de dimensionnement, sont actuellement étudiées dans le cadre d'autres projets de recherche). Les valeurs caractéristiques peuvent être déterminées en divisant la valeur de dimensionnement par un facteur partiel nominal γ_Q = 1,50.
- Les facteurs partiels ci-dessus sont valables pour le dimensionnement de nouvelles structures et pour l'évaluation des structures existantes lorsque les variables correspondantes n'ont pas été actualisées par des mesures directes.
- Pour l'évaluation des structures existantes, lorsque les dimensions ont été mesurées sur place et/ou que la résistance des matériaux a été actualisée à partir d'essais sur des échantillons prélevés sur la structure existante, les facteurs partiels peuvent être ajustés en utilisant la procédure décrite dans le présent rapport et les valeurs statistiques dérivées des mesures. De manière simplifiée, les facteur partiels suivants peuvent être admis :
    - Pour γ_S et γ_C , les valeurs indiquées à l'annexe A (Modification des facteurs partiels relatifs aux matériaux) de la norme EN 1992-1-1:2023 peuvent être utilisées ;

- Pour le poids propre de la structure, il convient d'utiliser les valeurs de γ_{G1} décrites ci-dessus ;
- Pour les autres actions permanentes, on peut admettre $\gamma_{G2} = 1{,}20$ si les dimensions sont mesurées sur la structure existante.

Summary

According to the partial safety factors method, introduced in structural concrete design codes in the middle of the last century, structural safety is ensured by performing limit state verifications using design values calculated with partial safety factors. In recent years, some efforts were made to establish a standard probability modelling framework. However, the sources of uncertainties covered by each partial factor are still a matter of discussion in the scientific community since they are not clearly defined in codes of practice and the related background documents. Moreover, the statistical distributions of the basic random variables are assumed according to the best knowledge at a specific time. As knowledge evolves, technological advancement progresses and more data is available, these statistical data should be updated and lead to either a confirmation or an update of the partial safety factors. The fact that some of the partial safety factors do not have a solid scientific base might lead to insufficient levels of safety in different scenarios (type of structures, failure modes, materials etc.), or, in some cases, lead also to excessively expensive structures (too safe). In addition, an adequate knowledge of the basic random variables covered by each partial factor is fundamental to improve decision-making when dealing with existing structures. Thus, to design safe and more economical structures, the aim of this report is to clarify the main uncertainties covered by each partial safety factor and to update the partial safety factors on the basis of updated statistical distributions if needed. To this purpose, it should be noted that within the frame of the Partial Safety Factor Format (PSFF), it is not correct to refer to an individual PSF; instead, one must consistently consider a set of PSF. In fact, in addition to the variability of each random variable, the extent to which these quantities contribute to the limit state function, which separates the safe structural domain from the unsafe one, must be considered. For instance, in the First Order Reliability Analysis Method (FORM), this contribution is represented by the sensitivity factors, which is the partial derivative of the limit state function with respect to the investigated variable. In this framework and since this report will mainly focus on road bridges, an effort will be put in quantifying uncertainties both on the resistance side and on the action side. Besides the structural self-weight, the traffic load and the pavement load variabilities are investigated.

Partial safety factors in structural concrete

Various sources of uncertainty affecting the resistance of reinforced concrete members and the corresponding partial safety factors are investigated. To this purpose, new statistical data are collected and evaluated. The simple, yet rigorous exponent sensitivity analysis approach is used for assessing the partial safety factors. In particular, the exponent sensitivity analysis approach is equivalent to perform a first order Taylor expansion of the resistance function in the logarithmic space of the basic random variables influencing the resistance. The exponent sensitivity represents local partial derivative of the logarithmic resistance with respect to each variable (assumed following a log-normal distribution). One of the advantages of this calculation methodology is that the exponent sensitivity factors are unitless and can be directly linked to the uncertainty through the influence of a given basic variable on the resistance model. In addition, the thoroughness of the exponent sensitivity analysis can be easily verified considering the units of each resistance variable.

To calibrate the partial safety factors on the resistance side without accounting for the variability on the action side, a common assumption generally made is to consider each component separately by assuming a fixed First Order Reliability Method (FORM) sensitivity factor for the resistance (R) and the action side (E). In this case, the sensitivity factors are assumed respectively $\alpha_E = -0.7$ and $\alpha_R = 0.8$. These values are given in EN 1990:2023 and the fib Model Code 2010 and are generally conservative accounting for a large number of scenarios.

Based on the above assumption, the exponent sensitivity analysis approach is used for five common resistance models for RC structures (axial tension, axial compression, bending, shear with shear reinforcement, punching shear). The results show that the exponents associated to the different geometrical and material parameters vary from one case to the other, indicating that the governing uncertainties vary correspondingly. The results of such analyses show that while a material factor approach (γ_S and γ_C) can be applied to a wide range of typical resistance models (axial tension and compression, bending, shear in the presence of sufficient shear reinforcement; where the material and the geometrical uncertainties are governing), a resistance factor approach (γ_V) is more appropriate for other specific resistance models (shear without shear reinforcement and punching shear; where the geometrical and the model uncertainties govern).

The model for the bending resistance of reinforced concrete sections is used as reference for the calibration of the partial factor for the yield strength of steel reinforcement. For the calibration of the partial factor for the concrete compressive strength, the model for the resistance of columns against axial compression is used. Both resistance models are commonly used in practice and represent cases where the material strengths variables have a dominating influence and present relatively high model uncertainties.

For the steel yield strength, the partial safety factor γ_S = 1.15 covering the material, model and geometrical uncertainties is confirmed. However, this approach can lead to unsafe designs for slabs with an effective depth smaller than 200 mm and can be overly conservative for deeper members. It is shown that a constant safety level and a more economic design could be obtained if design values of the effective depth (to cover the geometrical uncertainty explicitly and individually) are adopted together with a reduced partial factor γ_S.

For the concrete compressive strength, current partial factor γ_C = 1.50 is also confirmed. This value includes not only the material, geometrical and model uncertainties, but also those which relate to the production, transportation and casting of concrete.

Despite the fact that current values of γ_S and γ_C are confirmed, the conducted research, in addition to the possibility to reduce the partial factors in case the design value of the effective depth is used, also provides useful information for several practical cases:

- For the modification of partial factors for (i) enhanced quality control and (ii) measured values of geometrical data and the compressive concrete strength f_{ck} according to EN 13791 to be used for the assessment of existing structures.
- Clarification of the difference between cylinder concrete strength (measured on control specimens) and in-situ strength.
- Calculation of γ_C and γ_S for different values of the target reliability index (other than 3.8).
- For the safety format calibration of refined non-linear finite element analyses: it is important that by using these approaches, all material and geometrical uncertainties are treated consistently as by using conventional models. For this purpose, the statistical data (coefficient of variation and bias factors) for material and for geometrical values which have been assumed to justify the factors γ_C = 1.50 and γ_S = 1.15 are presented.

With respect to the resistance partial factor γ_V for punching shear and shear resistance of members without shear reinforcement, if geometrical uncertainties are covered by the resistance partial factor, γ_V = 1.40 is proposed. However, it is observed that a constant value of γ_V = 1.40 can lead to unsafe design of slabs with a shear resisting effective depth smaller than 200 mm and can be overly conservative for thicker slabs. Eventually, it is shown that a more constant safety level is achieved if the design value of the shear resisting effective depth is combined with a lower value of the partial factor γ_V.

Most of the results of this work have been implemented in the second generation of the European standard for the design of concrete structures (Eurocode 2 of 2023) and its

background document, so that they will be adopted implicitly in the future versions of the Swiss code for concrete structures.

Model uncertainties in action effects and load bearing capacity calculation in statically indeterminate structures

This work focusses on the uncertainties in calculating action effects and the global load bearing capacity of reinforced concrete and composite structures (steel-concrete). For the dimensioning and assessment of structures, it is common practice to compare action effects with sectional resistances. While model uncertainties on the resistance side have been extensively investigated as described above, the model uncertainty in the calculation of action effects in statically indeterminate systems has not been properly investigated yet. In particular, the model uncertainty in action effects and load bearing capacity calculations is investigated considering various mechanical models and failure modes. To collect a sufficient amount of data and perform statistical analyses, the experimental response of statically indeterminate systems is obtained adopting a simple and effective technique which allows using experimental results available in literature.

Compared to more refined models, a linear elastic model with uncracked sectional stiffness leads to larger CoV of the model uncertainty in load bearing capacity calculation; however, to a larger CoV correspond larger values of the mean, leading to similar tail's distribution, thus, similar safety margin as for more refined approaches (i.e. non-linear models). For linear elastic uncracked models, it can also be observed that an over-design of one or more components of a statically indeterminate system influences the CoV of the model uncertainty in action effects calculation. Regarding more refined calculation models, a lower CoV of the model uncertainty can be observed for the bearing capacity calculation while this is not always the case for action effects calculation, depending on the over-design ratio of the members;

For reinforced concrete structures, models based on limit analysis assuming unlimited deformation capacity, if performed without ductility requirements lead to very large CoV and potentially unsafe results. Limiting the deformation capacity, or verifying that ductility requirements are fulfilled reduces considerably the CoV. The failure mode influences the model uncertainty in load bearing capacity calculation but does not influence the model uncertainty in action effects calculation. Larger CoV for the load-bearing capacity calculation is observed for brittle systems independently of the calculation model.

For composite steel-concrete structures, when using a linear elastic model, the model uncertainty in load bearing capacity calculation is similar to the one obtained for reinforced concrete structures. Also, the section class, which is related to the failure mode, influences the model uncertainty in load-bearing capacity calculation regardless of the analysis performed, as observed for reinforced concrete structures. Finally, a decrease of the CoV is observed by limiting the deformation capacity when using plastic models. In addition to the assembled two-beams system, for composite structures these results are confirmed by investigating a continuous system assembled using the experimental responses of the simply-supported beams. Overall, based on the results for assembled two-beams systems, it can be assumed that the uncertainties in calculation of the load bearing capacity and, consequently, of the internal action effects are similar to those obtained for reinforced concrete structures.

By means of parametric analyses and investigated case studies, the partial safety factor γ_{Sd} that covers the uncertainties related to the action effects calculations, and is implicitly implemented in the partial factors γ_G and γ_Q on the action side, ranges between 1.05 and 1.15. It is important to note that γ_{Sd} factor does not account for uncertainties related to structural system variations during construction or structural modelling of complex structures. These additional uncertainties deserve to be investigated more in detail and significantly depend on the complexity of the structure, the construction method, the used tools and the experience of the designer.

Recalibration of partial safety factors for permanent loads

The calibration of the partial safety factor is generally performed to provide an acceptable level of safety for a wide range of design scenarios and each partial safety factor covers well-defined uncertainties related to the variability of one or more basic random variables, such as geometry, materials and models. Although the statistical distributions of the basic random variables are assumed according to the best knowledge at a specific time, as knowledge increases, technological advancement progresses and more data is available, these distributions should be updated and lead to either confirming or updating of the partial safety factors. On this basis, to update the partial factors on structural and non-structural self-weight, statistical distributions are updated using data collected on the Swiss road network and provided by institutions and private companies. Also, the variability of traffic loads is quantified based on weight in motion measurements performed during more than 20 years in multiple locations (~15 stations) located in Switzerland. Based on the updated statistical distributions, parametric analyses are performed to investigate the sensitivity of the partial factors and to estimate their value.

Structural self-weight variability of the reinforced concrete members is generally caused by geometric and concrete specific weight variability. By using tolerances as standard deviation of the geometrical parameters and statistical distributions available in literature, geometric variabilities appear to be less significant for large members. The CoV for structural self-weight of reinforced concrete members is generally between 3 and 6%.

Measurements in several existing road bridges in the Swiss road network show that the variability of the pavement thickness is generally influenced by pre-existing deformations and the bridge geometry. For the analysed cases, the mean thickness of the pavement is larger than the design value with the bias factor generally between 1.2 and 1.5. In some cases, the bias is larger than 2 suggesting that during resurfacing the nominal value of the pavement thickness was increased. The CoV of the overall pavement thickness is found between 10 and 20%, significant larger that for the structural self-weight, confirming values published in other countries.

For these reasons, two partial safety factors, respectively γ_{G1} for structural and γ_{G2} for non-structural self-weight are proposed. While the material partial factors have been calibrated independently of the other variabilities (to allow for a simple modification if needed), the two partial factors for permanent actions have been calibrated accounting for all variabilities to provide a more reliable assessment for all potentially governing combinations.

With this respect, materials strength variabilities are updated using data collected in Switzerland. Distributions are generally in line with values specified in Section 1. However, the CoV and bias factor of concrete strength for the analysed data are larger than data found in international literature. This over-strength is probably to be attributed to an increase in cement content to meet durability and workability criteria by producers.

The variability of the traffic load for the weekly maxima events is found between 10 and 18%. Extrapolation of 50-year maxima distributions depends significantly on the tail fitting accuracy of the starting weekly distribution. Considering both log-normal and Gumbel extreme-maxima distributions for the tail fitting of the starting distribution leads to CoV of the traffic load variability between 6 and 10%.

According to the parametric reliability analyses, the required value of γ_{G1} for self-weight to reach the target value of the reliability index $\beta_{tgt,50y} = 3.8$ lies between 1.1 and 1.2 while γ_{G2} for other permanent actions is between 1.3 and 1.8 in case the nominal pavement thickness is considered as reference value. Reliability analyses performed on selected case studies including various failure modes confirm that $\gamma_{G1} = 1.2$ and $\gamma_{G2} = 1.5$ lead in general to sufficiently safe results for the design of new and the assessment of existing structures. With respect to the reference value of the pavement thickness, an increase of 20% of the

nominal value as recommended in Eurocode 1 is justified. Reliability analyses performed on selected case studies including various failure modes confirm that γ_{G1} = 1.2 and γ_{G2} = 1.5, respectively for structural and non-structural self-weight lead to sufficiently safe results with respect to current values and in absolute terms.

Structural system changes during construction and significant differences between modelling of complex structures and actual behaviour are not accounted for in the partial safety factors on the load side described above. If relevant for the structural system, depending on its complexity and particularly in case of governing brittle failure modes, if the behaviour cannot be improved with sound detailing during the design process, the structure should be modelled in a reasonably conservative manner and the results interpreted accordingly.

Summary of proposed partial factors

Based on the investigations described in this report, the partial factors for persistent and transient design situations can be proposed for a target value of the reliability index $\beta_{tgt,50}$ = 3.8 (CC2).

- For reinforcing steel :
  - If the verification is performed with the nominal values of the geometric dimensions, the value γ_S = 1.15 is confirmed;
  - If the verification is carried out on the basis of the design values of the effective depth $d_d = d_{nom}$ - 15 mm, the partial factor for the reinforcement may be reduced to γ_S = 1.05.
- For concrete :
  - The value γ_C = 1.50 is confirmed.
- For structural steel :
  - The value γ_{M1} = 1.05 is confirmed.
- For shear stress in slabs without shear reinforcement and for punching according to EN 1992-1-1:2023 :
  - If the verification is carried out using the nominal values of the geometric dimensions, γ_V = 1.40;
  - If the verification is carried out on the basis of the design values of the effective depth $d_d = d_{nom}$ - 15 mm, the partial factor for shear and punching can be reduced to γ_V = 1.30.
- The partial factor γ_{Sd} covering the model uncertainties in the action effect calculation lies between 1.05 and 1.15 depending on the other uncertainties. This factor is implicitly accounted for in the partial factors γ_G and γ_Q. Alternatively, γ_G and γ_Q can be calibrated assuming following statistical values of the model uncertainty: bias factor μ = 1.0 and CoV = 6.5-8%. It has to be noted that these factors and statistical values do not account for potential uncertainties related to the modelling of complex structures and/or the influence of system changes in the case of structures with limited deformation capacity and limited possibility to redistribute internal forces at ultimate limit state.
- For permanent actions :
  - Since the uncertainties of the self-weight of structural and non-structural elements are different, it is recommended to use two separate partial factors, namely γ_{G1} for structural and γ_{G2} for non-structural elements
  - The default value of the factor for the structural self-weight is γ_{G1} = 1.35 as in the current SIA 260. γ_{G1} may be reduced to 1.20 in case the modelling of the structure is conducted by the designer in a sufficiently reliable manner (sufficient experience with respect to the type of structure / software used / influence of the modelling of the structure on the results based on similar calculations on similar structures) and if the influence of changes in the system during construction is taken into account in a sufficiently reliable manner (method used / material parameters assumed / experience of the designer with respect to the influence of assumptions on the results). The same reduction is allowed also in the case of statically determined structures.

    - The partial factor for the self-weight of non-structural elements γ_{G2} = 1.50 is proposed. For the pavement of road bridges, in addition to γ_{G2} = 1.50, the nominal thickness should be increased by 20% in accordance with EN 1991-1:2023 [128].
- For variable actions :
    - The design values are derived on the basis of reliability analyses (out of the scope of the present research since the calibration of traffic loads, including their design values, are currently investigated in other research projects). The characteristic values can be determined by dividing the design value by a nominal partial factor γ_Q = 1.50.
- The above partial factors are valid for the design of new structures and for the assessment of existing structures where the related variables have not been assessed by direct measurements.
- For the assessment of existing structures, where the dimensions have been measured on site and/or the material strengths have been assessed from tests on samples taken from the existing structure, the partial factors may be adjusted using the procedure described in this report and the statistical values derived from the measurements. As a first step, the following partial factors may be assumed:
- As a firsts step, the following partial factors can be assumed:
    - For γ_S and γ_C , the values provided in Annex A (Adjustment of partial factors for materials) of EN 1992-1-1:2023 may be used;
    - For the structural self weight, the values of γ_{G1} described above should be used;
    - For the other permanent actions, γ_{G2} = 1,20 may be used if the dimensions are measured on the existing structure.

1 The partial safety factors in structural concrete

1.1 Introduction

Partial safety factors for concrete and reinforcing steel covering the material, the geometrical and the model uncertainties are used since several decades in codes of practice for concrete structures to calculate the design values of the resistances R_d to be compared to the design values of the internal forces E_d in the verification of the Ultimate Limit State to ensure that $R_d \geq E_d$. The approach with an explicit verification of the Ultimate Limit State (ULS) has replaced the permissible stresses approach since the 1970s (in Switzerland, the verification for prestressed structures was conducted at ULS already according to SIA 162:1968 and for the general case, since its guideline SIA 34:1976). The partial safety factors for concrete and steel reinforcement are relatively stable since more than five decades although they have been calibrated at the beginning to ensure the same level of safety as previous standards based on the permissible stresses approach. Current values according to SIA 262:2013 [1] (namely $\gamma_C = 1.50$ and $\gamma_S = 1.15$) have been adopted from EN 1992-1-1:2004 [3]) whose calibration according to reliability analysis is described in its background document [23].

The theoretical bases of the calibration of the partial factors are still valid and the statistical values of the uncertainties covered by the partial factors for concrete and steel have evolved little in recent decades. Nevertheless, a recalibration of γ_C and γ_S is justified for several reasons:

- The statistical values of the model uncertainties should be consistent with the actual values which refer to the models used for the verification.
- With respect to the uncertainties related to the actual concrete compressive strength in the structure, there is a need for a clear definition of the effects covered and the assumed statistical values.
- For design formulae where the concrete strength is not accounted for in a linear manner (as for instance punching and shear in slabs without shear reinforcement, where the resistance is proportional to the concrete strength with an exponent of 1/3), there is a need of a recalibration and to avoid some shortcomings, and the definition of a new partial factor is suitable.
- For the sake of simplicity, the dominating geometrical uncertainties, as for instance the effective depth, are typically covered by the material partial factors γ_C and γ_S. Nevertheless, this simplification shows some shortcomings (is overly conservative for deep members, slightly unconservative for thin members). For this reason, the possibility to use an alternative format, where the verification is conducted on the basis of design values of the dominant geometrical dimension, can be useful to save material in dimensioning new structures or in assessing existing structures in a more reliable manner.
- The partial safety factors for materials have been calibrated on the basis of the most common cases (design formulae for bending and compression; typical material uncertainties; most common tolerance class in execution; new cast-in-place concrete members; verification based on nominal geometrical values; usual target value of the reliability index; etc.). Nowadays, exceptions are more and more common. For this reason, there is a need for a consistent procedure to adjust the partial factors for materials for other situations as for instance: (a) geometrical deviations fulfilling more stringent tolerance classes during execution (as for instance in precast elements); (b) calculation of the design resistance on the basis of geometrical values measured on the finished structure (for new and existing structures); (c) verification on the basis of the compressive concrete strength and/or the reinforcement yield strength assessed in the existing structure; (d) the use of other verification methods with different model uncertainties (as for instance Non-Linear Finite Element Analysis Methods, see next

point); and (e) the choice of another target value of the reliability index (current partial factors are based on $\beta_{tgt,50}$ = 3.8), for instance accounting for another reference period.

- The use of Non-Linear Finite Element Analysis Methods, where the same assumptions with respect to the material and geometrical uncertainties as for common analyses should be made in the calibration of their safety format. The same holds true for other design methods that could be developed in the future, where the design values should be calibrated using the same assumptions for the relevant uncertainties as described in this section.

For all these cases, not only a procedure, but also a clear definition of the material, geometrical and model uncertainties and other effects (e.g., difference between in-situ concrete strength and concrete strength measured on specimens) which are covered by the partial factors is needed.

The results of the research described in this section have already been implemented in the 2nd generation of Eurocode 2 for concrete structures (EN 1992-1-1:2023 [14]) and its background document [57], so that they will be adopted implicitly in the future versions of the Swiss code for concrete structures. The procedure for adjusting the partial factors for materials, as well as the statistical values presented in this section are also defined in a code-like formulation in the Annex A of EN 1992-1-1:2023 [14].

In the following of this section, the common assumptions in the partial factor format calibration and the typical partial factor formats for structural concrete are briefly reminded in Subsection 1.2. The exponent sensitivity analysis, whose application was instrumental on the calibration of the partial factor, are also introduced in the same subsection. In Subsection 1.3, the reference limit states, as well as the corresponding resistance models, investigated for the calibration of the basic partial factors γ_C and γ_S and the additional partial factor γ_V (for shear of members without shear reinforcement and for punching shear in the 2nd generation of Eurocode 2) are presented. Eventually, in Subsections 1.4, 1.5 and 1.6, the probabilistic modelling of the basic uncertainties and the detailed procedure adopted in the calibration of γ_S, γ_C, and γ_V are explained and discussed.

1.2 Typical partial factor formats and exponent sensitivity analysis approach

1.2.1 Typical partial factor formats in structural design codes

The safety verification in current design codes is mainly performed by verifying limit state functions adopting design values for the resistance and for the action effects, whose values are calculated with partial factors calibrated to ensure a target reliability level. In this subsection, the common assumptions in the partial factor format calibration and the corresponding typical partial factor formats for reinforced concrete structures in current design codes will be briefly reminded.

It should be noted that the definitions of the basic concepts of probability of failure P_f, reliability index β, target reliability index β_{tgt}, the First Order Reliability Method (FORM) sensitivity factors α_E and α_R in the probability-based structural safety theory will not be repeated in this subsection and can be consulted in other literatures (e.g.[2, 5, 6]).

In the partial factor calibration in current structural design codes, the first common assumption is to adopt standardized FORM sensitivity factors for the action effect and the resistance side. In the EN 1990:2023 [7] and the *fib* Model Code 2010 [8], the standardized values $\alpha_E = -0.7$ and $\alpha_R = 0.8$ are proposed for the FORM sensitivity factors provided that the ratio between the standard deviations of the action effect and the resistance is within the limit between 0.16 and 7.6. Using standardized values for the FORM sensitivity factors allows calibrating:

- the partial safety factors on the action and on the resistance sides separately;

- the partial safety factors for actions regardless of the type of construction material, which significantly simplifies the safety format used in practice.

On the basis of the standardised FORM sensitivity factors, the target reliability for the design resistance and the design action effect are simplified as:

$$P\{E(\mathbf{X}) \geq E_d\} = \Phi(\alpha_E \beta_{tgt}) \quad (1)$$

$$P\{R(\mathbf{X}) \leq R_d\} = \Phi(-\alpha_R \beta_{tgt}) \quad (2)$$

where $\mathbf{X}$ refers to the vector of the random variables representing the basic uncertainties involved, $P(\cdot)$ refers to the probability function and $\Phi(\cdot)$ refers to the cumulative probability function for standard normal distribution.

Another important simplification normally considered consists on lumping partial factors covering different basic variables. Such procedure allows reducing the total number of partial factors in the design format. In EN 1990:2023(E) [7], a number of simplifications are proposed in the safety format for the design resistance, resulting eventually in three different safety formats. A comparison of the different formats is summarized in Tab. 1.

***Tab. 1** Different formats of the design resistance according to EN 1990:2023 (E) [7], (refer to notation section for the definitions of symbols)*

	Formula	Model uncertainties	Material uncertainties	Geometrical uncertainties
General format	$R_d = \frac{1}{\gamma_{Rd}} R\left\{\frac{\eta X_k}{\gamma_m}, a_d, \sum F_{Ed}\right\}$	γ_{Rd}	γ_m	covered by γ_{Rd} with $a_d = a_{nom}$ or separately by $a_d = a_{nom} \pm \Delta a$
Material factor approach	$R_d = R\left\{\frac{\eta X_k}{\gamma_M}, a_d, \sum F_{Ed}\right\}$	covered by γ_M		covered by γ_M with $a_d = a_{nom}$ or separately by $a_d = a_{nom} \pm \Delta a$
Resistance factor approach	$R_d = \frac{R\left\{\eta X_k, a_d, \sum F_{Ed}\right\}}{\gamma_R}$	covered by γ_R		covered by γ_R with $a_d = a_{nom}$ or separately by $a_d = a_{nom} \pm \Delta a$

In the general format (first row in Tab. 1), the partial factors can be individually calibrated for the model, geometrical and material uncertainties. The design value of resistance (R_d) is defined as:

$$R_d = \frac{1}{\gamma_{Rd}} R\left\{\frac{\eta X_k}{\gamma_m}, a_d, \sum F_{Ed}\right\} \quad (3)$$

where γ_{Rd} is the partial factor associated with the uncertainty of the resistance model, and for geometrical deviations, if these are not modelled explicitly; η is a conversion factor accounting for scale effects, effects from moisture and temperature, effect of aging of materials, or any other relevant parameters; X_k is the characteristic value of materials or product properties; γ_m is a partial factor for a material property accounting for unfavourable deviation of the material or product properties from their characteristic values as well as

the random part of the conversion factor η ; a_d represents the design values of geometrical properties; and F_{Ed} represents the design values of actions used in the assessment of E_{Ed}.

Alternatively, to enhance the ease-of-use, the partial factors for different types of uncertainties may be combined into a partial factor γ_m for material properties (referred to as the "material factor approach", second row in Tab. 1):

$$R_d = R\left\{\frac{\eta X_k}{\gamma_M}, a_d, \sum F_{Ed}\right\} \tag{4}$$

or into a single partial factor γ_R for the resistance (referred to as the "resistance factor approach", third row in Tab. 1):

$$R_d = \frac{R\left\{\eta X_k, a_d, \sum F_{Ed}\right\}}{\gamma_R} \tag{5}$$

It should be emphasized that the partial factors for material strength variables (γ_M) in the "material factor approach" need to be calibrated to cover material, model and potentially also geometrical uncertainties (depending if design values a_d are also adopted for the governing geometrical variables) involved in the resistance model. Similarly, the partial factor for the design resistance (γ_R) in the "resistance factor approach" also need to be calibrated to cover all basic uncertainties (again, potentially with the exception of the geometrical uncertainties, if design values are considered for the geometrical variables). With respect to Eq. 5, it is also worth to mention that in some codes, the resistance design values are obtained by dividing the characteristic values with a factor $\gamma_R > 1$ (e.g. EN 1992-1-1:2004 [3]) whereas in other codes, the same result is obtained by multiplying the characteristic values with a strength reduction factor $\phi < 1$ (ACI 318-19 [9]).

In what regards specifically RC structures, it should be noted that the approach mathematically expressed in Eq. 4 is for instance considered in EN 1992-1-1:2004 [3], *fib* MC 2010 [8], the Chinese [10] and Canadian [11] codes to calculate the resistance associated to bending, axial force, shear and torsion of members with sufficient shear reinforcement, whereas Eq. 5 is applied in other cases, such as the verification of the shear resistance of members without or with insufficient shear reinforcement in EN 1992-1-1:2004 [3] and *fib* MC 2010 [8], or for all design formulae according to ACI 318-19 [9], AASHTO [12] and Australian [13] codes for concrete structures.

The suitable simplified safety format to be applied to a given type of structural resistance should be chosen on the basis of the variability of the shape of the corresponding limit state functions and on the dominating involved uncertainties. In the 2nd generation of Eurocode 2 [14] for the design of concrete structures, two basic partial factors according to the "material factor approach" are calibrated: γ_C for the concrete compressive strength and γ_S for the steel yielding strength. The two partial factors are calibrated so that the verification of a wide range of limit states commonly used in daily practice can be performed ensuring the required safety level (e.g. the resistance to axial load, bending, and combined axial load and bending). There are other more specific limit states where the combination of the partial factors γ_C and γ_S calibrated on the basis of a "material factor approach" cannot provide a sufficiently consistent reliability level and, for those cases, additional partial factors can be calibrated (this is the case of the partial factor γ_V calibrated following a "resistance factor approach" for both the shear resistance of members without sufficient shear reinforcement and the punching shear resistance). This matter is discussed in detail in Subsection 1.3.

1.2.2 Exponent sensitivity analysis

As it will be shown in the following, the so-called exponent sensitivity analysis is an efficient tool to facilitate the calibration of partial factors for the resistance of concrete structures. The shape of the limit state function in the standard normal space of the basic variables plays an instrumental role in the reliability analysis and, consequently, in the calibration of the partial factors. For the calibration of the partial factor on the resistance side, the limit state function is defined by $R(\mathbf{X}) - R_d = 0$ and its shape in the standard normal space depends not only on the sensitivity of the structural resistance model $R(\mathbf{X})$ to the involved basic variables $\mathbf{X}$, but also on the probability distributions of the basic variables.

In this work, in order to have a clear and explicit representation of the sensitivity of the resistance models to the basic variables, exponent sensitivity analyses are carried out [15,16]. The exponent sensitivity factors are calculated based on a power-multiplicative form approximation of the resistance functions:

$$R(\mathbf{X}) \approx C_0 \cdot \prod_{i=1}^{p} f_i^{n_i} \text{ where } \mathbf{X} = (f_1, f_2, ... f_p) \tag{6}$$

where f_i is the i^{th} basic variable in the resistance function, n_i is the corresponding exponent sensitivity factor and C_0 is the residual constant coefficient in the power-multiplicative form approximation of the resistance function.

The power-multiplicative form approximation presented in Eq. 6 is equivalent to perform a first order Taylor expansion of the resistance function in the logarithmic space of the basic variables. The exponent sensitivity factors can be calculated as the local partial derivative of the logarithmic resistance to the logarithmic basic variables [15]. The advantages lying on the calculation of the exponent sensitivity factors are:

- The exponent sensitivity factors are unitless and can be directly linked to the uncertainty through the influence of a given basic variable on the resistance model. When the basic uncertainties are modelled as lognormal distributions, the CoV of the resistance variable can be directly estimated based on the CoVs of the basic variables and the corresponding exponent sensitivity factors with Eq. 7:

$$V_R \approx \sqrt{n_i^2 \cdot V_i^2} \tag{7}$$

- The thoroughness of the exponent sensitivity analysis can be verified by comparing the units obtained on the right side of Eq.6 to the known units of the resistance variable (left side of Eq. 6), refer to [15] for details.

The precision of the estimated CoV in Eq. 7 depends on the nonlinearity of the resistance function in the logarithmic space. When the resistance function is strongly nonlinear (e.g. involving different failure modes; refer to [15] for examples), the values of the CoV estimated based on the locally calculated exponent sensitivity factors are not necessarily precise. However, when the exponent sensitivity analysis is performed for a wide range of applicable cases for a given resistance function, the results can provide valuable information about the ranges and trends of the sensitivity factors and the corresponding variability of the resistance variable [17]. This valuable information can thereafter be used to facilitate the partial factor calibration.

1.3 Considerations on the calibration of partial factors in structural concrete

1.3.1 Definition of the required partial factors

The partial factors required to achieve a given target reliability level vary with the shape of the limit state functions and, thus, implicitly depend on the structural resistance models. In order to have a quantitative comparison between different resistance models, an exponent sensitivity analysis is performed for five resistance models for the most common limit states governing the design of RC structures, namely:

1. The resistance of a reinforced tie subjected to axial tension;
2. The resistance of a reinforced column subjected to axial compression (neglecting second order effects);
3. The resistance of a reinforced beam segment subjected to bending, analysed with Bernoulli-Navier hypothesis (plane sections remain plane after deformation) and neglecting the concrete tensile strength;
4. The shear resistance of a beam with shear reinforcement, analysed with the closed-form resistance model of EN 1992-1-1:2023 (clause 8.2.3 [14]);
5. The resistance of a slab-column connection without shear reinforcement (punching shear), analysed with the closed-form resistance model of EN 1992-1-1:2023 (clause 8.4.3 [14]).

The results of the exponent sensitivity analysis for these different resistance models are shown in Fig. 1 as a function of the main variables.

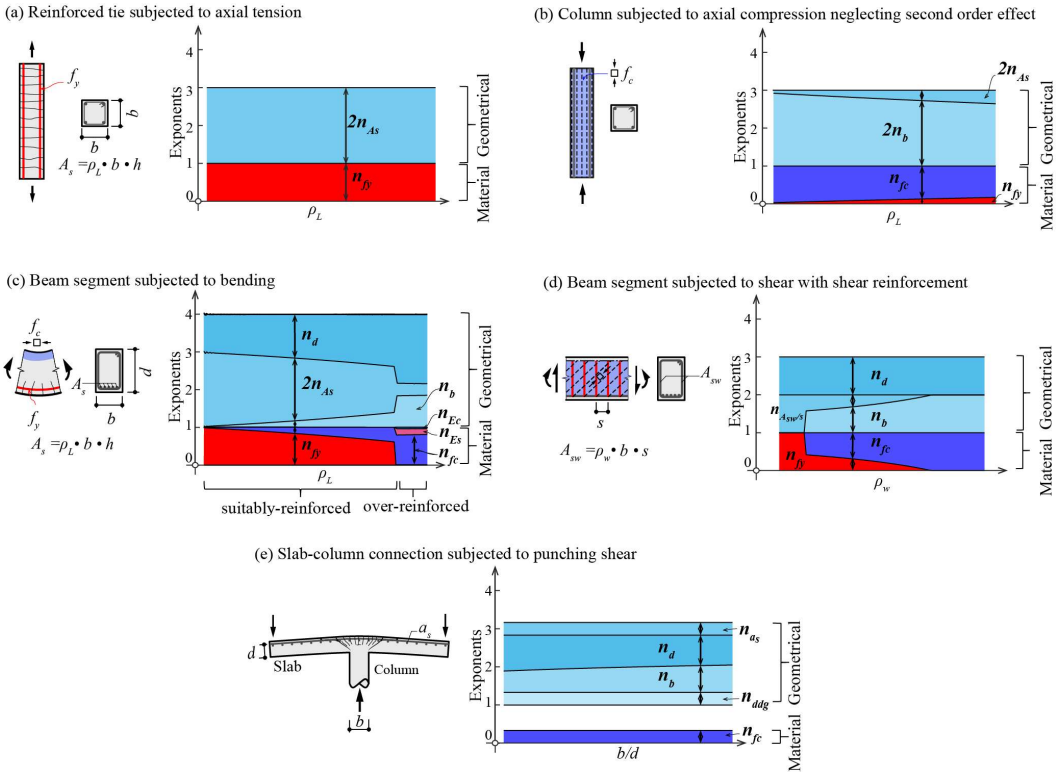

Fig. 1 *Results of the exponent sensitivity analyses [15] for five typical structural concrete resistance models: (a) RC member subjected to pure axial tension; (b) RC column subjected to pure axial compression; (c) RC beam subjected to pure bending; (d) RC beam with shear reinforcement subjected to shear and (e) slab-column connection with potential punching failure.*

The following observations can be made by comparing the results of the exponent sensitivity analyses of the five investigated resistance models:

- The results of this analyses confirm the significant differences among the models in terms of the sensitivities to the basic geometrical and material variables. The dominating material and geometrical variables (from a deterministic perspective) therefore differ from one limit state to the other.
- For the cases of flexure and shear, various failure regimes can be easily identified.
- Both the axial tension resistance model and the bending resistance model of suitably-reinforced cross-sections are dominated by the steel yield strength (with the exponent n_{fy} close to 1, refer to Fig. 1a and c), which indicates that they have similar level of material uncertainties. However, by comparing the sensitivity of geometrical variables in the two resistance models, it can be observed that the bending resistance model involves a higher level of geometrical uncertainties, since, in the former case, both the reinforcement area (A_s) and the effective depth (d) have an exponent close to 1. In addition, it is well-known that the bending load-bearing mechanism is more complex than the one associated with axial tension, which suggests that also a higher model uncertainty is potentially associated to the bending resistance model (the statistics of the uncertainty of the different resistance models are presented later in Subsection 1.4).
- Both the axial compression (Fig. 1b) and bending resistances (Fig. 1c) of over-reinforced cross-sections are dominated by the concrete compressive strength (with n_{fc} close to 1).
- For the punching shear resistance model (Fig. 1d), it can be observed that only one material strength variable is involved (f_c, as the closed-form equation represents a simplification of a more advanced mechanically-based model, refer to [18, 19] for details) and that its exponent is much lower than 1 (n_{fc} = 1/3). Regarding geometrical variables, it is important to note that the effective depth d has the highest exponent (n_d >1). The results also show that in the case of punching shear, the sum of the exponents of material variables is significantly lower than the sum of the exponents of geometrical variables and of the exponent of the model uncertainty (when the model uncertainty is assumed to be represented by a random variable θ multiplied to the resistance model, it has an exponent equal to 1).

The safety format suitable for each limit state should depend on the dominating uncertainties. If these are material variables, a material factor approach can be adopted; otherwise, if the model uncertainty is the dominating one, a resistance factor approach should be adopted. In more complex situations, a general format approach can be adopted.

The results of Fig. 1 show from a deterministic perspective that the resistance models can be distinguished into two types based on their sensitivity to the material strength variables f_c and f_y :

- Resistance models with $n_{fc} + n_{fy} \cong 1$: this type of models include resistance against an axial tension, compressive axial load, bending and shear of members with shear reinforcement. It should be noted that for bending with over-reinforced cross-section, the sum $n_{fc} + n_{fy}$ is smaller than 1, but the difference is relatively small and can still be considered to belong to this type.
- Resistance models with $n_{fc} + n_{fy} \ll 1$: the punching shear resistance belongs to this type. In addition, performing an exponent analysis as the one shown in Fig.1 to the shear resistance model of members without shear reinforcement allows showing that, also in that case, the model presents a low sensitivity to the material strength variables and belongs to this category.

The first type of resistance models (with $n_{fc} + n_{fy} \cong 1$) has high sensitivity to the material strength variables (comparable to the exponent of model uncertainty, $n_\theta = 1$). By combining the information of the exponents and the probability distributions of the basic uncertainties using Eq. 7 (the statistics of basic uncertainties will be presented in Subsection 1.4-1.6), it can be demonstrated that the material uncertainties are dominating for most models of this type. Due to this reason, a material factor approach can therefore be accepted for these

resistance models, with a partial factor applied to the concrete compressive strength (γ_C) and another to the steel reinforcement yield strength (γ_S).

On the contrary, for the second type (with $n_{fc} + n_{fy}$ significantly smaller than one), due to their low sensitivity to the material strength variables, the material uncertainties cannot be dominating anymore. A safety format based on a material approach is for this reason not suitable, as the partial factor of the material strength variable would have a low exponent in the design resistance equation, being therefore not effective. A safety format based on the resistance factor approach (refer to Tab. 1) results as a justified safety format alternative for these resistance models. Due to this reason, a partial factor γ_V, applied to the resistance model and calibrated on that basis, is thus justified for the punching shear resistance (this applies also for the case shear resistance of members without sufficient shear reinforcement).

1.3.2 Definition of reference models used for the calibration of the partial factors

For design purposes, it is suitable to have the same partial factors applied to a number of resistance models (associated to different limit states). This means that a choice has to be made with respect to reference resistance model to be used to calibrate each partial factor. The following criteria are established for that purpose:

- The reference model used in the calibration of the partial factor for a material strength should be a case in which this material strength variable is dominating (i.e. with an exponent sensitivity factor close to or equal to 1);
- The chosen reference model should be relevant for practice and have significant geometrical and model uncertainties in order to widen the applicability range of the calibrated partial factors.

Based on these criteria, γ_C is calibrated using the resistance model for the axial compression resistance of columns (as it is more likely to find situations in practice where the axial compressive resistance of columns is governing than the bending resistance of over-reinforced cross-sections) and γ_S is calibrated accounting for the bending resistance of suitably-reinforced concrete cross sections. The case of a reinforced concrete tie (see Fig. 1a) is not suitable since: (i) it is not a common case in practice; (ii) the model uncertainty is very small; and (iii) the geometrical uncertainty is also negligible (the uncertainty of the reinforcement area is indirectly accounted for in the uncertainty of the yield strength, since according to EN 10080:2005 [25], the latter is determined by dividing the measured yield force by the nominal reinforcement area). With respect to the partial factor γ_V, it can be calibrated on the basis of the resistance model for shear of members without shear reinforcement or punching shear. In fact, both models share the same principles [22] and the derived closed-form design expressions included in the EN 1992-1-1:2023 for the two cases present strong similarities (thus yielding equivalent trends in terms of material, geometrical and model uncertainties). Differences in the model uncertainties can be covered by adjusting the related calibration coefficients.

1.3.3 Assumptions and simplifications adopted in the calibration of partial factors

Accounting for the reference resistance models, the following simplifications and approximations are further assumed in order to achieve an analytical solution for the calculation of the partial factors γ_C, γ_S and γ_V:

- The probabilistic modelling of the basic uncertainties and of the resistance variable can be approximated by lognormal distributions.
- The standard deviation of the logarithm of the resistance variable (denoted as $\sigma_{\ln(R)}$) can be approximated by its CoV (denoted V_R). For a lognormal distribution variable, the

exact relationship between its standard deviation and CoV is: $\sigma_{\ln(R)} = (\ln(V_R^2 + 1))^{0.5}$. The approximation of $\sigma_{\ln(R)} \approx V_R$ is considered acceptable when $\sigma_{\ln(R)}$ is lower than 0.2.

- The material strength variable has an exponent close to 1 in the resistance solution when the "material factor approach" is adopted. When this assumption is valid (considered also as a criterion in the choice of the reference resistance model), the application of the partial factor to the material strength variable is equivalent to applying it to the resistance directly.

Based on the aforementioned assumptions, the value of the partial factors can be calculated with the following equations:

$$\gamma_M = \frac{\exp\left(\alpha_R \cdot \beta_{tgt} \cdot V_{RM}\right)}{\mu_{RM}} \tag{8}$$

$$V_{RM} = \sqrt{\sum n_i^2 V_i^2} \tag{9}$$

$$\mu_{RM} = \frac{R_m}{R_{nom}} = \prod \mu_i^{n_i} \tag{10}$$

where the subscript *M* is replaced by *S* for reinforcement, by *C* for concrete in compression and *V* for shear; V_{RM} is the Coefficient of Variation (CoV) of the resistance (accounting for the influence of (i) the material strength variability; (ii) the geometrical uncertainties and (iii) the model uncertainties on the resistance side; n_i is the exponent sensitivity factor for the i^{th} basic variable; V_i is the CoV for the i^{th} basic variable; μ_{RM} is the bias factor of the resistance represented by the ratio between the mean value of the resistance R_m and the nominal value of the resistance R_{nom}; R_{nom} is the nominal value of the resistance calculated with the design formula without partial factors, and μ_i is the bias factor for the i^{th} basic variable, representing the ratio between its mean value and its nominal value accounted for in the design formula (e.g. the characteristic value for material strength variables).

In the following subsections, the probabilistic modelling of the basic uncertainties involved as well as the exponent sensitivity factors of the corresponding basic variables in different failure modes of RC structures are discussed and the corresponding partial factor calibration is presented.

1.4 Calibration of partial factor for steel reinforcement

Following the discussions presented in Subsection 1.3.1, the bending resistance model of a suitably-reinforced rectangular cross section is used as reference for the calibration of the partial factor for the yield strength of steel reinforcement.

The bending resistance can be calculated adopting Bernoulli-Navier hypothesis (plane sections remain plane), neglecting the concrete tensile strength and considering a parabola-rectangle response of concrete (with strain limitation) in compression and an elastic-perfectly plastic response of steel reinforcement. These are the hypotheses adopted for the exponent analysis presented in Fig. 1b. In such case, the bending resistance model can be approximated by the following power-multiplicative equation (including the random variable θ_S for its model uncertainty):

$$R \approx C_0 \cdot f_y^{n_{fy}} \cdot A_s^{n_{As}} \cdot d^{n_d} \cdot \theta_S \approx C_0 \cdot f_y \cdot A_s \cdot d \cdot \theta_S \quad \text{with} \quad n_{fy} = n_{As} = n_d \approx 1 \tag{11}$$

Following the simplified form of the resistance function, the adopted distribution parameters of the yield strength f_y, the effective depth *d*, and the model uncertainty variable θ_S in the calibration of partial factor γ_S are listed in Tab. 2. The distribution parameters adopted to justify the same partial factor in SIA 262:2013 [1] derived from EN 1992-1-1:2004 (refer to

[23]) are also listed in Tab. 2 for the sake of comparison. It should be noted that, as already discussed, since the yield strength of steel reinforcement is typically calculated based on the measured axial tensile load resistance and the nominal reinforced area (without measuring the actual area) of reinforcement bars [24, 25], the statistics of f_y represent both the uncertainties of f_y and A_s. Due to this reason, the reinforcement area A_s is considered to be deterministic in the partial factor calibration. In the following, the considerations for the distribution parameters adopted for each basic variable are explained in detail.

***Tab. 2** Statistical values assumed to calibrate the partial factors for reinforcement (values in brackets refer to the assumptions to justify in EN 1992-1-1:2004, see [23])*

	Coefficient of variation V_i	**Bias factor μ_i**
Yield strength f_y	V_{fy} = 0.045 (0.040)	f_{ym}/f_{yk} = exp(1.645V_{fy})
Effective depth d	V_d = 0.050 (0.050)	μ_d = 0.95 (1.00)
Model uncertainty θ_S	$V_{\theta s}$ = 0.045 (0.025)	μ_s = 1.09 (1.00)
Coefficient of variation and bias factor of resistance for reinforcement	$V_{RS} = \sqrt{V_{fy}^2 + V_d^2 + V_{\theta s}^2} = 0.081$ (0.069)	$\mu_{RS} = \frac{f_{ym}}{f_{yk}} \mu_d \cdot \mu_{\theta s} = 1.115$ (1.068)

1.4.1 Statistics of yielding strength

Regarding the distribution of the material strength variable f_y, Tab. 3 shows the statistics of B500 reinforcement of different ductility classes in UK and in Switzerland collected in the two last decades. It can be observed that the CoVs are slightly higher than the value of 0.04 assumed in EN 1992-1-1:2004 (see Tab. 2). For this reason, a value of 0.045 is adopted. It has to be noted that with this assumption, the ratio $f_{ym} / f_{yk,spec}$ becomes 1.077, which is slightly lower than the measured values (second value is the bracket of Tab. 3). With respect to prestressing reinforcement, Kreis et al. [26] provided similar results ($V_{fp0.1}$ = 0.043-0.058 for the 0.1% proof strength $f_{p0.1}$ and V_{fp} = 0.025-0.043 for the tensile strength f_p).

***Tab. 3** Statistical values of the yield strength of B500 reinforcement ($f_{yk,spec}$ = 500 MPa, the values in the brackets refer to the number of tests and to the average value of the measured ratio $f_{ym} / f_{yk,spec}$)*

Ductility class	**Beeby/Jackson:2016 [Beeby, 2016]**	**CARES 2005-2006 [Cares, 2019]**	**EPFL 2015-2019 [EPFL, 2019]**
A	0.050 (1 803, 1.143)	0.051 (410, 1.140)	-
B	0.048 (10 480, 1.108)	0.040 (3 458, 1.104)	0.042 (104, 1.092)
C	0.040 (3 794, 1.092)	0.038 (300, 1.084)	-
All ductility classes	0.048 (16 077, 1.107)	0.043 (4 168, 1.107)	-

1.4.2 Statistics of effective depth

As already mentioned, the geometrical uncertainties related to the reinforcement area A_s are implicitly accounted for in the variability of the yield strength (since the latter is characterized on the basis of the nominal cross-sectional area [25]). For this reason, this geometrical uncertainty is not accounted for repeatedly in the partial factor calibration. In addition, as the exponent n_b takes relatively low values and the variability of b is small (detailed information provided in Subsection 1.5), it is assumed that its influence on the reliability of bending resistance is negligible (assuming $n_b \approx 0$). It thus results the variability of the effective depth d (assuming $n_d \approx 1$) as sole geometrical uncertainty involved in the calibration of γ_S.

The probabilistic modelling of the effective depth is based on the following sources:

- In the work of Ellingwood [27], it is considered for the effective depth of one-way slabs that:
  - $d_m = d_{\text{nom}} - 10$ mm and $\sigma = 12$ mm for top bars
  - $d_m = d_{\text{nom}} - 3$ mm and $\sigma = 9$ mm for bottom bars

where d_m refers to the mean value of the effective depth and σ refers to its standard deviation:

- In the JCSS Probabilistic Model Code (section 3.10.2) [28], it is proposed to adopt $d_m = d_{\text{nom}} - 10$ mm and $\sigma = 10$ mm.
- A comparison between the nominal and measured values of the effective depth of the hogging reinforcement in 140 punching tests conducted in the Structural Concrete Laboratory of Ecole Polytechnique Fédérale de Lausanne (Switzerland) between 2007 and 2015 (refer to Fig. 2) shows that the difference between the nominal and measured value has the same order of magnitude as the standard deviation (similarly to the relationship adopted by Ellingwood [27]).
- A comparison in practice between the nominal value according to drawings (based on the specified member height, cover and bar diameter), the effective depth considered in design (similar to nominal value) and the theoretical value based on the chosen reinforcement supports has shown that a part of the deviation between nominal and actual effective depth has its origin already during the design process.

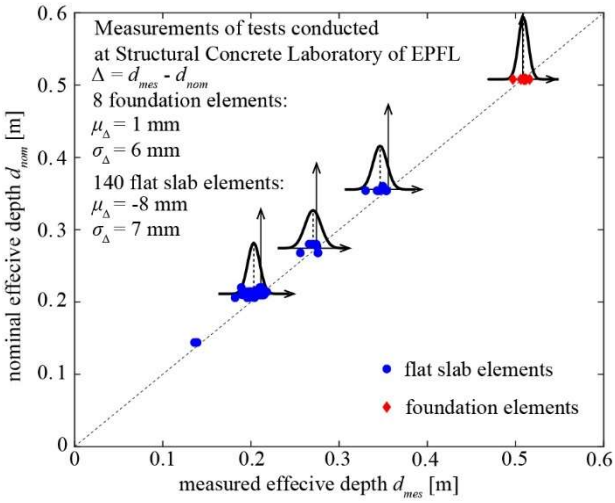

***Fig. 2** Statistics of effective depth measured on punching shear specimens tested at EPFL between 2007 and 2015 (all measured on saw-cuts).*

Based on these sources, a standard deviation of 10 mm is seen as a reasonable assumption. Nevertheless, since the statistical values described above refer to relatively thin members, they should be corrected by a law accounting for the size of the member. The latter can be calibrated on the basis of the tolerance of the location of ordinary reinforcement according to EN 13670:2009 [29]. As shown in Fig. 3a, the influence of the size of the member can be reproduced by the following formulae:

$$V_d = 0.05 \cdot (200 / d)^{2/3} \quad [d \text{ in mm}] \tag{12}$$

$$\mu_d = 1 - 0.05 \cdot (200 / d)^{2/3} \tag{13}$$

The resulting CoV of the effective depth *d* is represented in Fig. 3b.

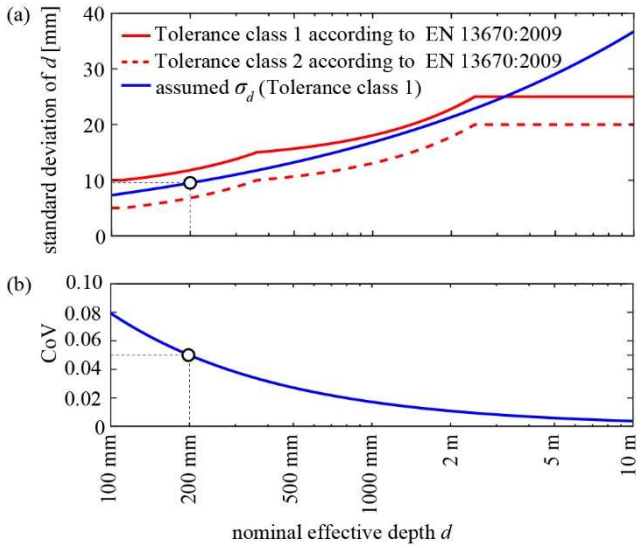

Fig. 3 *Standard deviation of the effective depth as a function of the member's size; (a) comparison between the assumed standard deviation and the tolerances of the location of ordinary reinforcement according to EN 13670:2009 and (b) resulting coefficient of variation (see Eq.(14)-(15), abscissae in logarithmic scale).*

1.4.3 Statistics of model uncertainty for the flexural resistance model

To quantify the model uncertainty related to bending, the flexural resistance measured in laboratory tests (denoted as $M_{R,exp}$) is compared to the resistance calculated (denoted as $M_{R,calc}$) according to the provisions of subsection 8.1 of EN 1992-1-1:2023 [14]. With this respect, the formulae are applied without partial factors and with the mean values reported in the publications. The database used by Foster et al. in [30] and Stewart et al. in [31] for calibrating the Australian Standard for concrete structures AS3600 is considered in the following.

The compression zone is considered in the calculation of the flexural resistance with a parabola-rectangle distribution of the concrete stresses. Regarding the stress-strain relationship for reinforcing steel, clause 5.2.4(2) in EN 1992-1-1:2023 [14] allows two approaches:

- (a) Linear-elastic/perfectly plastic behaviour without strain-hardening, and
- (b) Linear-elastic/plastic behaviour with strain hardening linearized between beginning of yielding and ultimate strength (stress f_t and strain ε_u, but with a strain not higher than $\varepsilon_{uk} / \gamma_S$).

The comparison between experimental and theorical results has been conducted following both approaches. With respect to the stress-strain relationship including strain hardening, the slope of the plastic branch (strain hardening modulus E_h) depends on the ductility class of the reinforcement. Assuming the minimum values (10% quantiles) of the ratio f_t / f_y and of the maximum strain ε_{uk} given in table C1.2 in Annex C of EN 1992-1-1:2023, modulus E_h becomes 1110 MPa for ductility class A, 840 MPa for class B and 1030 MPa for class C (Grade B500 reinforcement). Assuming the maximum value of ratio f_t / f_y for class C reinforcement, E_h becomes 2410 MPa. Since for most of the tests included in the used database, the actual strain hardening behaviour is unknown, a strain limit of $\varepsilon_u = 7.5\%$ and a ratio f_t / f_y = 1.2 has been adopted in the comparison ($E_h = 1380$ MPa for $f_y = 500$ MPa).

Fig. 4 shows the model uncertainty variable θ_S calculated as the ratio between the measured and the calculated flexural strength, $\theta_S = M_{R,exp} / M_{R,calc}$, for both modelling approaches (neglecting or accounting for strain hardening of steel reinforcement) as a function of the calculated reinforcement strains.

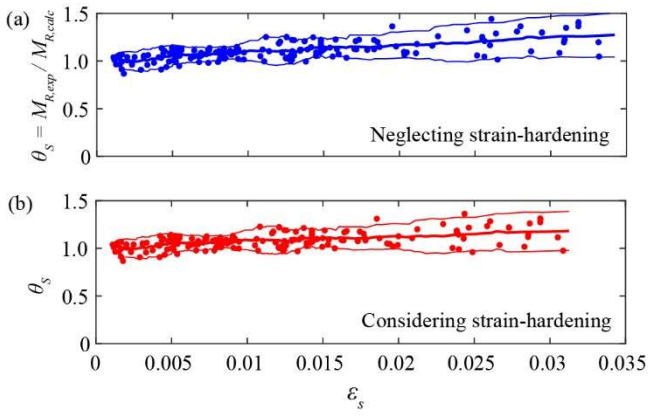

Fig. 4 *Comparison between calculated flexural resistance $M_{R,calc}$ (on the basis of section 8.1 and 5.2.4 of EN 1992-1-1:2023 [14]) and experimental measured value $M_{R,exp}$ as a function of the calculated steel stain for (a) the case strain hardening is neglected and (b) the case with strain hardening assuming $\varepsilon_u = 7.5\%$ and f_t / f_y = 1.2 (the thick curves refer to the moving averaged whereas the thin curves describe the upper and lower 5% fractiles, courtesy of data by S. J. Foster).*

The statistics of both cases are compared in Fig. 5. One can observe that:

- For small steel strains (failure dominated by concrete crushing with elastic reinforcement or with limited plastic strains), the bias factor $\mu_{\theta S}$ is close to 1.0. For this regime, the uncertainty of the resistance for practical cases will be governed by γ_C so that these cases should not be considered in calibrating γ_S.
- For large steel strains, the bias factor $\mu_{\theta S}$ increases significantly, not only for the case where strain hardening is neglected in the calculation, but also in the case strain hardening is accounted for. Such result is justified by the fact that: (1) the database contains also tests with ductile steels (with significant f_t / f_y ratios); (2) the model for bending according to EN 1992-1-1:2023 [14] underestimates the effect of strain hardening (since an average steel strain is considered, i.e. the strain localization in the crack region is neglected); (3) the concrete strain limit is probably underestimated in case of a strain localization which develops with steel yielding.
- The coefficient of variation $V_{\theta S}$ increases with the steel strain. This can be explained by the fact that steels with different strain hardenings are considered in the database.

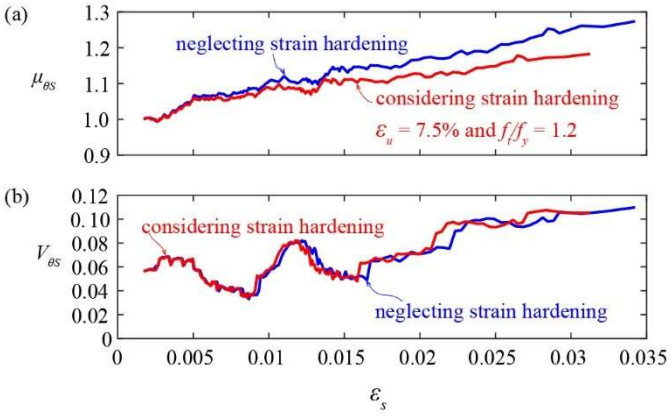

Fig. 5 *Statistics of the model uncertainty data for flexural resistance: (a) bias factor $\mu_{\theta S}$ = $M_{R,exp}$ / $M_{R,calc}$ and (b) coefficient of variation $V_{\theta S}$ of ratio $M_{R,exp}$ / $M_{R,calc}$.*

Based on the results shown in Fig. 5, the values of $\mu_{\theta S} = 1.09$ and $V_{\theta S} = 0.052$ can be assumed for the region governed by an average steel strain. In addition, it has to be considered that these variabilities depend also on the uncertainties related to the reported

data in the test reports. Using the procedure proposed by Ellingwood [27], the effect of these uncertainties can be removed from the actual model uncertainty as follows:

$$V_\theta = \sqrt{V_{\theta\tau}^2 - V_{test}^2 - \sum V_i^2} \tag{14}$$

where V_θ is the actual CoV of the model uncertainty, $V_{\theta\tau}$ is the CoV of the ratio $M_{R,exp}$ / $M_{R,calc}$ mentioned above, V_{test} represents the measurement uncertainties related to the failure load (errors in measuring the failure load, effect of supports friction, influence of different loading rates, effect of the test procedure, etc.) and V_i are the CoVs for the measured error of the geometrical and material variables. The following values are assumed for the CoVs: effective depth = 0.01; yield strength = 0.01 and concrete strength = 0.03. Accounting for all the measurement errors, the coefficient of variation of the flexural resistance $V_{\theta S}$ can be reduced from 0.052 to 0.045.

1.4.4 Calibration of γ_S using the nominal value of the effective depth

By using Eq. 8 and assuming $\alpha_R = 0.8$, $\beta_{tgt} = 3.8$ (for the ultimate limit state of structures with medium consequences class with a 50 years reference period according to EN 1990:2023 [7]) and the above-mentioned distribution parameters, the partial factor γ_S becomes:

$$\gamma_S = \frac{f_{yk}}{f_{yd}} = \frac{\exp\left(\alpha_R \cdot \beta_{tgt} \cdot V_{RS}\right)}{\mu_{RS}} = \frac{\exp\left(0.8 \cdot 3.8 \cdot \sqrt{0.045^2 + 0.050^2 + 0.045^2}\right)}{\exp(1.645 \cdot 0.045) \cdot 0.95 \cdot 1.09} = 1.15 \tag{15}$$

which is unchanged with respect to current practice.

1.4.5 Alternative using the design value of the effective depth

As already discussed above, the distribution parameters for the geometrical uncertainties assumed in the calibration of γ_S are valid only for members with an effective depth of approximately 200 mm (for the hogging reinforcement). For thinner members, the geometrical variability (in terms of coefficient of variation V_d) will be higher, so that a higher partial factor γ_S would be required to ensure that the target reliability index is reached. On the contrary, for larger members (and also for sagging reinforcement), a lower partial factor γ_S could be justified (refer to Fig. 3). To overcome this shortcoming, and to achieve a more uniform level of safety, the verification can be conducted using design values of the effective depth (instead of nominal values, requiring the geometrical uncertainties to be covered by a material partial factor). This possibility is already considered in the general format for the resistance design value R_d according to EN 1990:2023 [7] (refer to Eq. 3). The term a_d in Eq. 3 refers the design value of the geometrical property and its value is defined based on the sensitivity of the resistance to the deviation in the relevant geometrical property (refer to clause 8.3.7 of EN 1990:2023 [7]):

- When the structural design is sensitive to deviations in a geometrical property, the design value of the parameter a_d should be calculated as:

$$a_d = a_{nom} \pm \Delta a \tag{16}$$

- On the contrary, when the structural design is not significantly sensitive to the deviation of a given geometrical property, the design value can be simply assumed as:

$$a_d = a_{nom} \tag{17}$$

where a_{nom} is the nominal value of the geometrical property and Δa is the deviation in the geometrical property.

In what regards the sensitivity of the bending resistance to the effective depth as geometrical property, and as previously shown and discussed, Eq. 17 is theoretically only

applicable for thick members. This fact indicates that the design value of the effective depth (Eq. 16) should be used instead of its nominal value (Eq. 17).

The deviation in the effective depth Δa can be obtained by minimizing the difference between the target reliability index β_{tgt} and the achieved index β (see Fig. 6b) or by aiming at achieving an almost constant partial factor (see Fig. 6a). As shown in Fig. 6, consistent results can be obtained with the values of $\gamma_S = 1.04$ and $\Delta d = 19$ mm for hogging reinforcement and $\Delta d = 11$ mm for sagging reinforcement. For the sake of simplicity, a constant value of Δd can be adopted in the calculation of the design value of the effective depth:

$$d_d = d_{nom} \pm \Delta d \tag{18}$$

where the value of $\Delta d = 15$ mm is proposed for both hogging and sagging reinforcement.

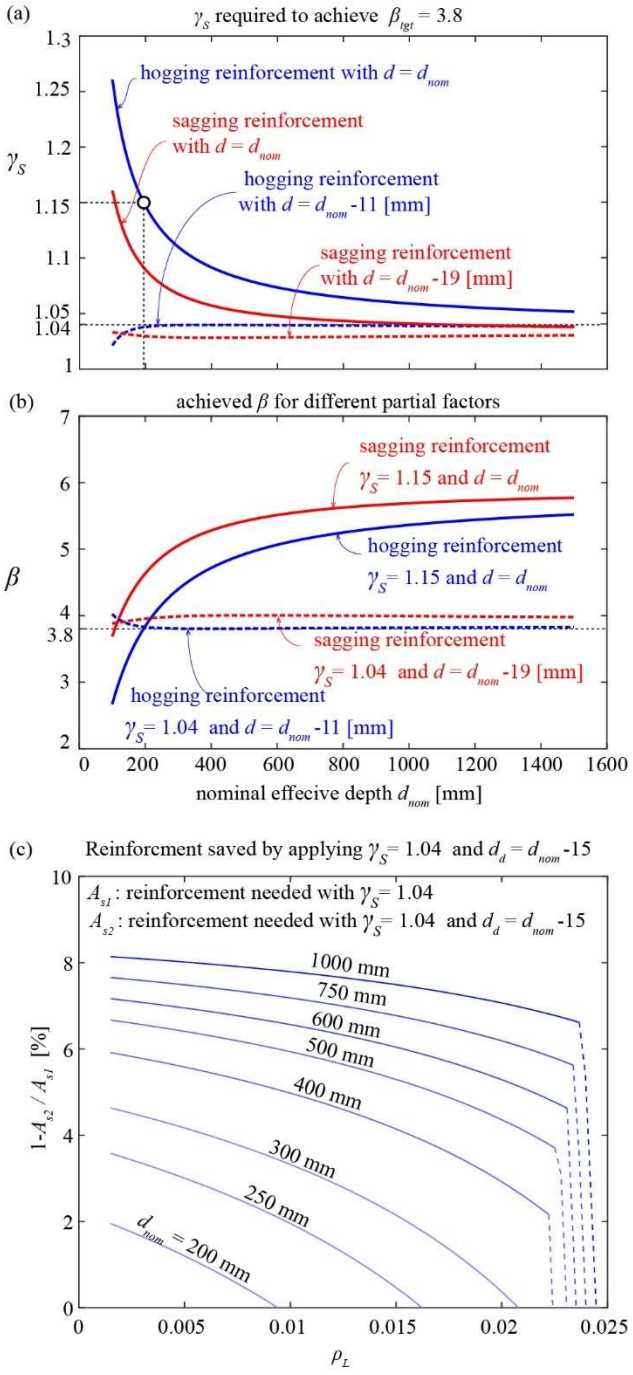

Fig. 6 *(a) Required partial factor to achieve the target reliability index β_{tgt}; (b) achieved reliability indexes with the assumed partial factor γ_S (solid curves refer to the approach using nominal values of the effective depth whereas dashed curves refer to the case using design values of the effective depth) and (c) Reinforcement saved by applying $\gamma_S = 1.04$ and $\Delta d = 15$ mm instead of $\gamma_S = 1.15$ to achieve the same design bending resistance (assumed $h_{nom} = d_{nom} + 50\text{mm}$, $b_{nom} = 0.6 \cdot d_{nom}$, $f_{yk} = 500\text{MPa}$ and $f_{ck} = 30\text{MPa}$, the dashed part of the curves represent cases with over-reinforced cross-section).*

It has to be emphasized that this approach allows to obtain, not only a more constant safety level (avoiding an unsafe design for thin members), but also a more economical and environmentally-friendly design (particularly for deep members). The ratio of reinforcing steel that can be saved by adopting the design effective depth approach is shown in Fig. 6c.

1.5 Partial factor for concrete in compression

As discussed in Subsection 1.3.1, the most frequent case where the concrete compressive strength is the dominating material strength is the axial compression resistance of columns. Due to this reason, it is used as the reference model for the calibration of γ_c.

The axial compression resistance of centric loaded reinforced concrete columns can be approximated as follows when the contribution of both longitudinal and confinement reinforcement is neglected:

$$R \approx \eta_{is} \cdot f_c \cdot A_c \cdot \theta_c \tag{19}$$

Following the simplified form of the resistance function, the distribution parameters of f_c, A_c, and the model uncertainty variable θ_C adopted in the calibration of partial factor γ_C in EN 1992-1-1:2023 [14] are listed in Tab. 4 (the detailed justification of these distributions are explained in the following subsections). The distribution parameters assumed in the justification of the same partial factor in EN 1992-1-1:2004 (refer to [23]) are also listed in Tab. 4 for comparison.

In the following, the considerations for the distribution parameters adopted for each basic variable are explained in detail.

Tab. 4 *Statistical values assumed to calibrate the partial factor for concrete (adopted in Table A.3 of EN 1992-1-1:2023 [14], values in brackets refer to the assumptions to justify $\gamma_C = 1.50$ in EN 1992-1-1:2004, see [23])*

	Coefficient of variation V_i	**Bias factor μ_i**
Compressive strength f_c (control specimen)	V_{fc} = 0.100 (0.150)	f_{cm}/f_{ck} = exp(1.645V_{fc})
In-situ factor $\eta_{is} = f_{c,ais} / f_c$	$V_{\eta is}$ = 0.120 (0.000)	$\mu_{\eta is} = 0.95$ (0.85)
Concrete area A_c	V_{AC} = 0.040 (0.050)	$\mu_{AC} = 1.00$ (1.00)
Model uncertainty	$V_{\theta C}$ = 0.070 (0.050)	$\mu_{\theta C}$ = 1.02 (1.00)
Coefficient of variation and bias factor of resistance for concrete	$V_{\mathrm{RS}} = \sqrt{V_{fc}^2 + V_{\eta is}^2 + V_{Ac}^2 + V_{\theta C}^2} = 0.176$ (0.166)	$\mu_{\mathrm{RC}} = \frac{f_{cm}}{f_{ck}} \cdot \mu_{\eta is} \cdot \mu_{AC} \cdot \mu_{\theta C} = 1.142$ (1.088)

1.5.1 Definition with respect to the compressive concrete strength

The partial factor for concrete γ_C applies to the characteristic concrete compressive strength which can be either specified (and controlled according to EN 12390-3:2019: Testing hardened concrete – Part 3: Compressive strength of test specimens [32]) or determined according to EN 13791 [33] on the basis of tests on core samples extracted from the executed structure. Furthermore, the control cylinder specimens can be casted at a main plant or on-site in a ready mix plant. On the other side, the partial factor γ_C is determined on the basis of reliability analysis accounting for the actual uniaxial in-situ concrete compressive strength in the structure. With this respect, it is important to clearly differentiate between the following definitions of the concrete compressive strength (refer to Fig. 7):

- $f_{c,spec}$: specified uniaxial concrete compressive strength
- $f_{c,cyl}$: concrete compressive strength of the control specimens casted at a main plant (cylinders), or on-site in a ready mix plant (no transportation)
- $f_{c,ais}$: actual uniaxial in-situ concrete compressive strength in the structure

- $f_{c,is}$: compressive strength of a core taken at a test location within a structural element or precast concrete component expressed in terms of the strength of a 2:1 core of diameter > 75 mm

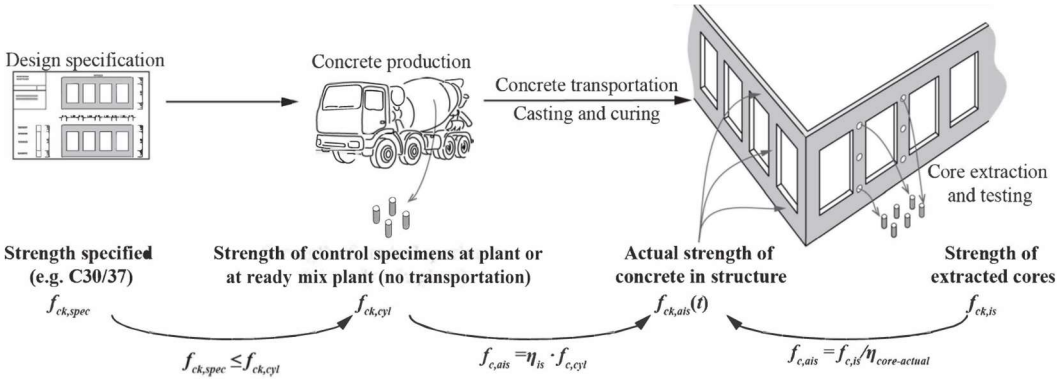

Fig. 7 *Representation of different concrete compressive strengths (figure adapted from [57])*

The difference between $f_{c,spec}$ and $f_{c,cyl}$ depends on:

- The strength margin decided by the concrete producer
- The variability of concrete components and production (at location of production)
- The seasonal variability (typically, with a lower concrete strength in summer)
- The variability of manufacture, curing and testing of control specimens

The difference between $f_{c,cyl}$ and $f_{c,ais}$ (accounting for with coefficient η_{is}) depends on:

- The effects of casting, vibration, curing and temperature
- The effect of consolidation of fresh concrete (mainly bleeding, refer to [34])
- The anisotropy (difference between horizontal and vertical concrete strength resulting from bleeding, refer to [34])
- The effect of transport and W/C (water to cement ratio) modification between mixing and casting

The difference between $f_{c,ais}$ and $f_{c,is}$ (accounted for with coefficient $\eta_{core-actual}$) depends on:

- The damage sustained during core extraction
- The potential uncorrected effect of length-diameter ratio (theoretically, the concrete strength $f_{c,is}$ should refer to cores with an aspect ratio 2:1, but the actual aspect ratio can be slightly different or the relationship for transforming the concrete strength from different aspect ratios can be inaccurate)
- The core diameter (since the cores are typically smaller than the control specimens used to measure $f_{c,cyl}$, there is a size effect [35, 36, 37, 38, 39])
- The effect of the moisture condition on the core [39, 40, 41, 42]

The distribution parameters of the variables defining the different definitions of concrete compressive strength can be determined based on the following available information:

- $f_{c,cyl}$: as a part of the quality control after production
- $f_{c,is}$: statistical evaluation of the results of core testing
- $\eta_{core-actual}$: by comparing the results of cylinder tests and cores extracted from cylinders
- η_{is} : by comparing the results of cylinder tests and cores extracted from a structural member, accounting also for $\eta_{core-actual}$

1.5.2 Statistical values of the concrete compressive strength $f_{c,cyl}$

In the past, the standard deviation of $f_{c,cyl}$ (or $f_{c,cube}$) has often been defined based on the work by Rüsch and co-workers [43], who concluded that, for different types of construction sites and quality controls, a standard deviation of about 5 MPa can be assumed for $f_{c,cube}$ > 30 MPa (see Fig. 8). Interestingly, the referred authors also observed that the standard deviation was smaller for mass production or for ready-mix (they found a reasonable fit with a constant coefficient of variation $V_{fc} = 0.136$ for mass production (at main plant) and $V_{fc} = 0.115$ for ready-mix concrete, see Fig. 8).

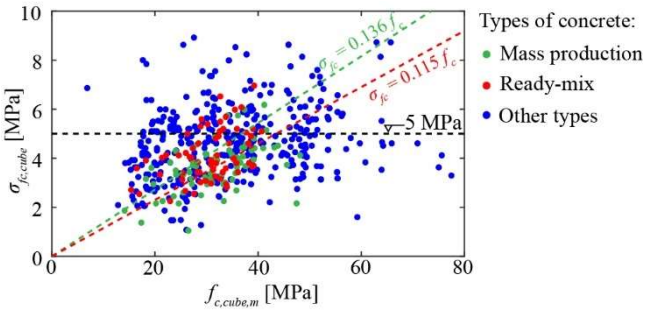

Fig. 8 *Standard deviation of the cube strength as a function of the mean value of the concrete strength according to [43] for all types of construction sites and productions (green markers for mass production red markers for ready-mix concrete and blue markers for other types, reproduced based on the data from [43]).*

Since the work by Rüsch et al. [43] (more than 50 years ago), the concrete production and the quality control have evolved significantly, so that more updated statistical data can nowadays be considered. According to Fig. 9, which shows the results by Foster et al. [30], Bartlett & MacGregor [44] and Torrenti [45], the CoV of concretes produced in the last decades is lower than the values presented by Rüsch et al. [43]. In addition, as shown by Torrenti & Dehn [46], who considered additional recent data (particularly from Germany), the CoV decreases for higher concrete strengths. To account for such effect, the mentioned authors proposed as a best fit the following relationship: $V_{fc} = 0.100 \cdot (f_c / 40)^{-2/3}$, see dashed curves in Fig. 9. Nevertheless, as it is later shown in this document, this effect has little influence on the calibration of the partial factor, so that $V_{fc} = 0.100$ for in-situ concrete and $V_{fc} = 0.060$ for precast concrete can considered without a significant loss of generality.

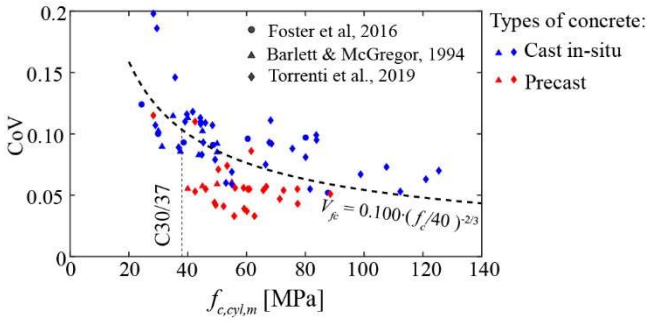

Fig. 9 *Coefficient of variation of concrete compressive strength as a function of the mean value according to (a) Foster et al. [30], Bartlett & MacGregor [44], Torrenti [45] and Torrenti & Dehn [46].*

1.5.3 Statistical values of factor η_{is} for new in-situ structures

It is well-known since more than a century that the concrete compressive strength in an actual structure differs from the concrete strength measured on control specimens (cubes and cylinders). It is further known that the concrete compressive strength can even vary within a structural member resulting from casting (for a comprehensive literature review since 1915, see Moccia et al. [34]). This phenomenon has been confirmed by numerous researchers who have compared the strength of control specimens ($f_{c,cyl}$ or $f_{c,cube}$) to the strength of cores with the same aspect ratio (2:1 for cylinders and 1:1 for cubes) extracted from the actual structure. Since one of the most relevant effects on the actual in-situ concrete strength attributes to the phenomena occurring during the first minutes/hours after casting (mainly the bleeding process, where the water in excess in fresh concrete migrates upwards due to the settlement of solid particles which leads to an accumulation of water on the upper layer of concrete and particularly under the coarse aggregates [34]), the distribution of η_{is} mainly depends on:

- The location where the cores are extracted (typically $\eta_{is} < 1.0$ in the upper layer and $\eta_{is} > 1.0$ in the bottom layer, see Fig. 10), and
- The direction of the core extraction (typically, the horizontal concrete strength in the upper layers is more affected by the bleeding phenomenon than vertically extracted cores [47]).

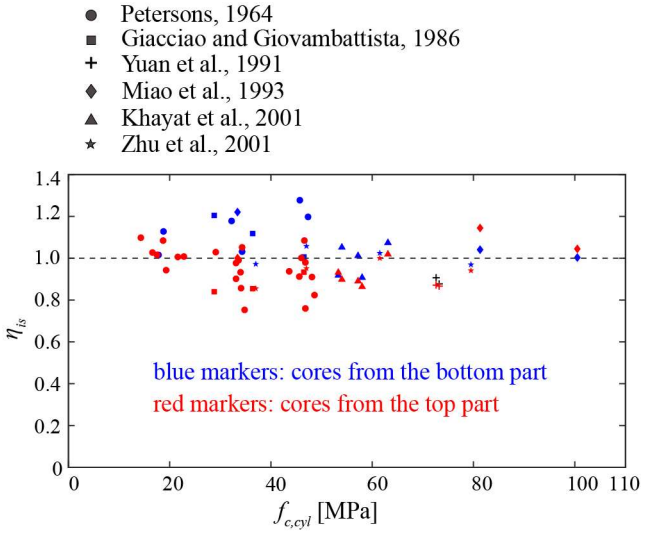

Fig. 10 *Ratio η_{is} between the concrete strength in the structure $f_{c,ais}$ and the cylinder strength $f_{c,cyl}$, red and blue markers refer to the top and bottom part of the member, respectively (has been calculated as $\eta_{is} = f_{c,ais} / f_{c,cyl} = (f_{c,is} / \eta_{core-actual}) / f_{c,cyl}$) assuming $\eta_{core-actual} = 0.95$, figure adapted from Moccia et al. [34].*

In addition to the comparison between extracted cores and control specimens, also compression tests on larger specimens extracted from an actual structural member confirm this effect (see Fig. 11). As shown by Moccia et al. [34], this effect can be accentuated by the presence of transverse reinforcement (due to the development of voids under such reinforcement), although it can also be mitigated in case confinement reinforcement is provided.

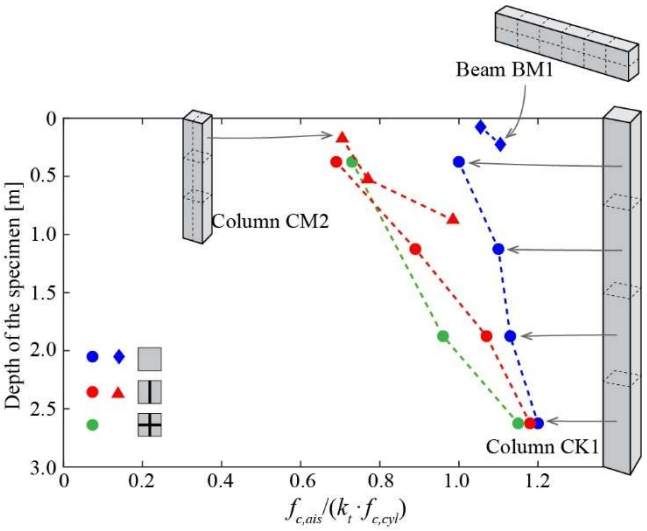

Fig. 11 *Ratio between the average compressive strength measured on specimens cut out from Column CK1, CM2 and Beam BM1 ($f_{c,ais}$) and the cylinder strength $f_{c,cyl}$ (adjusted with factor k_t accounting for the effect of the speed of loading, refer to [34]): specimens extracted from a 3m high column (CK1), a 1.05m column (CM2) and a beam (BM1) under in-situ conditions (the blue curve and the blue dot refer to unreinforced members, the red and the green curve refer to members with transverse reinforcement not acting as confinement), adapted from Moccia et al. [34].*

For determining the statistical values of coefficient η_{is} to be used for the calibration of the partial factor γ_C, the following approaches can be adopted:

1. By statistical evaluation of tests available in literature;
2. By ensuring full consistency with the standard for the assessment of in-situ compressive strength in structures;
3. By referring to the assumptions for calibrating other structures.

Regarding the first approach, the statistical data of the values plotted in Fig. 10 can be used:

- Top layer (upper 20% of the height, red markers in the figure): 40 values, $\mu_{\eta is} = 0.95$, $V_{\eta is} = 0.095$
- Bottom layer (bottom 20% of the height, blue markers in the figure): 23 values, $\mu_{\eta is} = 1.05$, $V_{\eta is} = 0.105$

If one assumes that the measurements from the top and the bottom layers are equally represented, then the statistical values become: $\mu_{\eta is} = 1.00$, $V_{\eta is} = 0.11$.

It has to be noted that these values refer mostly to results of laboratory tests where compaction and curing have been most likely conducted in a more accurate manner than in practice. Therefore, for practical cases (at least for in-situ structures), one can expect the statistical values to be less favourable (especially the coefficient of variation). On the other hand, the observed variability can partially be related to the difference between the actual in-situ strength $f_{c,ais}$ and the core strength $f_{c,is}$ (variability of coefficient $\eta_{core-actual}$, see Fig. 7). With this respect, the results of a comprehensive experimental programme by Haavisto et al. [39] show that for cores ≥ 80 mm (height and diameter), the CoV of the strength of cores extracted from cylinders produced from the same batch is slightly higher than the CoV of the cylinder strength (5.3% instead of 3.7%) and the CoV of factor $\eta_{core-actual}$, (in this case, $f_{c,ais} = f_{c,cyl}$) is 5.4% (a similar value of $V_{\eta core-actual}$ is given by Bartlett et al. [44]: between 4% and 5.5% for cores Ø100-150 mm). By combining these data with the CoV of 0.11 reported above, the CoV of η_{is} becomes $(0.11^2-0.054^2-0.053^2+0.037^2)^{1/2}$ = 0.088.

A detailed investigation based on the interpretation of 1080 cores extracted from members cast using 108 mixes is presented by Bartlett & MacGregor [48, 49, 50]. The statistical values of η_{is} based on cores extracted from mid-height of the member (or averaged between top and bottom parts) are:

- $\mu_{\eta is} = 0.948$ for members with h < 450 mm,
- $\mu_{\eta is} = 1.032$ for members with h ≥ 450 mm,
- $V_{\eta is} = 0.139$ for all members.

In what refers to the variability within the member (mostly related to the location over its height), Bartlett & MacGregor [50] proposed to consider it with an additional variable with a CoV of: $V_{\eta is-location} = 0.063$ for laboratory cast columns, 0.069 for laboratory cast shallow members and 0.099 for the case of an in-situ bridge. A more recent evaluation of these statistical data performed by Bartlett [51], and conducted for the calibration of the Canadian Standard A23.3-4, led to the following conclusions: a value of $V_{\eta is} = 0.113$ should be adopted for cast-in-place members, whereas the additional coefficient of variation to account for the geometrical variability $V_{\eta is-location}$ given by Bartlett [51] is confirmed.

With respect to the second approach (consistency with the standard for the assessment of in-situ compressive strength in structures), EN 13791:2018 (section 9) [33] and Annex I of EN 1992-1-1:2023 contain the following relationship:

$$f_{ck} = \frac{f_{ck,is}}{0.85} \tag{20}$$

Which can be justified as follows:

$$f_{c,is} = \eta_{is} \cdot \eta_{core-actual} \cdot f_{c,cyl} \tag{21}$$

Assuming lognormal distributions and independency between all random variables, the CoV, the mean and the characteristic values of $f_{c,is}$ become:

$$f_{cm,is} = \mu_{\eta is} \cdot \mu_{\eta core-actual} \cdot f_{cm,cyl} \tag{22}$$

$$V_{fc,is} = \sqrt{V_{\eta is}^2 + V_{\eta core-actual}^2 + V_{fc,cyl}^2} \tag{23}$$

$$f_{ck,is} = f_{cm,is} \cdot \exp(-1.645 \cdot V_{fc,is}) \tag{24}$$

and since :

$$f_{ck} = f_{cm,cyl} \cdot \exp(-1.645 \cdot V_{fc,cyl}) \tag{25}$$

the relationship between f_{ck} and $f_{ck,is}$ can be expressed as:

$$f_{ck} = f_{ck,is} \cdot \frac{\exp(1.645(\sqrt{V_{\eta is}^2 + V_{\eta core-actual}^2 + V_{fc,cyl}^2} - V_{fc,cyl}))}{\mu_{\eta is} \cdot \mu_{\eta core-actual}} \tag{26}$$

Considering the assumed distribution parameters for the basic variables listed in Tab. 5, Eq. 26 becomes $f_{ck} = f_{ck,is} / 0.86$, which is approximately equivalent to Eq. 20.

Tab. 5 *Distribution parameters for basic variables related to $f_{ck,is}$*

	Coefficient of variation V_i	**Bias factor μ_i**
f_c	0.100	$f_{cm}/f_{ck} = \exp(1.645 V_{fc})$
η_{is}	0.120 (assumed)	1.00 (For cores extracted from all regions)
$\eta_{core-actual}$	0.05 (assumed according to [39] and Bartlett & MacGregor [44])	0.95 (1/1.06 according to [52])

It should be noted that in the derivation of the relationship between f_{ck} and $f_{ck,is}$ in Eq. 20 (Annex I of EN 1992-1-1:2023 [14]), the bias factor of η_{is} is taken as 1.00 assuming that cores are extracted from all regions in the structure (see Tab. 5). This is a conservative assumption since Eq. 20 is usually used to estimate the characteristic cylinder strength f_{ck} based on the value of $f_{ck,is}$ (characteristic strength of cores extracted from existing structures).

With respect to the calibration of other standards, the following distribution parameters have been assumed:

- Calibration of in EN 1992-1-1:2004: according to [23], the value $\gamma_C = 1.50$ accounts for a coefficient $\eta_{is} = 0.85$ without an explicit mention about its variability. According to König et al. [53], this value (already considered in the justification of in ENV 1992-1-1:1991 [54]) has been intended as a characteristic value;
- Canadian Standard A23.3-04 [11]: according to Bartlett [51], the resistance factor for concrete in compression has been calibrated on the basis of following values: $\mu_{\eta is} = 1.03$, $V_{\eta is} = 0.113$ (these values referring to the average strength in the member). To account for the in-situ strength variability within the member as well as the number of batches used to case the member, an additional factor is considered (whose mean value is 1.00 with an CoV equal to 0.13 for cast in-place structures, see also [52]);
- Australian Standards AS3600:2018: according to [55] and [30], the calibration of the resistance factor for concrete in compression in the latest Australian Standard is based on following assumptions: $\mu_{\eta is} = 0.88$, $V_{\eta is} = 0.12$ (these values being based on a previous work [56]). The work by Bartlett & MacGregor [49] is also mentioned as a confirmation of the assumed value of $V_{\eta is}$.

Based on these considerations, the following distribution parameters for η_{is} can be adopted:

- Mean value: $\mu_{\eta is} = 0.95$
- Coefficient of Variation: $V_{\eta is} = 0.12$

With respect to the mean value, it accounts for the unfavourable case where the internal force has been transferred across the weakest part of the member as in columns (Fig. 12a), walls not sensitive to buckling (as for instance walls for the introduction of concentrated

loads, see Fig. 12(b)), members with sagging moments (Fig. 12(c)) or compression fields in large members subjected to shear forces as shown in Fig. 12(d) and (e).

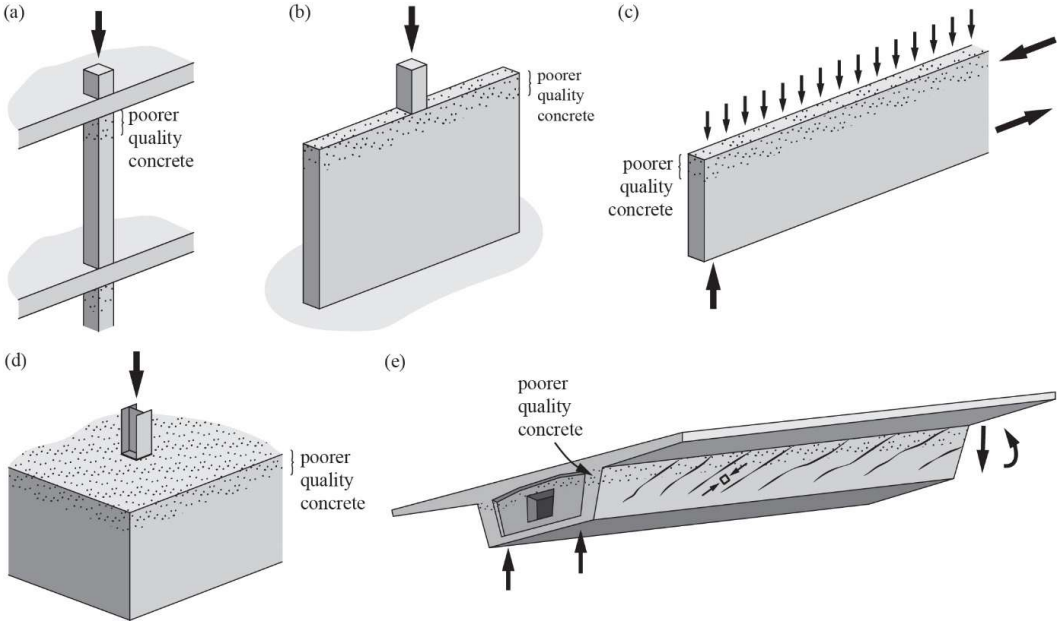

Fig. 12 *Examples of structural members where the region with poor concrete quality can be governing (Figure adapted from [57]).*

It should be noted that the above-mentioned effects shall be also considered in the derivation of the distribution parameters of the model uncertainties. This is accounted for by deducing the effect of the variability of η_{is} (reasonable values reproducing the conditions in test specimens) from the distribution parameters of the model uncertainties assumed based on the statistics of test data (as proposed by Ellingwood et al. [27]).

1.5.4 Statistical value of the geometrical uncertainties for calibrating γ_c

As mentioned above, columns can be considered as typical members where the partial factor γ_C plays a major role. For the dimensions of the cross sections of these members, a standard deviation of 6 mm can be assumed according to Ellingwood et al. [27]. Since this value refers to common dimensions, it should be corrected accordingly to a similar law as prescribed for the construction tolerances. As shown in Fig. 13, the evolution of the tolerances according to EN 13670:2009 [29] can be reasonably described by a power law with an exponent of 1/3 in the region of interest, so that following standard deviation of the column width *b* can be adopted:

$$\sigma_b = 6 \cdot (b / 300)^{1/3} \quad [b \text{ in mm}] \tag{27}$$

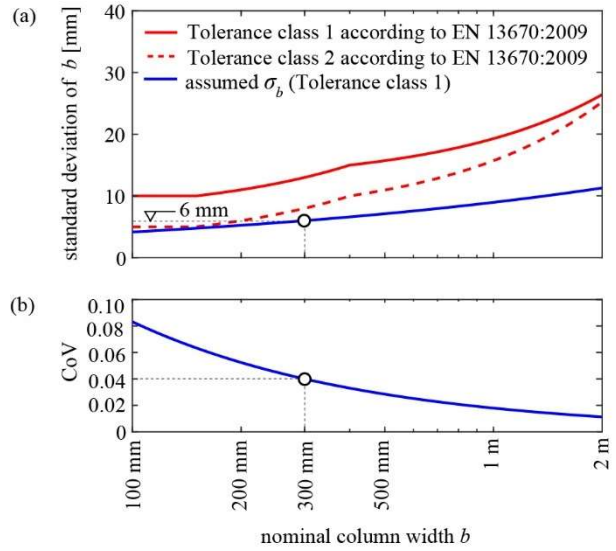

***Fig. 13** Comparison of the evolution of the assumed standard deviation of the column width (Eq. 27) with the tolerance according to EN 13670:2009 (a) and (b) resulting CoV of the column area (Eq. 28).*

Assuming that for a square column with dimension $b \times b$, both dimensions are fully correlated (a conservative assumption), the CoV of the concrete area becomes:

$$V_{Ac} = 2 \cdot V_b = 0.04 \cdot (300 / b)^{2/3} \qquad [b \text{ in mm}] \tag{28}$$

As shown in Fig, 13, the CoV of the column area varies between 0.01 and 0.05 for columns with standard dimensions. It should be noted that the factor 2 in Eq. 28 is replaced by $\sqrt{2}$ in case the two dimensions of the cross section are statistically independent. Nonetheless, as the geometrical uncertainty associated to the cross-section area of the column is not dominant compared to material and model uncertainties, a constant value $V_{Ac} = 0.04$ can be assumed (the influence of this choice will be discussed later).

1.5.5 Statistical values of the model uncertainty for calibrating γ_c

The comparison between the experimental results of short column members (without second order effects) and calculated values according to the provisions of Section 8.1 of EN 1992-1-1:2023 [14] has been conducted in [58] for the cases without and with load eccentricity. For cylinder strengths not higher than 100 MPa, the mean values of the ratio $N_{R,\exp} / N_{R,calc}$ is 1.02 and its coefficient of variation is 0.087. Since the latter is affected by the uncertainties in the reported data (typically nominal dimensions of the test specimens, variability of the strength of the control specimens $f_{c,cyl}$ and η_{is}), the actual coefficient of variation of the model uncertainty can be reduced according to Eq. 14. With $V_{test} = 0.02$ (variability of load measurements in tests), $V_{Ac} = 0.02$ (variability of cross-section area in tests), $V_{fc} = 0.03$ (variability of concrete cylinder strength in tests) and $V_{\eta is} = 0.03$, the CoV of the model uncertainty $V_{\theta C}$ is reduced from 0.087 to 0.070.

1.5.6 Calibration of γ_c

The coefficient of variation and the bias factor of the resistance can be calculated on the basis of the uncertainties defined above using:

$$V_{RC} = \sqrt{V_{fc}^2 + V_{\eta is}^2 + V_{Ac}^2 + V_{\theta C}^2} = \sqrt{0.100^2 + 0.120^2 + 0.040^2 + 0.070^2} = 0.176 \tag{29}$$

$$\mu_{RC} = (f_{cm} / f_{ck}) \cdot \mu_{\eta is} \cdot \mu_{Ac} \cdot \mu_{\theta C} = \exp(1.645 \cdot 0.100) \cdot 0.95 \cdot 1.00 \cdot 1.02 = 1.142 \tag{30}$$

By using Eqs. 8- 10, adopting $\alpha_R = 0.8$, $\beta_{tgt} = 3.8$ and on the basis of the above-mentioned distribution parameters, the partial factor γ_C becomes:

$$\gamma_C = \frac{\exp\left(\alpha_R \cdot \beta_{tgt} \cdot V_{RC}\right)}{\mu_{RC}} = \frac{\exp\left(0.8 \cdot 3.8 \cdot 0.176\right)}{1.142} = 1.49 \cong 1.50 \tag{31}$$

which confirms current practice.

It has to be noted the CoV of the concrete compressive strength measured on control specimens V_{fc} intervenes both in the numerator and in the denominator of Eq. 31, so that it has a limited influence on the resulting partial factor γ_C (see Fig. 14a). This is the reason why neglecting the influence of the variation of CoV as a function of the concrete compressive strength on the CoV of the reference resistance model V_{RC} is seen as an acceptable approximation. With respect to the CoV of the variation of the geometrical uncertainty V_{Ac} , also in this case, neglecting the influence of the cross-section area remains as a reasonable approximation (see Fig. 14b).

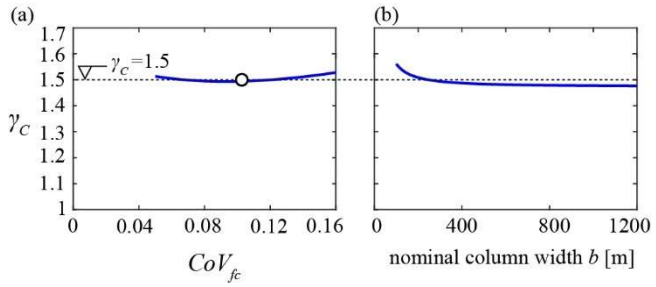

Fig. 14 *Influences on the resulting partial factor γ_C of (a) the CoV of the compressive strength (of control specimens, see also Fig. 9) and (b) of the size of the cross section (see also Fig. 13).*

In case the concrete strength is assessed according to Section 8 of EN 13791 [33], the uncertainties of $f_{c,cyl}$ and η_{is} are merged in the derived distribution parameters based on the statistics of the core strength ($V_{fc,is,corr}$ and $\mu_{fc,is}$). For this reason, the terms $V_{fc,is,corr}$ and $\mu_{fc,is}$ replace the terms $(V_{fc}^2 + V_{\eta is}^2)^{0.5}$ and $(f_{cm} / f_{ck}) \cdot \mu_{\eta is}$ in Eq. 29 and 30) based on the assumption of a Student t distribution.

It should be noted that the applicability of the partial factors γ_C and γ_S to other structural resistance models depends on the shape of the resistance model (in terms of the sensitivity to material and geometrical variables) and on the corresponding model uncertainty. A discussion regarding the applicable condition of γ_C and γ_S to other resistance models is provided in Appendix I of this work.

1.6 Partial factor for shear and punching shear without shear reinforcement

The calibration of the partial factor for the punching shear resistance model is presented in the following in a similar manner as presented by [20]. A similar work by [21] for the shear formulae has shown similar results, so that the same partial factor γ_V can be used for both cases. This is an expected and acceptable approach considering that the formulae for shear and for punching shear share the same theoretical background and show evident similarities [22].

For the simple case of internal medium-size square columns supporting not too slender slabs, the design value of the punching shear resistance formula (refer to Formulae 8.94, 8.92 and 8.97 of EN 1992-1-1:2023 [14]) can be reformulated as:

$$V_{Rd,c} = \frac{25.1}{\gamma_V}\sqrt{b_{0.5}} \cdot d_V \cdot A_s^{1/3} \cdot f_{ck}^{1/3} \cdot s^{-1/3} \cdot d_{dg}^{1/3} \cdot a_p^{-1/6} \cdot \beta_e^{-1} \tag{32}$$

where $b_{0.5}$ is the control perimeter, d_V is the shear-resisting effective depth, s is the spacing of the hogging flexural reinforcement, d_{dg} is a size parameter describing the failure zone roughness (depending on the concrete type and its aggregate properties), a_p is the maximum distances from the centroid of the control perimeter to the point where the bending moment in the slab is zero and β_e is a coefficient accounting for the concentrations of the shear forces along the control section. For medium-sized columns ($b \approx 1.5 d_v$), the square root of the control perimeter $b_{0.5}$ can be approximated as:

$$\sqrt{b_{0.5}} = \sqrt{4b + \pi d_v} \cong 2.64 \cdot b^{1/3} \cdot d_v^{1/6} \tag{33}$$

where b is the column width, so that Eq. 32 becomes:

$$V_{Rd,c} = \frac{66.3}{\gamma_V} d_V^{7/6} \cdot b^{1/3} \cdot A_s^{1/3} \cdot f_{ck}^{1/3} \cdot s^{-1/3} \cdot d_{dg}^{1/3} \cdot a_p^{-1/6} \cdot \beta_e^{-1} \tag{34}$$

For the most sensitive variables appearing in Eq. 32, namely d_V and f_{ck} (where the sensitivity depends on the exponent in Eq.32 and on their variabilities represented by their corresponding CoVs), the same coefficients of variation V_i and bias factors μ_i adopted for calibrating γ_S and γ_C can be used for calibrating γ_V. For the other variables, the following assumptions can be made:

- Column width b : as defined in Eq. 27, namely $V = 0.02$ for $b = 300$ mm and $\mu = 1.00$
- Reinforcement area A_s : $V = 0.02$ and $\mu = 0.97$ (according to [59])
- Bar spacing s: $V = 0.05$ and $\mu = 1.00$ (it is assumed that the governing reinforcement is distributed over a width of 2.0 m with a standard deviation of 100 mm)
- Size parameter d_{dg} describing the crack roughness on the basis of $D_{\max}$: $V = 0.10$ and $\mu = 1.00$
- Distance a_p: $V = 0.15$ and $\mu = 1.00$ (this variability is related to the errors in calculating the position of point of contraflexure, namely stiffness assumptions, calculation methods, etc., the proposed values are based on author's experience)
- Coefficient β_e : considered in this calibration as deterministic, considering that its variability has already been considered in the provisions defining it.

The variabilities of the these less sensitive variables are lumped in a random variable defined as "Residual uncertainties", with the following distribution parameters:

$$V_{res,V} = \sqrt{\left(\frac{0.02}{3}\right)^2 + \left(\frac{0.02}{3}\right)^2 + \left(\frac{0.05}{3}\right)^2 + \left(\frac{0.10}{3}\right)^2 + \left(\frac{0.15}{6}\right)^2} = 0.046 \tag{35}$$

$$\mu_{res,V} = 1.00^{1/3} \cdot 0.97^{1/3} \cdot 1.00^{1/3} \cdot 1.00^{1/3} \cdot 1.00^{1/6} \cong 1.00 \quad (36)$$

1.6.1 Statistics of the model uncertainty for calibrating γ_V

The comparison between test experiments on isolated slab specimens and the calculated resistance according to subsection 8.4 of EN 1992-1-1:2023 (using mean values provided in test reports) gives a bias factor between 1.07 and 1.09 and a coefficient of variation between 0.11 and 0.13 [60]. Also in this case, the coefficient of variation $V_{\theta\tau}$ of the ratio $V_{R,\exp} / V_{R,calc}$ contains the uncertainties related to the reported data in the test reports and can be corrected adopting Eq. 14 (suitably adapted accounting for the different exponents in Eq. 34). With this respect, the following distribution parameters can be considered:

- Measurement and definition of the failure load: $V = 0.03$ and $\mu = 1.00$
- Shear resisting effective depth d_v: $V = 0.01$ and $\mu = 1.00$ (in most of recent tests, the effective depth has been measured on saw-cuts after testing)
- Concrete cylinder strength $f_{c,cyl}$: $V = 0.03$ and $\mu = 1.00$ (CoV according to EN 12390-1: 2001, Table 1)
- In-situ factor η_{is}: $V = 0.05$ and $\mu = 1.00$
- Column width b: $V = 0.01$ and $\mu = 1.00$
- Reinforcement area A_s: $V = 0.02$ and $\mu = 0.97$ (almost all test reports provide nominal values only)
- Bar spacing s: $V = 0.00$ and $\mu = 1.00$ (the number of bars in the width of the control specimens can be considered as deterministic)
- Size parameter d_{dg} describing the crack roughness on the basis of $D_{\max}$: $V = 0.10$ and $\mu = 1.00$ (almost all test reports provide specified values)
- Distance a_p: $V = 0.05$ and $\mu = 1.00$ (the variability depends on the position of the load introduction, the distance between the slab edge and load introduction and accounts also the act that some of the tests are not perfectly axisymmetric)
- Coefficient β_e: $V = 0.015$ and $\mu = 1.015$ (this is due to the fact that punching tests are never perfectly centric; for the eccentricity, the vectorial average is null, but the scalar average is larger than 0). For the test eccentricity, it is assumed $\mu_e = 5$ mm and $\sigma_e = 5$ mm; β_e is calculated according to Table 8.3 of EN 1992-1-1:2023 for a typical test specimen with b_b =400 mm

With these distribution parameters, the CoV of the model uncertainty is reduced from 0.12 to 0.107 and the bias factor increased from 1.07 to 1.10.

1.6.2 Calibration of γ_V using the nominal value of the effective depth

For the sake of simplicity, the exponent of the effective depth in Eq. 34 is assumed to be equal to 1.0. With this simplification, the CoV and the bias factor of the resistance function can be calculated accounting for the exponents in Eq. 34 as :

$$V_{RV} = \sqrt{\left(\frac{V_{fc}}{3}\right)^2 + \left(\frac{V_{\eta is}}{3}\right)^2 + V_d^2 + V_{\theta V}^2 + V_{resV}^2}$$
$$= \sqrt{\left(\frac{0.100}{3}\right)^2 + \left(\frac{0.120}{3}\right)^2 + (0.050)^2 + (0.107)^2 + (0.046)^2} = 0.137 \quad (37)$$

$$\mu_{RV} = \left(\frac{f_{cm}}{f_{ck}} \cdot \mu_{\eta is}\right)^{1/3} \cdot \mu_d \cdot \mu_{\theta V} \cdot \mu_{resV} = \left(\exp(1.645 \cdot 0.100)\right)^{1/3} \cdot 0.95^{1/3} \cdot 0.95 \cdot 1.10 \cdot 1.00 = 1.085 \quad (38)$$

Adopting $\alpha_R = 0.8$ and $\beta_{tgt} = 3.8$, the partial factor becomes:

$$\gamma_V = \frac{\exp(0.8 \cdot 3.8 \cdot V_{RV})}{\mu_{RV}} = \frac{\exp(0.8 \cdot 3.8 \cdot 0.137)}{1.085} = 1.40 \quad (39)$$

This result is similar to the value obtained for γ_C, but it has to be noted that the two partial factors have a significant different origin. In the case of γ_C, the dominant uncertainties are related to the material strength variables (factor η_{is} and $f_{c,cyl}$), whereas in the case of γ_V, the dominating uncertainty is related to the resistance model since the concrete strength appears in the resistance function with an exponent of 1/3. As shown in Fig. 15, where the contributions to the CoV of the resistance model as a function of the effective depth are depicted, also the effect of the geometrical uncertainty can become significant for thin slabs (the value of $V_{RV} = 0.137$ given above is valid for $d_v = 200$ mm). These findings are important, since in the adjustment of the partial factors in the case of the assessment of existing structures, the assessment of the concrete strength can have a significant influence on γ_C, whereas its influence on γ_V is significantly smaller.

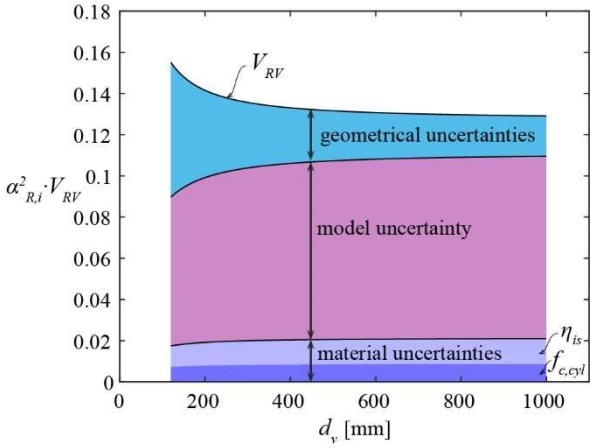

Fig. 15 *Contribution of different basic uncertainties to the coefficient of variation of the resistance function according to Eq. 37 as a function of the effective depth ($\alpha_{R,i}$ represents the FORM sensitivity factor for each basic uncertainty, calculated as $\alpha_{R,i} = n_i \cdot V_i / V_{RV}$).*

1.6.3 Calibration of γ_V using the design value of the effective depth

The fact that the variability of the effective depth can become significant for thin members (in a similar manner as observed in the calibration of γ_S) leads to a slightly insufficient value of the reliability index β for those cases if a constant value of the partial factor $\gamma_V = 1.40$ is adopted (see the blue curves in Fig. 16a-b for $d_V < 200$ mm). On the other hand, $\gamma_V = 1.40$ is overly conservative for thick members. To avoid these shortcomings, the verification of the shear and punching resistances of members without shear reinforcement may be conducted using design values of the shear resisting effective depth. As shown in Fig. 16b (refer to red curves), an almost constant safety level is obtained using $\gamma_V = 1.29$ and $d_d = d_{nom} - 15$ mm. This possibility has been adopted in EN 1992-1-1:2023.

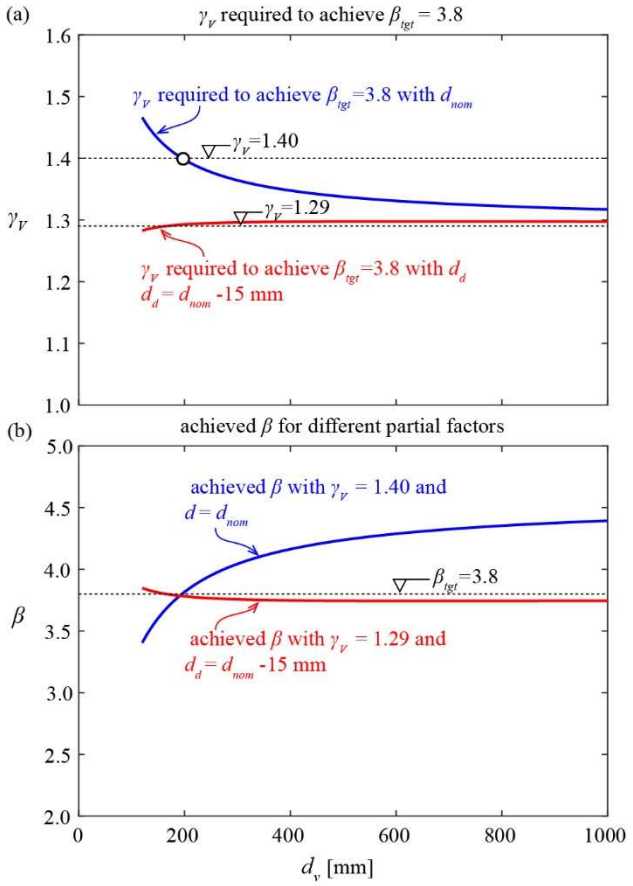

Fig. 16 *Required partial factors γ_V to achieved the target reliability index $\beta_{tgt} = 3.8$ (a) and (b) obtained reliability indexes with the assumed partial factors γ_V (blue curves refer to the approach using nominal values of the effective depth whereas red curves refer to the case using design values of the effective depth).*

1.7 Conclusions

This work presents a new calibration of the partial factors for the design of reinforced concrete structures by applying the methodology proposed by the European standard for Structural Design EN 1990:2023 [7] together with the most relevant data associated to the different sources of uncertainties available in the literature. In addition, an explicit description of the methodology and the assumed statistical values of all uncertainties allow the adjustment of the partial safety factors in case more precise values for a given situation are available. This is typically the case for the assessment of existing structures, when geometrical and material values are assessed on site, or when more refined verification methods are used (as for instance Non-Linear Finite Elements Analysis Methods). This procedure as well the statistical values described in this section have been adopted by the 2nd generation of Eurocode 2. Such calibration is performed in a transparent and simple, yet rigorous, manner on the basis of the content included in Annex A of the 2nd generation of Eurocode 2 (EN 1992-1-1:2023 [14]). The most relevant findings presented in this section are summarized in the following:

- The application of the exponent sensitivity analysis approach to five of the most common resistance models for RC structures (axial tension, axial compression, bending, shear with shear reinforcement, punching shear of slabs without shear reinforcement) enables showing that the exponents associated to the different geometrical and material parameters vary from one case to the other, which indicates that the governing uncertainties can also vary correspondingly. The results of such analyses show that while a material factor approach (γ_S and γ_C) can be applied to a wide range of typical resistance models (axial tension and compression, bending, shear in the presence of sufficient shear reinforcement; where the material and the geometrical uncertainties are governing), a resistance factor approach (γ_V) is more appropriate for other specific resistance models (shear without shear reinforcement and punching shear; where the geometrical and the resistance model uncertainties govern).
- The model for the bending resistance of suitably reinforced concrete sections is used as reference for the calibration of the partial factor for the yield strength of steel reinforcement. For the calibration of the partial factor for the concrete compressive strength, the model for the resistance of columns against axial compressive force is used. Both resistance models are commonly used in practice and represent cases where the material strengths variables have a significant influence (with an exponent close to 1) together with the model uncertainties.
- For the steel yield strength, the calibrated value of the partial factor is equal to γ_S=1.15 confirming current practice if the geometrical uncertainties are to be covered by the material partial factors. This approach can lead to unsafe designs for slabs with an effective depth smaller than 200 mm. It is shown that a constant safety level and a more economic design could be obtained if design values of the effective depth are adopted together with a reduced partial factor γ_S. Such approach has been adopted as an alternative in the 2nd generation of Eurocode 2.
- For the concrete compressive strength, the calibrated value of the partial factor is equal to γ_C=1.50, confirming again current practice. This section demonstrates how the different sources of uncertainties related to the production, transportation, casting and testing of concrete are considered in the calibration of its associated partial factor.
- With respect to the resistance partial factor γ_V for punching shear and shear resistance of members without shear reinforcement, its calibration is shown for the former resistance model, yielding a value of γ_V=1.40 (if geometrical uncertainties are to be covered by this factor also). A similar value could also be obtained by using the shear resistance model of members without shear reinforcement. Like the case of the material factor γ_S, it is also observed that a constant value of γ_V=1.40 can lead to unsafe design of slabs with a shear resisting effective depth smaller than 200 mm. Eventually, it is shown that more constant safety level and more economic designs can be achieved if design values of the shear resisting effective depth are combined with a lower value of the partial factor γ_V. Such approach is also proposed as alternative in the 2nd generation of Eurocode 2.

2 Model uncertainties in action effects and load bearing capacity calculation in statically indeterminate reinforced concrete structures

2.1 Introduction

The design process of reinforced concrete structures typically consists of three main steps. First, the structure is conceived considering the constrains and requirements. Experience and empirical rules (e.g., span/depth ratios) govern this phase, which results in the definition of the structural members geometry. Second, the relevant load cases are identified and the action effects are calculated by means of idealised models. Finally, with the geometry and the action effects for each section, the reinforcement is designed and dimensioned so that the sectional resistance is larger than the action effects. If the initial geometry of the structure is not suitable, the process can be repeated.

Typically, to calculate actions effects in statically indeterminate structures, engineers assume a linear-elastic uncracked mechanical behaviour of the structure, neglecting the influence of the reinforcement on the stiffness. The main advantages of these assumption are that the stiffness of the members does not depend on the load level and consequently no iteration is required. Thus, the process is direct and the results are easily obtainable, making these assumptions suitable for practical applications. However, for statically indeterminate systems (Fig. 17a and 17b), a linear-elastic uncracked behaviour does not provide a completely realistic prediction of the action effects. In fact, because cracking is neglected, so is the ensuing redistribution of internal forces.

In spite of that, the sectional resistance is generally calculated considering cracking of concrete and non-linear behaviour of materials, assuming that each section or member can reach its design resistance. This assumption is not consistent with the assumptions for the calculation of the stiffness, however, it is certainly true if all sections have a sufficient deformation capacity. However, a premature failure of the system can occur if this is not the case. To illustrate this scenario, Fig. 17c shows the evolution of the bending moment (in absolute value) in the sagging and hogging section of a continuous beam under a distributed load q (see Fig. 17a [61]). Several regimes can be observed: (1) uncracked behaviour; (2) cracking in the hogging region, with the hogging moment increasing less than the sagging moment; (3) cracking of the sagging region, with the hogging moment increasing again more rapidly and (4) plastic regime with reinforcement's yielding in the hogging region. In the presented case, after some plastification of the reinforcement in the hogging region, due to insufficient deformation capacity (failure of the compression zone or of the reinforcement in tension), the sagging section is unable to reach its design resistance, leading to failure of the system for a load $q^* < q_d$, which is the theoretical failure load predicted assuming an elastic uncracked mechanical behaviour. Compared to the predicted linear elastic behaviour (dashed lines in Fig. 17c), not only the actual load-bearing capacity can be underestimated ($q^* < q_d$), but also in terms of actual internal forces, deviations can be expected (differences between continuous lines and dashed lines). These deviations are one of the components contributing to the uncertainty in calculating action effects.

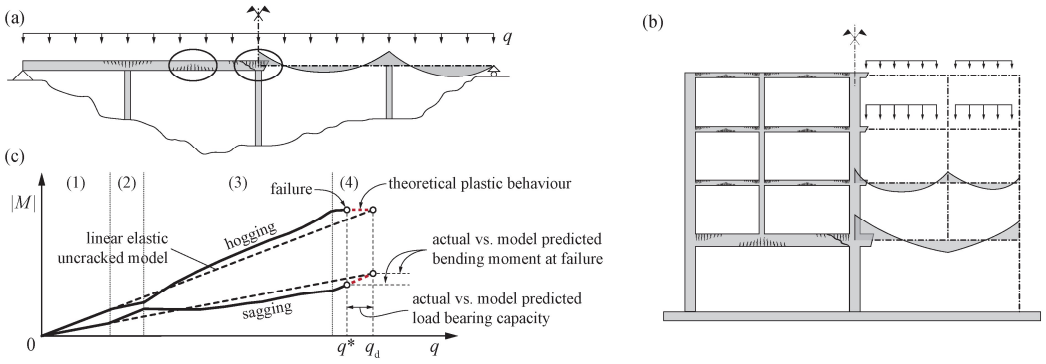

Fig. 17 *Redistribution of forces: (a) continuous beam, (b) frame system; (c) bending moment redistribution between the hogging and the sagging section of a continuous beam with regimes (1)-(4) (see explanation in the text) and premature failure of the hogging section.*

To ensure structural safety, most current codes of practice adopt a semi-probabilistic design approach. Accordingly, limit state verifications are performed by means of design values and adequately calibrated Partial Safety Factors (PSFs), which cover uncertainties related to geometry, materials, actions effects and models, as shown in Fig. 18. Regarding the uncertainty in model assumptions (idealization of the actual structure), previous research was mainly focused in investigating the model uncertainty related to the sectional resistance, while little effort was put in investigating the uncertainty in action effects. Depending on the type of action, for the ratio of the actual internal force to the calculated value, the JCSS Probabilistic Model Code [28] recommends a log-normal distribution with mean equal to 1.0 and CoV between 0.05 and 0.2. However, the origin of this recommendation is not clear. As stated in the JCSS Probabilistic Model Code (part 3, section 3.9.3), to obtain those values "… *a more or less standard structural Finite Element Model has been kept in mind"* without specifying the adopted mechanical behaviour. The authors assume that the recommended values are based on a linear elastic uncracked mechanical behaviour.

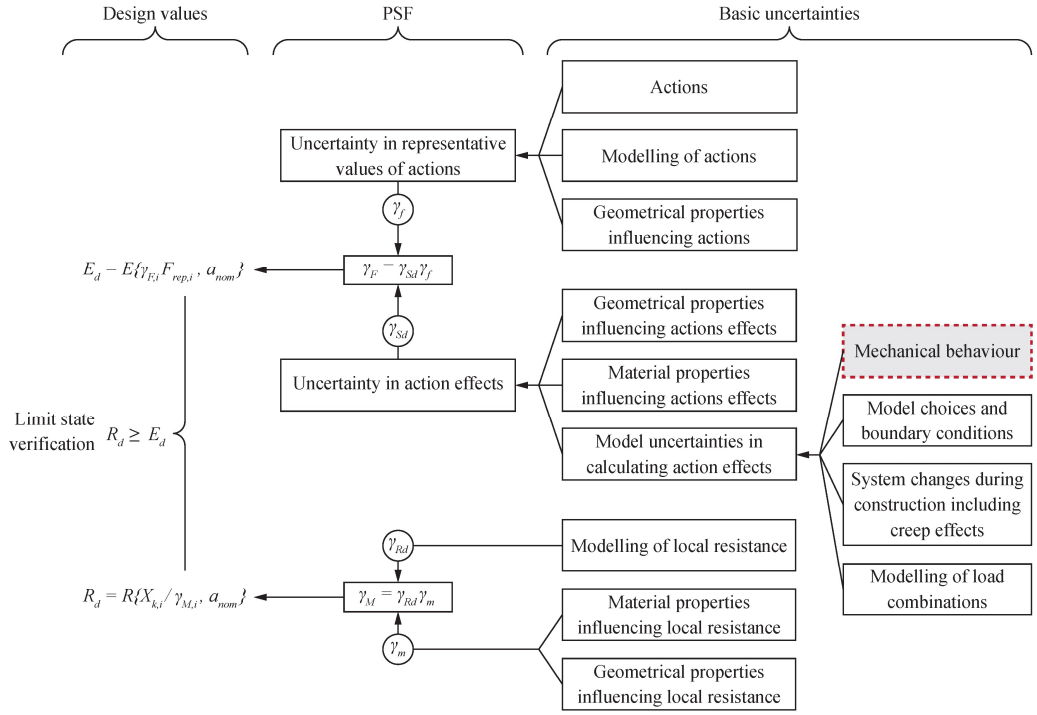

Fig. 18 *Basic uncertainties and corresponding partial safety factors (PSFs), figure adapted from [2] and [65], notation consistent with [7].*

Regarding codes of practice, in EN 1990:2002 [2], the model uncertainty in action effects is implicitly covered by the partial factors for permanent and variable actions (γ_G and γ_Q). However, for particular verifications, the designer is allowed to decouple the model uncertainty in action effects, γ_{Sd}, from the uncertainty in the representative values of actions, γ_g and γ_q. In those cases, the recommended value for γ_{Sd} is between 1.05 and 1.15, consistent with the prescriptions of the first codes dealing with the topic, which proposed a factor γ_{Sd} equal to 1.15 [64]. This value was originally proposed to consider uncertainties related to the calculation methodology and tools ("*moderately careful or uncertain studies and calculations*", in French *"études et calculs moyennement soignés ou incertains"*, [64]), while statically indeterminate systems and redistribution of forces were not explicitly mentioned. Additional literature review on this topic can be found in [65]. In the latest available draft of EN 1990:2023 [7], the model uncertainty in action effects is still covered by the partial safety factor for permanent and variable actions, presented with slightly different notation ($\gamma_F = \gamma_f \cdot \gamma_{Sd}$). It is also specified that γ_F may be used for both linear and non-linear calculation, although the different verification types may differ: local verifications for linear analyses, global verifications for non-linear analyses. In EN 1990:2023 [7], except for some specific design cases, no recommended values of γ_{Sd} are specified. It is worth noting that one of the possible disadvantages of considering γ_{Sd} on the actions side is the impossibility to consider the mode of failure of the system (brittle vs. ductile), as it depends on the sectional resistance model.

Interestingly, the approach of codes of practice nowadays does not account for the type of system in terms of uncertainties in modelling and determination of action effects. For statically determinate systems, the calculation of action effects is only influenced by equilibrium and geometry, whereas the stiffness and the mechanical behaviour have no influence on the results, provided that second order effects can be neglected. For statically indeterminate systems, however, additional phenomena and basic uncertainties contribute to the uncertainty in action effects, as can be schematically observed in Fig. 18, adapted from [65] and [2], notation consistent with [7]. As shown in Fig. 17, one of the main components influencing the calculation of action effects is modelling of the mechanical behaviour. Indeed, any model is a simplification of the actual structure and leads to a different degree of accuracy and precision. Generally, more complex models lead to more precise but not necessarily more accurate results and they require additional parameters and calculation time, often involving iterative processes and more complex interpretation of results. Also, time-dependent deformations due to creep can influence the uncertainties in action effects. Another phenomenon that can increase the uncertainty in action effects, is the system change during construction (casting of concrete parts which constitute a statically indeterminate structure at different times time or/and assembly of precast members). Generally, in the design process, the model of the structure is generated as a whole and the totality of the load is applied at once, including self-weight. In actual structures, however, self-weight is applied according to construction stages, permanent load is incrementally applied after construction and live loads are applied sporadically. In statically indeterminate systems, this sequential application of the loading can lead to internal force redistributions, increasing the uncertainty in action effects. In addition, the internal forces are affected by the uncertainties related to the actual creep behaviour, the age of concrete at system change and the time at activation of self-weight (removal of propping or scaffolding). Finally, combinations of different actions, which is generally a task left to the designer, can lead to further uncertainties in calculating action effects.

As numerical models evolve, they are becoming more and more complex, giving designers many options to model a structure. For instance, the modelling of boundary conditions, the type of elements, the interaction between different element types and the adopted solver can influence the calculated action effects. As there is no standard for modelling structures, these choices are left to the discretion and the experience of the designer, leading to further uncertainties in the value of action effects.

The aim of this work is to contribute to quantifying the model uncertainty in action effects and load-bearing capacity calculations of reinforced concrete structures and clarify whether

the failure mode of the system influences this uncertainty. This investigation focuses on uncertainties related to the mechanical behaviour of the structure, see highlighted box in Fig. 18, by comparing tests results and calculated values. Uncertainties related to geometrical variability effects on model uncertainties and system changes are not considered. Based on updated distributions, the partial safety factor γ_{Sd} is calculated by means of parametric analyses and case studies. Finally, uncertainties covered by γ_{Sd} are clarified and practical implications are discussed.

2.2 Investigated structural system and practical relevance

Since there is little experimental data available on statically indeterminate systems, it cannot be used to perform statistical analyses. To overcome these difficulties, the experimental response of statically indeterminate systems is obtained by assembling the response of simply supported beams tested in a 3-point bending setup. This technique has already been used by [65] with structural members exhibiting brittle failure modes. It is also applicable to reinforced concrete systems where both brittle and ductile failure modes can occur. The deformability of supports is also considered by supporting beams on reinforced concrete columns tested under concentric uniaxial load.

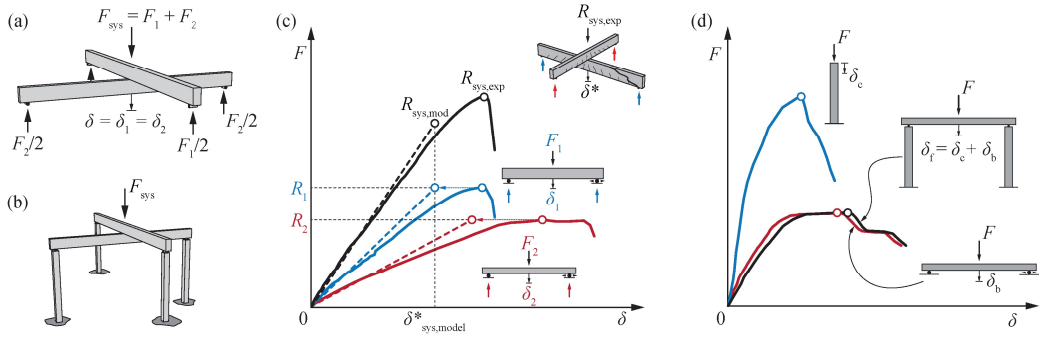

Fig. 19 *(a) Assembled system with beams on infinitely rigid supports and (b) supported by columns; (c) experimental response of the system (black) assembled with beams (red and blue) and linear-elastic uncracked model prediction (dashed); (d) Force-deflection (F-δ) response of a beam tested in a 3-point bending setup (red), a column tested in compression (blue) and a beam supported by two columns (black).*

For the case presented in Fig. 19a, the response of the assembled system in terms of force-displacement relationship (*F-δ*) is obtained by combining the response of various beams crossing at midspan. For compatibility reasons, the force applied to the system for a given displacement is the sum of the forces required to produce that same displacement in each of the beams composing the system, see Fig. 19c. For the statically determinate systems with a beam supported on columns, which constitute the indeterminate system shown in Fig. 19b, the displacement at midspan is obtained by adding the displacement of both members as shown in Fig. 19d.

The theoretical response predicted by the model is obtained by using the same technique, where the *F-δ* response of each beam is calculated using several models. As an example, Fig. 19c shows the experimental *F-δ* response of a system composed of two beams and the response of a linear elastic model. It is important to note that the model uncertainty related to the sectional resistance calculation is not considered. For this reason, the predicted resistance of each beam is equalled to the experimental resistance (in Fig. 19c $R_{1,mod} = R_{1,exp}$ and $R_{2,mod} = R_{2,exp}$). With this assumption, the load-bearing capacity predicted by the elastic model for the system presented in Fig. 19c is lower than the experimental one ($R_{sys,exp}$), which results from the superposition of the two experimental load-displacement curves.

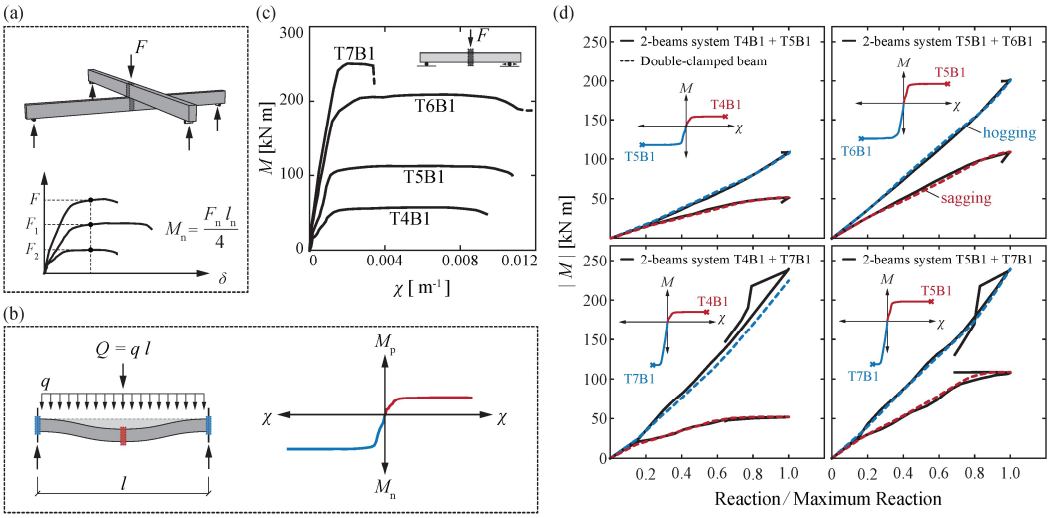

Fig. 20 *(a) F-δ response of an assembled 2-beams system; (b) double-clamped beam and assumed M-χ relationship; (c) experimental M-χ relationships of beams used in the comparison; (d) comparison of bending moment evolution as a function of the load for the 2-beams system (continuous curves) and the double-clamped beam (dashed curves).*

To assess whether the assembled 2-beams system (Fig. 20a) is representative of redistributions occurring in a continuous beam (Fig. 20b), action effects in each beam of the system are compared with those in a double-clamped beam in the sagging and hogging sections. The double-clamped beam is subjected to both a distributed load q and a concentrated force at midspan $Q = q \cdot l$. All beams used in the comparison have been tested by [76], have the same cross section ($b \times h = 200 \times 400$ *mm*) and variable longitudinal reinforcement ratios ($0.4\% < \rho_l < 1.8\%$). The moment-curvature (*M-χ)* relationships (measured over a length equal to the effective depth of the corresponding beam) are shown in Fig. 20c. In the double-clamped beam, the sagging and hogging bending moment are calculated using the measured *M-χ* relationship to fulfil equilibrium and compatibility. The shear deformations are neglected. Fig. 20d shows the bending moments at midspan of the 2-beams system as well as the sagging and hogging bending moments in the double-clamped beam as a function of the normalized load. It can be observed that the bending moment at midspan of each beam in the 2-beams system (continuous curves) closely follows the bending moment in the double-clamped beam (dashed red at midspan and dashed blue at the clamped end). For the case shown in the bottom left of Fig. 20d (system T4B1 + T7B1), the resistance of the midspan section of the double-clamped beam is extremely under-designed and its deformation capacity is not sufficient to allow the clamped section to reach its designed resistance. Overall, except for cases where sections are extremely under-designed, the redistribution of forces in the assembled system is a good approximation of the redistributions occurring in a continuous beam. Even when sections are under-designed, Fig. 20d shows that the redistribution of internal forces between the 2-beam system and the continuous beam is very similar up to failure. Thus, the assembled 2-beams system is representative of several practical cases, including double-clamped beams and continuous beams.

2.3 Definitions

2.3.1 Random variables

Depending on the type of analysis performed and the code of practice used, structural verifications can be performed by comparing action effects to sectional resistances (approach typically used in the design of new structures) or by comparing the load-bearing capacity directly to the actions (approach often used in the assessment of existing structures). In the present work, these two approaches are defined as *local* and *global*

verification methods. For statically determinate structures, both methods lead to the same result, whereas for statically indeterminate structures, the results are typically different. The local verification method is typically used in combination with linear elastic analyses (or analyses with partial redistribution of internal forces) whereas the global verification method is used with non-linear analyses or calculations based on limit analysis.

To cover both cases, two random variables are defined in this report. The global random variable θ_{QR} is defined in Eq. 40, where $R_{sys,exp}$ is the experimental load-bearing capacity of the 2-beams assembled system and $R_{sys,mod}$ is the theoretical load-bearing capacity predicted by the model, see Fig. 21a.

$$\theta_{QR} = \frac{R_{sys,\exp}}{R_{sys,\mathrm{mod}}} \tag{40}$$

The local random variable θ_E is defined in Eq. 41, where $E_{j,mod}$ is the theoretical action effect in each member of the system (predicted by the model) and $E_{j,exp}$ is the experimental action effect for the theoretical load-bearing capacity ($R_{sys,mod}$). The random variables are graphically illustrated in Fig. 21a. The action effects (E_j) are proportional to the force carried by each beam (F_j) at each load step where j is index of the beam in the assembled system.

$$\theta_{E,j} = \frac{E_{j,\exp}}{E_{j,\mathrm{mod}}} = \frac{F_{j,\exp}}{F_{j,\mathrm{mod}}} \quad \text{with} \quad F_j = \frac{E_j}{\kappa_j} \quad \textit{and} \quad j=[1,2] \tag{41}$$

As already mentioned, the aim of the present report is to investigate the model uncertainty in action effects related to the modelling of the mechanical behaviour. The model uncertainty related to calculation of the sectional resistance is not considered, in fact, it is removed by equalling the theoretical predicted resistance of each member of the system to the experimental value.

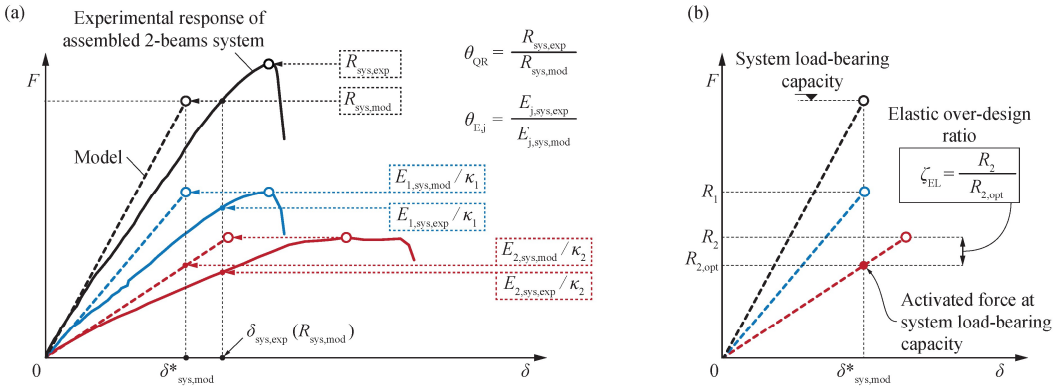

Fig. 21 *(a) Global and local random variable definition, respectively θ_{QR} and θ_E, for the shear force at the support $\kappa_1 = \kappa_2 = 0.5$ and for the bending moment at midspan $\kappa_1 = 4/l_1$ and $\kappa_2 = 4/l_2$; (b) elastic over-design ratio definition, ζ_{EL}.*

2.3.2 Elastic over-design ratio

Overdesign of a section can result from several sources. Generally, structures are dimensioned by considering the envelope of action effects calculated using a linear elastic uncracked model for the relevant load combinations. As failure can occur for a specific load combination, this leads to some sections being over-designed with respect to others. Another source is often related to detailing and serviceability requirements (like minimal reinforcement ratio, limitation of deformations and cracking control) or fatigue and fire

requirements. In addition, the effective amount of reinforcement provided is often slightly larger than calculated, to accommodate commercially available reinforcement bars and convenient spacings. Sometimes, simplicity of construction leads to uniform reinforcement diameters, leading to possible over-design. Finally, if various failure modes are involved, the uncertainty of the resistance model could also lead to over-design of some sections. To account for these effects, the *elastic over-design ratio*, defined in Eq. 42 is introduced to investigate the model uncertainty for action effects.

$$\zeta_{EL} = \frac{R_j}{R_{j,opt}} \tag{42}$$

This ratio is graphically represented in Fig. 21b and, by definition, cannot be lower than unity as it is calculated on members that do not cause the failure of the system.

2.4 Database and considered models

A database of 93 beams and 75 columns was collected. Tab. 6 and 7 shows details of the beams and columns database. All beams and columns used in the simulations have well documented *F-δ* experimental responses, including the post-peak branch and well as documented material and geometrical properties. For beams, only 3-points bending tests are considered.

***Tab. 6** Database of beams tested in a 3-points bending setup*

Reference	number of tests	Span l_b [mm]	Effective depth d [mm]	Longitudinal reinf. ratio ρ_l [%]	Shear reinf. ratio ρ_w [%]	f_c [MPa]	f_y [MPa]
[77]	5	1600-2700	175	0.32-2.29	0.15-0.26	44.4	460
[76]	21	2000-6000	176-565	0.13-1.94	0.13-0.38	30.9	587-595
[78]	2	2000	170	0.30-1.22	0	34.4-35.3	562-573
[79]	11	645-1075	215	3.77	0.45-1.81	52.0	414
[80]	8	5400	875-925	0.50-1.75	0-0.08	21.0-38.0	550
[81]	1	10800	1890	0.74	0	33.6	455
[82]	12	3600-6840	457	1.72-3.46	0-0.20	22.6-43.5	440-445
[83]	3	3000	372	1.51	0-0.21	55.2	464
[84]	2	1400	210	2.46	0.5	42.0	418-426
[85]	3	4200	340-348	0.23-2.10	0.36	35.3-45.9	336-507
[86]	6	1175-1952	235-244	3.29-3.60	0.22-0.32	37.0-42.2	402-436
[87]	6	1400	160-210	0.84	0-0.19	40.3	510-520
[88]	4	2800-7700	556	0.89	0	32.6-35.6	713
[89]	6	1600	140-210	0.80-1.6	0-0.20	39.9	520
[90]	3	3000-5000	460	1.37	0.09-0.19	23.8-27.0	495

***Tab. 7** Database of columns tested under uniaxial compression*

Reference.	number of tests	Width b_c [mm]	Slenderness ratio λ_G	ρ_l [%]	*fc* [MPa]	*fy* [MPa]
[91]	24	305	4.0	1.72-3.66	31.3-40.0	372-438
[92]	19	200-600	3.0-4.5	1.50-2.50	33.2	247-475
[93]	6	267-600	3.0	0.28	42.8	458-494
[94]	26	267-600	3.0	0.28	42.8	458-494

Among the beams included in the database, 46 failed in flexure and 47 in shear. Because one of the aims of this report is to clarify whether a brittle or a ductile mode of failure influences the model uncertainty, the deformation capacity is determined from the reported load-deformation relationships. To this aim, the indicator of the deformation capacity of each beam, which is used to distinguish between ductile and brittle behaviour, is calculated as the ratio between the deformation at 90% of the experimental post-peak branch δ_R and the predicted elastic uncracked ultimate displacement δ_y, see Fig. 22a for a graphical representation.

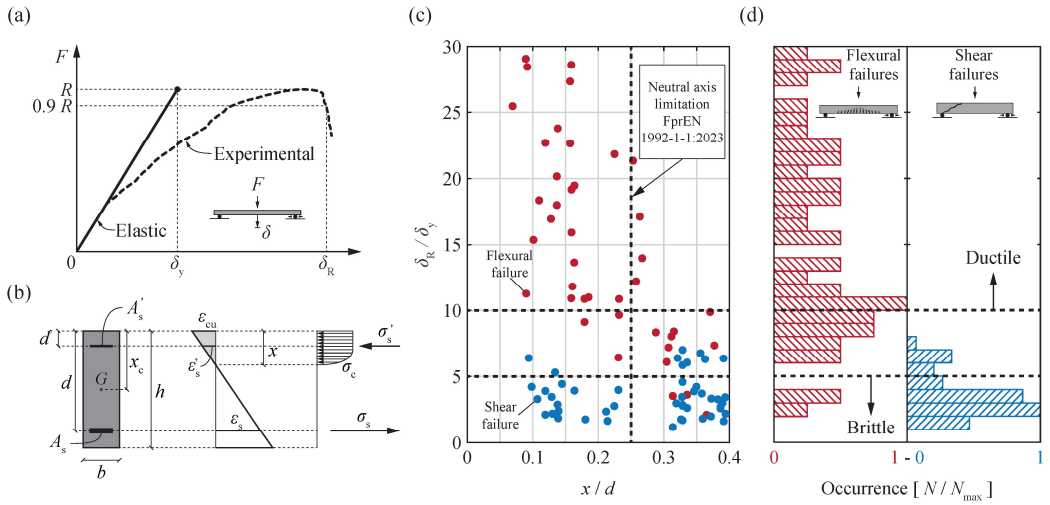

***Fig. 22** (a) F-δ response of a beam tested in a 3-point bending setup with definition of δ_y and δ_R; (b) strain profile of a RC beam section at Ultimate Limit State (ULS); (c) beams grouped based on their deformation capacity ratio at failure, failure modes and the neutral axis depth; (d) histogram of the deformation capacity ratio by failure mode (bending in red and shear in blue).*

The failure is assumed to be ductile if the deformation capacity ratio is larger than 10 and brittle if it is smaller than 5 (intermediate behaviour for $5 \leq \delta_R / \delta_y \leq 10$). Fig. 22c shows the deformation capacity ratio plotted against the depth of the neutral axis calculated according to EN 1992-1-1:2023 [95] (see definition in Fig. 22b). It can be observed that beams that fail in bending and respect the condition imposed by EN 1992-1-1:2023 for performing plastic analyses ($x/d \leq 0.25$) [95], generally exhibit a ductile behaviour. As shown in Fig. 22c and in the histograms of Fig. 22d, shear failures lead to brittle or intermediate behaviour.

All columns included in the database have a square cross section (width b_c between 250 and 600 mm) and a geometrical slenderness ratio of the specimen λ_G, (defined as the ratio of the height of the column over the width b_c) between 3 and 4. None of the columns exhibit a buckling failure.

2.4.1 Moment-curvature relationships and calculation models

Besides the Linear Elastic Uncracked model (LEU), five additional models are considered to evaluate the model uncertainty in action effects. An overview of the models is given in Tab. 8 and the corresponding *M-χ* relationships are shown in Fig. 23a.

For the LEU model, the flexural stiffness is calculated according to Eq. 43. In the Linear Elastic Fully-Cracked model (LEFC), all sections are assumed to be fully cracked before applying the load, and the flexural stiffness is calculated according to Eq. 44 where the location of the neutral axis is calculated according to Eq. 45.

$$EI_{LEU} = E_c \cdot \frac{b \cdot h^3}{12} \tag{43}$$

$$EI_{LEFC} = b \cdot d^3 \cdot E_c \cdot \left[\frac{1}{3} \cdot \left(\frac{x}{d} \right)^3 + n \cdot \rho_l \cdot \left(1 - \frac{x}{d} \right)^2 + n \cdot \rho_l' \cdot \left(\frac{d'}{d} \cdot \frac{x}{d} \right)^2 \right] \tag{44}$$

$$x = d \cdot (\rho + \rho') \cdot n \cdot \left(\sqrt{1 + 2 \cdot \frac{\rho + \rho' \cdot \frac{d'}{d}}{n \cdot (\rho + \rho')^2}} - 1 \right) \quad with \quad \rho = \frac{A_s}{b \cdot d} \quad \rho' = \frac{A_s'}{b \cdot d} \tag{45}$$

where $n = E_s/E_c$ is the ratio between elastic moduli of steel and concrete. In the Tri-Linear model (3L), the section is uncracked until the cracking moment M_r according to Eq. 46 is reached. For cracked sections, tension stiffening is accounted for by shifting the *M-χ* line by a value equal to $\Delta\chi t_s$, calculated according to Eq. 47, as shown in Fig. 23a, see [96]. The Quadri-Linear model, with and without limitation of the deformation capacity, respectively 4L and 4L-LIM, is identical to the 3L model up to the level of the resisting moment M_R. Thereafter, the *M-χ* relationship has an infinite plastic plateau in the 4L model while in the 4L-LIM model, the curvature is limited to match the experimental displacement at peak load. Finally, the behaviour of the Non-Linear model (NL), in brown in Fig. 23a, is obtained by discretizing the section in fibres, with each concrete fibre having a uniaxial stress-strain response calculated according to EN 1992-1-1:2023 [95] for the compression zone and an elastic-brittle behaviour in tension. The reinforcement is modelled by fibres with an elastic-perfectly plastic stress-strain response.

$$M_r = f_{ct} \cdot \frac{EI_{LEU}}{E_c \cdot (h - x)} \tag{46}$$

$$\Delta\chi_{Ts} = \frac{3}{8} \cdot \frac{1}{n \cdot \rho_T} \cdot \chi_r \qquad \rho_T = \rho \cdot \frac{5 \cdot d}{h} \qquad \chi_r = \frac{M_r}{EI} \tag{47}$$

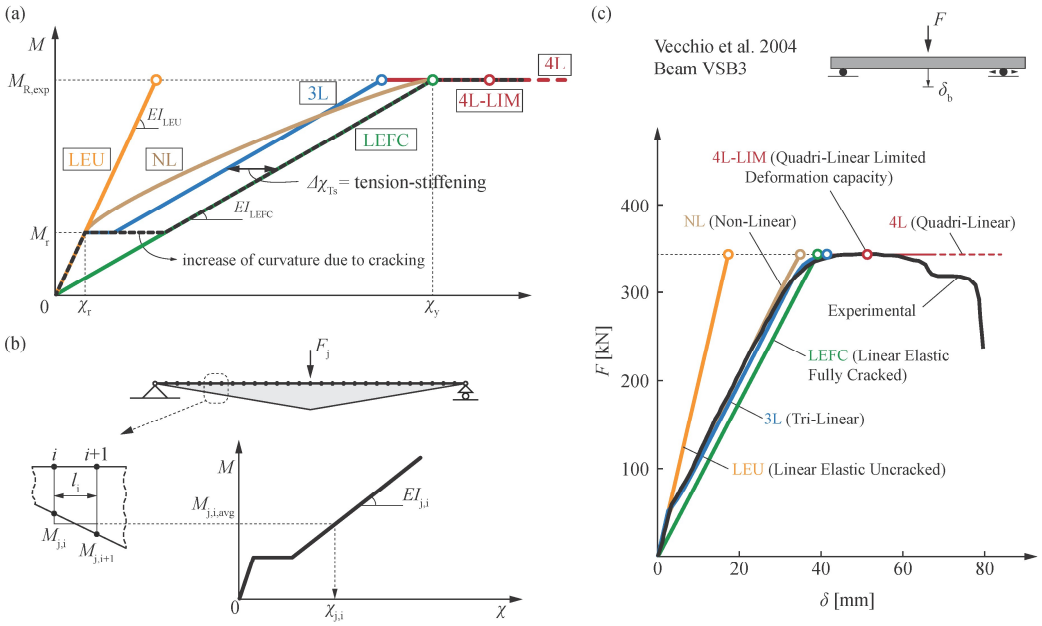

Fig. 23 *(a) Assumed M-χ relationships for the various models; (b) computation of the deflection; (c) example of the experimental and predicted F-δ responses for beam VSB3 [82].*

Fig. 23b shows the methodology used for calculating the force-displacement relationship of the simply supported beams for the 3L model. At each load step, the beam is discretized and the displacement is calculated by updating the flexural stiffness of each element based on the calculated bending moment. For beams without shear reinforcement, the displacement due to shear deformations is calculated using the mechanical model proposed by [97], which is based on [88]. For beams containing shear reinforcement, the model proposed by [98] is used. Fig. 23c shows the experimental *F-δ* response of a simply supported beam (in black, beam VSB3 by [82]) and the theoretical response predicted by the various models.

Tab. 8 *Implemented models for beams*

Name	Symbol	*M-χ*	Section	Shear deformation	Tension stiffening	Concrete *σ-ε*	Steel *σ-ε*
Linear Elastic Uncracked	LEU	Linear	Uncracked	No	No	Elastic	Elastic
Linear Elastic Fully-Cracked	LEFC	Linear	Fully-cracked	No	No	Parabola rectangle	Elastic
Tri-Linear	3L	Tri-Linear	Uncracked/ Fully-cracked	Non-linear	Yes	Parabola rectangle	Elastic/ Plastic
Quadri-Linear	4L	Quadri-Linear	Uncracked/ Fully-cracked	Non-linear	Yes	Parabola rectangle	Elastic/ Plastic
Quadri-Linear-Limited	4L-LIM	Quadri-Linear	Uncracked/ Fully-cracked	Non-linear	Yes	Parabola rectangle	Elastic/ Plastic
Non-Linear	NL	Non-Linear	Variable	Linear	No	Parabola rectangle	Elastic/ Plastic

The *F-δ* response of the columns is modelled using either a linear elastic model (LE) or a non-linear model (NL). In the LE model, both concrete and the reinforcement constitutive laws are assumed linear-elastic, Fig. 24a. In the non-linear model (NL), the constitutive law of concrete proposed by Guidotti et al. 2011 [99] is used, and the increase of strength and deformation capacity due to transverse reinforcement is considered according to [100]. The reinforcement is modelled by an elastic-perfectly plastic stress-strain behaviour. Fig. 24b shows the experimental *F-δ* response of a column tested under uniaxial compression (column CAM1 by [93]) and the theoretical response predicted by the two models.

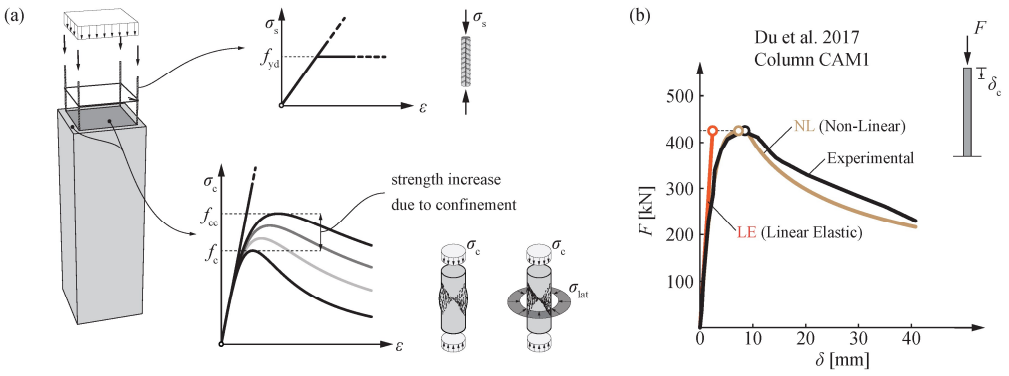

Fig. 24 *(a) Materials stress-strain for linear elastic and non-linear model; (b) example of the experimental and predicted F-δ responses for column CAM1 [93].*

2.4.2 Examples of two beams assembled systems

Fig. 25 shows the experimental and theoretical response, as predicted by the Linear Elastic Uncracked model, of three characteristic systems. In Fig. 25a, the failure of the system is controlled by beam 1 in the experimental response and by beam 2 in the model prediction. Due to concrete cracking, the relative decrease of flexural stiffness for beam 2 is larger than for beam 1 and, since beam 1 fails in a brittle manner, so does the assembled system. This cannot be predicted by the LEU model, that in this case leads to an unsafe prediction (load-bearing capacity larger than the experimental value, $\theta_{QR} < 1$). A slightly larger theoretical load-bearing capacity with respect to the experimental is also observed in Fig. 25b, where both beams have a relatively ductile behaviour, but their peak resistance occurs for significantly different displacements. A rather different result is shown, however, in Fig. 25c, where the experimental peak resistance is reached for a similar displacement in both beams, leading to a experimental load-bearing capacity of the 2-beams system which is larger than the value predicted by the model. It must be noted that the examples in Fig. 25 are for illustrative purposes and are not exhaustive.

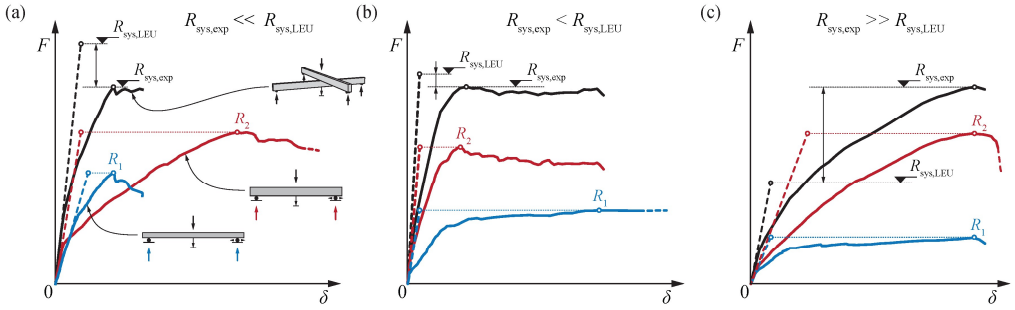

Fig. 25 *Examples of theoretical (Linear Elastic Uncracked model) and experimental response of 2-beams assembled systems: (a) beam DB0530M [80] and S130 [86]; (b) beam DR572 [89] and T1A1 [76]; (c) beam DR382 [89] and VSC2 [82].*

2.5 Results

The combination of the 93 beams described in Tab. 6 allows to produce up to 4278 two-beams systems with the corresponding experimental behaviours. For all the assembled systems, the internal forces and the theoretical load-bearing capacity is determined according to the models defined above.

2.5.1 Presentation of the results and distribution fitting

Fig. 26a shows the log-normal probability-plot of θ_E defined in Eq. 41 where the internal forces $E_{j,mod}$ are calculated using the linear elastic uncracked model (LEU). The logarithm of the random variable (x-axis) is plotted against the normal quantile in terms of standard deviation σ (y-axis). The red, blue and green distributions correspond respectively to ζ_{EL} smaller than 1.1, 1.25 and 5 while the continuous line represents the fitting LN distribution. This type of graphical representation allows to graphically verify if a LN distribution is a good fit for a random variable. In fact, data lying on a straight line indicate an exact LN distribution and the slope corresponds to the coefficient of variation (CoV). Whether a LN distribution is suitable to represent the tail of the distribution has already been discussed in the past. According to [101], to compare different propositions, a simple fitting criterion with an arbitrary choice of the distribution is practically non-verifiable and there is a need to have standardized distribution types to perform adequate comparisons. The present report accounts for these considerations and, accordingly, a LN distribution is adopted to describe θ_E and θ_{QR}. In fact, besides being a good fit for the distribution of θ_E as shown in Fig. 26, the comparison with the recommendations of [28] is facilitated.

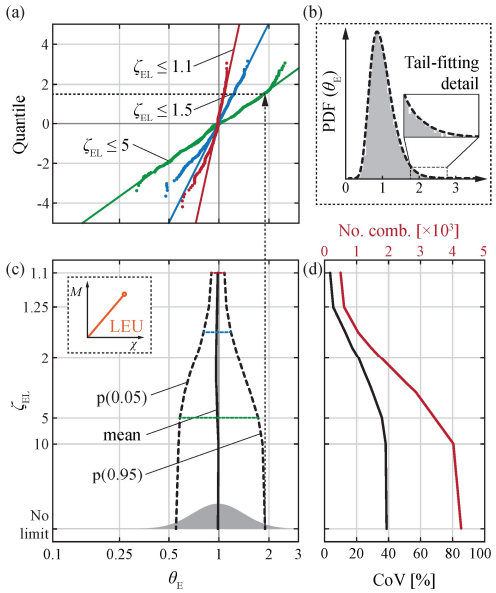

Fig. 26 *(a) Probability plot of θ_E using a Linear Elastic Uncracked model and (b) detail of the tail fitting; (c) graphical representation of the distribution parameters with varying elastic over-design ratio; (d) CoV (black) and number of combinations (red).*

It can be observed that the LN distribution is a good fit for the distribution, including the tail regions. Fig. 26b shows the histogram of θ_E and the detail of the upper tail fitting. Because θ_E is defined as the ratio between the experimental action effect and the calculated one, the values in the upper tail region are the unsafe cases where $E_{exp} > E_{mod}$. The dashed line in Fig. 26a represents the fitting of the data with a LN distribution (fitting performed using a linear least-squares fitting algorithm, tail values larger than the 95th percentile of the data are weighted by a factor equal to 2). Parametric analysis combined with graphical checks show that this fitting parameters allow to have a good approximation of the tail of the distribution when the model uncertainty in action effects calculation is determining (upper tail values, θ_E >1) and a good fit of the rest of the distribution when the model uncertainty is not determining, see probability plots in Figure 26a.

Fig. 26c shows the distribution parameters of θ_E (mean, 5th and 95th percentile) with varying elastic over-design ratio (ζ_{EL}). If one of the beams is largely over-designed compared to the other (large ζ_{EL}), redistribution of the force is more likely to occur, resulting in a larger uncertainty in determining action effects and leading to an increase of the coefficient of variation of θ_E, see Fig. 26d. However, as shown in Fig. 20d, if the elastic over-design ratio

is very large (ζ_{EL} > 2), the assembled system is not necessarily representative of a practical case. In Fig. 26c, it can be observed that the mean of the distribution is always close to unity. This is due to the fact that, if the action effect is overestimated in one member, it is generally underestimated in the other. The red line in Fig. 26d shows the number of systems that is possible to assemble for a given limit of ζ_{EL}. At least 500 systems are analysed for each ζ_{EL} value, which is sufficient to perform statistical analyses.

2.5.2 Discussion of the results

Using the same format proposed in Fig. 26, Fig. 27a shows the distribution parameters of θ_E (mean, 95th percentile and CoV) for the LEU, LEFC, 3L and NL models (the results of the LEU model are already discussed in the previous section, they are presented again to allow for a comparison). For the LEFC model, very large CoVs can be observed. This is due to the fact that the flexural stiffness can be largely underestimated. For instance, if the failure of the system occurs with limited cracking in one of the beams (actual experimental behaviour), the action effect can be considerably underestimated considering the beam fully cracked. The probability for this scenario to occur is larger for large values of ζ_{EL} since the system has a higher probability to fail with one member still in the uncracked state. On the other hand, for the tri-linear (3L) and the non-linear model (NL), ζ_{EL} has a limited influence on the distribution of θ_E. In fact, for these models, the flexural stiffness depends on the load level, leading to a satisfactory prediction of the displacement and the internal forces for each load step. Since non-linear shear deformations and tension stiffening are considered in the tri-linear model (3L), but not in the non-linear model (NL), displacements are generally better predicted for the former and lead to a smaller CoV. Fig. 27b shows the distribution of θ_E using the LEU model for systems exhibiting brittle and ductile failure modes (for details about the failure mode classification see Fig. 22). Since the LEU model better describes the behaviour of brittle systems (uncracked section), for a given ζ_{EL} smaller CoVs are obtained for brittle systems than for ductile systems (see Fig. 27b).

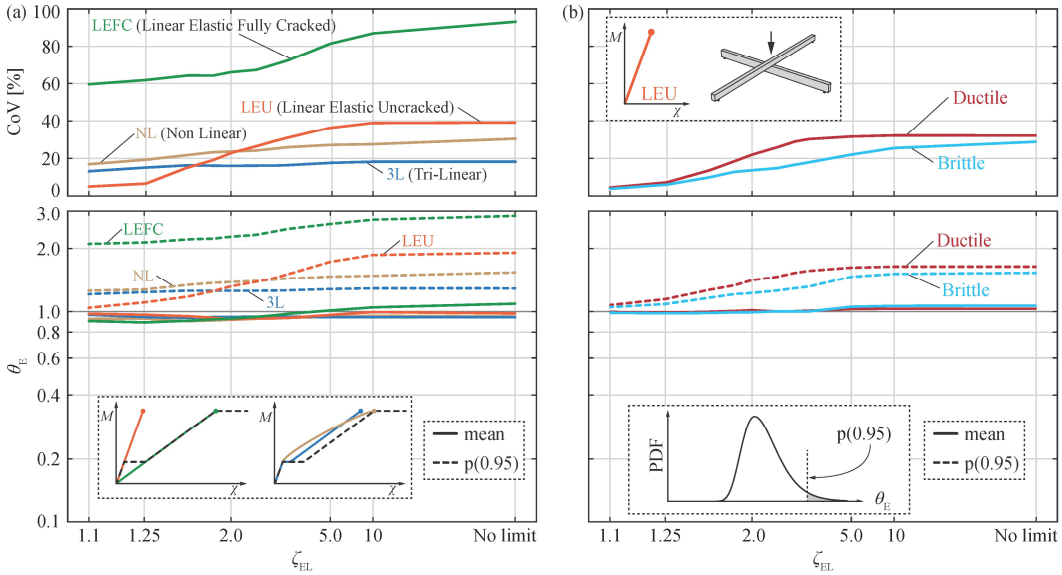

Fig. 27 *CoV (top) and distribution parameters (bottom) of θ_E: (a) for various models and (b) for the Linear Elastic Uncracked model with various ductility degrees.*

Fig. 28 shows the CoV and the distribution parameters of θ_{QR} according to Eq. 40 (ratio between the experimental and calculated load-bearing capacities, mean, 5th percentile and CoV) for the various models. Unlike θ_E, for which the values in the upper tail region are the less safe, for θ_{QR} the unsafe values are located in the lower tail (θ_{QR} < 1), where the experimental load-bearing capacity (R_{exp}) is smaller than the one predicted by the model (R_{mod}). As for θ_E, ζ_{EL} does not influence the distribution of θ_{QR} for the 3L and NL models. On the other hand, it does for the LEU and LEFC models, but this influence is less

pronounced than for θ_E. Two major trends can be identified: (1) the mean value of θ_{QR} tends towards unity with increasing refinement of the model (see continuous lines in the bottom of Fig. 28); (2) the CoV decreases with increasing refinement of the model (top of Fig. 28). The combination of these two phenomena leads to a 5th percentile of the distributions which is almost constant ($p(0.05)$ ~ 0.95-0.98 for all the analysed models) despite the fact that the complexity and the calculation time for refined models increases considerably. A good compromise for estimating the load-bearing capacity of the system is achieved by using the LEFC model which does not require an iterative process for the assessment of an existing structure, but for which the reinforcement needs to be known in each section to determine the fully cracked flexural stiffness (this means that for designing a new structure, an iteration is needed).

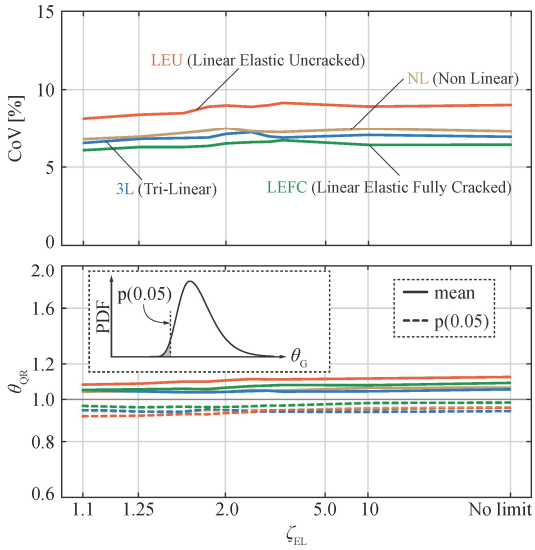

Fig. 28 *CoV (top) and distribution parameters (bottom) of θ_{QR} for various models.*

Fig. 29 shows the statistical values of θ_{QR} for brittle and ductile systems using the LEU and the 3L models. As already mentioned, ζ_{EL} only influences the results of the distribution of θ_{QR} for the LEU model whereas it has no influence for the 3L model. For both models, brittle systems exhibit a larger CoV compared to ductile systems (see Fig. 29, top). Also, due to the redistribution of forces, the mean value of the distribution is larger for ductile systems. In fact, both the 3L and the LEU model do not consider plastic deformations, thus underestimating on average the load-bearing capacity for ductile systems and leading to a larger safety margin ($R_{sys,exp} > R_{sys,mod}$). This does not occur for brittle systems that do not undergo plastic deformations, leading to mean values closer to unity. The combination of these two effects leads to a larger 5th percentile of θ_{QR} for ductile systems (~ 1.00) compared to brittle systems (~ 0.90).

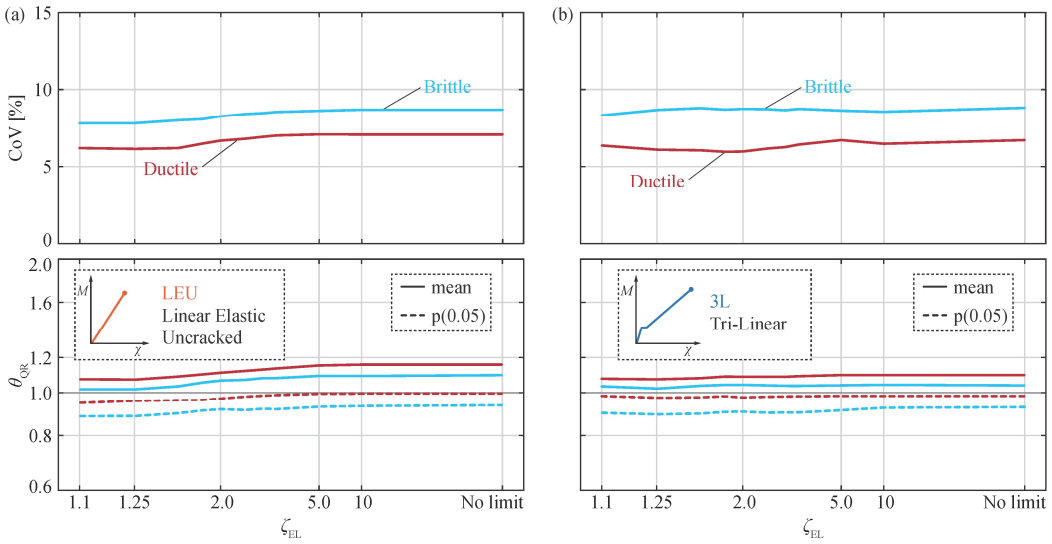

Fig. 29 *CoV (top) and distribution parameters (bottom) of θ_{QR} for ductile and brittle systems: (a) using the LEU (Linear Elastic Uncracked) model and (b) using the 3L (Tri-Linear) model.*

2.5.3 Plastic models

If a quadrilinear model (Quadri-Linear, 4L) with a plastic plateau without deformation limit is used, the results will be identical to a rigid plastic investigation according to limit analysis. In this case, the random variable θ_{QR} cannot be larger than one. In fact, the theoretical load-bearing capacity ($R_{sys,mod}$), is always equal to the sum of the single resistances of the individual beams. For the experimental load-bearing capacity of the system ($R_{sys,exp}$), this scenario occurs only if the experimental peak resistance of the individual beams in the 2-beams assembled system is reached for the same displacement, as shown in Fig. 25c. The CoV of the θ_{QR} values for the 4L model are shown in Fig. 30a. The 4L model allows for unlimited redistribution between the members of the 2-beams system. However, the beams included in the database exhibit both brittle and ductile failure modes, thus, redistribution in the assembled 2-beams system can be limited. This leads to large values of CoV for the 4L model (see Fig. 30a). As an example, the probability-plot of θ_{QR} for $\zeta_{EL} \leq 2$ is presented in Fig. 30c. It must be noted that the mean value of the log-normal distribution it is not meaningful for the cases where the maximum value is limited (i.e. to 1 for the 4L model). In fact, in these cases, a log-normal distribution is not suitable to represent the whole distribution but only the lower-tail, see Fig. 30c for the 4L model. However, this choice allows performing comparisons between the different models.

If the deformation capacity of the beams is limited to the experimental displacement at peak resistance, as in the 4L-LIM model, the CoV of θ_{QR} decreases and does not depend on ζ_{EL}, see Fig. 30a. Moreover, the 5th percentile of the distribution is closer to unity than for the 4L model. Also, since the deformation capacity is the same as the experimental one, the predicted load-bearing capacity is not necessarily equal to the sum of the single members resistance and the value of θ_{QR} is not limited to 1.0 as can be observed in Fig. 30c. If the 4L model is used for systems assembled with beams failing in bending and complying with the requirements according to EN 1992-1-1:2023 [95] (4L-LIM-REQ model), the CoV of θ_{QR} reduces considerably with respect to the 4L and 4L-LIM models and the 5th percentile is very close to unity, see Fig. 30a. The limitations mentioned above for the 4L-LIM-REQ model are shown in Fig. 30b and include the depth of the neutral axis according to [95] ($x/d \leq 0.25$, Fig. 22b) and the relative resistance of the critical sections ($0.5 \leq R_1/R_2 \leq 2$).

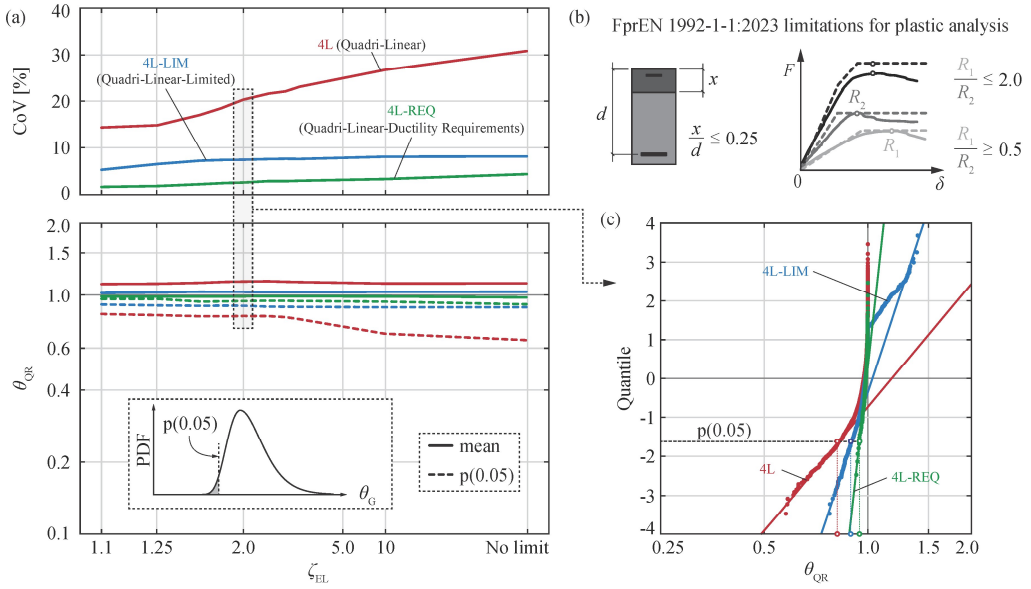

Fig. 30 *(a) CoV (top) and distribution parameters of θ_{QR} for a Quadri-Linear model with a plastic plateau (4L in red), a Quadri-Linear model with limitation of the deformation capacity (4L-LIM in blue) and a Quadri-Linear model with a plastic plateau used for beams respecting the requirements of EN 1992-1-1:2023 (4L-REQ in green); (b) requirements according to EN 1992-1-1:2023 [95] to perform plastic analyses without explicit checks on the deformation capacity (4L-REQ model); (c) probability plots for the presented models with ζ_{EL} = 2.*

2.5.4 Deformability of supports

Fig. 31 shows the comparison of the 2-beams system investigated above with the same system supported on columns (see insert in Fig. 31a). A slenderness ratio λ_G = 10 is considered for all columns without accounting for 2nd order effects and only cases where column resistance is not governing are considered. The load-deformation relationships are produced with the methodology presented in Fig. 19d. The results are presented in Fig. 31 in terms of CoV and mean values of θ_E and θ_{QR} (case with ζ_{EL} = 1.1). Regardless of the model considered, the CoV of θ_E shows a decrease of 1 to 3% while the mean values of θ_E also decrease. With respect to θ_{QR} defined as in Eq. 40, a reduction of the mean values and the CoV can also be observed (minor reduction in the case of the CoV). These results can be explained by the fact that the deformability of supports leads to an increased redistribution of forces.

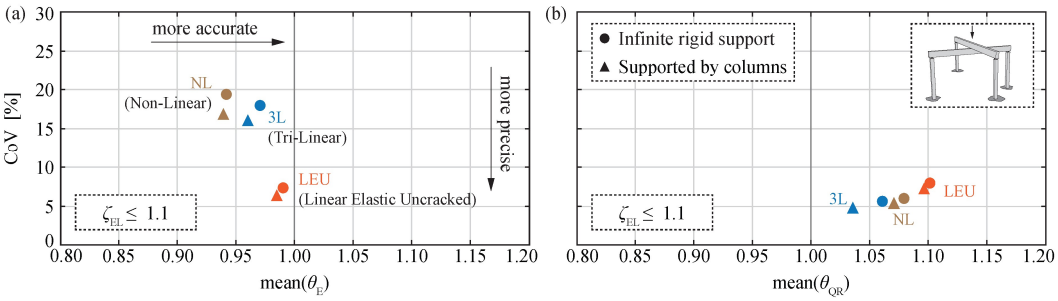

Fig. 31 *CoV and mean values of the of (a) θ_E and (b) θ_{QR} for the 2-beams system on infinitely rigid supports and supported by columns (slenderness ratio λ_G = 10).*

2.6 Case study: reinforced concrete frame

As already mentioned, the model uncertainties related to the calculation of action effects are usually covered by the partial factors for permanent and variable actions (γ_G and γ_Q). In EN 1990:2023 [7], γ_G and γ_Q are obtained by multiplying γ_{Sd} with γ_g and γ_q, which cover respectively the model uncertainty in action effects and the uncertainty in the representative values of the actions, see Fig. 18. To estimate the value of γ_{Sd} based on the distribution parameters of θ_E, reliability analyses are performed on the 1st floor beam of the RC frame, shown presented in Fig. 32. To account for various ratios between structural and non-structural self-weight, the spacing between frames, *s*, is varied between 4 and 12 m, see Fig. 32b. This variation covers also the ratio between the structural and non-structural self-weight in bridges, however, this ratio can be generally larger than 3 for long-span bridges. The building is designed for a design life of 50 years and for various intended uses. For each intended use, design loads are assumed according to [102]. Only gravity actions are considered, wind and seismic actions are assumed to be carried by a bracing system. In all case studies, action effects are calculated using a linear elastic model with uncracked sectional stiffness (LEU).

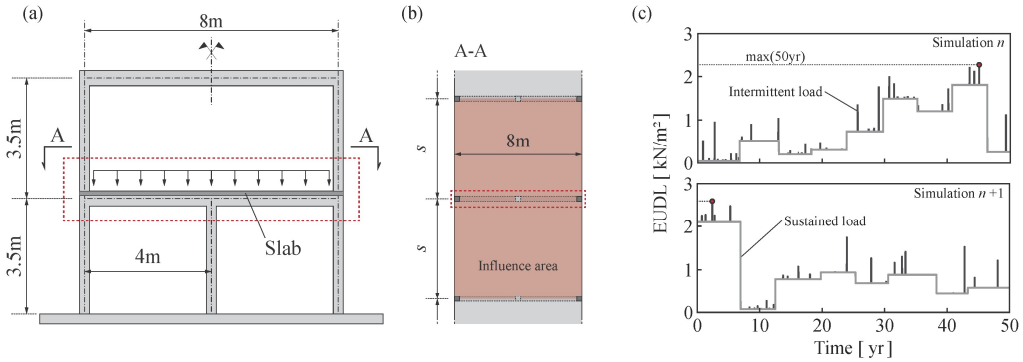

Fig. 32 *(a) Elevation and (b) plan view of the investigated office building; (c) simulations of 50-year live load for s=6 m.*

The variability of the structural self-weight, denoted by G_1, is modelled considering the geometrical and the specific weight variability according to [28]. For non-structural self-weight, G_2, a general model is not available since it largely depends on the types of building and on common construction practices of different countries. In this report, the variability of G_2 is modelled using a discrete choice model to consider a large number of possible combinations of screed, insulation, flooring, ceiling and partition walls. For each of the above components, mean values and CoV are defined based on experience on similar buildings in Switzerland. Fig. 33a shows the normal probability-plot of G_1 and G_2 distribution resulting from 10'000 simulations. Besides showing that a normal distribution is a good fit for G_1 and G_2, it can be observed that the CoV of G_2 is much larger than of CoV of G_1, which reflect the large variability of non-structural self-weight in buildings. These results refer to a building with an intended use as an office and a spacing *s* equal to 6 m. The live load, *Q*, is modelled according to part 2 of the JCSS report [28] with the influence area assumed as shown in Fig. 32b (shaded red area). Each simulation lasts 50 years and leads to a maximum value of EUDL (Equivalent Uniform Distributed Load) as shown in Fig. 32c. Fig. 33b shows the log-normal probability-plot of the live load distribution, *Q*, resulting from 10'000 simulations. It confirms that a LN distribution is a good fit for the distribution of *Q*. Besides the office space, the other investigated uses are: residence, hotel, lobby, retail and classroom. The same methodology described above and shown in Fig. 32c is used to determine the distribution of *Q* for each intended use and spacing of the frame, *s*.

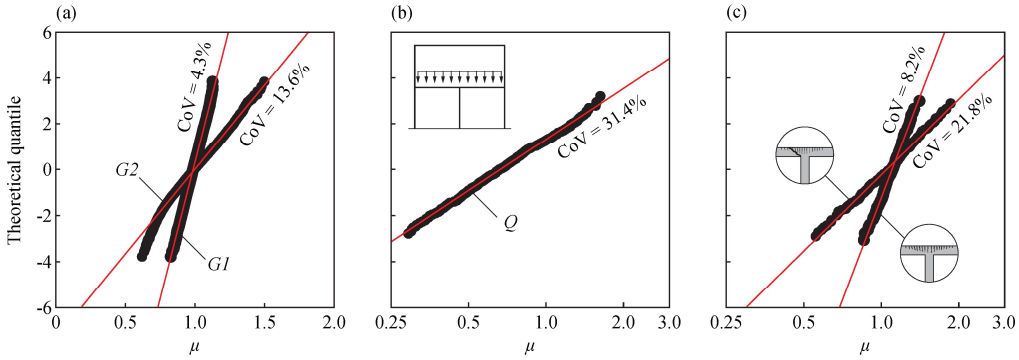

Fig. 33 *(a) Normal probability-plot of G_1 and G_2; (b) log-normal probability-plot of Q; (c) log-normal probability plot of the sectional resistance R for flexural failure and shear failure; s=6m, intended use as office, design life of 50 years.*

Tab. 9 presents the characteristic load values and the distribution parameters as a function of the spacing *s* for an intended use as office space. The representative value of the non-structural self-weight is calculated considering the mean values of the discrete choice model. It has to be noted that, according to EC1 [102] linear load of partition walls cannot exceed 3 kN/m to assume the load uniformly distributed. This threshold is satisfied in the discrete choice model used for calculating the distribution of G_2.

Tab. 9 *Characteristic value and distribution parameters of G1, G2 and Q for an intended use of the building as office space and increasing spacing (s) between frames*

s [m]	G_{1k} [kN/m]	G_{2k} [kN/m]	Q_k [kN/m]	G_{1k}/G_{2k}	G/Q	Distributions					
						G_1 [kN/m]		G_2 [kN/m]		Q [kN/m]	
						Mean	CoV [%]	Mean	CoV [%]	Mean	CoV [%]
4	17.4	12.4	12.0	1.41	2.49	0.99	4.48	12.9	13.6	0.79	35.0
5	24.2	15.5	15.0	1.56	2.64	0.99	4.42	16.1	13.6	0.73	32.7
6	31.9	18.6	18.0	1.71	2.80	0.99	4.34	19.3	13.6	0.69	31.4
7	40.4	21.7	21.0	1.86	2.96	0.99	4.29	22.5	13.6	0.66	30.2
8	48.0	24.8	24.0	1.94	3.03	0.99	4.27	25.8	13.6	0.63	29.4
9	58.3	27.9	27.0	2.09	3.19	0.99	4.23	29.0	13.6	0.61	28.7
10	67.2	31.0	30.0	2.17	3.27	0.99	4.21	32.2	13.6	0.60	27.8
11	79.2	34.1	33.0	2.32	3.43	0.99	4.18	35.4	13.6	0.59	27.9
12	92.3	37.2	36.0	2.48	3.60	0.99	4.15	38.6	13.6	0.57	27.6

The shear resistance and resisting bending moment, denoted respectively with R_{Shear} and R_{Flex}, are calculated according to Section 8 of EN 1992-1-1:2023 while their variability is calculated using the statistical distributions of materials strength, geometric and models variabilities according Section 1 of this report. Fig. 33c shows that a log-normal distribution is a good fit for both resisting moment and shear resistance calculation variabilities. It can also be observed that the CoV of the shear resistance calculation is much larger than the resisting moment calculation. This is mainly due to the large uncertainty in the model uncertainty for the calculation of the shear resistance for members with shear reinforcement, see [104].

Tab. 10 *Statistical parameters of the random variables used to perform reliability analysis for the investigated case studies. If a range is given, the value varies for buildings with different spacing s and intended use*

Variable	Distribution	μ	V [%]
E_{G1}	Normal	0.98 1.00	4.1 4.9
E_{G2}	Normal	1.00	13.6
E_{Q}	Log normal	0.55 0.80	19.1 58.3
$R_{Flex.}$	Log-normal	1.09 1.12	8.1 8.4
R_{Shear}	Log normal	1.07 1.14	20.4 22.9
θ_E	Log-normal	1.00	6.5

Tab. 10 presents the distribution parameters of the random variables used to perform the reliability analyses for all the investigated case studies. The limit state function is formulated in the classical form as shown in Eq. 48. The uncertainty in calculating action effects is considered as an independent random variable that multiplies the action effects calculated using the adopted mechanical model. In the presented case studies, a Linear Elastic Uncracked (LEU) model is adopted, and each section is designed so that $R/E = 1$. Therefore, the distribution of θ_E is assumed for a LEU mechanical behaviour considering $\zeta_{EL} \leq 1.1$ as shown in Tab. 10, see Fig. 27.

$$g(R,E) = R - E = R - (E_{G1} + E_{G2} + E_Q) \cdot \theta_E \tag{48}$$

$$\gamma_{Sd} = \mu_{\theta E} \cdot \exp(\alpha_{\theta E} \cdot \beta_{tgt} \cdot V_{\theta E}) \qquad \text{with} \qquad V_{\theta E} < 20\% \tag{49}$$

Sensitivity factors α, are calculated for each variable using the FORM (First Order Reliability Method) analysis. Based on the sensitivity factor relative to the model uncertainty in action effects ($\alpha_{\theta E}$), the partial safety factor γ_{Sd} is calculated using Eq. 49 where $\beta_{tgt,50y}$ is assumed equal to 3.8 according to EN 1990:2023 [7]. The choice of β_{tgt} depends on the level of risk acceptance at the societal level and is not treated in this report. For details regarding the FORM analysis and the derivation of the partial safety factors, refer to [105]. In addition to the case studies described above, a parametric study was performed to investigate the influence of V_Q, V_R and G/Q on γ_{Sd}. In particular, V_Q is varied between 15 and 70%, V_R is varied between 5 and 25% and G/Q is assumed equal to 1.5 and 3.5, where $G = G_1 + G_2$.

Fig. 34a and 34b present the results of the parametric analysis while Fig. 34c and 34d present the results of the investigated case studies. For all plots two axis labels are provided, on the left axis indicating the value of $\alpha_{\theta E}$, on the right indicating the corresponding value of γ_{Sd} calculated using Eq. 49.

Fig. 34a shows the variation of $\alpha_{\theta E}$ and γ_{Sd} as a function of V_Q for various values of V_R while Fig. 34b shows the variation of $\alpha_{\theta E}$ and γ_{Sd} for two selected values of V_R with G/Q equal to 1.5 and 3.5. Generally, results from the parametric analyses show that $\alpha_{\theta E}$, and consequently $\gamma_{Sd,}$ decrease with increasing values of V_R and V_Q. Also, the ratio G/Q has no influence if V_R is large, on the other hand, if V_R is small, an increase of γ_{Sd} is observed for larger values of G/Q. Fig. 34c and 34d show that the results obtained from the investigated case studies are within the boundaries found with the parametric analyses.

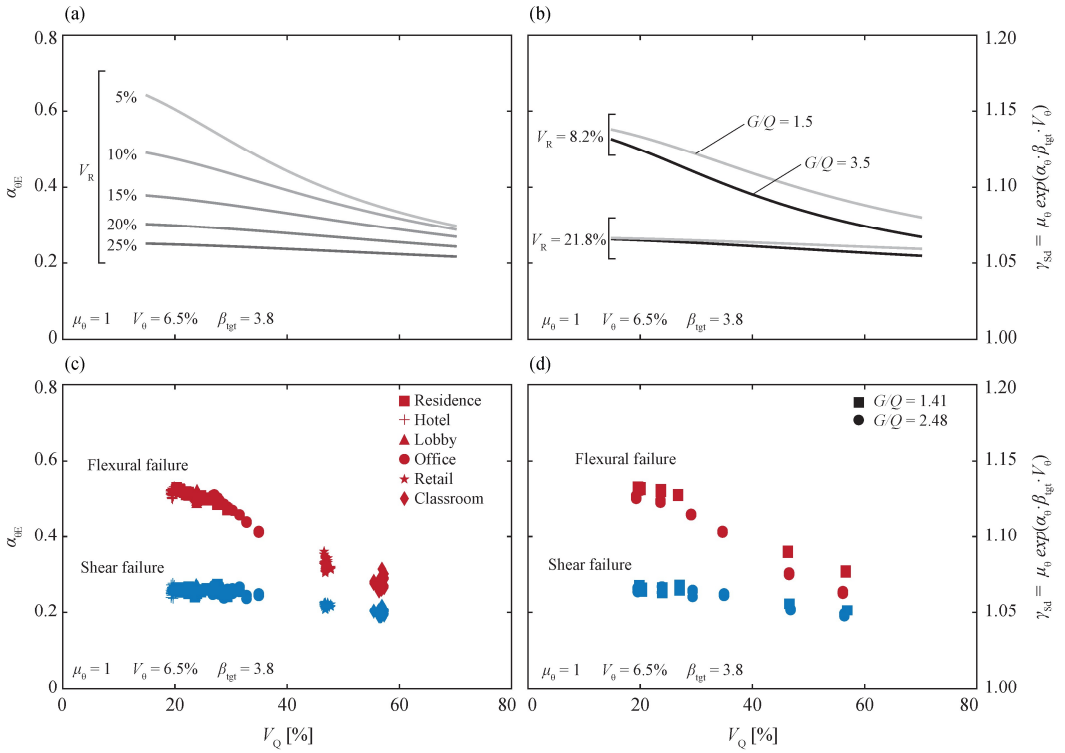

Fig. 34 *$\alpha_{\theta E}$ and corresponding γ_{Sd} as a function of V_Q resulting from: (a) parametric analysis for various V_R; (b) parametric analysis for two selected V_R and G/Q = 1.5 and 3.5; (c) case studies for various V_R; (d) case studies for two selected V_R and G/Q = 1.5 and 3.5.*

These results can be explained considering that the sensitivity factors, α, represent the weight of each random variable for a defined limit state function and the sum of their square is equal to unity by definition. Thus, if the weight of one variable increases in the limit state function, the weight of the other variables must decrease. This explains the finding that for flexural failures (with lower CoVs of the resistance model), the required γ_{Sd} factor is larger than for shear failures (where the CoV of the resistance model is significantly larger). Nevertheless, this influence can be compensated by the fact that for flexural failures, which are typically more ductile than shear failures (see Fig. 22), the load-bearing capacity shows smaller uncertainties (smaller CoV and higher mean value of ratio θ_{QR} as shown in Fig. 29. In other words, underestimating an action effect when the behaviour is ductile behaviour has typically smaller consequences then when it is brittle.

Based on the results of the parametric analysis, the performed simulations and the obtained distributions of θ_E, it is reasonable to assume a value of γ_{Sd} between 1.05 and 1.15 as initially specified by [64] but based on significantly different motivations. It is important to note that the model uncertainty related to changes of the structural system during construction (including the redistributions due to creep) is not covered by the estimation of the factor γ_{Sd} presented in this report. This means that for structural systems subjected to significant system changes (e.g. high-rise buildings), a sensitivity analysis should be performed to determine the most relevant parameters influencing the calculation of action effects and load bearing capacity.

It is a matter of fact that the model uncertainty related to the action effects significantly depends on the complexity and the level of statical indeterminacy of the structure. In fact, only the influence of geometrical uncertainties can have an influence in statically determinate structures, whereas the uncertainties can increase for highly indeterminate complex structures. In addition, for complex structures, additional uncertainties can be expected with respect to the models implemented in commercial analysis software tools and the choices by the designer in modelling the structures. This applies for linear elastic calculations, but also to a larger extent for nonlinear analyses. These considerations, which

were not the aim of the present work, deserve to be investigated in the future also accounting for the increasing complexity of the analysis tools used nowadays.

2.7 Conclusions

This section investigates the model uncertainty in action effects and load-bearing capacity calculations for statically indeterminate concrete structures accounting for the type of mechanical model used and for various failure modes. Based on the presented investigations, the main conclusions are:

1. Compared to more refined models, the Linear Elastic Uncracked model leads to larger CoV of model uncertainty in load bearing capacity calculation (θ_{QR}); however, the mean of the distribution is larger, leading to similar tail's distribution, thus, similar safety margin;
2. For Linear Elastic Uncracked models, an over-design of one or more components of a statically indeterminate system influences the CoV of the model uncertainty in action effects calculation (θ_E);
3. Refined calculation models lead to more accurate results and generally to lower CoV of the internal forces ratio θ_E and of the load bearing capacity ratio θ_{QR};
4. The failure mode influences the model uncertainty in load bearing capacity calculation but it does not influence the model uncertainty in action effects calculation. Larger CoVs of θ_{QR} are observed for brittle systems, independently of the calculation model.
5. Plastic calculation models with unlimited deformation capacity, if performed without ductility requirements (4L), lead to very large CoV and can lead to unsafe results. Limiting the deformation capacity, or verifying that ductility requirements are met reduces considerably the CoV.
6. Considering supports deformability allows larger redistribution of forces and leads to slightly smaller CoV.
7. Parametric analyses and investigated case studies show that the partial factor γ_{Sd} to cover the uncertainties of the internal force calculation ranges between 1.05 and 1.15. It must be noted that the estimated γ_{Sd} factor does not account for uncertainties related to structural system variations during construction or structural modelling of complex structures. These additional uncertainties, which deserve to be investigated more in detail, significantly depend on the complexity of the structure, the construction method, the tools used and the experience of the designer.

3 Model uncertainties load bearing capacity calculation of steel-concrete composite structures and partial factor for structural steel

3.1 Introduction

In parallel to the more thorough study on conventional reinforced concrete (RC) structures, a similar investigation is presented in this report on steel-concrete composite structures. In fact, since in Switzerland steel bridges are rare compared to steel-concrete composite beam bridges, this study focuses on the latter (i.e. steel bridges are not considered). As already mentioned, the aim of this investigation is to quantify the model uncertainty in action effects related to the modelling of the mechanical behaviour. The model uncertainty related to calculation of the sectional resistance is not considered, It is removed by making the theoretically predicted resistance of each member of the statically indeterminate composite system equal to the experimental value. By adopting the same technique used for RC structures and presented in Chapter 2, one wants to determine whether the composite structures behaviour is similar to that of RC structures; in other words, to determine if the model uncertainty covered by the partial factor γ_{Sd}, see Fig. 18 and [135], should be differentiated in function of the material/code and its respective design modelling assumptions. Although the analysis technique is similar to that used for RC systems, some differences in the mechanical modelling and verification methods do exist and are discussed herein.

But before, in this introduction, a discussion on the partial factor for structural steel is conducted, again in analogy to that for concrete and reinforcing steel. The introduction ends with a section on random variables definition in model uncertainty.

In the first part of this Chapter, the technique already proposed and validated for textile reinforced concrete [65] and RC beams in Chapter 2 is used to assemble statically indeterminate structures. Specifically, experimental force-displacement responses (F-δ) are obtained by assembling simply supported steel-concrete composite beams tested in a 3-point bending setup, Fig. 35 illustrates such a system. In a second part, the technique is further developed to relate such systems to continuous steel-concrete composite beams and study those.

To illustrate the concept, in Fig. 35 one can see that the experimental response of the system (“sys”) is obtained by superposing two simply supported beams crossing each other at the concentrated load application point. Note that the composite beams represented are in this case both subjected to positive bending. By imposing a displacement at the loading point and knowing the experimental F-δ response (load-deflection) of each beam as obtained from the literature, the F-δ response of the system can be determined by adding the force acting in each member of the system simulating a displacement-controlled test. Thus, prior to any analysis in this investigation, an experimental database with all relevant and sufficiently well reported tests was created and is presented in the next section.

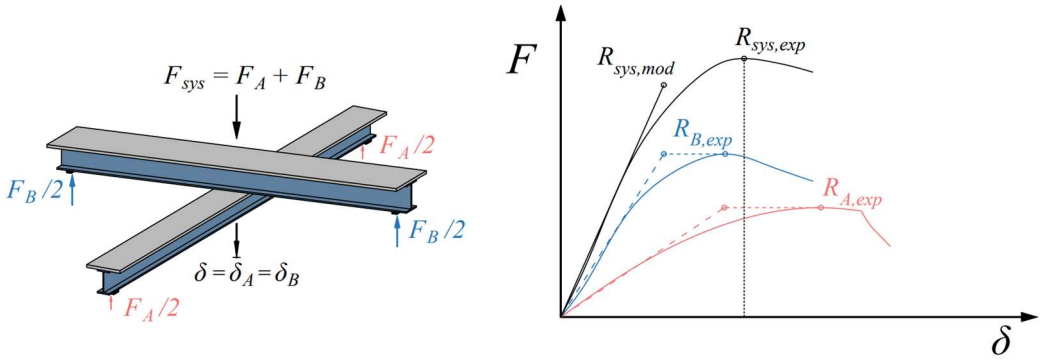

Fig. 35 *Example of assembled system with two composite beams; experimental response of the system (black) assembled with beams (red and blue) and linear-elastic uncracked model prediction (dashed).*

3.1.1 Partial resistance factor for structural steel

According to SIA codes

For the design of new structures, the SIA 260 and SIA 263 codes prescribe the use of a characteristic value of yield strength f_{yk}, or of the ultimate strength, f_{uk} (usually denoted simply as f_y and f_u), which are related to a certain value of elastic yield strength R_e *or* ultimate strength R_m "guaranteed" by the manufacturers, usually defined as 5% fractiles of the respective distributions [66]. For structural steel, the resistance side factor of safety – γ_M – is equal to 1.05 for cross-section, element and stability checks, which all depend on f_y [67]. This factor covers the material uncertainties (specific to steel properties f_y and E) and the model uncertainties (in the resistance models).

For existing structures, to update the value of resistance used in the examination of a structure, it is required by Annex C of SIA 269 to define a target safety level by means of the reliability index β_0 (SIA 269, Annex B.1: "The structural safety requirement is specified using the target value of the reliability index or by the individual risk.") [68]. As introduced by Table 2 of Annex B of SIA 269, the target value β_0 is a function of the consequences of a structural failure r and the efficiency of interventions EFM. The estimation of both r and EFM as a function of actual cost (cost of failure, repair, safety and risk reduction) requires many assumptions. Instead, one can also assume some reasonable values for these two quantities, which leads for example for a highway bridge to assume: important consequences of a failure ($5 < r < 10$), and efficiency of interventions EFM = 1 (according to SIA 269 Annex B.3, which yields a reliability index $\beta_0 = 4.4$.

Then, following the assumption of Annexes C.1 and C.2 of SIA 269, it is presumed that the resistance parameter of interest, here the yield strength, follows a log-normal distribution and the updated examination value can be obtained as given below, equ. (50) and (51):

$$f_{yd,act} = f_{ym,act} \cdot e^{(\alpha_R \beta_0 \delta_R - \delta_R^2)} \tag{50}$$

with :

$$\delta_R^2 = \ln(v_{R,act}^2 + 1) \tag{51}$$

Note that the definition of the characteristic value of, for example, yield strength f_{yk} as a fractile of the distribution, is not needed here.

According to current knowledge as well as developments within the Eurocode 2nd generation, the approach described in the Swiss codes (SIA 269:2011) for updating

material properties for existing structures is somewhat inconsistent with the safety factor calibration framework for the design of new structures. In the SIA for new structures, the safety factors are calibrated using the material and model uncertainties present in the various load-bearing capacity verifications. But, in the evaluation of the updated design value of $f_{yd,act}$, see Eq. 50, the term δ_R (representing the variability accounted for in the design value calibration) only depends on the statistical distribution of the steel yield strength, thus the inherent uncertainty in the resistance model or empirical equation is not accounted for in $f_{yd,act}$. Therefore, it seems that the approach following the guidelines of SIA 269:2011 is somewhat simplistic compared to the inherent nature and origin of the current safety factors. Furthermore, as was the case in the first generation of Eurocodes, the current safety factors result in safety levels that are not necessarily uniform across all design equations and "not even within a single design rule" as stated by Knobloch et al [71].

Proposed partial resistance factors in line with the upcoming Eurocode 3 Part 1-1, EN 1993-1-1:2022 [70]

In view of the above observations, to retain the current format of equations proposed by the Swiss standards with the corresponding factors of safety, a consistent method for obtaining characteristic (i.e. nominal) values for both new and existing structures is to base the calibration on the steel production requirements that are introduced in Annex E of EN 1993-1-1:2022 [70] as well as in accordance with EN 1990. Even if the new informative Annex E is about calibration of partial factors for buildings and not bridges, interest is less pointed towards the actual calibration values to be used in the new Eurocode 3, which stay similar to the former ones, but more on the information about steel properties presented in Table E.1 of Annex E [70].

As a matter of fact, during the recent SAFEBRICTILE project [73], whose aim was to contribute to the harmonization of reliability levels across design rules for steel structures, material and geometrical properties of various steel products were consistently collected [71]. Based on the collected data, statistical distributions for the most relevant mechanical and geometrical properties for a wide range of products and grades commonly used in Europe were specified. The latter are now included in Tables E.1 and E.2 of Annex E of EN 1993-1-1:2022. The distributions, assumed log-normal, are specified with their mean value, coefficient of variation (CoV), 5% fractile and 0.12% fractile values [71]. As mentioned by Knobloch et al., the last two values “may mainly be used by producers of steel construction products to verify the compatibility of their production statistics with the basic assumptions underlying the recommended values of γ_M in the standard” [71]. This is in line with the Swiss prescription of a minimum requirement for the 5% fractile that needs to be guaranteed by producers and which is related to a characteristic value of material strength used in design. Also, SAFEBRICTILE concluded that the value of the partial safety factor γ_{M1} :

1. γ_{M1} =1.0 as recommended in EN 1993-1-1 for stability verifications is only justified when the nominal values are directly taken as $f_y = R_{eH}$ and $f_u = R_m$ (the lower value of the specified range) from the relevant product standard.
2. when using the values in the tables of the design codes (EN 1993-1-1:2022 or SIA 263:2014) for steel according to EN 10025 (all parts), EN 10210 (all parts) and EN 10219 (all parts) and Table 5.2 for steel according to EN 10149 (all parts), the partial safety factor γ_{M1} shall be increased.

In the current National Annex for Switzerland, γ_{M1} =1.05 is used. This adequately covers the difference between option 1) and 1) based on reviews by ETH Zurich [74].

Thus, the safety factors $\gamma_{M0} = \gamma_{M1} = 1.05$ cover the choice of option b) with sufficient reliability and are already well established in Switzerland by SIA 263. Finally, defining the safety factors γ_{M0} and γ_{M1}, which are both used in verifications with f_y as the strength value, with the same numerical value is also based on practical considerations: this avoids inconsistencies and “jumps” in the load-bearing capacity at the transition between structural components with and without a stability issue.

Regarding existing structures, the authors believe the approach and Table E.1 of Annex E of EN 1993-1-1:2022 also apply for structural steels since those produced in the early 1970s with the introduction of the Euronorm 25/72 [72] and the starting of a European steel properties database [73]. However, in this case, it is proposed to compare the statistical distribution of the measured R_{eH}, or R_m, against the one specified by Table E.1, which can lead to the four situations described in Fig. 36. If it cannot satisfy a steel grade listed, cases c or d, then in order to obtain an equivalent production steel grade, it is proposed that the nominal steel grade that would correspond in Table E.1, i.e. the value $f_{y,nom}$, is varied such that the test result distribution satisfies the production requirements with regard to this equivalent steel grade. For example, in the case of R_{eH}, the ratio $R_{eH,mean}/R_{eH,min}$ and CoV assumed for the presumed steel grade are to be considered to find the nominal steel grade value $f_{y,nom}$ and thus the f_{yk}, to be used in the verifications [75]. Examples of following both the approach from Annex C of SIA 269 and the one presented above lead to either similar values or conservative ones with the adapted Annex E approach, which is logical since it includes more uncertainty sources.

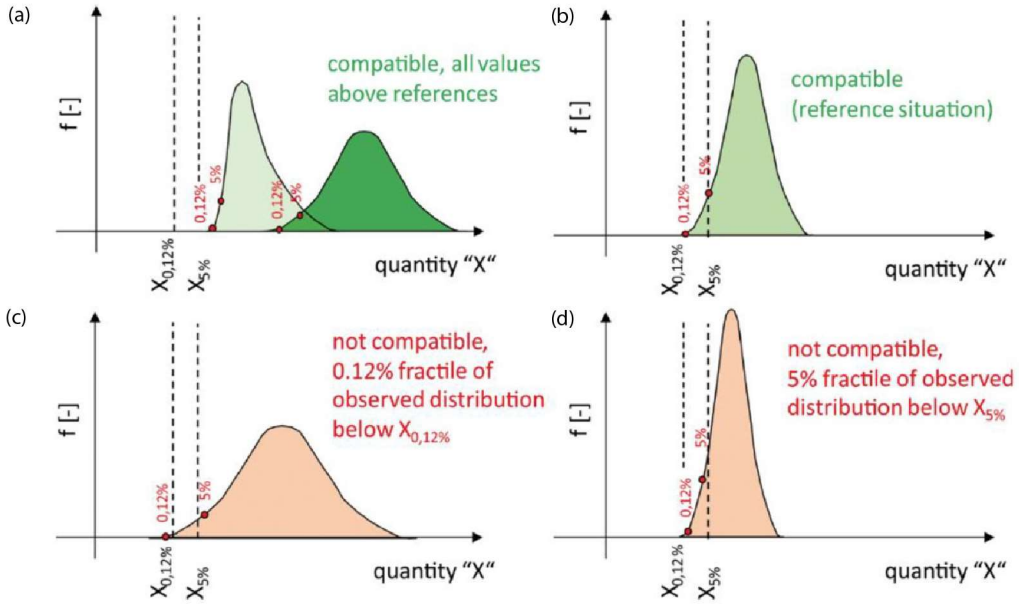

Fig. 36 *Schematic representation of the verification procedure for production data for compatibility with annex E [71].*

3.1.2 Model uncertainty, random variables definition

In design and modern codes, the quantification of the model uncertainty is based on the global load bearing capacity of the system (Annex C of EN 1990:2023 [7]). Also, the sectional resistance is often calculated considering material's non-linearities while action effects are usually calculated with a simplified linear-elastic mechanical behaviour, incl. in the case of composite structures [108]. In some rare cases, plastic analyses or non-linear analyses are performed to determine action effects and load-carrying capacity. In this investigation, the model uncertainty related to the calculation of the sectional resistance (and the resistance of each beam) is not investigated. On the other hand, the load-bearing capacity of the system adopting various mechanical behaviour is investigated. In other words, the random variable is referred to as the model uncertainty related to the global load-bearing capacity θ_G, as defined in the previous chapter, Equ. [40] and [65], repeated below for simplicity:

$$\theta_G \equiv \theta_{QR} = \frac{R_{sys,exp}}{R_{sys,mod}} \tag{52}$$

Two typical cases of mechanical behaviour modelling are shown in Fig. 37, where:

$R_{sys,exp}$ peak value of sum of experimental responses (black in Fig. 37)

$R_{sys,mod}$ sum of the individual model *F-δ* responses (blue in Fig. 37 left and red in Fig. 37 right) at $\delta_{sys,mod}$, determined as the peak value of the modelled response of the cross-beam system

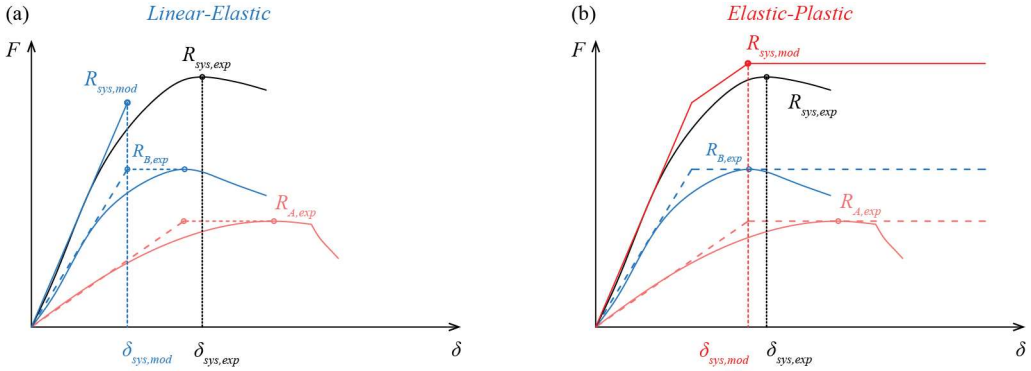

Fig. 37 *Modelling of the mechanical behaviour: a) linear-elastic and b) elastic-plastic.*

Herein, the resulting distribution of the random variable θ_{QR} is fitted with a log-normal distribution and to graphically check the accuracy of the tail distribution approximation, data are represented in a probability plot, see previous Section for details on this representation. As for the reinforced concrete elements, the tail fitting is performed on the 5th percentile of the overall data; essentially the latter will be used to discuss the results. Note that by computing a 5th percentile, one uses the most commonly defined percentile level for representative values. In this way, some considerations concerning the model partial factor value, namely γ_{Sd}, can also be made.

3.2 Experimental database collection

The first step of the work is the collection of test data to perform the analyses. To do this, careful gathering and screening was undertaken to collect enough simply supported beam tests. The experiments retained in the database must contain well-documented information (geometry, load-displacement response, material properties). Unfortunately, there is limited literature on experiments with typical bridge girders. Most of the data collected reflect experiments on composite beams with cross-sectional dimensions closer to those used in conventional building designs. Nevertheless, it was possible to collect the results of 81 experiments. This set of experiments includes both beams tested under positive (45) and negative bending (36). The failure mode observed during the experiments was either in shear, in fracture of steel or crushing of concrete. The screened literature list is summarized in Tab. 11.

***Tab. 11** References for the composite beams database*

Author	Year	Title	Positive M	Negative M
Barbato et al. [109]	2014	Probabilistic nonlinear response analysis of steel-concrete composite beams	1	-
Wang & Chung [110]	2006	Integrated analysis and design of composite beams with flexible shear connectors under sagging and hogging moments	4	2
Toprac [111]	1965	Strength of three new types of composite beams	6	-
Gattesco [112]	1999	Analytical modelling of nonlinear behaviour of composite beams with deformable connections	1	-
Nie et al. [113]	2007	Experimental study of partially shear-connected composite beams with profiled sheeting	5	3
Nie et al. [114]	2004	Experimental studies on shear strength of steel concrete composite beams	2	-
Fabroccino et al. [115]	1998	Non-linear analysis of composite beams under positive bending	1	-
Fabroccino & Pecce [116]	2000	Experimental tests on steel-concrete composite beams under negative bending	-	3
Zhao et al. [117]	2011	Simplified nonlinear simulation of steel-concrete composite beams	2	2
Yan et al. [118]	2017	Numerical and parametric studies on steel-elastic concrete composite beams	1	-
Zhang et al. [119]	2020	Experimental and theoretical study on longitudinal shear behaviour of steel-concrete composite beams	8	-
Zhou et al. [120]	2020	Experimental investigation of the vertical shear performance of steel-concrete composite girders under negative moment	-	5
Men et al. [121]	2020	Behaviour of steel-concrete composite girders under combined negative moment and shear	-	7
Men et al. [122]	2021	Web shear buckling of steel concrete composite girders in negative-moment regions	-	5
Men et al. [123]	2022	Shear capacity investigation of steel-concrete composite girders in hogging moment region	-	6
Ban & Bradford [124]	2013	Flexural behaviour of composite beams with high strength steel	3	-
Zhao & Yuan [125]	2010	Experimental studies on composite beams with high-strength steel and concrete	2	-
Chapman & Balakrishnan [126]	1964	Experiments on composite beams	7	-
Hoffmeister [127]	1997	Plastische Bemessung von verbundkonstruktionen unter verwendung realitätsnaher Last-verformungsansätze	-	1
Gomez Navarro [128]	2001	Experimental study of the behaviour of composite beams under negative bending moments	-	2
Baldwin [129]	1973	Composite bridge stringers	2	-
TOTAL			45	36

For each experiment, the following information is collected and kept in the database (in an Excel sheet, with separate files containing the numerical values of the *F-δ* curves):

- Material properties: Yield strength of steel (flange and web if given), concrete compressive strength, reinforcement yield strength.
- Geometrical properties: steel section dimension, (built-up or rolled section), slab height and width, span length.
- Slab connection: full or partial connection, connectors rigidity and strength
- Load configuration
- Test results: Ultimate Load, Ultimate Moment, Shear ratio ($V_{ult}/V_{w,pl}$), *F-*δ response.

3.3 Two-beams assembled system

3.3.1 Sectional analyses

Three different types of section analyses are performed to predict the moment-curvature (M-χ) relationships. The structural section analysis models are simple and are intended to reflect the types of analysis that are performed by the majority of engineers, see Fig. 38. In most cases, the Linear-elastic (*LE*) model is used to determine the distribution of forces within the structure and to determine the load-carrying capacity, while knowing that a certain margin can exist thanks to the redistribution of forces if plastic hinge formation can happen. This means that the structure is designed according to the resistance of the element that reaches yielding first.

In some cases, a plastic analysis can also be performed to consider the redundancy of a system and the redistribution of internal forces. In this case, the simplest and most efficient way is to use an elastoplastic (*EP*) model with or without imposed deformation capacity. This model is equivalent to the *LE* model until reaching the yielding limit, then a plateau is defined, which can have a deformation capacity limit or not.

A type of cross-sectional behaviour models more representative of reality consists of Non-Linear (*NL*) models. *NL* models can be defined in multiple ways, depending on the non-linearities accounted for. Non-linearities can arise from material non-linearity (constitutive law) or geometric non-linearity. In the current study, it has been chosen to only account for material non-linearity. This choice is explained by the fact that most of the structural analyses carried out by engineers use simple and efficient models such as the *LE* and *EP* models. It is rare that highly refined non-linear models are used, so it seemed that the consideration of the non-linearity of the material(s) is sufficient to be representative of engineering practice, without considering more complex models in the current study (i.e. with geometric non-linearities).

To determine *LE* and *EP* models slope, the NL curve (rigidity) initial slope in the elastic stage is used, see next subsections.

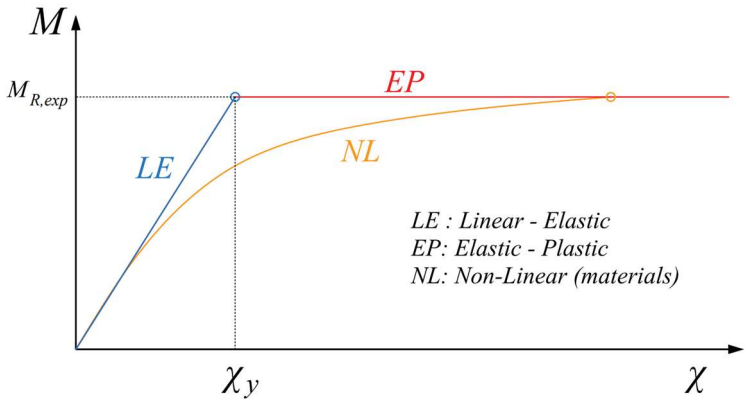

Fig. 38 *Sectional analysis models.*

3.3.2 Non-Linear model

This paragraph presents the assumptions used in the non-linear model to determine the moment-curvature relationship of steel-concrete composite sections. The section analysis is performed numerically using a fibre-based model, Fig. 39 presents the algorithm procedure. The material properties are experimental values taken from the test database.

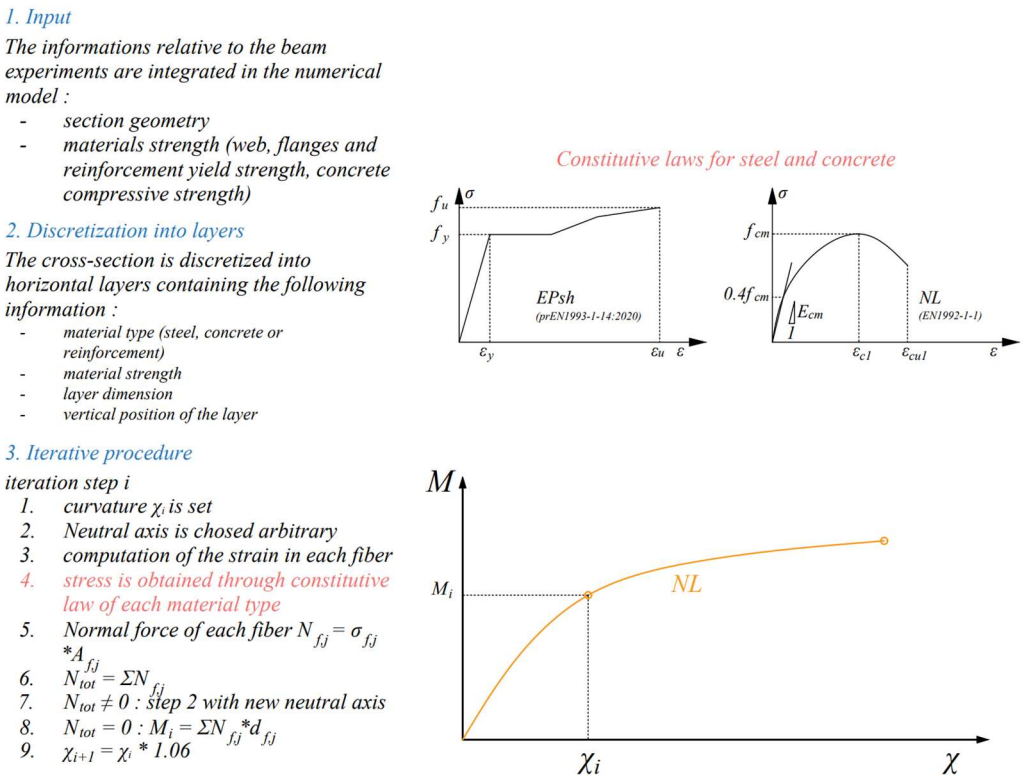

Fig. 39 *Algorithm procedure for the non-linear model.*

The ultimate curvature is reached when one of the extreme fibre fractures. If the section is subjected to positive bending: the concrete slab crushes, or the bottom steel flange fractures. Under negative bending, the slab is not considered but the fracture of the reinforcement becomes determining (over the fracture of the steel in compression, the experiments being designed to avoid flange stability problems, see also the subsection on the influence of the section class). The fracture criteria for the fibres are thus conventionally fixed as the following: ε_{cu1} = 3.5‰ for concrete (specific deformation at crushing) and ε_u = 5% for all steels (specific deformation at ultimate strength).

The initial elastic stage slope (rigidity) of the NL curve is used to define the *LE* and *EP* models slope.

3.3.3 Structural analyses load-deflection response

The different moment-curvature relationships were calculated using the models presented above. With this information, the load-displacement curves (*F*-δ response) can be determined for each beam and each model (LE, EP, and NL) as presented in Fig. 40. The computation is performed analytically by integrating the curvature along the beam, respecting the boundary conditions. For each load step, the deflection at midspan can be determined and the load-deflection curve can be constructed until reaching the experimental failure load.

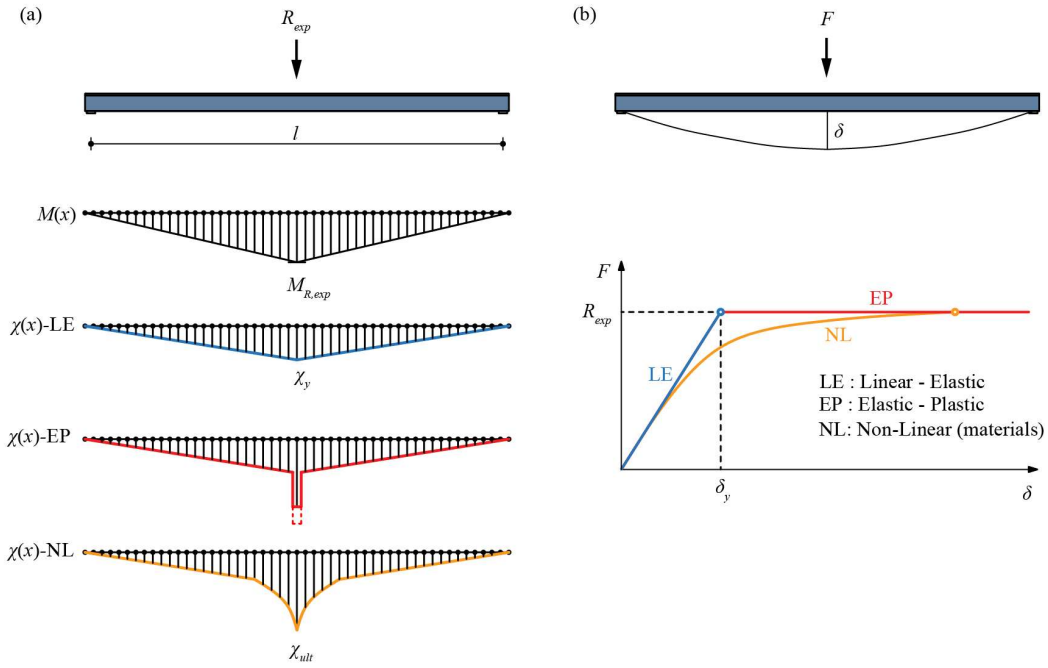

Fig. 40 *Algorithm procedure for the non-linear model: (a) bending moment $M(x)$ and curvature $\chi(x)$ along the beam and (b) the resultant F-δ curves for different analysis approaches.*

Each of the beams obtained from the literature presented in Tab. 11 was analysed to determine the *F*-δ responses according to the different models investigated. In addition, the experimental *F*-δ curves have been digitized, which allow to perform comparisons.

3.3.4 Response of the assembled two-beams systems

As described in the introduction, structural responses of statically indeterminate structures are determined by combining the experimental *F*-δ responses of two simply supported beams as shown in Fig. 41. To evaluate the model uncertainty, the *F*-δ response of the system is compared with the response of the models resulting from the structural analyses adopting various mechanical behaviours.

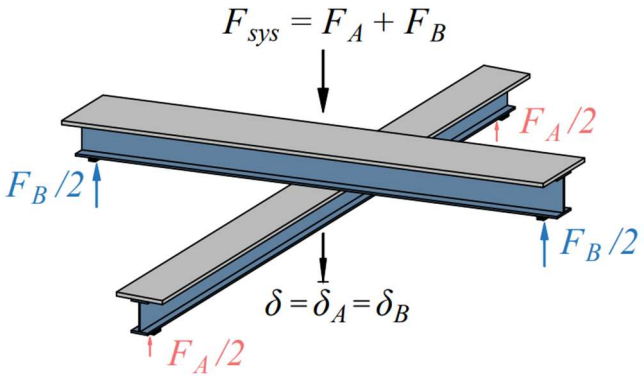

Fig. 41 *Illustration of the statically indeterminate system assembled with two simply supported beams.*

In total, four different mechanical models are compared as illustrated in Fig. 42. In addition to the three models presented in Subsection 3.3.1, an additional model is investigated: Elastic-Plastic with limited deformation capacity (*EPLim*). This model is implemented to reduce uncertainties related to the deformation capacity before failure of one of the beams. For the model with limited deformation capacity, the deformation capacity of each beam is

limited by imposing it as the deflection at the peak load, as reported in the experimental *F-δ* responses. The use of limited deformation capacity can be explained by the section class requirements to perform plastic analyses.

These four models are believed to be representative of common engineers' practice in the calculation of internal forces and load-bearing capacity.

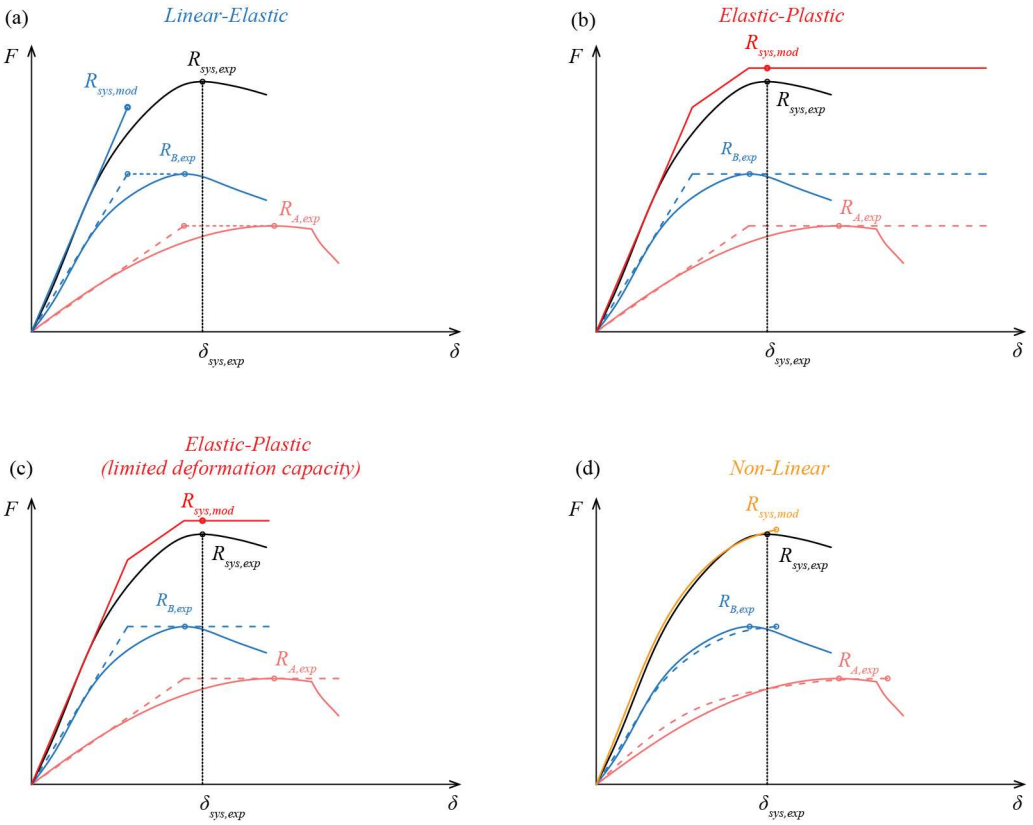

Fig. 42 *Four mechanical models to study the response of the assembled two-beams system: (a) Linear-Elastic; (b) Elastic-Plastic; (c) Elastic-Plastic (limited deformation capacity) and (d) Nonlinear.*

3.3.5 Ductility class indicators

Initially, differentiation according to the type of action (positive or negative bending) was used as a mean of differentiating ductile from brittle behaviour. Observing the results, no significant correlation with the failure mode was noticeable.

Then, to better differentiate the type of failure behaviour considering instability effects, the ductility of each beam according to the experimental force-displacement response was used. Herein, the ductility indicator chosen is the ratio between the displacement at failure δ_R and the displacement at first yield δ_y, see Fig. 43. The first yield displacement δ_y is calculated with the elastic stiffness of the section (according to the geometric characteristics of the section and yield strength of materials given in the test report). As for the displacement at failure δ_R, it is characterized as the maximum displacement before failure or when the resistance falls to 90% of the maximum bearing capacity of the beam (if a downward part is observed in the experimental force-displacement response).

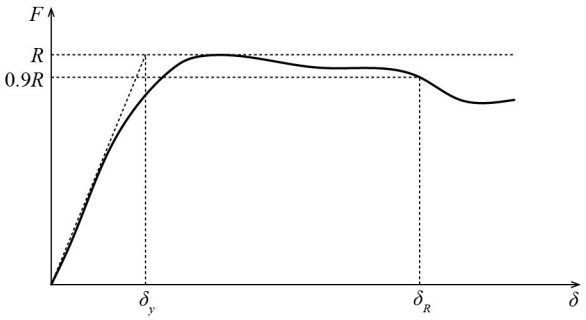

Fig. 43 *Typical experimental force-displacement response and beam ductility indicator.*

Furthermore, each experimental beam was classified according to the standardized ductility indicator, namely its cross-section class. This is the criterion in structural steel codes for defining the allowed calculations methods in section and/or for calculating internal forces, each beam being classified according to slenderness limits for its web and flanges in function of the panel supporting conditions and loading mode. Tab. 12 summarizes the most restrictive slenderness limits given in EN 1993 [130], that is for panels in pure compression. These limits were chosen because in composite beams under negative bending, most of the web panel is under compression.

Tab. 12 *Cross section class definitions and corresponding slenderness limits*

Cross-section class	Internal forces	Section resistance	h_w/t_w (web)	c/t_f (flange)
1	Plastic	Plastic	< 33 ε	< 9 ε
2	Elastic	Plastic	< 38 ε	< 10 ε
3	Elastic	Elastic	< 42 ε	< 14 ε
4	Elastic	Elastic reduced		

Where the expression for the steel grade coefficient is:

$$\varepsilon = \sqrt{\frac{235}{f_y}} \tag{53}$$

The indicators ductility and cross-section class are evaluated in Fig. 44a and 44b by plotting the ductility of each beam against the web slenderness (as this is the main determinant panel in our case), in order to establish whether a significant relationship could be observed.

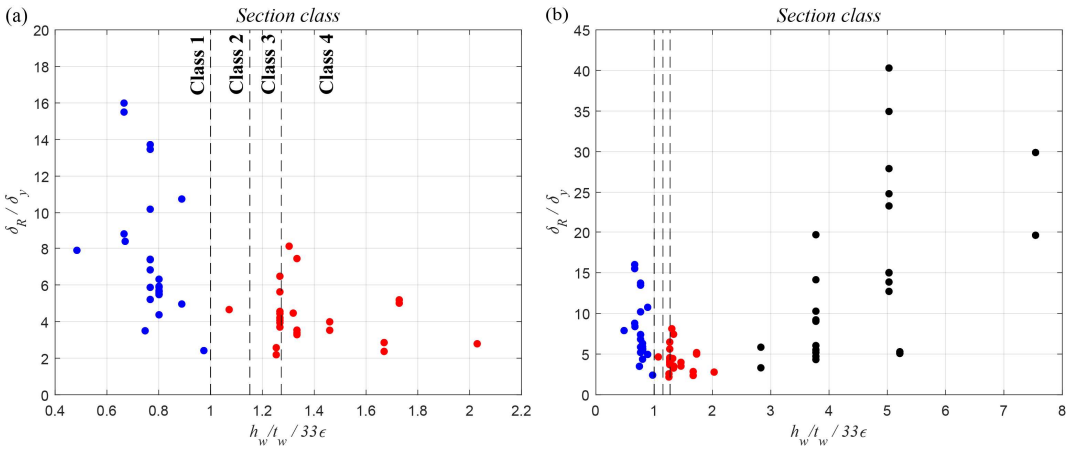

Fig. 44 *Web slenderness* h_w/t_w *against beam ductility a) beams with medium web slenderness, up to 2.2, b) all beams, incl. those with high web slenderness.*

Most of the sections of class 1 (blue dots) are very ductile, while the ductility tends to decrease for the higher classes of sections (red dots). In Fig. 44b, the black dots represent beams with high web slenderness that are closer to a bridge-type section, but were designed to study shear force behaviour and contain stiffeners to be able to use the contribution of the web panels with a direct tensile force. In this case, the rotation capacity necessary to activate this tension diagonal through the web panel must be sufficiently large, which in some cases results in quite high ductility values. Furthermore, as these experimental beams shown in Fig. 44b were tested in shear (with very short spans), it implies that the section could not even reach the plastic moment resistance and therefore the ductility indicator (as we calculate it) is all the greater because δ_y is reached earlier.

3.3.6 Discussion of the results

Herein, only the analyses carried out with the cross-system combinations regrouped in function of their cross-section classes are presented in detail. The experiments are separated into 2 groups: the first group containing beams with section class 1 and the second group containing beams classified as class 2 and above. The cross-system combinations therefore do not consider the moment direction (positive or negative), but the cross-section class. First the section classes 1 are combined together, then the higher classes are combined with each other, while the last type of combination consists of a class 1 beam with a beam class 2 and above. A summary of the processed combinations is given in Tab. 13. Since beams classified as class 1 are usually those under positive bending, a comparison between these two classification schemes can be made and is presented below. All the same for beams classified as 2, 3, or 4, which are most likely to be under negative bending, and the combinations of the above that are typical of a combination M+ and M-.

The main results are presented in terms of the global model uncertainty (θ_G) obtained by performing the analyses according to the different mechanical models presented above (*LE, EP, EPLim, NL*). For each model, the results are represented in the form of a probability plot. The data are fitted with a lognormal distribution. The lognormal probability plots also allow checking the accuracy of the tail distribution approximation. On the x-axis is reported the random variable θ_G (logarithmic value) while on the y-axis is reported the normal quantile in terms of standard deviation. For an exact log-normal distribution, the points should represent a straight line in the probability plot.

Tab. 13 *The different models and cross system combinations between cross-section classes*

	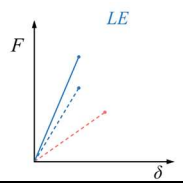	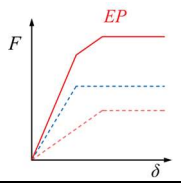	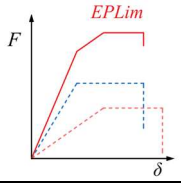	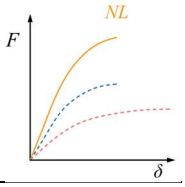
CLASS 1 - CLASS 1	903 comb.	903 comb.	903 comb.	903 comb.
CLASS 2/3/4 - CLASS 2/3/4	595 comb.	595 comb.	595 comb.	595 comb.
CLASS 1 - CLASS 2/3/4	1505 comb.	1505 comb.	1505 comb.	1505 comb.

3.3.7 Linear-Elastic model results

Fig. 45 shows the log-normal probability-plot of θ_{QR} defined in Eq. 41 obtained with the LE model. Note that in this figure and herein, the legend in blue correspond to whole dataset statistics, whereas the legend in red correspond to tail approximation statistics. For the tail

approximation, one can observe that the 5th percentile is always around the value 1.0. For the combinations between class 1 beams the tail fitting of the actual distribution is close along the curve. The behaviour is not linear but the gap is nevertheless small. The same is true for beam combinations of class 2 and higher. The behaviour is quite homogeneous over the whole distribution. When the two class types are combined, a linear behaviour is obtained on the lower half of the curve with a rather low coefficient of variation, which reflects quite well the determining cases when the weakest beam (class 2 and higher) reaches failure.

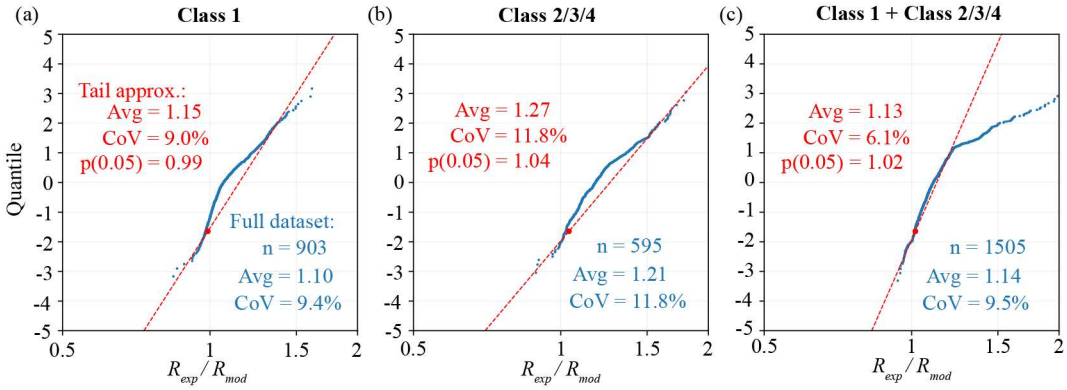

Fig. 45 *Probability plots of θ_{QR} for LE model and cross-sections combinations composed of:(a) Class 1 only (b) Class 2/3/4 combined and (c) Class 1 with Class2/3/4.*

3.3.8 Elastic-Plastic model results

For class 1 sections, better approximation of the lower tail distribution and a fractile 5% ($p(0.05) = 0.90$) are obtained, see Fig.46. The coefficient of variation is relatively small 6.1%. The main reason for this good fit is that the most extreme values have been removed because the elements with brittle behaviour are not part of the first group due to the classification according to the cross-section.

On the other hand, for classes with a cross-section greater than 1, different behaviour can be observed. In this case, the EP analysis shows values that can be very low. The lower part of the distribution has a very different shape from the rest of the distribution with a very high $CoV = 31.3\%$. Nevertheless, this result is expected because the EP model is not suitable for this section type as it does not allow for ductile behaviour.

When the two types of sections are combined, an intermediate behaviour can be observed in Fig. 46a and 46b. Having at least one of the beams with ductile behaviour allows for an improvement by tightening the distribution compared to the fully brittle case.

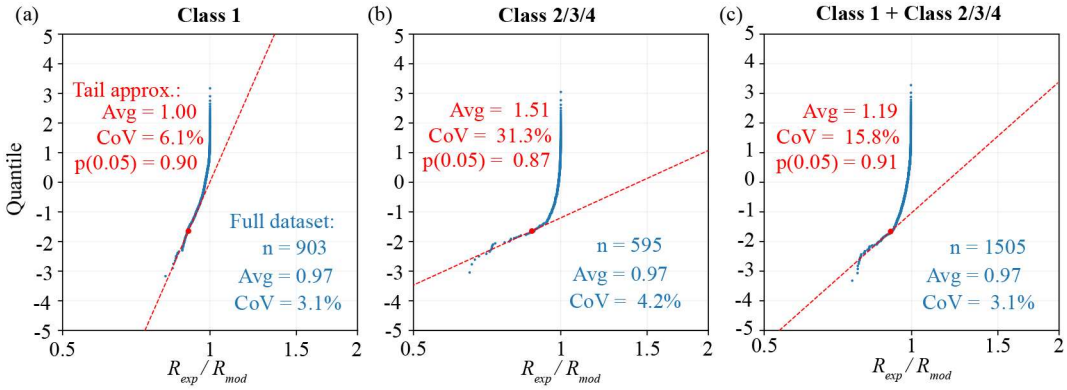

Fig. 46 *Probability plots of θ_{QR} for EP model and the different cross-sections combinations composed of:(a) Class 1 only (b) Class 2/3/4 combined and (c) Class 1 with Class2/3/4.*

3.3.9 Elastic-Plastic model with limited deformation capacity results

When considering the deformation capacity observed during the experiment within the EPLim model, see Fig. 47, for experiments using beams with cross-section class 1, the results remain identical to the EP case (Fig. 46) because their ductile behaviour allows a large deformation capacity and thus the addition of this constraint in the model has no impact on the results. On the contrary, for experiments using beams with a more brittle behaviour, this additional parameter allows to improve the results by avoiding overestimating the deformation capacity. The 5% fractile $p(0.05) = 0.92$ and the coefficient of variation $CoV = 22.9\%$ are improved.

For the combination of 2 types of behaviour (1 ductile beam and 1 brittle beam), considering the deformation capacity of the brittle beam leads to a significant improvement in the probability distribution of the results. This implies that a plastic calculation, to a certain extent, could be used if the deformation capacity of each section is carefully considered (i.e. some redistribution can be admitted as long as the deformation capacity of the beams with a rather brittle behaviour is not overestimated).

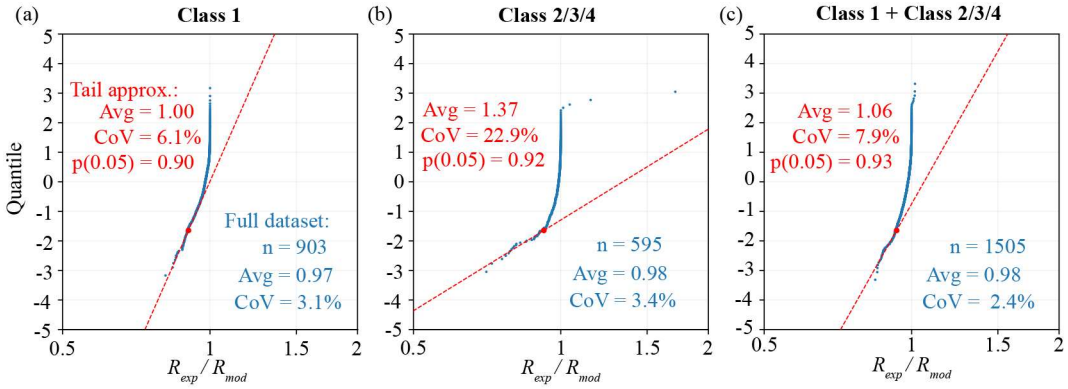

Fig. 47 *Probability plots of θ_{QR} for EPLim model and the different cross-sections combinations composed of:(a) Class 1 only (b) Class 2/3/4 combined and (c) Class 1 with Class2/3/4.*

3.3.10 Non-Linear model results

The non-linear model results as probability plots of θ_{QR} in Fig. 48 provide a good approximation for ductile beams with a distribution tail that precisely follows a lognormal distribution. In this case, considering the non-linearity allows for a good approximating of the real behaviour of the statically indeterminate cross system.

For larger cross-sectional areas, however, different behavioural modes are observed at the other extreme of the distribution. These different modes are due to the instabilities that these experimental beams may experience. If the behaviour is close to brittle, then the model results can become bad because the model only considers the non-linearity of the materials and not the instability problems, thus making the model no longer suitable.

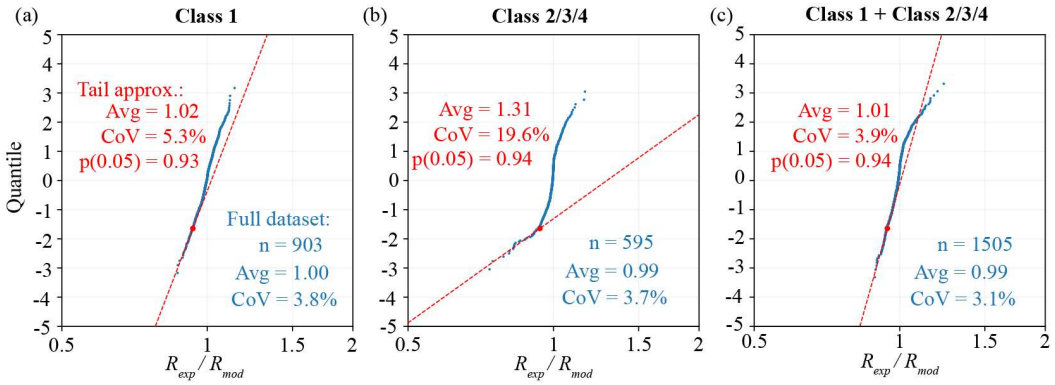

Fig. 48 *Probability plots of θ_{QR} for NL model and the different cross-sections combinations composed of:(a) Class 1 only (b) Class 2/3/4 combined and (c) Class 1 with Class2/3/4.*

3.3.11 Summary tables and discussion

In the following tables, the results for θ_{QR} for the different models and cross system combinations, separated according to the two differentiations: moment direction (M^+ & M^-) or cross-section classes (1 & 2 or higher), are summarized and compared.

First, when looking at Tab. 14, an improvement in the 5th percentile and in the tail fitting/ lower tail approximation (represented by the Mean and CoV) for the cross-section class 1 combinations can be observed. This can be attributed to the removal of the more brittle beams from this group.

Tab. 14 *Comparison of all results of θ_{QR} for the different models and cross system combinations for positive moments or cross-sections class 1 (in blue whole dataset statistics, in red tail approximation statistics)*

	M+/M+			Class1/Class1		
	Mean.	**CoV %**	**p(0.05)**	**Mean.**	**CoV %**	**p(0.05)**
LE	1.17	15.0		1.10	9.4	
	1.15	8.7	0.99	1.15	9.0	0.99
EP	0.96	4.8		0.97	3.1	
	1.28	22.3	0.87	1.00	6.1	0.90
EPLim	0.97	3.3		0.97	3.1	
	0.99	6.1	0.89	1.00	6.1	0.90
NL	0.97	3.4		1.00	3.8	
	0.99	6.2	0.89	1.02	5.3	0.93

Tab. 15 *Comparison of all results of θ_{QR} for the different models and cross system combinations for negative moments or cross-sections classes 2, 3 and 4*

	M-/M-			Class2+/Class2+		
	Mean	**CoV %**	**p(0.05)**	**Mean**	**CoV %**	**p(0.05)**
LE	1.18	12.4		1.21	11.8	
	1.09	4.5	1.01	1.27	11.8	1.04
EP	0.98	1.6		0.97	4.2	
	0.97	1.8	0.95	1.51	31.3	0.87
EPLim	0.98	1.6		0.98	3.4	
	0.97	1.8	0.95	1.37	22.9	0.92
NL	0.99	2.1		0.99	3.7	
	0.98	1.9	0.95	1.31	19.6	0.94

In Tab. 15, no improvement when using the cross-section classification can be observed. A reduction of fractile 5% values is noticeable because the ductile cases considered in the first analysis are removed and thus the tail behaviour is closer to what we expect (i.e. it removed what could be seen as outliers before, too ductile as designed for shear study). As discussed in the previous subsections, the experiments and their combinations show different behaviour, with the lower part of the distribution having a very different shape from the rest of the distribution.

Tab. 16 *Comparison of all results for the different models and cross system combinations for negative/positive moments or cross-sections class 1 with classes 2, 3 and 4*

	M+/M-			Class1/Class2+		
	Mean	**CoV %**	**p(0.05)**	**Mean**	**CoV %**	**p(0.05)**
LE	1.14	9.3		1.14	9.5	
	1.17	7.8	1.02	1.13	6.1	1.02
EP	0.97	3.4		0.97	3.1	
	1.40	23.7	0.93	1.19	15.8	0.91
EPLim	0.97	3.2		0.98	2.4	
	1.22	16.0	0.93	1.06	7.9	0.93
NL	0.99	3.6		0.99	3.1	
	1.25	16.3	0.95	1.01	3.9	0.94

In Tab. 16, one can see that the 5th percentile values are not improved with the use of the cross-section classification, but a better approximation of the lower tail can be observed, with in particular a large reduction of the CoV values.

From the above, it is concluded that:

- The section class, which can be said to be linked to the failure mode, appears to influence the model uncertainty of action effects calculation regardless of the analysis performed. Systems combining Class1 beams only show lower CoV and smaller 5th

percentile than combinations of Class1/Class2+. Furthermore, Class1/Class2+ show lower CoV than Class2+/Class2+ combinations.

- Since a better representation and modelling of the different beam behaviour within an indeterminate static system can be achieved by relying on the cross-section classification, one shall always refer to the cross-section classification to validate the use of linear or plastic internal forces redistribution. Also, this is an interesting result as this classification is used every day by engineers in practice and potentially provides an elegant solution for differentiating the value of the model uncertainty partial factor in the verification of the global load-bearing capacity of indeterminate static systems.
- There is also a clear observation of 2 regimes, a relationship between the failure mode and the θ_{QR} distribution shape.
- The model uncertainty reduces when more refined analyses are performed. However, and inversely, the work effort increases in terms of input data, time and calculation complexity.

The main questions that remain are the representativity of both the beam in a cross system and the database used in this section to determine the resulting probability density functions for the random variable θ_{QR} and the corresponding values of the model partial factor γ_{Sd}. The indeterminate static systems modelled should be representative of common structural systems in practice. Referring to our research domain, this corresponds to continuous composite bridges. The crossing of a ductile and brittle beam can be considered as the model that is the closest to our common structural system but are two beams crossing each other at midspan representative of our common longitudinal structural system?

This question is addressed in the following subsections by proposing an extension of the modelling technique using the results from experiments on simple composite beams to continuous composite longitudinal structural systems.

3.4 Longitudinal continuous systems

To extend the results obtained on cross systems, crossing of two simply supported beams (SSB), another statically indeterminate system is hereby studied. It must be ensured that this hypothetical system can be representative of a common longitudinal system such as a continuous composite bridge. It is therefore necessary to analyse and relate both systems, to observe how to adequately represent the behaviour of a continuous beam by superposing or combining simply supported beams.

In this case, it seems appropriate to combine beams that are loaded in different directions (i.e. positive and negative bending) which allows the representation of both the sagging and the hogging regions of a continuous girder. Since this is an over-constrained problem, different conditions analysis between both systems are carried out, namely static and kinematic (using curvature as well as displacements). It is shown, by further modelling of both systems using different beams, that they lead to similar relations.

3.4.1 Static conditions

The first step is to investigate the static conditions that must be satisfied for each of the two static systems chosen. Fig. 49 shows the determination of the load-carrying capacity for each system. To explain the reasoning, the simplified assumption that both beams in the cross-system have equal span lengths is made.

As for the longitudinal system, it is defined as a symmetrical two spans system with the same properties as the assembled two-beams system (identical span length and the cross-sections are taken from the crossed system (i.e., sagging region = SSB under positive bending, hogging region = SSB under negative bending). This means that ultimate moment capacity is equal in both systems. The longitudinal system is loaded with two identical concentrated forces located in the centre of each span. To compare both systems, the

maximum load-carrying capacity is determined assuming that plastic hinges can form in both the hogging region and the sagging regions (plastic design).

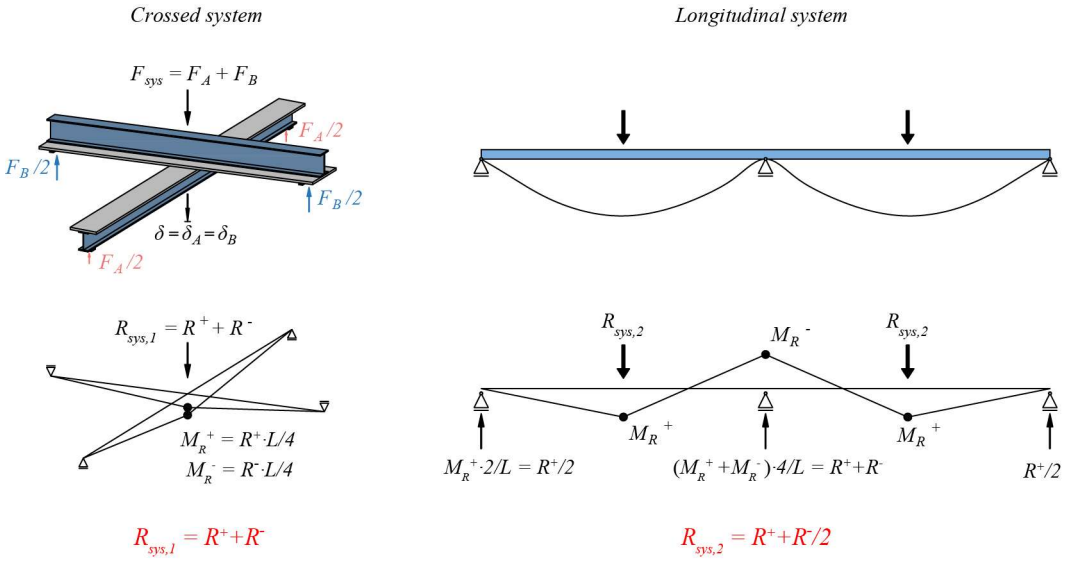

Fig. 49 *The two statically indeterminate systems considered and their respective static conditions requirements.*

After analysing both systems as summarized in Fig. 49, the cross-system configuration does not reflect the behaviour of a continuous beam. This is because the section subjected to negative bending has an equal "weight" to that of the positive section, whereas in the longitudinal system the bearing capacity is influenced twice as much by the capacity of the sagging regions. To be statically equivalent, the crossed system must contain 3 beams. Two times the same beam (in case of a symmetric longitudinal system) in positive bending for one beam submitted to negative bending.

3.4.2 Kinematic conditions

The second step is now to investigate the kinematic conditions of both systems, and it is less obvious to find a relationship between them. On the one hand, the experimental database contains isostatic beam deflections, which are quite different from the deflections of a continuous girder. On the other hand, analysing and comparing beam deflections of different systems is possible, even after concrete cracking and during redistribution of internal forces by integrating the curvature along each beam as presented in Subsection 3.3.4 to obtain the load-deflection response of each system.

In the static cross-span system, the imposed displacement at mid-span is identical for each beam, but for continuous girders this assumption must be confirmed. To represent as best as possible the response of a continuous system using the same experimental database, the method is to approximate the deflection of a continuous beam by the deflections of simply supported beams. Let's define first the sagging and hogging regions. Fig. 50 represent the elastic moment distribution along a 2 spans continuous beam loaded as before with two identical concentrated forces located in the centre of each span. Based on the elastic moment distribution and consideration about the concrete cracking zone under hogging, a total length of the hogging zone equal to 0.6L is assumed (to be validated later, see Subsection 3.4.3).

The reasoning is now to consider each part of the continuous beam as a separate isostatic system (to be able to refer back to experimental data) and at the same time ensure the continuity of the deflection along the whole continuous beam. This means that at the zero moment points (points of intersection) the displacements must be equal, $\delta_{imp,2} = \delta_{imp,1}$, as presented in Fig. 51. Note that this does not ensure continuous slope at the points of intersection.

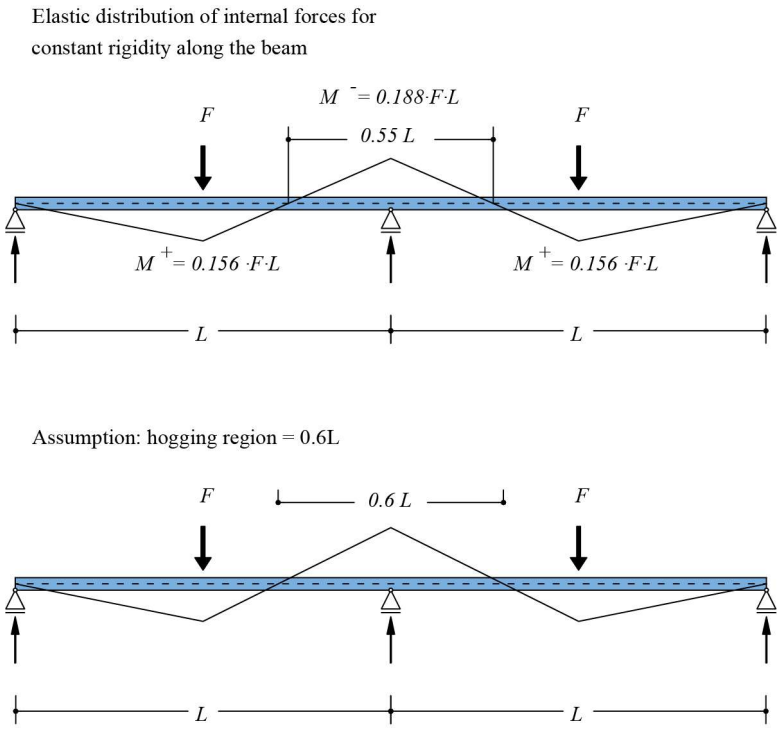

Fig. 50 *Two-spans continuous beam with elastic moment distribution and definition of hogging and sagging regions.*

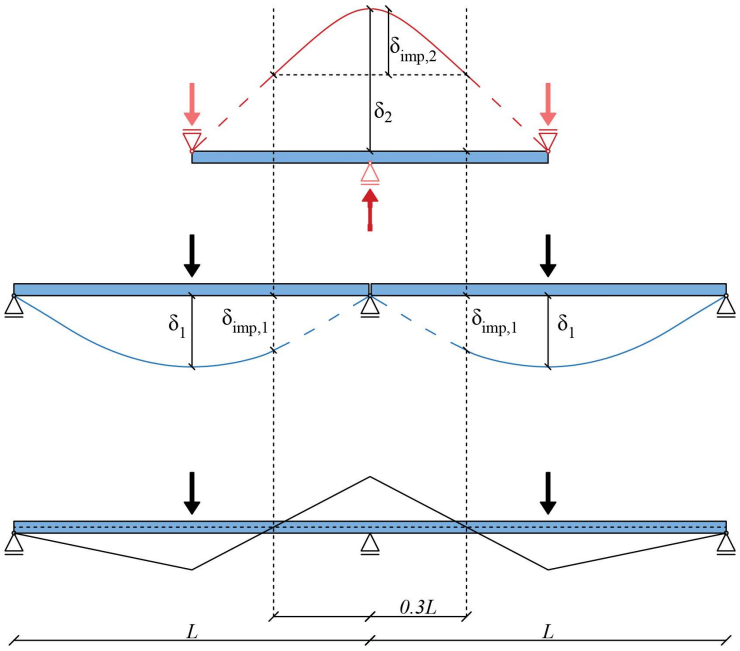

Fig. 51 *Kinematic conditions imposed on the two-spans continuous beam.*

For comprehension purpose, analysis is made separately for sagging and hogging region. Considering the sagging region, an approximation from simply supported beam to continuous beam mid-span displacement is done by comparing the behaviour of both systems. In Fig. 52, deflection of isostatic beams that are not connected at intermediate support is shown in blue and that of the continuous system is plotted in black. Considering constant rigidity along the beam, the mid-span displacements in the elastic range can be computed. In this case, the mid-span displacement of the continuous beam can be taken as approximately 70% of the displacement of the same beam if simply supported.

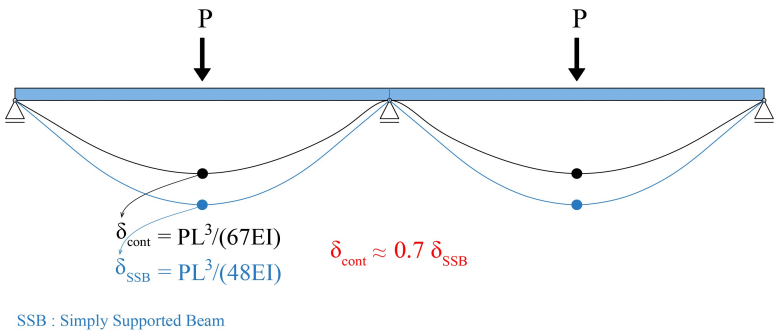

Fig. 52 *Comparison between deflections at midspans from a two-span continuous beam and two Simply Supported Beams (SSB).*

The focus is now put on the intersection between the 2 regions, as a relationship between the mid-span displacement and the one at the point where bending moment is null needs to be found. Considering the rotation diagram along the beam, it is possible to determine this relationship using the assumption that the hogging region is equal to 0.6 times the span length (see Fig. 50). Considering the integration of the curvature along the beam, as presented in Fig. 53, it is possible to estimate the ratio between null moment and mid-span deflections as being equal to 80%. However, as the assumption of a constant rotation in the hogging part of the beam has been made, the value found is slightly overestimated. Furthermore, the analysis was done based on the deflection of an isostatic beam. In the case of the continuous beam, it is expected that the deflection at the point of zero moment is lower since the rotation at the intermediate support must be equal to zero. An approximation closer to reality would lead to lower ratio values, around 0.65-0.7, instead of considering 0.8. Finally, one shall note that this factor is also largely influenced by the difference in stiffness between the hogging and the sagging regions. In composite bridges, stiffnesses at supports are usually significantly higher since applied moments are higher and cracking has to be limited. Thus both the steel section as well as the rebars quantity (typically 1.5% vs 0.8% [131] are higher at supports, which also explain why the ratio values are lower.

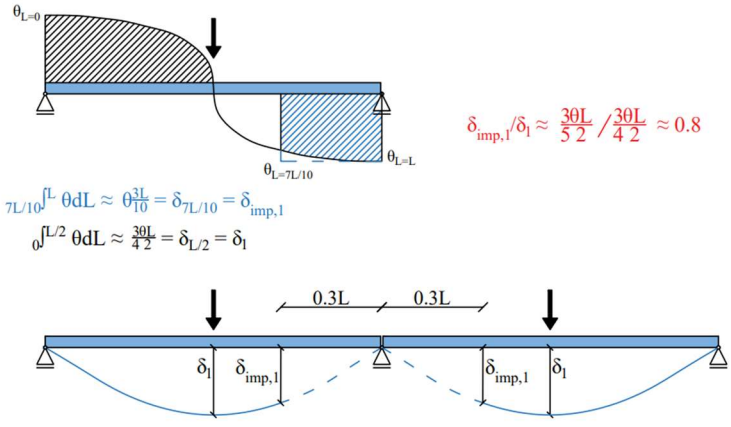

Fig. 53 *Relationship between curvature and displacements at the intersections ($\delta_{imp,1}$) and mid-span locations (δ_1).*

Concerning the hogging region, it is straightforward to determine the ratio between the deflection of the simply supported beam and the one at the intersection. With the assumption made on the hogging region length (0.6 times the span length), the displacement can be calculated from the deflection of the isostatic system and it is equal to 0.6^2 for a concentrated load at mid-span (which is represented by the intermediate support reaction in our case).

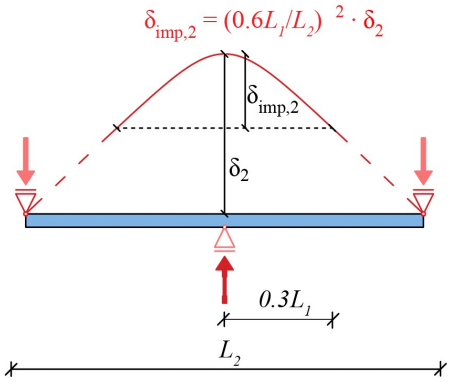

$L_1 = L$: span of the assumed two-span continuous beam

L_2 : span of the experimental SSB used for representing the hogging region

Fig. 54 *Relationship between displacements at the intersections ($\delta_{imp,2}$) and support location (δ_2).*

3.4.3 Summary and validation of the conditions between static systems

To confirm the assumptions made in determining the forces and deflection relationships given in Fig. 55, validation according to some simple cases has been performed. A random selection of sectional behaviour was chosen, and the two systems were modelled to check whether the behaviour matched the relationships derived from the static and kinematic conditions. Four cases were analysed with, for the span section, always the same moment-curvature relationship. For the support section, 4 different moment-bending relationships are given in Fig. 56; they were chosen to observe the influence of the stiffness ratios between the two sections and are given in Tab. 17. In addition, case A was defined to show a brittle behaviour (no plastic behaviour as indicated by the dotted line in Fig. 56).

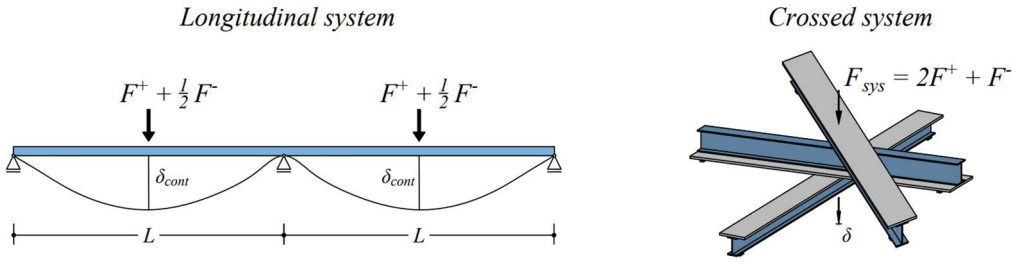

	Longitudinal system	Simple span combination (or cross system)		
	(L, 2P, δ_{cont})	(L_1, F^+, δ_1)	(L_2, F^-, δ_2)	(L_1, F^+, δ_1)
Force (F)	$2F^+ + F^-$	F^+	F^-	F^+
Deflections (δ_i)	δ_{cont}	$0.7\,\delta_1$	$\delta_1 = (0.6L_1/L_2)^2/0.65\,\delta_2 = 0.55\,\delta_2$	$0.7\,\delta_1$

Fig. 55 *Summary of the forces and deflection relationships linking the longitudinal (continuous beam) and the simple span combination systems.*

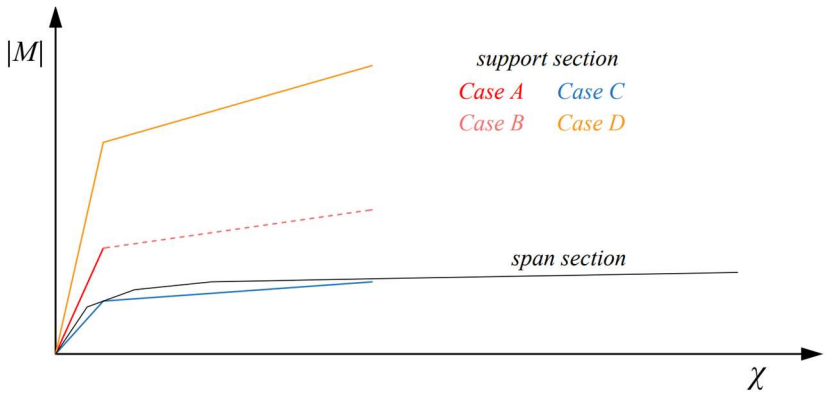

Fig. 56 *Validation cases, span and support moment-curvature relationships.*

Tab. 17 *The different stiffness ratios and behaviour type for the four cases analysed*

	Stiffness ratio (I_{sup}/I_{span})	**Support section behaviour (brittle/ductile)**
CASE A	1.5	brittle
CASE B	1.5	ductile
CASE C	0.75	ductile
CASE D	3	ductile

3.4.4 CASE A

The results for case A are shown in Fig. 57. The dashed lines show the deflections according to a simply supported beam for the support section (**red**) and for the span section (**black**). The line (**blue**) defines the behaviour of the continuous beam. For the span section the correction factor is taken as 0.7 as described in Fig. 55; according to the same figure, the correction for the support section should be 0.55, based on the assumptions and analysis carried out. It turns out that to obtain a behaviour identical to the continuous beam, in this case with a stiffness ratio equal to 1.5, the necessary correction should be taken as 0.68. The dashed line with black crosses is performed by adding both force-displacement responses of the simply supported beams after correction factor for the imposed displacement (which represent the crossed system). It is observed in Fig. 57 that first yield at midspan is reached at the same point for both systems, and the failure (occurring at the support section) is attained for the same displacement.

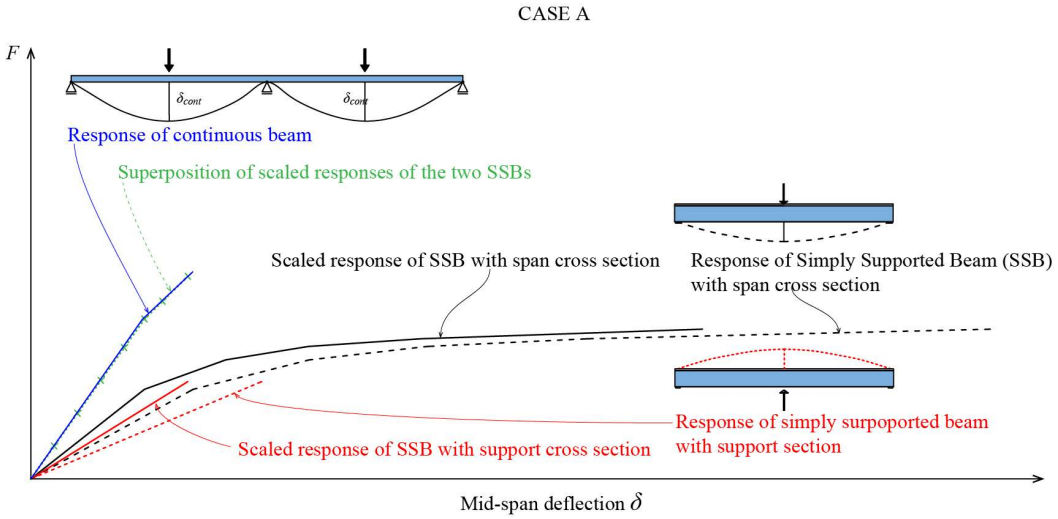

Fig. 57 *Forces-deflection curves for case A.*

3.4.5 CASE B

For case B, the moment-curvature relation is equivalent to the case A with the exception that the support section shows ductile behaviour. Again, a correction factor of 0.68 is applied to the simply supported beam result of the support section. The resulting curve (dashed line with black crosses) show that the behaviour of the continuous beam (**blue**) can still be well approximated, see Fig. 58.

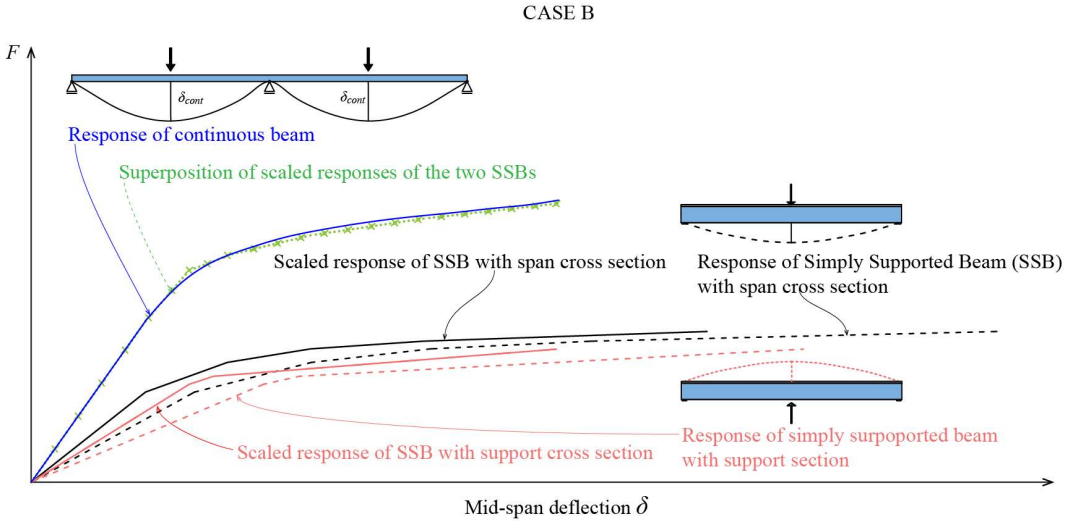

Fig. 58 *Forces-deflection curves for case B.*

3.4.6 CASE C

For case C, the stiffness ratio between support and span section is lower than previously and equal to 0.75. This time, the needed correction factor is smaller, since the span section is stiffer. Also, the hogging moment region becomes smaller, and the span region behaviour is more important in this case. The correction factor applied this time is equal to 0.55 to get a good approximation of the simulated curve (dashed line with black crosses) with the continuous beam behaviour (**blue**), both in terms of shape and values, see Fig. 59.

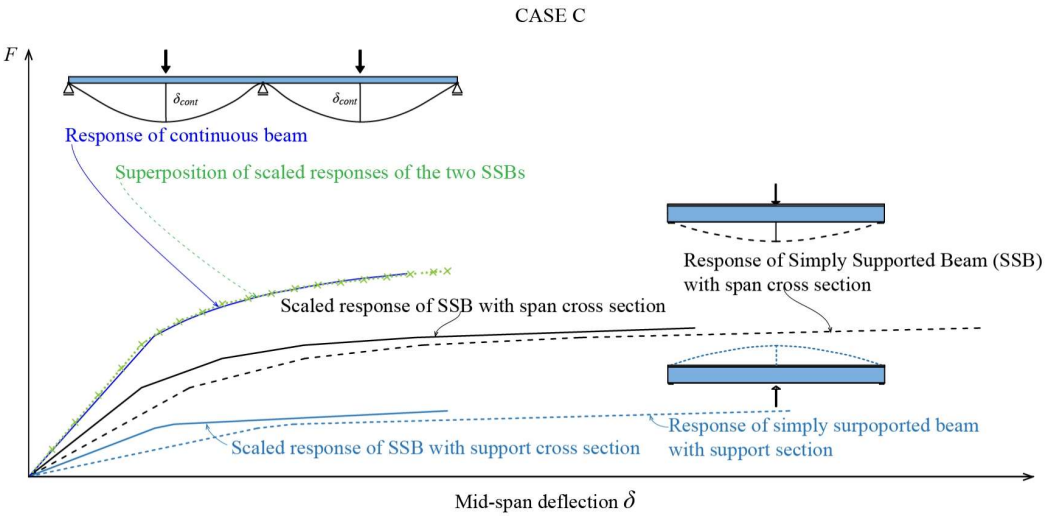

Fig. 59 *Forces-deflection curves for case C.*

3.4.7 CASE D

As the stiffness ratio is now increased to 3 between support and span section, the behaviour of the support is now more important in simulating the behaviour of the continuous system. As shown in Fig. 60 the correction factor needed is now 0.8 to get a good approximation of the simulated curve (dashed line with black crosses) with the continuous beam behaviour (**blue**), both in terms of shape and values.

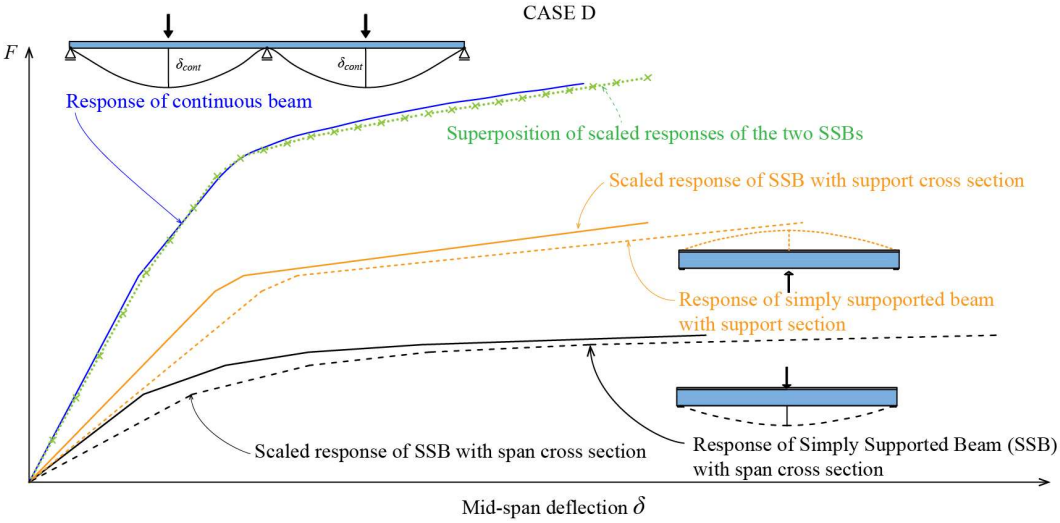

Fig. 60 *Forces-deflection curves for case D.*

3.4.8 Recapitulation of main results and correction factors

For the 4 cases, the correction factors for the imposed displacement are given in Tab. 18.

Tab. 18 *Summary of correction factors for the imposed displacement*

	CASE A	CASE B	CASE C	CASE D	1st estimate
Span correction	0.7	0.7	0.7	0.7	0.7
Support correction	0.68	0.68	0.55	0.8	0.7

Based on the results obtained for these 4 cases, one can observe that the correction factor for the span section is a good approximation to convert from the simply supported system behaviour to the continuous beam one. However, for the support section, the correction factor value varies and depends on the stiffness ratio between both sections. Nevertheless, even if the support correction factor ranges between 0.5 and 0.8, the average is nearly the same as the factor for the span section and in first approximation the results of cases C and D can be considered as rather extreme cases. Thus, to best represent the continuous systems by means of cross systems, the value 0.7 as a first estimate can be used for both correction factors. Furthermore, the cross system without correction of the imposed deflection can be considered representative enough and the results would not improve by adding a random variable on this correction factor.

In all of the above cases, the comparisons have been performed for simply supported beams with equivalent span length. It goes without saying that if the two beams do not have the same span length, the force-displacement response of the beam tested in negative bending must be corrected with respect to the span length of the beam in positive bending, i.e. with the following factor $(L_1/L_2)^2$ as presented in Fig. 55.

3.5 Approaching continuous system behaviour (composite bridges)

Using the reasoning developed in the previous section, a new set of simulated tests is created to represent longitudinal systems (continuous composite bridges). The approach here differs from the one for concrete structures for two reasons linked to the focus on composite girder bridges:

- The stiffnesses at supports are usually significantly higher, as shown by the larger steel sections as well as rebars quantity used in these regions.
- Their design is predominantly influenced by the low ductility of composite beams, especially in the intermediate support areas. This is due in particular to the web's slenderness which can get very high.

In span regions, the ductility problem is not predominant because almost the entire web is subjected to tension, which eliminates the problems associated with stability. In the most common case, the span sections are considered to have a very ductile cross-section class (class 1), whereas the cross-section class at the supports is easily class 3 or 4. This means, among other things, that the design of such a structure should not admit plastic redistributions from the support to the span sections due to the low ductility of the support section(s), which considerably complicates the design and requires a fastidious verification according to elastic stress distributions within the sections. Nevertheless, thanks to the doctoral studies of Ducret [132] and Lääne [133], it has been shown that a certain redistribution can be admitted between the support and span internal forces as even in class 4 the resisting moment can be sustained under a certain rotation range. Considering the available rotational capacity at the support, it was shown that a plastic calculation in span is possible as long as the sagging moment does not exceed 90% of the plastic moment capacity (which limits the plastification and thus the rotation in span so as not to require too much rotation capacity at the support). This criterion should allow for the support section to maintain its resistance (even for section classes 4, the reduced elastic resistance EER) while the span section is in the plastic behaviour.

To best reflect the behaviour of a composite bridge, it was decided to combine experimental beams according to the classifications that can be found in a composite bridge. The assembled system always consists of 3 beams (2 simply supported beams tested under positive loading and 1 beam submitted to negative moment classified as cross-section class 3 or 4).

***Tab. 19** First assembling scheme, completely symmetrical longitudinal system*

	Assembled longitudinal system		
	1st beam (span)	**2nd beam (support)**	**3rd beam (span)**
	(L_1, F^+_1, δ_1)	(L_2, F^-_2, δ_2)	(L_3, F^+_3, δ_3)
Force (F)	F^+_1	$(L_2/L_1)\ F^-_2$	Identical to 1st
Deflections (δ_i)	δ_1	$(L_1/L_2)^2\ \delta_2^-$	Identical to 1st
Cross-section class	1	3 or 4	Identical to 1st
Nb of experimental beams available	36	28	NA

In a first assembling scheme, the analysis is performed by duplicating the experimental beam representing the span region. This allows to represent a completely symmetrical longitudinal system; Tab. 19 gives the information needed to assemble the system, which leads to a total of 1008 possible combinations. If the beam representing the support section does not have the required length (i.e. the same length), it can nevertheless be adapted using the length ratios for both the imposed displacement and the force. These adjustments allow to obtain the same bending moment-deflection behaviour, the difference being only in the integration of the curvature diagram on a span length corrected to be equal to that of the reference beam (i.e. the span beam section under sagging moment).

In a subsequent assembling scheme, an additional variable is added by using a different beam for each of the two spans as presented in Tab. 20, which leads to a total of 36288 possible combinations. However, to remain consistent, it is necessary that the system remains symmetrical (the spans on each side of the support must be of equal length). This ensures an approximately equal negative section area on each side of the support. It is therefore necessary to also correct the 3rd experimental beam (representing the second span) to adjust its length in relation to the 1st experimental beam.

***Tab. 20** Second assembling scheme, non-symmetrical into symmetrical longitudinal system*

	Assembled longitudinal system		
	1st beam (span)	**2nd beam (support)**	**3rd beam (span)**
	(L_1, F^+_1, δ_1)	(L_2, F^-_2, δ_2)	(L_3, F^+_3, δ_3)
Force (F)	F^+_1	$(L_2/L_1)\ F^-_2$	$(L_3/L_1)\ F^+_3$
Deflections (δ_i)	δ_1	$(L_1/L_2)^2\ \delta_2$	$(L_1/L_3)^2\ \delta_3$
Cross-section class	1	3 or 4	1
Nb of experimental beams available	36	28	36

3.5.1 Models

In addition to the four models used in the previous sections, two models are added to represent the differentiation between span and support behaviour with moment-rotation:

- Allowing the beam in span and under sagging moment to behave elastic-plastic and reach its plastic capacity while limiting the support section to its elastic limit capacity (EPLE) (plLE),
- Allowing the beam in span and under sagging moment to behave elastic-plastic but only reach 90% of its plastic capacity while limiting the support section to its elastic limit capacity (EP90LE) (plLE90%)

The assembled longitudinal systems behaviour will be compared using now in total six (instead of four as previously) different models as presented in Fig. 61.

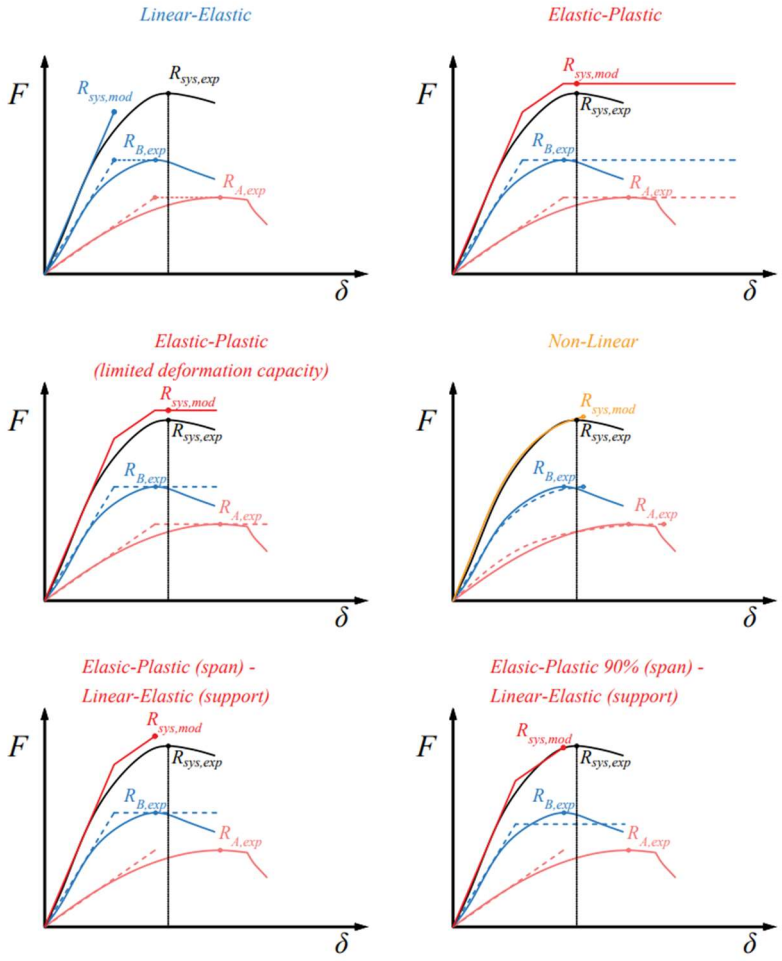

Fig. 61 *The six models compared to study the assembled longitudinal systems.*

3.5.2 Linear-Elastic model results

The results obtained with the LE model are shown in Fig. 62. The results are very similar for both assembling schemes (completely symmetrical or not symmetrical longitudinal systems).

The linear elastic model leads to an over-design ratio as it does not consider any ductility, as already observed with the cross system in Subsection 3.3. This elastic over-design ratio influences the model uncertainty, the distribution shape for load bearing capacity (θ_{QR}). The behaviour is quite homogeneous over the whole distribution. The 5th percentile is slightly above unity and the CoV are low. The assumption that there is no redistribution possible from the support to the span sections is in contradiction with the usual behaviour of such systems, even if made out of cross-section classes 2 to 4.

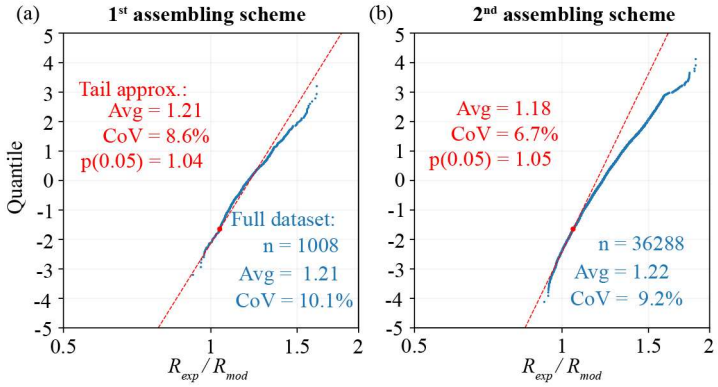

Fig. 62 *Probability plots of θ_{QR} for the LE model for the (a)1st and (b)2nd assembling scheme of longitudinal system, see Tab. 19 and 20 respectively.*

3.5.3 Elastic-Plastic model results

For the EP model, it is again the least conservative of all (i.e. similarly to cross systems) with 5th percentile values around 0.92, see Fig. 63. The results are quite similar for both assembling schemes, with a better tail distribution fit for the scheme 2.

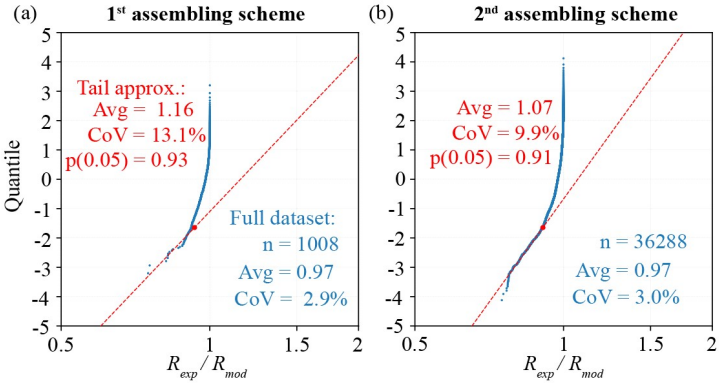

Fig. 63 *Probability plots of θ_{QR} for the EP model for the (a)1st and (b)2nd assembling schemes of longitudinal system.*

3.5.4 Elastic-Plastic model with limited plasticity results

The resulting probability plots of θ_{QR} for this model are very similar to the previous results from the EP model, which means that the added constraint of plasticity limitation does not play any role.

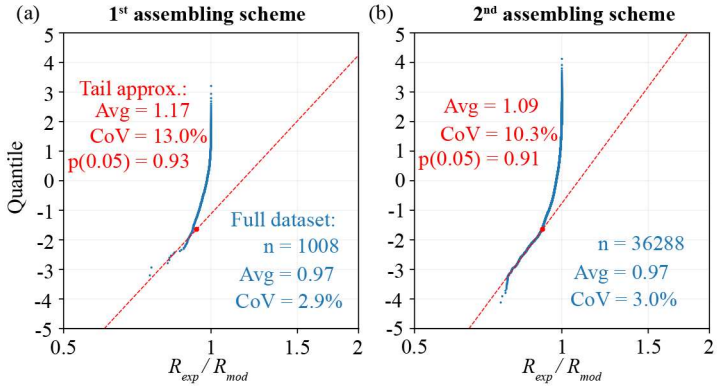

Fig. 64 *Probability plots of θ_{QR} for the EPLim model for the (a)1st and (b)2nd assembling schemes of longitudinal system.*

3.5.5 Non-linear model results

The resulting probability plots of θ_{QR} for the NL model shown in Fig. 65 provide a very good approximation of the real behaviour with a distribution tail that follows precisely a lognormal distribution, as was already the case for the statically indeterminate cross system. Given that the beams behaviour is sufficiently ductile, the nonlinearity allows for a good approximation of the real behaviour of the longitudinal system. This reflects well the usual behaviour of such systems.

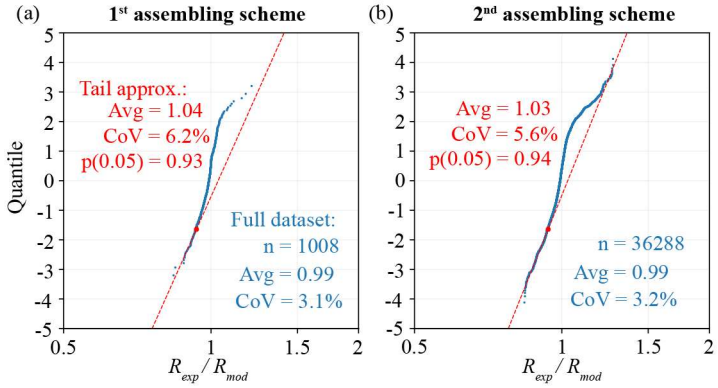

Fig. 65 *Probability plots of θ_{QR} for the NL model for the (a)1st and (b)2nd assembling schemes of longitudinal system.*

The second scheme, which has 36 times the combinations of the first but more uncertainty due to the correction on the 3rd beam, leads to very similar values, with a slight reduction of the CoV of the tail approximation.

These good results can be traced back to the behaviour of the longitudinal system, with redistribution between the support and the span sections, with plastification in the spans and sufficient rotation capacity at the support section. In this model, the support section does not remain elastic up to failure, as shown in in Fig. 61. This condition will be enforced in the two last models, namely (EPLE) and (EP90LE).

3.5.6 Elastic-Plastic model in span only, elastic on support (EPLE)

The resulting probability plots of θ_{QR} for this model are among the least conservative, with the EP model. This is not surprising since it considers redistribution and plastic behaviour in span section. The behaviour is quite homogeneous over the whole distribution. Thus, as long as the support section rotates without losing its strength, i.e. without exceeding its elastic capacity, the model should give good predictions. This is indeed the case with 5th percentile values between 0.96 and 0.92. The CoV however is quite high in comparison with the other models, so there is room for improvement. This could be the case with the next and last model EP90LE.

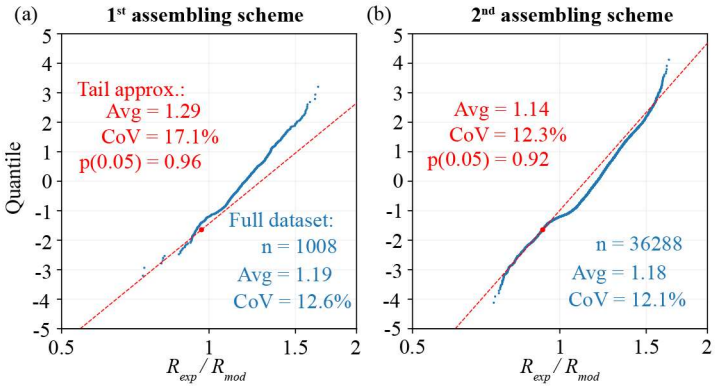

Fig. 66 *Probability plots of θ_{QR} for the EPLE model for the (a)1st and (b)2nd assembling schemes of longitudinal system.*

3.5.7 Elastic-Plastic model in span limited, elastic on support (EP90LE)

The resulting probability plots of θ_{QR} of this model are as expected somewhat better than those from the EPLE model. The 5th percentile values are very close to unity and the CoV are smaller than with the previous model. This is in line with previous works, but does not constitute a confirmation of the correctness of the limitation to 90% of in-span plastic capacity since there is no requirement on the rotation needed to reach this load capacity.

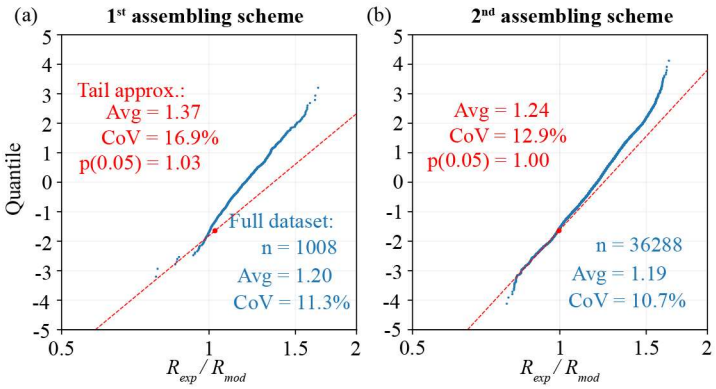

Fig. 67 *Probability plots of θ_{QR} for the EP90LE model for the (a)1st and (b)2nd assembling schemes of longitudinal system.*

3.5.8 Summary of models of longitudinal system and discussion

A summary of all results of θ_{QR} is given in Tab. 21. When compared with the results from the cross system, see Tab. 14, Tab. 15 and Tab. 16, one can see that the models show the same trends, with a reduction of 5th percentile values when considering plastic behaviour and also probability plots and tail behaviour closer to the expected distribution. Not surprisingly, the models that consider redistribution and plastic behaviour in span section give good results. The best results are obtained with model EP90LE, with the beam

in span and under sagging moment allowed to behave elastic-plastic but only reach 90% of its plastic capacity while limiting the support section to its elastic limit capacity. Thus, under the assumption that the support section rotates without losing its strength, i.e. below that of its elastic capacity, it is a good choice to use this model in design. The validity of this requirement is not part of this research, it has been studied and validated in previous works [132, 133].

With respect to the corresponding value of the partial factor, it was not possible to carry out a complete study as for the reinforced concrete. However, when compared the values found in Tab. 21 are similar to values for the model uncertainty related to the global load-bearing capacity found for the reinforced concrete structures as can be seen in Tab. 22 Thus, it is reasonable to conclude, with the same limitations inherent to this report, that the partial factor γ_{Sd} to cover the uncertainties of the internal force calculation ranges between 1.05 and 1.15.

***Tab. 21** Comparison of all results of θ_{QR} for the different models of longitudinal system*

	1st assembling scheme (completely symmetrical, 1008 comb.)			2nd assembling scheme (36288 comb.)		
	Avg.	**CoV %**	**p(0.05)**	**Avg.**	**CoV %**	**p(0.05)**
LE	1.21	10.1		1.22	9.2	
	1.21	8.6	1.04	1.18	6.7	1.05
EP	0.97	2.9		0.97	3.0	
	1.16	13.1	0.93	1.07	9.9	0.91
EPLim	0.97	2.9		0.97	3.0	
	1.17	13.0	0.93	1.09	10.3	0.91
NL	0.99	3.1		0.99	3.2	
	1.04	6.2	0.93	1.03	5.6	0.94
EPLE	1.19	12.6		1.18	12.1	
	1.29	17.1	0.96	1.14	12.3	0.92
EP90LE	1.20	11.3		1.19	10.7	
	1.37	16.9	1.03	1.24	12.9	1.00

***Tab. 22** Comparison of results of θ_{QR} between Reinforced concrete and steel-concrete structures*

	RC structures			Composite structures		
	Avg.	**CoV %**	**p(0.05)**	**Avg.**	**CoV %**	**p(0.05)**
LE cracked	1.16 to 1.23	9.1 to 12.9	0.99 to 1.00	1.18 to 1.21	6.7 to 8.6	1.04 to 1.05
3-linear	1.13 to 1.30	8.5 to 17.2	0.97 to 0.98			
EPLim				1.09 to 1.17	10.3 to 13	0.91 to 0.93
EP90LE				1.24 to 1.37	12.9 to 16.9	1.00 to 1.03

3.6 Conclusions

To quantify the model uncertainty in calculating the load-bearing capacity for statically indeterminate composite structures, an experimental database with all relevant and sufficiently well reported tests on composite beams was created; it includes both beams tested under positive (45 tests) and negative bending (36 tests). This database is an achievement and can be used and extended in the future. The study on statically indeterminate structures built with this database reached the following conclusions:

- The section class, which can be said to be linked to the failure mode, appears to influence the model uncertainty of the load-bearing capacity calculation regardless of the analysis performed;
- Since a better representation and modelling of the different beam behaviour within an indeterminate static system can be achieved by relying on the cross-section classification, one shall always refer to the cross-section classification to validate the use of linear or plastic internal forces distribution;
- This classification being used every day by engineers in practice, potentially provides an elegant solution for differentiating the value of the model uncertainty partial factor (γ_{Sd}) in the verification of the global load-bearing capacity of indeterminate static systems;
- The representativity of the beam in a cross system and the database used has been shown to have the potential to be extended to a more common structural system in practice, namely continuous composite bridges;
- There is also a clear observation of 2 regimes, a relationship between the failure mode and the θ_{QR} distribution shape;
- Plastic and non-linear models, used to calculate the load bearing capacity, give lower CoV if performed with limiting the deformation capacity. Also mean values closer to unity are observed for θ_{QR};
- The partial factor γ_{Sd} to cover the uncertainties of the internal force calculation can be taken similarly to reinforced concrete structures, i.e. it ranges between 1.05 and 1.15. Further differentiation with the section classification was not addressed in this study and would need to perform a large parametric study. Also, as for reinforced concrete structures, it must be noted that additional uncertainties, which depend on the complexity of the structure, the construction method, the tools used and the experience of the designer deserve to be investigated more in detail.

4 Recalibration of partial safety factors for permanent loads in bridges

4.1 Introduction

In this Section, the partial safety factors (PSFs) for permanent actions, used for designing new structures and for the assessment of existing ones, are updated for the case of reinforced concrete (RC) road bridges based on available statistical distributions of geometrical, material, traffic and model uncertainties. In road bridges, permanent loads result from the self-weight of structural and non-structural elements, which include the pavement, safety barriers and if present, non-structural curbs. In the latest available draft of EN 1990:2023 [135], the recommended partial safety factor for all permanent loads, denoted with γ_{Gi}, is equal to 1.35 and covers the uncertainty in the representative value of permanent loads and the model uncertainty in action effects calculation. For the model uncertainty in action effects calculation, the JCSS Probabilistic Model Code [28] recommends a Log-Normal distribution with mean 1.0 and CoV between 0.05 and 0.20, but no clear background is provided. These values are confirmed in Sections 2 and 3 of this report (additional references on this topic can be found in [65] and in Section 2). As mentioned above, the recommended values of PSFs for structural and non-structural self-weight EN 1990:2023 [135] are the same. However, the latest available draft of EN 1991-1-1:2023 [138] recommends to assume a deviation of the pavement thickness of [-20%, +20%] or [-20%, +40%] depending on whether the pavement has already been replaced or not. In order to clarify whether these values are reasonable, data collected from measurements on various bridges in Switzerland will be analysed and it will be assessed whether there is a need to decouple the two partial safety factors for structural and non-structural self-weight, respectively. Traffic variability will also be considered using Weight In Motion (WIM) data collected in several locations in Switzerland. To estimate the partial safety factors, parametric reliability analyses, covering a wide range of scenarios, are performed based on the updated statistical distributions using the First Order Reliability Method (FORM). Finally, to investigate if a sufficient level of safety is achieved with the proposed partial safety factors, reliability analyses are performed using more refined methods on selected case studies.

4.2 Statistical uncertainties influencing structural self-weight

The self-weight of structural members in concrete bridges is affected by three main variables: (1) the specific weight of concrete, (2) the dimensions of concrete and (3) the reinforcement content (typically expressed in kg/m^3 and calculated on the basis of nominal dimensions). The bar diameter, the geometry and the specific weight of the reinforcement show also some variability affecting the self-weight, but these are negligible since the production is highly optimized and standardized. The same considerations apply also to composite bridges, where the largest source of variability for the structural self-weight is generally related to the reinforced concrete deck. Fig. 68a shows the probability-plot of the specific weight of concrete obtained from around 3’500 samples (150×150×150 mm) collected in Western Switzerland between 2014 and 2021 (courtesy by TFB SA, only samples with an air content smaller than 2.5% are included in the analysis). These data are obtained from raw concrete samples produced using siliceous limestone aggregate found typically in the Swiss plains (specific weight equal to 26.7 kN/m^3). The resulting CoV, neglecting the lowest part of the distribution, is 1.4%, significantly smaller than the value recommended by the JCSS report of 4% [28] (which is based on the publication 115 of the CIB report [139]). It is also much smaller than the value proposed by Ellingwood of 10% [27], however, this value also included the geometric and reinforcement content variability, therefore, not directly comparable. It must be noted that the values shown in Fig. 68a refer to the production of concrete in a limited area, thus, different statistical values could be

found in similar studies in different locations where several aggregate types and petrography's can be found.

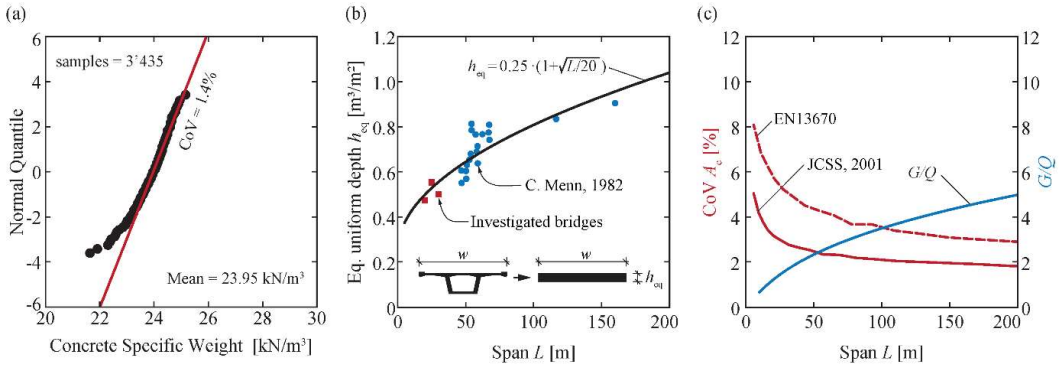

Fig. 68 *(a) Normal probability-plot of concrete specific weight; (b) equivalent bridge deck thickness as a function of the span (values from Menn, 1982 [141] in blue circles and some investigated bridges of Tab. 23 in red squares); (c) CoV of the sectional area (A_c) variability using tolerances as standard deviations [142] (dashed red) and statistical distributions according to the JCSS report [28] (contionuous red); ratio of permanent load over traffic load (G/Q) for varying span in blue.*

Fig. 68c shows the coefficient of variation of the sectional area for increasing span of the bridge assuming that tolerances according to [142] correspond to standard deviations (dashed red line) and using the statistical distributions recommended by the JCSS report [28] (continuous red line). It can be observed that the importance of the geometric variability decreases with increasing cross-sectional dimensions. In fact, tolerances do not increase linearly and are limited for elements larger than a fixed threshold (e.g. 30 mm for cross-sectional dimensions larger than 2'500 mm [142]). Thus, the geometrical variability has a relatively small influence on bridges with spans larger than 30 m.

Although geometric variability has a stronger influence on the structural self-weight of short span bridges, in these cases permanent loads are generally less significant compared to traffic loads. This is illustrated in Fig. 68c (continuous blue curve), where the ratio between permanent load (obtained from the empirical relationship plotted in Fig. 68b) and characteristic traffic loads (according to SIA 261:2020 [143]) is presented as a function of the span length *L*. One can observe that the ratio *G / Q* varies between 0.5 for bridges with a short span (~10 m) and 4 for bridges with longer spans (~50-100 m).

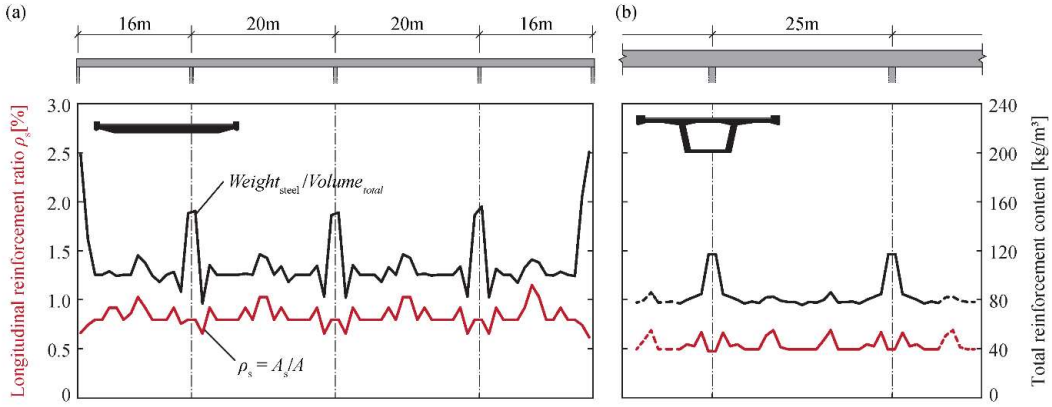

Fig. 69 *(a) Longitudinal reinforcement ratio (red) and reinforcement content expressed in kg/m³ (black): (a) bridge Haute-Rive built in 1972 and (b) bridge Brocard built in 1964, see Tab. 23.*

Figs. 69a,b show the reinforcement content in two reinforced concrete bridges calculated using the original drawings considering both prestressing and passive reinforcement. While the longitudinal reinforcement ratio (red line) is almost constant along the longitudinal axis of the bridge, the reinforcement content expressed in kg/m^3 increases close to the supports due to increased shear reinforcement and the more heavily reinforced transversal elements. However, close to the supports, as the load is directly transmitted to the latter, the reinforcement weight is less significant for the action effects. It must be noted that the reinforcement content in a bridge depends on several factors, such as the amount of prestressing, the structural system and the year of construction (generally, the reinforcement ratio of new structures being larger compared to older structures due to current more stringent requirements in terms of durability and serviceability as well as a reduced amount of prestressing).

4.3 Statistical uncertainties influencing non-structural self-weight

In addition to the structural self-weight, other non-structural loads contribute to the permanent load in road bridges. These include pavement, safety barriers and, if present, non-structural curbs. The same considerations made in the previous section for reinforced concrete elements apply also to reinforced concrete curbs while lane separation elements and safety barriers should be considered according to the corresponding specifications. In this Section, the self-weight variability of the pavement is investigated whereas the variability of the other permanent actions is neglected. In particular, since the variability of the pavement thickness has a larger impact than the specific weight variability, the focus will be put on the former while the pavement specific weight variability is assumed based on available literature [144, 145, 146]. Specifically, in this Section, a mean value of 24.0 kN/m^3 and a CoV = 4% is assumed, as found by Hugenschmidt on bridges that were demolished in Switzerland [147].

Fig. 70a shows some typical cases of pavement thickness variability in the transversal and longitudinal direction. In particular, in the transversal direction, thickness variations occur mostly due to pre-existing deformations of the deck before surfacing which are generally caused by self-weight, transversal prestressing or imperfections during construction. In the longitudinal direction, two main scenarios can occur as illustrated qualitatively in Fig. 70a: if the precamber and the deformations caused by prestressing exceed those caused by self-weight, the pavement will be typically thicker close to the supports while in case of non-prestressed bridges or if precamber and prestressing are not sufficient to compensate deformations caused by self-weight, the pavement is typically thicker at midspan. In addition, the imperfections of the concrete surface just after casting add an aleatory component to the variability of the pavement thickness. An additional source of uncertainty is related to the resurfacing of the pavement with partial replacement and correction of the deflections/settlements after some decades. The effects described above can be more or less significant and are generally combined in actual bridges.

Fig. 70c shows the pavement thickness for one of the analysed bridges as part of this work using the Ground-Penetrating-Radar (GPR) technique. GPR measurements are performed by emitting electromagnetic waves which are reflected differently by the materials composing the different layers (i.e. bituminous pavement, concrete substrate). The propagation time of the electromagnetic waves is then recorded and converted to a dimension by determining the propagation speed of the wave in each layer. In all the analysed bridges, including this example, the propagation speed in the pavement is calibrated by means of control cores extracted at various locations along the bridge (red dots in Fig. 70c). For details about GPR measurements and calibration see [147, 148, 149]. The plot in Fig. 70c shows that, in this case, in the transversal direction, the pavement is up to 50% thicker close to the edges. Also, the mean value of the thickness is significantly larger than the specified nominal value defined in the original drawings, suggesting that the pavement thickness was probably increased during resurfacing. Fig. 70b shows the ratio between the mean of the measured thickness and the specified nominal value for 7 bridges

build between 1963 and 1994 which were investigated as part of this research (raw data provided by Bridgology SA), see Tab. 23 for details.

Tab. 23 Details of the bridges where pavement thickness measurements are performed, raw data provided by Bridgology SA

Bridge	Location	Construction year	Typology	Span [m]	Nominal thickness [m]	μ*	CoV [%]
Viaduc du Brocard	A21 Martigny-G. St. Bernard (km. 60.060)	1964	Box-girder	19.6-25.0	0.050	1.3-1.7	17.0-20.02
Pont de Rive-Haute	A21 Martigny-G. St. Bernard (km. 250.875)	1972	Hollow-Core Slab	16.0-20.0	0.050	2.3-2.4	16.3-19.3
Jonction de Vennes	N9 Lausanne (km. 7.039)	1963	Hollow-Core Slab	39.0	0.070	2.0-2.2	19.0-21.6
Passage Supérieur Le Daillet	N9 Sion-Sierre (km. 105.161)	1992	Multi-beam	33.5	0.060	1.4	9.4-10.8
Passage Supérieur Sierre-Ouest	N9 Sion-Sierre (km. 113.392)	1992	Slab	36.0	0.075	1.3-1.4	11.1-13.9
Viaduc des Îles Falcon (Nord)	N9 Sion-Sierre (km. 116.104)	1994	Box-girder	27.4-73.0	0.075	1.1-1.4	10.8-13.8
Viaduc des Îles Falcon (Sud)	N9 Sion-Sierre (km. 116.104)	1994	Box-girder	27.4-73.1	0.075	1.1-1.3	8.4-9.9

*The bias is defined as the mean of the measured thickness in each span over the nominal thickness:
$\mu = t_{pav,mean} / t_{pav,nomina}$

It can be observed that the bias factor μ, defined as the ratio between the measurements mean and the nominal thickness for each span, is generally between 1.1 and 1.7, which justifies the increase of the nominal value recommended by [138] of 20 or 40%. The mean measured thickness is never found to be smaller than the nominal value. Also, it can be observed that for smaller spans, the bias ratio increases. This could be related to the fact that for short span bridges, the pavement thickness can depend mainly from requirement related to the level of the approaching road.

Considering the equivalent thickness of the concrete section, h_{eq}, as shown in Fig. 68b and a standard pavement thickness of 100 mm, the pavement weight is relatively more significant for smaller spans than for larger ones, accounting up to 25% of the total permanent load for spans between 8 and 12 m. Since the bias is also larger in those cases, potentially unsafe scenarios are more likely to occur. Considering all the measurements within each span, the CoV of the pavement thickness ranges between 8.4 and 21.6%, see Tab. 23. Despite a slightly larger upper limit, these values are in line with previous researches which presented a CoV between 8 and 15% [145, 146].

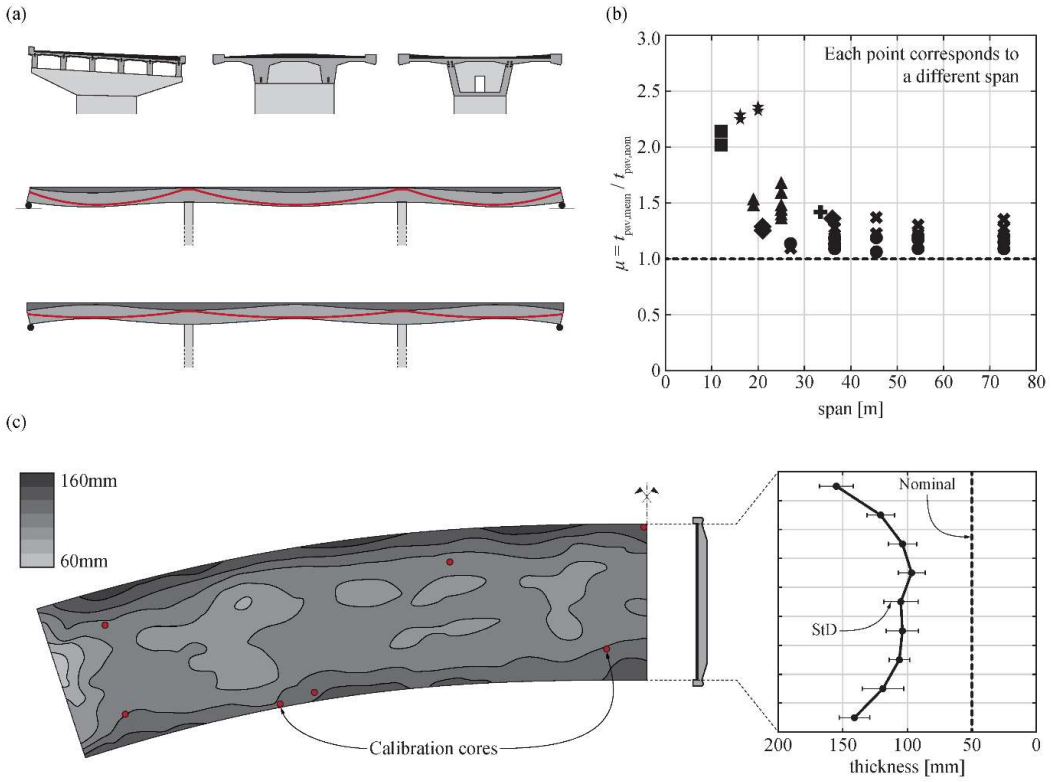

Fig. 70 *Typical pavement thickness variability in road bridges (a) qualitative transversal and longitudinal distributions; (b) ratio between the actual mean and the nominal pavement thickness as a function of the span for the investigated bridges; (c) greyscale map of the measured pavement thickness of the Rive-Haute bridge as an example, see Table 23 (raw data provided by Bridgology SA and analysed as part of this research)*

4.4 Updating of other statistical uncertainties

In addition to the variability of the permanent loads in road bridges described above, an accurate estimation of the variability on the resistance side and of the traffic loads is necessary to calibrate the PSFs. In fact, all variabilities contribute to the limit function, which separates the safe structural domain from the unsafe one. In the First Order Reliability analysis Method (FORM), the relative contribution of the single variabilities is represented by the sensitivity factors, α, which is the partial derivative of the limit state function with respect to the investigated variable. Per definition, the sum of the squares of all sensitivity factors corresponds to 1.0. Thus, if the weight of one variable increases, the weight of all the others must decrease (see [105] for further details on the meaning of the sensitivity factors and FORM analysis). Therefore, to accurately estimate the sensitivity factor of the permanent loads, in the following sections, the variability of the materials parameters, traffic loads and resistance models will be investigated.

4.4.1 Materials strength

Regarding the reinforcement yield strength, f_y, assumptions made in Section 1 of this report are assumed for new structures. For existing structures, these assumptions are verified on the basis of an existing database referring to steel produced in Switzerland [151]. The data of more than 2'500 tests conducted between 1960 and 1994 for steel classes IIIa and IIIb according to SIA 162 [152] (specified 5% characteristic value $f_{yk} \approx 451$MPa) are considered in this evaluation. Figs 71a and 71b show the mean and the CoV of the reinforcement yield strength, f_y, as a function of the year of production and of the bar diameter. The mean value increased with time, associated also with a decrease of the CoV. This was most likely due to the optimization of the industrial production processes over time. For bars with larger diameters, the yield strength shows a decreasing trend. In some cases, when products are categorized by steel type (based on the producer), the distribution deviates from the typical Log-Normal (LN) distribution, see difference between Roll-S and Box-Ultra in Fig. 71c. This was perhaps the result of two different products grouped under the same designation. In fact, the two distributions can clearly be identified and show similar CoV. Overall, the CoV resulting from the analysed data for existing structures is in line with Section 1 where a CoV = 4.5% has been assumed for new structures. These values are also confirmed by other publications [154, 24]. Previous researches [156, 27] report larger CoV, up to 10-12%, however, they are based on a more limited amount of data and different steel grades. With respect to the variability of the actual cross-section of the reinforcement bars, it is implicitly accounted for in the evaluation of the yield strength since the latter is calculated on the basis of the nominal cross-sectional area.

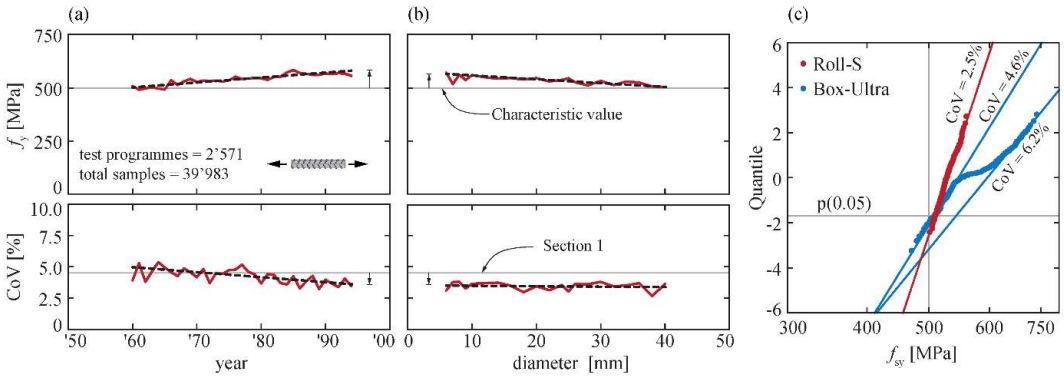

Fig. 71 *Mean and coefficient of variation of steel yield strength, respectively top and bottom: (a) as a function of time; (b) as a function of the bar diameter; (c) log-normal probability plot of two common steel products available in Switzerland.*

Fig. 72a shows the log-normal probability-plot of the yield strength (proof-stress at 0.1% irreversible strain) and the tensile strength of prestressing strands, respectively. The

probability-plot of the Young's modulus is presented in Fig. 72b. Data refer to tests carried out in Switzerland in the period between 1968 and 1979 (see [26]). In particular, Fig. 72a shows that the CoV of the yield strength of prestressing strands is similar to that of passive reinforcement, confirming the assumptions made in Section 1, namely CoV = 4.5% and is consistent with value reported by other researches [158, 27, 159, 154, 30]. In addition, the mean value of the Young's modulus is equal to 195 GPa with a CoV of 2.8%. This value is also consistent with results published by other researchers [158].

Fig. 72c shows the probability-plot of the concrete compressive strength at 28 days ($f_{c,cube,28}$) of various concrete strength classes (C20/25, C25/30, C30/37, C35/45). Distributions are obtained from ~3'500 compression tests performed on concrete cubes with an edge size of 150 mm in Western Switzerland between 2014 and 2021. Tests include concretes used in residential buildings and engineering works with a void content lower than 2.5% and various exposure classes, see Tab. 24 for details.

Tab. 24 *Distribution parameters of the concrete compressive strength variability at 28 days, data provided by TFB SA for samples with void content lower than 2.5%, collected in Western Switzerland between 2014 and 2021. The columns on the right refer to the concrete classification on the basis of the exposure (defined as concrete type according to the Swiss national annex to EN 206 [161])*

Strength Class	Number of tests	Mean $f_{c,cube,28}$ [MPa]	CoV [%]	$P(0.05)$ [MPa]	Type	Number of tests	Exposure Class	Mean $f_{c,cube,28}$ [MPa]	CoV [%]	$P(0.05)$ [MPa]
C20/25	86	35.5	14.1	27.9	A	86	XC1, XC2	35.5	14.1	27.9
C25/30	737	43.8	18.9	31.6	A	227	XC1, XC2	40.0	17.2	29.8
					B	347	XC3	41.3	14.4	32.3
					D	120	XC4, XD1, XF2, XF3, XD2a	53.2	10.4	44.6
					P2	43	ND	50.8	9.9	43
C30/37	2470	51.7	14.2	40.6	A	75	XC1/XC2	44.8	13.6	35.8
					B	121	XC3	56.9	9.2	48.7
					C	1583	XC4/XF1	51.1	11.8	41.8
					F	173	XC4, XD3, XF2, XD2b, XAA	52.1	15.2	40.2
					G	438	XC4, XD3, XF4, XD2b	56.1	15.9	42.7
					P2	80	ND	62.5	13.3	49.8
C35/45	167	59.2	10.9	49.2	C	83	XC4, XF1	56.7	8.7	48.9
					F	40	XC4, XD3, XF2, XD2b, XAA	63.5	11.3	52.4
					G	44	XC4, XD3, XF4, XD2b	62.6	8.0	54.7

Data follows a log-normal distribution (see Fig. 72) which is in line with recommendations of [28] and [135]. As it can be observed, the actual characteristic value of each concrete class (defined as the 5th percentile of the distribution) is generally slightly higher than the specified value (difference from 1.6 to 4.2 MPa). Also, the difference between mean value and 5th percentile varies between 7.6 and 12.2 MPa, which is more or less in line with the typical assumption (between 8 and 10 MPa, see [95]). Besides the strength class, on the right-hand side of Tab. 24, concrete samples are classified based also on their exposure class, see [161]. Tab. 24 shows that a larger mean compressive strength is generally obtained for concretes with more stringent exposure requirements (e.g. for a C30/37 strength class, $f_{c,cube,28}$ of Type G concrete typically used in engineering works is 56.1 MPa while that of Type A typically used in buildings is 44.8 MPa). This over-strength is related to the minimal cement content requirements and to the fact that exposure requirements are often governing in the mix design. This justifies also the large mean compressive strength of concretes used for underwater piles and slurry walls (Type P2). Overall, the resulting CoV for the concrete compressive strength is located in the upper range of results

published in the literature, see Section 1 and Torrenti & Dehn [46]. The empirical rule: f_{cm} - f_{ck} = 8 MPa, provided in EN 1992-1-1:2023 [95] is generally confirmed, although, slightly higher values are obtained. However, it must be noted that these values are specific to the current Swiss concrete production situation which will probably evolve due to environmental requirements.

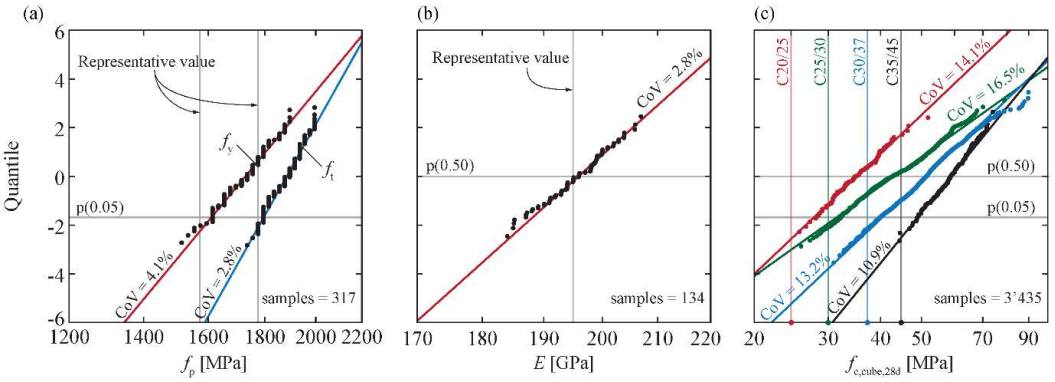

Fig. 72 *Log-normal probability plot of: (a) yield strength (red) and tensile strength (blue) of prestressing strands; (b) elastic modulus of prestressing strands; (c) concrete compressive strength at 28 days ($f_{c,cube,28}$) for various concrete strength classes (all exposure classes included in the analysis), see Tab. 24.*

4.4.2 Traffic loads

The aim of this investigation is not to reproduce a realistic scenario from the structural point of view but to quantify the variability of the traffic loads without considering the uncertainties related to the calculation of action effects and the transversal load distribution. To this purpose, a simply supported bridge with a width of 3 m (single lane) and span varying between 6 and 24 m is used, as shown in Fig. 73a.

Traffic load is simulated using Weight In Motion (WIM) measurements which were performed during more than 20 years at 14 stations located in Switzerland. After being classified considering the vehicle type, the measurements are combined and directly applied on the structure (this simulation procedure is denoted as “direct WIM” in the following, for details regarding WIM data classification and generation of direct-WIM loads, see [163]). Action effects calculated from direct WIM simulations are then compared with those obtained using a representative load model, assumed according to the SIA 261:2020 [143], which is derived from EN 1991-2:2003 [164]. As already mentioned, the aim of this investigation is to quantify the variability of the traffic load in terms of CoV of the action effects. Since the investigated bridge is not representative of a real case (single lane), the bias of the action effects (E_{WIM} /E_{REP}) is not significant for this investigation. For this reason, the adjustment factors $\alpha_{act,Q,i}$ and $\alpha_{act,q,i}$ are set equal to 1.0 (not in accordance with SIA 261:2020 [143]).

Direct WIM simulations are performed using both the weekly maxima traffic loads distribution, obtained from WIM measurements, and the 50-year maxima traffic loads distribution, derived from the weekly maxima as explained further on. To determine the 50-year maxima distribution, the weekly maxima events are considered as Independent-Identically-Distributed (IID) variables. Based on this assumption, if $F_X(x)$ is the common Cumulative Distribution Function (CDF) of the weekly maxima traffic load, and $F_N(y)$ is the CDF of the 50-year maxima traffic loads, with $Y = \max\{X_1, X_2, \ldots, X_N\}$, $F_N(y)$ is obtained from Eq. 54, with N equal to the number of weeks in 50 years (~2’607). Thus, the CDF of Y, the 50-year maxima distribution is obtained by taking the N^{th} power of the CDF of X, the weekly maxima distribution.

$$F_N(y) = P\left[(X_1 < y) \cap (X_2 < y) \cap \ldots \cap (X_N < y)\right] = \left\{F_X(y)\right\}^N \quad (54)$$

If *N* is a large number, the 50-year maxima distribution is either a Gumbel Extreme Values (GEV) Type-I or a Type-II depending on the tail approximation of the IID variable. In particular, if the tail of the Probability Density Function (PDF) of the weekly maxima distribution follows a Log-Normal (LN) or a GEV Type-I distribution, the 50-year maxima distribution will be a GEV Type-I (for additional details about the theoretical derivation and sample maxima distributions, see [165]).

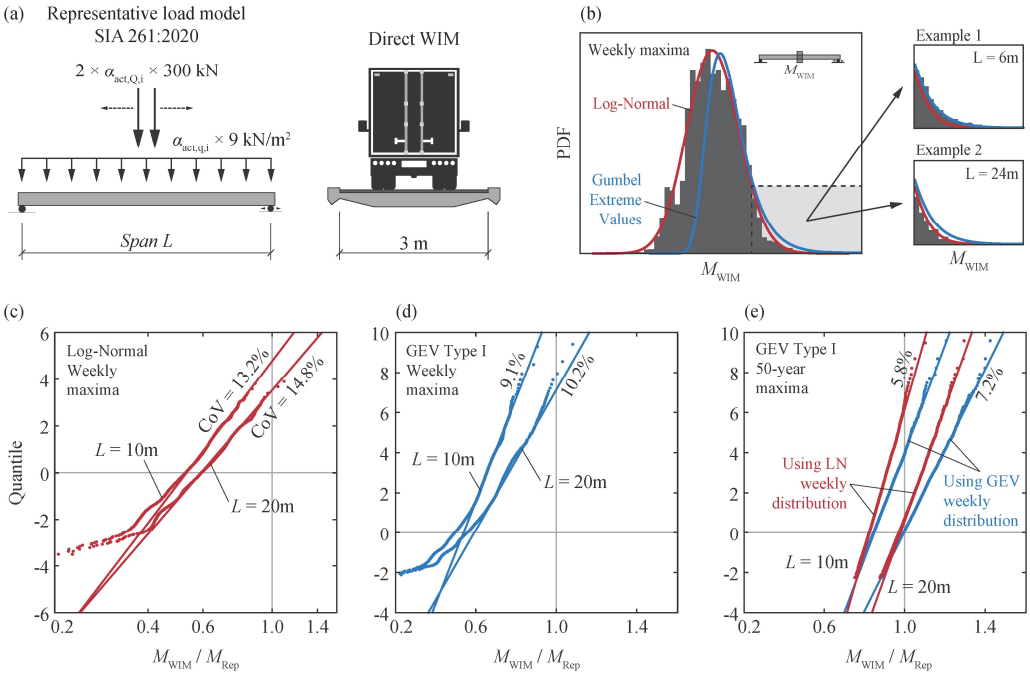

Fig. 73 *(a) Investigated structural system and representative load model according to [143] with the adjustment factors* $\alpha_{act,Q,i} = \alpha_{act,q,i} = 1.0$*; (b) typical histogram of the bending moment at midspan obtained from the weekly maxima direct WIM simulation (*E_{WIM}*) and tail fitting using a LN (red line) and a GEV Type-I distribution (blue line) with tail fitting details; (c) ratio between the bending moment at midspan obtained from direct WIM simulation with weekly maxima distribution and the bending moment at midspan obtained with the representative load model (*M_{WIM}/M_{Rep}*), tail fitted using a LN distribution for a span of 10 m and 20 m; (d) same data presented in (c) but tail fitted using a GEV Type-I distribution; (e) 50-year maxima distributions resulting from the weekly maxima distributions presented in (c) and (d).*

Fig. 73b shows a typical histogram obtained for the bending moment at midspan using the weekly maxima traffic distribution and the tail fitting using both a LN and a GEV Type-I distribution presented respectively in red and blue. As presented in the tail fitting details of Fig. 73b, with example 1 and 2 corresponding respectively to a span of 10 and 20 m, the most suitable distribution type depends on the specific case. Since the accuracy in approximating the tail fitting of the weekly maxima distribution influences significantly the distribution of the 50-year maxima and it is not possible to know a priori the best tail fitting distribution, both, a LN and a GEV Type-I distributions are used in the following to fit the tail of the weekly maxima distribution for each span L. Fig. 73c shows the probability-plot of the ratio between the bending moment at midspan obtained using the traffic weekly maxima distribution (M_{WIM}) and the bending moment obtained with the representative load model (M_{REP}) fitted using a LN distribution for a span L = 10 m and L = 20 m. The same cases are presented also in Figs 73d but using a GEV Type-I distribution. In Figs 73c and 73d, the fitting is performed considering only points on the upper part of the distribution (P > 0.5). Fig. 73e shows the resulting 50-year maxima distribution using the weekly distributions of Fig. 73c and 73d. Since the PDF tail of the GEV Type-I distribution shows a slower decrease than the LN distribution, it leads to larger bias and CoV. Based on the analysed spans, the CoV of the traffic load effects is found between 10% and 18% for the weekly maxima traffic load distribution and between 6% and 10% for the 50-year maxima traffic load distribution.

4.4.3 Variability of resistance calculation

The variability of the sectional resistance calculation is quantified by means of Monte-Carlo simulations performed considering the variability of the materials strength, the calculation models and the geometry. More specifically, this work focuses in quantifying the variability of the resisting bending moment calculation and the variability of the shear resistance calculation for members with shear reinforcement. To this purpose, the models provided in Section 8 of EN 1992-1-1:2023 [95] are implemented (provisions 8.1.1 and 8.1.2(1) for bending and 8.2.3(1-3,5,7,8) for shear). In addition, to investigate the influence of the cross-sectional dimensions (see Fig. 68c), a concrete section with constant width and depth, h, varying between 0.35 m and 1.4 m is investigated.

The variability of the materials strength is assumed according to Section 1 of this report while the geometric variability is assumed according to [28], except for the effective depth which is assumed according to Section 1, see Tab. 25. With regard to the model uncertainty for the calculation of the resisting bending moment, with failure occurring on the steel side, the value proposed in Section 1 is assumed while the model uncertainty for the calculation of the shear resistance in members with shear reinforcement is assumed according to [104]. Tab. 25 gives an overview of the statistical parameters used to perform the Monte-Carlo simulations. For details on the implemented models, see EN 1992-1-1:2023 [95].

Tab. 25 *Statistical distributions assumed for performing Monte-Carlo analyses to quantify the variability of shear resistance for members with shear reinforcement and bending moment resistance for RC members*

Random variable	CoV – V [%]	Bias - μ	Reference
f_c	10.0	1.18	Section 1 and Subsection 4.3
η_{is}	12.0	0.95	Section 1
f_y	4.50	1.08	Section 1 and Subsection 4.3
d	$5\cdot(200/d)^{2/3}$	$1 - 0.05\cdot(200/d)^{2/3}$	Section 1
A_c	2.0 – 6.0	1.00	JCSS report, 2001 [28]
$\theta_{R,Flex,steel}$	4.50	1.09	Section 1
$\theta_{R,Shear}$	19.4	1.11	Pejatovic et al. [104]

Fig. 74a and 74b show the resulting CoV (V_R) and the bias factor (μ) for the calculated resistances as a function of the section depth h. For each section depth, 10’000 simulations

are performed for both shear resistance and bending moment resistance to determine the coefficient of variation and the bias factor. Fig. 74c shows the probability plot for the case of h = 0.35 m.

Fig. 74a shows that for the calculation of the bending moment, the CoV decreases with increasing depth, h. This is due to the fact that the relative variability of the effective depth (d) is less significant for larger members. In fact, according to the formula in Tab. 25, an effective depth d = 1.2 m leads to μ =0.985 and V = 1.51% whereas for d = 0.2 m, μ =0.95 and V = 5%. On the other hand, for the calculation of the shear resistance, the variability of the effective depth is less significant, leading to a less pronounced reduction of CoV for larger members. Fig. 74b shows that for the shear resistance calculation, the bias varies between 1.20 and 1.25 while for the calculation of the bending moment, the bias varies between 1.14 and 1.16.

It can be noted that, regardless of the beam depth, the coefficient of variation V_R is much larger for the calculation of the shear resistance than for the calculation of the resisting bending moment. This is mainly due to the large model uncertainty for shear resistance calculation, see Tab. 25. Fig. 74c shows also that a Log-Normal (LN) distribution is a good fit for the resistance variability both for the calculation of shear and bending moment resistance, in line with the recommendations of [28] and Section 1.

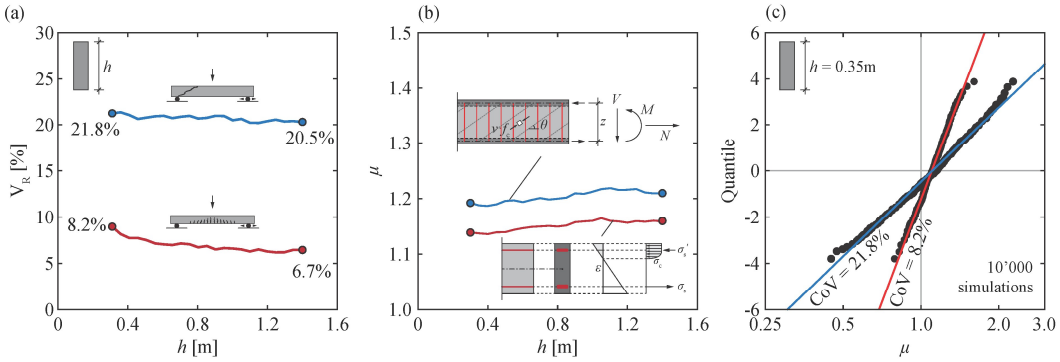

Fig. 74 *Variability of bending moment and shear resistance calculation for a beam with fixed width and varying depth between 0.35 m and 1.4 m: (a) V_R and (b) μ; (c) LN probability-plot of sectional resistance calculation for a beam with depth equal to 0.35 m.*

4.5 Calibration of γ_{G1} and γ_{G2} using FORM

As already discussed in the previous sections, the variability of the structural and non-structural self-weight is significantly different in road bridges. Therefore, the partial safety factor for permanent loads, γ_{Gi}, is treated separately for structural and non-structural self-weight, denoted with γ_{G1} and γ_{G2}, respectively. To estimate their values, parametric FORM analyses are performed covering a wide range of scenarios. The statistical distribution parameters of action effects (E), sectional resistance (R) and model uncertainty in action effects calculation (θ_E) are presented in Tab. 26.

The statistical distributions of the actions effects due to the structural and non-structural self-weight, respectively E_{G1} and E_{G2}, are obtained on the basis of the considerations made in the previous sections which are resumed in Tab. 27 and 28. To account for the large uncertainty related to the traffic loads, a wide range of CoVs is considered on the action effects due to the latter (V_{EQ}). Also, since the variability of the sectional resistance calculation varies largely depending on the failure mode, the latter is investigated considering a wide range of the CoV (V_R). Finally, the statistical distribution parameters of the uncertainty in action effects calculation are assumed according to Section 2. In particular, for a Linear Elastic model with uncracked sectional stiffness, a CoV of 6.5% is assumed as shown in Tab. 26.

Regarding the representative values of the actions, the self-weight for reinforced concrete members is calculated using the nominal dimensions and the specific weight equal to 25 kN/m^3 [138], including the reinforcement. The pavement load is calculated considering a representative thickness of the pavement of 100 mm (i.e., not accounting for the increase of 20-40% recommended in [138]) and the specific weight equal to 24 kN/m^3 [138]. Finally, the representative value of the traffic load (Q) is considered as a function of the permanent loads ($G = G_1+G_2$). Specifically, the ratio of the action effect due to permanent loads over the action effects due to traffic loads E_G/E_Q, is assumed equal to 4 and 0.5, which correspond respectively to a long and a short span bridge.

The limit state function is formulated in the classical form as in Eq. 55 while γ_{Gi} is calculated according to Eq. 56 with the sensitivity factors, α, obtained from the FORM analyses. Besides the uncertainty related to the representative value of the permanent loads, γ_{Gi} covers also the model uncertainty in the action effects calculation, denoted with θ_E. Thus, to account for this uncertainty, α_{Gi}, V_{Gi} and μ_{Gi} are calculated as in Eq. 57.

The value of $\beta_{tgt,50y}$ is assumed according to [135], equal to 3.8. Indeed, the choice of β_{tgt} depends on the risk acceptance at a societal level and is not treated in this work.

$$g(R,E) = R - E = R - (E_{G1} + E_{G2} + E_Q) \cdot \theta_E \tag{55}$$

$$\gamma_{Gi} = \mu_{Gi} \cdot exp(\alpha_{Gi} \cdot \beta_{tgt} \cdot V_{Gi}) \tag{56}$$

$$\alpha_{Gi} = \sqrt{\alpha_{gi}^2 + \alpha_{\theta E}^2} \qquad V_{Gi} = \sqrt{V_{gi}^2 + V_{\theta E}^2} \qquad \mu_{Gi} = \mu_{gi} \cdot \mu_{\theta E} \tag{57}$$

Tab. *26* Distribution type and parameters of random variables used for the parametric analyses

Random variable	CoV – *V* [%]	Bias - μ	Reference
EG1	Normal	1.00	3-6
EG2	Normal	1.10-1.30	15-25
EQ	Log-normal	0.7-1.0	4-26
R.	Log-normal	1.09-1.12	4-24
θE	Log-normal	1.00	6.5

Fig. 75 shows the sensitivity factors α, smaller than 1 by definition, and the partial safety factors γ, larger than 1, obtained from the parametric analysis as a function of the coefficients of variation V_R and V_Q. As already mentioned, two ratios of E_G/E_Q are investigated, namely 4 and 0.5, which correspond respectively to a long and short span bridge (the ratio total permanent load / total live load (G/Q) for bridges with increasing span is shown in Fig. 68c). For a long-span bridge, Fig. 75a and 75c show that V_Q does not influence γ_{G1} and γ_{G2} while an increase of V_R leads to smaller values of γ_{G1} and γ_{G2}. In fact, since traffic loads are less significant compared to permanent loads, their variability does not lead to a remarkable change of the sensitivity factor (α), and consequently on the partial factors (γ). On the other hand, for short span bridges, an increase of both V_Q and V_R leads to a decrease of γ_{G1} and γ_{G2}. Overall, for the investigated scenarios, the required value of γ_{G1} varies between 1.1 and 1.2, whereas γ_{G2} varies between 1.3 and 1.8.

Based on the results of the parametric analysis, the proposed values for γ_{G1} and γ_{G2} are 1.2 and 1.5, respectively. To cover the cases where γ_{G2} is larger than 1.5, an increase of the representative value of the pavement thickness as required in [102] and in [138] is justified (an increase of the nominal value by 20% covers the cases where γ_{G2} is larger than 1.5: 1.2×1.5 = 1.8).

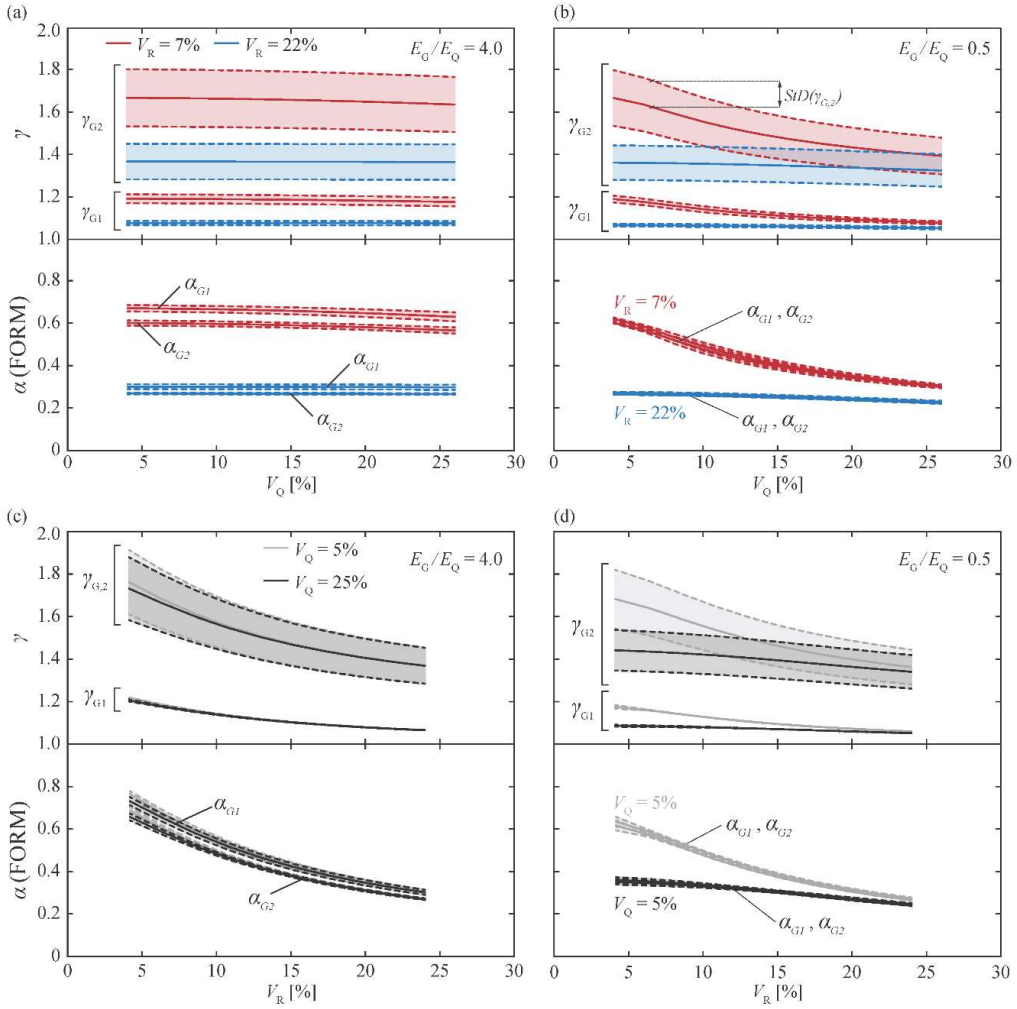

Fig. 75 *α_{G1} , α_{G2} [0,1] and γ_{G1} , γ_{G2} (>1) as a function of V_Q and V_R for a road bridge with E_G/E_Q equal to 4 and 0.5, which correspond respectively to a long and short span bridge.*

4.6 Validation of the proposed partial factors for a particular case

To investigate if a sufficient level of safety is achieved with the proposed partial safety factors, more refined reliability analyses are performed on two bridges with a maximum span of 20 and 30 m, respectively. Fig. 78a shows the longitudinal scheme and the transversal cross-section of the investigated bridges.

Both bridges are designed to fulfil the requirements of traffic loads for new bridges, according to [143], and for existing bridges according to [168], while representative permanent loads are calculated according to [138] (but no increase of the nominal pavement thickness is considered). Dimensioning is performed according to Section 8 of EN 1992-1-1:2023 [95] with a reinforcement ratio in the tension zones ranging between 0.4 and 0.8% and the post-tensioning tendons designed to carry the remaining required tension force at ULS (the average compressive concrete stress due to prestressing P/A_c is 1.75 and 2.05 MPa for the bridge with maximum span of 20 m and 30 m, respectively). The considered partial factors for the dimensioning are $\gamma_S = 1.15$ and $\gamma_C = 1.50$ whereas the currently recommended partial factors for the permanent actions $\gamma_{G1} = \gamma_{G2} = 1.35$ as well as the proposed combination $\gamma_{G1} = 1.20$ and $\gamma_{G2} = 1.50$ are considered. The strain difference in the prestressing steel and the hyperstatic moments due to prestressing are calculated considering: (i) an initial prestressing stress of $0.7 \cdot f_{pk}$, (ii) the tendon's geometry

shown in Fig. 77c, (iii) the friction losses according to EN 1992-1-1:2023, and (iv) 15% losses due to relaxation, shrinkage and creep.

For the refined reliability analyses, the variability of the geometry and the specific weight is modelled considering that a certain correlation exists between two points in the same element. This correlation is expressed by the Pearson correlation coefficient, which is denoted with ρ_{cc} and is calculated according to [28] as shown by Eq. 58, where δ is the correlation length, characteristic of the member type (e.g. equal to 6 m for slabs and walls and 10 m for reinforced concrete beam) and Δr is the distance between the points. The parameter ρ_{cc0} represents the correlation between two far away points in the same element.

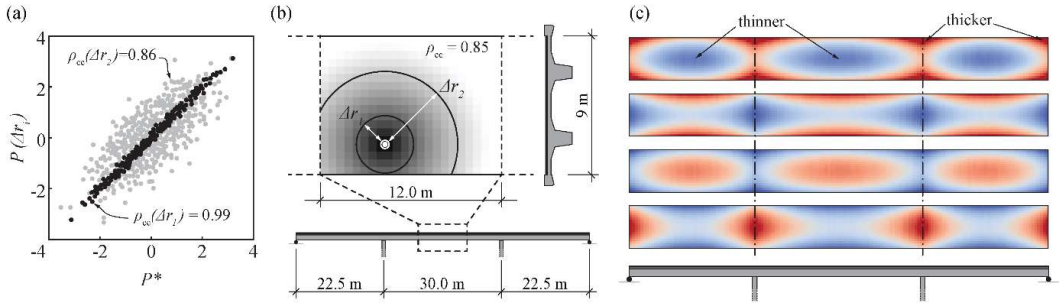

Fig. 76 *(a) Property of a reference point P* and property of a point at a distance Δr_1 and Δr_2 considering the Pearson correlation coefficient ρ_{cc}; (b) decrease of ρ_{cc} from a reference point; (c) typical simulations of pavement thickness variability in road bridges.*

Fig. 76a illustrates the correlation between the property of a reference point, *P**, and the property of two different points, $P(\Delta R_1)$ and $P(\Delta R_2)$, part of the same structural element, respectively at a distance Δr_1 and Δr_2 from the reference point, see Fig. 76b. Fig. 76b shows the decrease of ρ_{cc} as a function of the distance Δr. For a distance between the points larger than the characteristic length (δ), $\rho_{cc} = \rho_{cc0}$, with $\rho_{cc0} = 0.85$ in this particular case, assumed according to [28]. If multiple points are involved, instead of a single coefficient, the correlation is represented by a symmetric matrix [$n \times n$] with n equal to the number of investigated points. The symmetry of the matrix is due to the fact that ρ_{cc} is calculated considering only the distance between points and not the direction.

$$\rho_{cc}(\Delta r) = \rho_{cc} + (1 - \rho_{cc0}) \cdot \exp\left(-(\Delta r / \delta)^2\right) \quad with \quad \rho_{cc0} = 0.85 \tag{58}$$

Correlation of the pavement thickness and specific weight in different points of the same bridge is modelled using the same procedure and the characteristic length δ = 6 m.

Fig. 76c presents the resulting pavement thickness modelled by discretizing the surface of the bridge deck and implementing the longitudinal, the transversal and the aleatoric variability (see Subsection 4.3). The correlation is implemented using the methodology described above. The longitudinal and transversal thickness variabilities, which account for the pre-existing deformations, are modelled assuming a parabolic profile in both directions with the ratio $t_{long,support} / t_{long,midspan}$ and $t_{transv,center} / t_{transv,edge}$ defined by the distribution presented in Tab. 28. Tab. 27 presents the distribution parameters assumed for modelling the variability of the structural self-weight. The geometric variability is modelled according to [28] as shown in Fig. 68c. For the reinforcement content, the statistical parameters presented in Tab. 27 are assumed, see also Fig. 69.

Tab. 27 *Statistical parameters for modelling of the structural self weight*

Random variable	CoV – *V* [%]	Bias – *μ*	Mean value
Ac	2.0 – 5.0	1.00	-
pconcrete [kN/m3]	4.0	-	24.0
Reinforcement content [kg/m3]	15.0	-	130.0

Tab. 28 *Statistical parameters for modelling of the pavement load*

Random variable	CoV – V [%]	Bias – μ	Mean value
$t_{long,support}$ / $t_{long,midspan}$	20.0	1.00	-
$t_{transv,center}$ / $t_{transv,edge}$	20.0	1.00	-
t / $t_{nominal}$	4.0	1.00	-
Vol / $Vol_{nominal}$	22.0	1.25	-
ρ_{pav} [kN/m^3]	4.0	-	24.0

The aleatoric variability, $t / t_{nominal}$ is not related to pre-existing deformations but to imperfections of the concrete substrate and paving placing precision. The variability of the total volume of the pavement is defined by a distribution with mean 1.25 and CoV of 22%, in line with previous research and the findings of this work. It is important to note that cases where the nominal thickness is increased as a maintenance strategy are not considered as variability.

To obtain the variability of the action effect at a given position for both structural and non-structural load, a Monte-Carlo simulation is performed using the statistical distributions in Tab. 28 and 27. For each draw, the load pattern (load of each discretized element) is defined accounting also for the correlation and the action effect at a given position is calculated using a finite element (FE) model with 2D elements as shown in Fig. 77a.

Due to the large number of simulations, the influence surfaces / lines are calculated for each investigated cross-section and internal force (i.e. shear and bending moment). Subsequently, the action effect (E), is calculated by performing fast matrix operations. As an example, Fig. 77b shows the influence surface of the bending moment at midspan for one beam of the half-section.

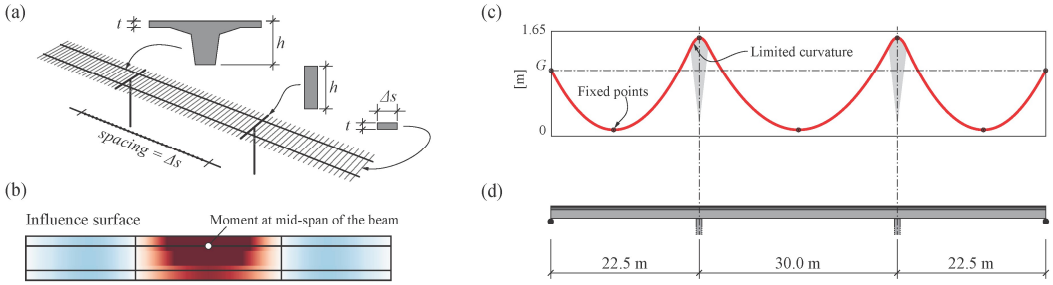

Fig. 77 *(a) FE model for calculation of influence lines/surfaces; (b) influence surface of the moment at midspan of the beam; (c) automatically determined profile of the prestressing tendon given the constraints on the curvature and the mandatory passing points; (d) longitudinal profile of the investigated bridge.*

For both investigated bridges (maximum spans of 20 and 30 m, respectively), 2×2×2 = 8 different scenarios are investigated, as presented in Tab. 29. Specifically, they include two different traffic configurations (unidirectional and bidirectional), two vehicle typologies (up to 42 t or 96 t, i.e., without and with mobile cranes) and two distribution types for fitting the tail of the WIM weekly maxima traffic loads (LN and GEV Type-I). For each scenario, reliability analyses are performed at the support and midspan section, denoted respectively with S1 and S2 in Fig. 78a. The following failure modes are considered: (1) shear failure for sections S1, (2) flexural failure with failure occurring on the steel side for both sections S1 and S2 (3) flexural failure with failure occurring on the concrete side for section S1. For the bridge with maximum span of 20 m and 30 m the ratio between the neutral axis depth and the effective depth in section S1, is respectively $x/d = 0.36$ ($x = 469$ mm) and $x/d = 0.40$ ($x = 625$ mm), justifying such a failure mode. As a comparison with the parametric reliability analysis, the ratio E_G / E_Q for the sections of the investigated bridges

ranges between 0.55 and 1.25, thus, covered by the limit cases of 0.5 and 4.0 considered for the FORM calibration of γ_{G1} and γ_{G2} shown in the previous subsection.

Tab. *29* *Scenarios considered for calculation of the reliability index β_{50y}*

Scenario	Traffic configuration	Vehicles class	Weekly maxima tail-fitting
1	Unidirectional	Including mobile cranes	GEV
2	Unidirectional	Including mobile cranes	LN
3	Unidirectional	Without mobile cranes	GEV
4	Unidirectional	Without mobile cranes	LN
5	Bidirectional	Including mobile cranes	GEV
6	Bidirectional	Including mobile cranes	LN
7	Bidirectional	Without mobile cranes	GEV
8	Bidirectional	Without mobile cranes	LN

The traffic load variability is considered using the WIM measurements introduced in Section 4.3.2 while the variability of the structural and non-structural self-weight is modelled using the methodology presented above. The variability of the resistance calculation is calculated as in Subsection 4.3.3 while the variability of the model for calculation of action effects is assumed according to Section 2, as for the parametric analysis.

To reduce the time needed to perform the crude Monte-Carlo (MC) reliability analyses, the Importance Sampling technique (MC-IS) is adopted. Accordingly, a FORM analysis is first performed to determine the design point and subsequently, the Monte-Carlo simulations are then performed around that point. This technique requires a smaller number of simulations to determine the reliability index β (see [169] for details about Monte-Carlo analysis and the Importance Sampling technique).

The limit state function is formulated in the classical form as for the parametric reliability analyses in Eq. 55. For each analysis, the limit state function is evaluated ~100’000 times to calculate the reliability index β. Overall, for all the investigated scenarios, sections and failure modes, ~5’000’000 simulations were performed.

Fig. 78b-d and 78e-g show the β_{50y} obtained from the MC-IS reliability analyses. The points corresponding to the same scenario refer to the different sections, failure modes, partial factors for permanent loads and different spans investigated. It can be observed that the β_{50y} obtained with the proposed partial factors γ_{G1} and γ_{G2} is similar to the one obtained with the current partial safety factors. Thus, the overall structural safety remains unchanged. However, the partial safety factors reflect better the uncertainties they are supposed to cover. This observation is further supported by the fact that β_{50y} is generally less dispersed with the newly proposed values. Fig. 78b-d shows that for new bridges, regardless of the scenario, β_{50y} is generally larger than 4.5, indicating that a safety margin is present if compared to the target value $\beta_{tgt,50y}$ = 3.8. On the other hand, β_{50y} calculated using reduced traffic loads for existing bridges shown in Fig. 78e-g, is much closer to $\beta_{tgt,50y}$ (however, it must be noted that for existing structures, the value of $\beta_{tgt,50y}$ may be reduced).

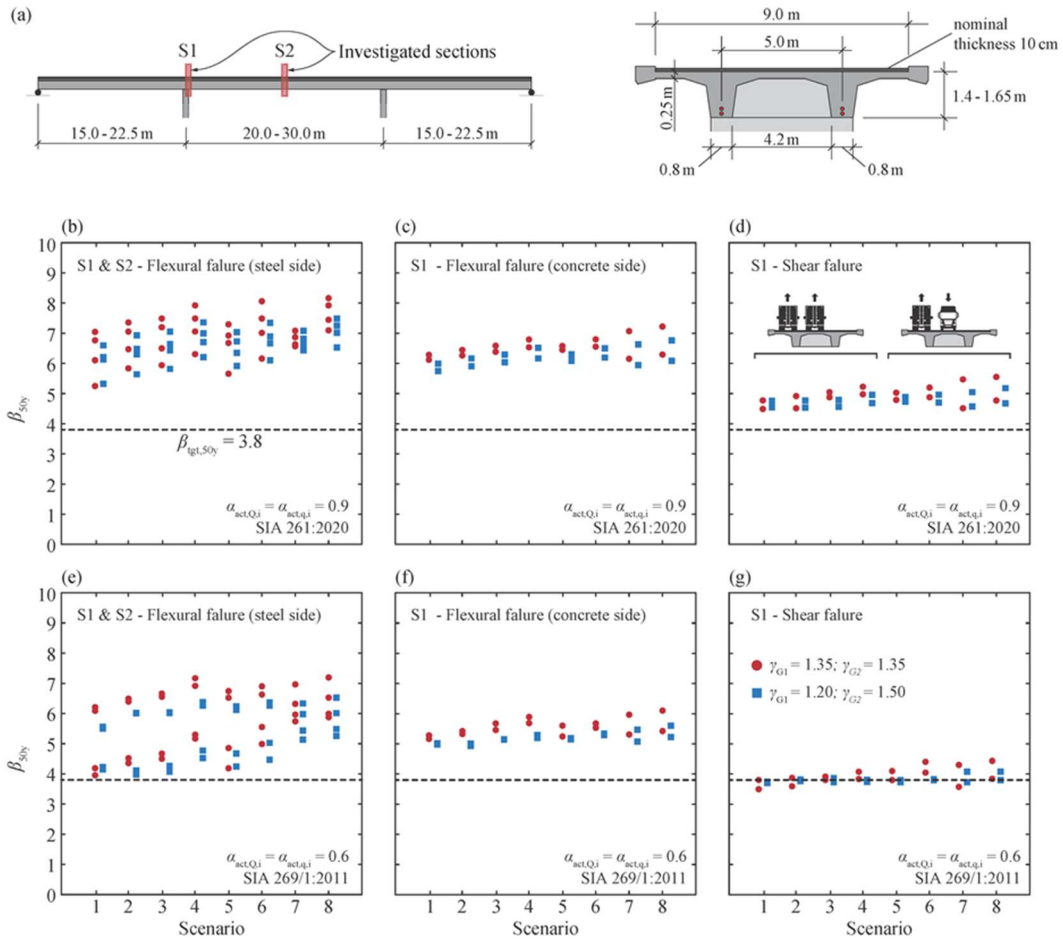

Fig. 78 *(a) Longitudinal scheme and cross-section of the investigated bridges, resulting β_{50y} calculated with the current (circles) and the proposed partial safety factors (squares): (b-d) considering adjustment factors $\alpha_{act,q,i}$ and $\alpha_{act,Q,i}$ according to [143] for new structures and (e-g) according to [168] for existing structures. The blue squares have been shifted to the right to improve readability of the plots, however, they refer to the same scenario as the red circles.*

4.7 Modelling of the structure, evolutions of structural system and designer's choices

It has to be noted that the proposed values for the partial safety factors γ_{G1} and γ_{G2} are based on the model uncertainties for the action effects analysed in Sections 2 and 3. As already discussed in Section 2, the model uncertainty related to the action effects significantly depends on the complexity and the level of statical indeterminacy of the structure. In fact, in statically determinate structures, where the internal forces depend almost only on the actions and on equilibrium, the model uncertainty related to the internal forces is very small and only depends on the geometrical uncertainties which has an almost negligible effect. In these cases, the assumed values for the model uncertainties of the action effects calculation can be considered as overly conservative. At the other side, for highly indeterminate complex structures, the model uncertainties can be significant, particularly in the case of system changes during construction. With this respect, the exact construction sequence is not necessarily known during the design, the creep deformations which affect the redistributions of internal forces are also affected by significant uncertainties, and above all, these effects are usually not accounted for in a detailed manner. In this context, the deformation capacity of the critical cross sections associated to the governing failure modes plays also a significant role. In case of ductile behaviour, all

these types of uncertainties have little influence on the load-bearing capacity since plastic redistributions of the internal forces can adjust a difference between calculated and actual internal forces (see Section 2). On the other side, for brittle behaviour, the possibility of a redistribution of internal forces is limited, so that the model uncertainties in the actions affect calculation can play a major role. In addition, for complex structures, additional uncertainties can be expected with respect to the models implemented in commercial analysis software tools and the choices by the designer in modelling the structures. This applies for linear elastic calculations, but also to an even larger extent for nonlinear analyses. These considerations, which were not the aim of the present work, deserve to be investigated in the future also accounting for the increasing complexity of the analysis tools used nowadays which can give to the designer the impression of a precision which cannot be reached for the reasons explained above.

To solve these problems, an increase of the complexity in the analysis, the consideration of a larger number of load combinations and scenarios, as well as a detailed analysis of the effects related to system changes during construction are not necessarily to be recommended. Also, designer's choices regarding structural modelling a complex structure in an apparently more detailed manner can lead to further uncertainties in calculating action effects. In fact, the increasing complexity of commercially available software makes it more difficult to verify the assumptions. For instance, the modelling of the load, the selection of the finite element, the interaction between different finite elements, the definition of the reference axis, the modelling of prestressing, the modelling of the system changes etc. are more or less conscious choices whose influences should be evaluated by the designers. In addition, an analysis with increasing complexity can even be counterproductive since it would increase the probability of human errors. According to the authors, it is more reasonable to invest time in thinking which is the most suitable and reasonably safe modelling, trying to evaluate qualitatively the potential uncertainties and interpret correctly the results.

These considerations are not the aim of this paper and further effort should be put in investigating this topic.

4.8 Conclusions

This section investigates the sources of structural and non-structural self-weight variability in road bridges along with other variabilities influencing structural safety in reinforced concrete structures. Based on the presented work, the main findings are:

1. Structural self-weight variability in bridges is mainly caused by geometrical, reinforcement content and concrete specific weight variability. Geometrical variabilities are less significant for large members. The CoV for structural self-weight of common members is generally between 3 and 6%;
2. Variability of the pavement thickness in a road bridge can be significant. For each span of the investigated bridges, the ratio between the measurements mean and the nominal thickness is generally located between 1.1 and 1.7 (larger for smaller spans). Considering all the measurements within each span, the CoV of the pavement thickness ranges between 8.4 and 21.6%. In some cases, the ratio between the measurements mean and the nominal thickness is larger than 2 suggesting an increase of the nominal value during resurfacing;
3. Distribution parameters of materials strength based on Swiss measurement are generally in line with values specified in Section 1. However, the CoV and bias factor of concrete strength for the analysed data are larger than data found in international literature. This over-strength is probably to be attributed to an increase in cement content to meet durability and workability criteria by producers;
4. The variability of the traffic load for the weekly-maxima events is found between 10 and 18%. Extrapolation of 50-year maxima distributions depends significantly on the tail fitting accuracy of the starting distribution. Considering log-normal and Gumbel distributions for the tail fitting leads to CoV of the traffic load variability between 6 and 10%;
5. According to the parametric reliability analyses, the required value of γ_{G1} for self-weight to reach the target value of the reliability index $\beta_{tgt,50y} = 3.8$ lies between 1.1 and 1.2 while γ_{G2} for other permanent actions is between 1.3 and 1.8 in case the nominal pavement thickness is considered as reference value. Reliability analyses performed on selected case studies including various failure modes confirm that $\gamma_{G1} = 1.2$ and $\gamma_{G2} = 1.5$ lead in general to sufficiently safe results for the design of new and the assessment of existing structures. With respect to the reference value of the pavement thickness, an increase of 20% of the nominal value as recommended in Eurocode 1 is justified;
6. Structural system changes during construction and significant differences between modelling of complex structures and actual behaviour are not accounted for in the partial safety factors on the load side described above. If relevant for the structural system, depending on its complexity and particularly in case of governing brittle failure modes, if the behaviour cannot be improved with sound detailing during the design process, the structure should be modelled in a reasonably conservative manner and the results interpreted accordingly.

5 Proposed partial factors

Based on the investigations described in this report, the following partial factors for persistent and transient design situations are proposed for a target value of the reliability index $\beta_{tgt,50}$ = 3.8 (CC2).

- For reinforcing steel:
  - If the verification is conducted with nominal values of the geometrical dimensions, the value γ_S = 1.15 is confirmed
  - If the verification is conducted on the basis of design values of the effective depth $d_d = d_{nom} - 15$ mm, the partial factor for reinforcement may be reduced to γ_S = 1.05.
- For concrete:
  - The value γ_C = 1.50 is confirmed.
- For structural steel:
  - The value γ_{M1} = 1.05 is confirmed.
- For shear in slabs without shear reinforcement and for punching according to EN 1992-1-1:2023:
  - If the verification is conducted with nominal values of the geometrical dimensions, the value γ_V = 1.40;
  - If the verification is conducted on the basis of design values of the effective depth $d_d = d_{nom} - 15$ mm, the partial factor for shear and punching may be reduced to γ_V = 1.30.
- The partial factor γ_{Sd} covering the model uncertainties in the action effect calculation lies between 1.05 and 1.15 depending on the other uncertainties. This factor is implicitly accounted for in the partial factors γ_G and γ_Q . Alternatively, γ_G and γ_Q can be calibrated assuming following statistical values of the model uncertainty: bias factor μ = 1.0 and CoV = 6.5-8%. It has to be noted that these factors and statistical values do not account for potential uncertainties related to the modelling of complex structures and/or the influence of system changes in the case of structures with limited deformation capacity and limited possibility to redistribute internal forces at ultimate limit state.
- For the permanent actions:
  - Since the uncertainties of the self-weight of the structural elements and the non-structural elements are different, it is recommended to use two separate partial factors, namely γ_{G1} for structural and γ_{G2} for non-structural elements.
  - The default value of the factor for the structural self-weight is γ_{G1} = 1.35 as in current SIA 260. γ_{G1} may be reduced to 1.20 in case the modelling of the structure is conducted by the designer in a sufficiently reliable manner (sufficient experience with respect to the type of structure / software used / influence of the modelling of the structure on the results based on similar calculations on similar structures) and if the influence of changes in the system during construction is accounted for in a sufficiently reliable manner (method used / material parameters assumed / experience of the designer with respect to the influence of the assumptions on the results). The same reduction is allowed also in the case of statically determinate structures.
  - The partial factor for the self-weight of non-structural elements γ_{G2} = 1.50 is proposed. For the pavement of road bridges, in addition to γ_{G2} = 1.50, the nominal thickness should be increased by 20% in accordance with EN 1991-2:2023 [138].
- For the variable actions:
  - The design values are derived on the basis of reliability analyses (out of the scope of the present research since the calibration of traffic loads, including their design values, are currently investigated in other research projects [170, 171]). The characteristic values can be determined by dividing the design value by a nominal partial factor γ_Q = 1.50.

- The above partial factors are valid for the design of new structures and for the assessment of existing structures where the related variables have not been assessed by direct measurements.

- For the assessment of existing structures, where the dimensions have been measured on site and/or the material strengths have been assessed from tests on samples taken from the existing structure, the partial factors may be adjusted using the procedure described in this report and the statistical values derived from the measurements. As a first step, the following partial factors may be assumed:
  - For γ_S and γ_C , the values provided in Annex A (Adjustment of partial factors for materials) of EN 1992-1-1:2023 may be used;
  - For the structural self-weight, the values of γ_{G1} described above should be used;
  - For the other permanent actions, γ_{G2} = 1.20 may be used the dimensions are measured on the existing structure.

Appendixes

I Applicable range of the combination of partial factors γ_c and γ_s

The aim of this appendix is to give a simple illustration of the applicable condition for the combination of the two basic partial factors, γ_C and γ_S.

As is pointed out in Subsection 1.3, for the cases where the sum of the exponents n_{fc} and n_{fy} is significantly lower than 1, the partial factors applied to material strength variables are not suitable anymore. Due to this reason, in the following, only the resistance models with the sum of n_{fc} and n_{fy} is equal to or close to 1 is considered ($n_{fc} + n_{fy} \cong 1$). For this type of cases, the applicable range depends on the variability of the basic uncertainties involved, as well as the shape of the resistance function.

The typical resistance models for the design of RC structures analysed in Subsection 1.3 will be used as references to help explain the applicability of γ_C and γ_S.

In terms of the shape of the resistance functions, the models analysed in Subsection 1.3 can be categorized into three types, namely:

- Type I: the axial compression and tension force resistance model neglecting second order effect and confinement reinforcement (Fig. 1a-b of Subsection 1.3.1):

  $$R \cong C_0 \cdot (f_y \cdot A_s)^{nfy} \cdot (f_{c,ais} \cdot A_c)^{nfc} = C_0 \cdot (f_y \cdot A_s)^{nfy} \cdot (f_{c,ais} \cdot b^2)^{nfc}$$

  For this type of resistance models, the contribution from longitudinal reinforcement depends on the yield strength f_y and the reinforcement area A_s, while the contribution from concrete depends on the compressive strength $f_{c,ais}$ and the cross-section area A_c ($A_c = b^2$ for square cross-section). Due to this reason, f_y and A_s share the same exponent n_{fy}. Similarly, $f_{c,ai}$ and A_c share the same component n_{fc}.
- Type II: the bending resistance for a suitably reinforced beam (Fig. 1c of Subsection 1.3.1):

  $$R \cong f_y \cdot A_s \cdot d \cdot (1 - \frac{f_y \cdot A_s}{2 \cdot f_{c,ais} \cdot b \cdot d}) \cong C_0 \cdot f_y \cdot A_s \cdot d \cdot (\frac{f_{c,ais} \cdot b \cdot d}{f_y \cdot A_s})^{nfc}$$

  $$\cong C_0 \cdot (f_y \cdot A_s \cdot d)^{nfy} \cdot (f_{c,ais} \cdot b \cdot d^2)^{nfc}$$

  For the bending resistance model, in addition to f_y and A_s, the contribution from longitudinal reinforcement also depends on its effective depth d (which influences the lever arm between the tension and compression chord); similarly, in addition to $f_{c,ais}$, the contribution from concrete depends on the width of the cross-section b and the effective depth d. It should be noted that since the effective depth d has an exponent two in the part of the equation representing the contribution of concrete strength.
- Type III: the shear resistance of a beam with shear reinforcement analysed with the closed-form model (clause 8.2.3 of EN 1992-1-1:2023) [14](Fig. 1d of Subsection 1.3.1):

  $$R = C_0 \cdot (f_y \cdot A_{sw} / s \cdot d)^{nfy} \cdot (f_{c,ais} \cdot b \cdot d)^{nfc}$$

  For the shear resistance model, the contribution of the shear reinforcement depends on its cross-section area A_{sw} and spacing s, and also on the effective depth d of the longitudinal reinforcement. On the other hand, the contribution of concrete depends on the width of the cross section b and the effective depth d. Due to this reason, the geometrical variables A_{sw} and s has the same exponent as f_y, and b has the same exponent as $f_{c,ais}$.

These three generalized types can be considered as the typical forms for the resistance models for reinforced concrete structures. For example, the eccentric axial load resistance model can be considered as a combination of the axial force resistance (Type I) and the bending resistance model (Type II). It is thus useful to use these three general types to discuss the problem of the applicable range of the combination of the two basic partial factors.

When γ_C and γ_S are applied, the achieved reliability level for a given resistance model can be calculated by rearranging formulae (Eqs. 8-10 of Subsection 1.3.3). The result is:

$$\beta = \frac{\ln(\gamma_C^{n_{fc}} \cdot \gamma_S^{n_{fy}} \cdot \mu_{RM})}{V_{RM} \cdot \alpha_R} \tag{1}$$

$$V_{RM} = \sqrt{\sum n_i^2 V_i^2} = \sqrt{\sum n_{j,geo}^2 V_{j,geo}^2 + n_{fc}^2 V_{fc}^2 + n_{fc}^2 V_{\eta is}^2 + n_{fy}^2 V_{fy}^2 + n_\theta^2 V_\theta^2} \tag{2}$$

$$\mu_{RM} = \frac{R_m}{R_{nom}} = \prod \mu_i^{n_i} = \prod \mu_{j,geo}^{n_{j,geo}} \cdot \mu_{fc}^{n_{fc}} \cdot \mu_{\eta is}^{n_{fc}} \cdot \mu_{fy}^{n_{fy}} \cdot \mu_\theta \tag{3}$$

Where $n_{j,geo}$, $V_{j,geo}$ and $\mu_{j,geo}$ refers to the exponent sensitivity factor, the CoV and the bias factor for the j^{th} geometrical variable; V_θ and μ_θ refers to the CoV and bias factor for the model uncertainty (all basic uncertainties are assumed to follow lognormal distribution).

It can be observed that for the three generalized types of resistance models, the contribution of geometrical and material uncertainties to the variability of the resistance model depends on the exponent partition between n_{fy} and n_{fc}. Similarly, the effect of the partial factors γ_C and γ_S also depends on the values of these two exponents. For a given resistance model belonging to the three generalized types, when the range of n_{fy} (or equivalently of n_{fc}) is known, the applicability of the partial factors γ_C and γ_S depends on its model uncertainty.

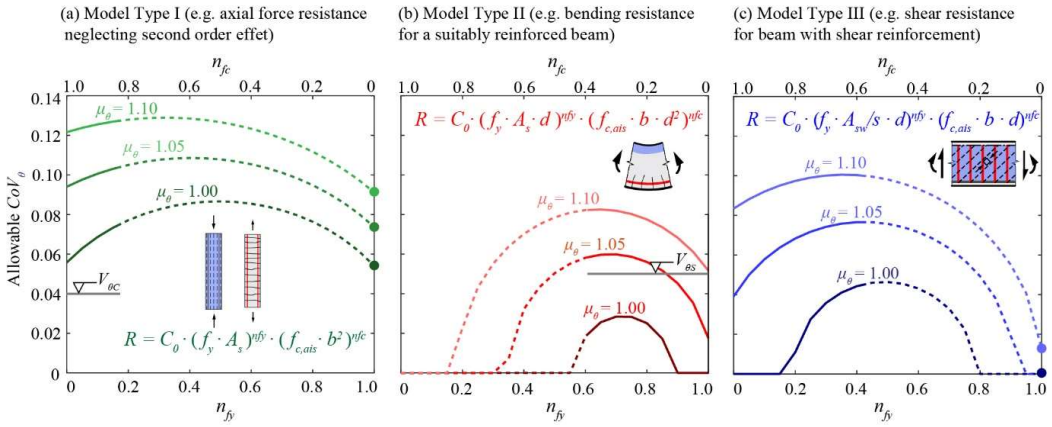

Fig. 1 *Envelop of the allowable CoV for model uncertainty for different types of models to achieve the target reliability with the combination of γ_C and γ_S for (a) Model Type I; (b)Model Type II and (c) Model III (solid parts of the curves and the solid markers represent the ranges of n_{fy} and n_{fc} that correspond to the cases analysed in Subsection 1.3, see Fig. 1 of Subsection 1.3.1).*

When the probabilistic modelling of the geometrical and material variables introduced in Subsection 1.4-1.7 are assumed, the allowable model uncertainty to achieve exactly the target reliability (β_{tgt}) for the three generalized types of resistance models can be calculated. Assuming d_{nom} = 200 mm, the allowable CoV of the model uncertainty for different levels of μ_θ (bias in the model uncertainty) is plotted in Fig. 1 of this appendix. The CoV of model uncertainty of the axial compression resistance model ($V_{\theta C}$) and the bending resistance model ($V_{\theta S}$) are also plotted in Fig. 1a-b of this appendix respectively. It can be observed that:

- Due to the different contributions of geometrical uncertainties, the allowable model uncertainties differ significantly for the three types of resistance models;
- For the axial compression resistance model and the bending resistance model, it is confirmed that the combination of γ_C and γ_S will yield conservative design results for the analysed cases since their model uncertainties are lower than the allowable levels.

This simple analysis shows that the combination of γ_C and γ_S can potentially be applied to a variety of different resistance models for RC structures when the distribution parameters of the model uncertainty fall within the applicable range. When the resistance model takes a more complex form that cannot be categorised to the three generalized model types, the applicability of γ_C and γ_S can be tested by calculating the achieved reliability level with Eqs. 1-3 of this appendix based on a proper exponent analysis covering the application range of the resistance model.

Notation

Notation for Section 1	
a_d	The design value of a geometrical property
a_{nom}	The nominal value of a geometrical property
a_p	The maximum distances from the centroid of the control perimeter to the point where the bending moment in the slab is zero
a_s	The ratio of cross section area over spacing of flexural reinforcement in flat slab
b	The width of the cross section
$b_{0.5}$	The control perimeter for punching shear resistance model
b_b	Geometric mean of the minimum and maximum overall widths of the control perimeter
d	The effective depth of the cross section
d_d	Design value of the effective depth of the cross section
d_{dg}	The size parameter describing the failure zone roughness
d_m	Mean value of the effective depth
d_{mes}	Measured value of the effective depth
d_{nom}	Nominal value of the effective depth
d_V	The shear-resisting effective depth
f_c	Concrete compressive strength
$f_{c,ais}$	Actual uniaxial in-situ concrete compressive strength in the structure
$f_{c,cyl}$	Concrete compressive strength of the control specimens (cylinders)
$f_{c,cube}$	Concrete compressive strength of the control specimens (cubes)
$f_{c,is}$	Compressive strength of a core taken at a test location within a structural element or precast concrete component expressed in terms of the strength of a 2:1 core of diameter > 75 mm
f_{ck}	Characteristic concrete compressive strength
$f_{ck,is}$	Characteristic concrete in-situ strength
$f_{c,spec}$	Specified product uniaxial concrete compressive strength
f_i	The i^{th} basic variable in the resistance function
f_p	Tensile strength of prestressing steel
$f_{p0.1}$	The 0.1% proof-stress of prestressing steel
f_s	Stress at ultimate limit state of reinforcement defined by Robert Maillart
f_t	Tensile strength of reinforcement
f_y	Yield strength of steel reinforcement
f_{yd}	Design value for steel yield strength
f_{yk}	Characteristic value for steel yield strength
$f_{yk,spec}$	Specified characteristic value for steel yield strength in product grading
f_{ym}	Mean value of steel yield strength
k_t	Factor accounting for the effect of the speed of loading for concrete specimen

h	The height of the cross section
n_i	The exponent sensitivity factor for the i^{th} basic variable in the resistance function
n_{fc}	The exponent sensitivity factor for f_c
n_{fy}	The exponent sensitivity factor for f_y
s	The spacing of shear reinforcement
A_s	Cross section area of concrete
A_s	Cross section area of flexural reinforcement
A_{sw}	Cross section area of shear reinforcement
C_0	the residual constant coefficient in the power-multiplicative form approximation of the resistance function
E_d	Design action effect
E_h	Strain hardening modulus
F_{Ed}	The design values of actions used in the assessment of E_d
M_{Rd}	Design flexural resistance of cross section
$M_{R,exp}$	The flexural resistance measured in laboratory tests
$M_{R,calc}$	The calculated flexural resistance
$N_{R,exp}$	The resistance of short columns measured in laboratory tests
$N_{R,calc}$	The calculated resistance of short columns
P_f	Probability of failure
R_d	Design resistance
R_m	The mean value of the resistance variable
R_{nom}	The nominal value of the resistance variable
X_k	The characteristic value of a material or product property
V_i	The CoV of the i^{th} basic variable in the resistance function
V_R	The CoV of the resistance variable
$V_{R,exp}$	The punching shear reistance measured in laboratory tests
$V_{R,calc}$	The calculated punching shear resistance of slab-column connections
V_{RM}	The CoV of the resistance accounting for the influence of material, geometrical and model uncertainties
$V\eta_{is\_location}$	The CoV of of the variability of η_{is} within a structural member
α_E	The First Order Reliability Method (FORM) sensitivity factor for action effect
α_R	The FORM sensitivity factor for resistance
$\alpha_{R,i}$	The FORM sensitivity factor for the i^{th} variable in the resistance model
β	Reliability index
β_e	A coefficient accounting for the concentrations of the shear forces along the control section of punching shear
β_{tgt}	Target reliability index
σ	Standard deviation of a random variable
$\sigma_{ln(R)}$	Standard deviation of the logarithm of the resistance variable
γ_C	Partial factor for concrete compressive strength

γ_S	Partial factor for steel yield strength
γ_V	Partial factor for the punching shear resistance model without shear reinforcement
γ_{Rd}	Partial factor associated with the uncertainty of the resistance model
γ_m	Partial factor for a material property
γ_M	Partial factor for a material property in the “material factor approach”
γ_R	Partial factor for the resistance variable in the “resistance approach”
ε_S	Strain of reinforcement steel
ε_u	Ultimate strain of reinforcement steel
ε_{uk}	Characteristic ultimate strain of reinforcement steel
θ_C	Model uncertainty variable accounted for in the calibration of γ_C
θ_S	Model uncertainty variable accounted for in the calibration of γ_S
η	The conversion factor for a material
$\eta_{core\text{-}actual}$	The coefficient representing the difference between $f_{c,ais}$ and $f_{c,is}$
η_{is}	The in-situ factor for concrete strength
μ_i	The bias factor for the i^{th} basic variable
μ_{RM}	The bias factor of the resistance represented by the ratio between its mean value and its nominal value
ρ_L	Longitudinal reinforcement ratio
ϕ	Strength reduction factor in ACI 318-19
$\mathbf{X}$	Vector of basic variables in structural resistance model
Δa	The deviation in the geometrical property a

Notation for Section 2 and 3	
RC	Reinforced Concrete
PSF	Partial Safety Factor
CoV	Coefficient of Variation
LE	Linear Elastic
LEU	Linear Elastic Uncracked
LEFC	Linear Elastic Fully-Cracked
NL	Non Linear
4L	Quadri Linear with plastic plateau
4L-LIM	Quadri Linear Limited deformation capacity
4L-REQ	Quadri Linear with plastic plateau and ductility requirements
3L	Tri-Linear
F	Force
δ	Displacement
δ_y	Displacement at maximum load predicted with a linear elastic uncracked model
δ_R	Displacement at 90% of the F δ post-peak branch

R	Load-bearing capacity
R_{exp}	Experimental load-bearing capacity
R_{mod}	Theoretical predicted load-bearing capacity
M	Bending moment
M_r	Cracking bending moment
M_R	Resisting bending moment
χ	Curvature
χ_r	Curvature at the cracking bending moment
χ_R	Curvature at the resisting bending moment
θ_{QR}	Global random variable
θ_E	Local random variable
E_{exp}	Experimental action effect
E_{mod}	Theoretical predicted action effect
l_c	Column height
λ_G	Geometrical slenderness of a column (height / width)
l_b	Beam span
b	Width of the section
b_c	Square column section width
d	Effective depth of a cross section
c	Concrete cover
x	Neutral axis depth
x_c	Center of gravity of the concrete section
ρ_l	Bottom longitudinal reinforcement ratio
ρ'_l	Top longitudinal reinforcement ratio
ρ_w	Shear reinforcement ratio
f_c	Concrete compressive strength (uniaxial)
f_{ct}	Concrete tensile strength
f_y	Steel yielding strength
E_c	Concrete elastic modulus
E_s	Steel elastic modulus
n	E_s / E_c
EI	Flexural stiffness
$\Delta\chi_{Ts}$	Decrease of curvature due to tension stiffening
q	Distributed load
Q	Concentrated force
ζ_{EL}	Elastic over-design ratio
γ_F	Partial factor for actions including model uncertainties [7]
γ_f	Partial factor for action values [7]

γ_G	Partial factor for permanent actions including model uncertainties [2]
γ_g	Partial factor for representative values of permanent actions [2]
γ_Q	Partial factor for variable actions including model uncertainties [2]
γ_q	Partial factor for representative values of variable actions [2]
γ_{Sd}	Partial factor covering uncertainty in action effects (model uncertainty)
γ_M	Partial factor for the material including model and geometrical uncertainties
γ_m	Partial factor for material properties
γ_{Rd}	Partial factor covering uncertainty in the resistance model
F_{rep}	Representative value of action variables
X_k	Characteristic value of material strength
a_{nom}	Nominal value of geometrical variables
E_d	Design value of actions
R_d	Design value of resistance
σ	Standard deviation
α	Sensitivity factor

Notation for Section 4	
RC	Weight In Motion
WIM	Partial Safety Factor
FORM	First Order Reliability Method
MCIS	Monte-Carlo Importance-Sampling
IID	Independent-Identically-Distributed
CDF	Cumulative Distribution Function
PDF	Probability Density Function
GEV	Gumbel Extreme Values
LN	Log-Normal
CoV	Coefficient of Variation
GPR	Ground Penetrating Radar Measurements
PSF	Partial Safety Factor
PSFF	Partial Safety Factor Format
β	Reliability index
f_c	Concrete strength
f_y	Steel yield strength
f_{pk}	Characteristic value of the tensile strength of prestressing steel
ρ_s	Sectional reinforcement ratio
A_c	Concrete area
h_{eq}	Equivalent depth of concrete deck
w	Width of concrete element

G	Permanent load
G_1	Structural self-weight
G_2	Non-structural self-weight
Q	Live load
θ_E	Model uncertainty in action effect calculation
Vol	Volume
α	Sensitivity factor
α_{act}	Actualisation factors for the traffic load model
V	Coefficient of Variation of the resistance
μ	Bias factor

References

References for Section 1

[1] SIA, **"SIA 262 :2013 Construction en béton"**, Zurich, 2013.

[2] CEN, **"EN 1990:2002 Basis of Structural Design"**, Brussels, Anglais, 2002.

[3] CEN, **"EN 1992-1-1:2004 Design of concrete structures, Part 1-1: General rules and rules for buildings"**, Brussels, 2004.

[4] CEB, **"Bulletin 127 Manuel sécurité des structures: 1ère partie"**, 1-316, Paris, 1980.

[5] König, G.& Hosser, D., **"The simplified level II method and its application on the derivation of safety elements for level I"**, Comité Euro-International du Béton (CEB), Bulletin No. 147, pp. 147-224, Lausanne, Switzerland, 1981.

[6] Melchers, R. E., **"Structural reliability analysis and prediction 3rd ed."**, Wiley, Hoboken, N.J, 2018.

[7] CEN, **"EN 1990:2023 Basis of structural and geotechnical design"**, 171, Brussels, 2023.

[8] FIB, **"fib Model Code for Concrete Structures 2010"**, fib, First Edition, UK, 2013.

[9] ACI, **"Building Code Requirements for Structural Concrete (ACI 318-19) and Commentary on Building Code Requirements for Structural Concrete (ACI 318R-19)"**, American Concrete Institute, 623 p., Farmington Hills, USA, 2019.

[10] GB 50010-2010, **"GB 50010-2010: Code for Design of Concrete Structures"**, Ministry of Housing and Urban-Rural Development of the People's Republic of China, 427, Beijing, Chinese, 2010.

[11] CSA, **"CSA Standard A23.3-14: Design of concrete structures"**, Canadian Standard Association, Ottawa, Canada, 2014.

[12] AASHTO, **"AASHTO LRFD Bridge Design Specifications, 9th Edition"**, Washington D.C., USA, 2020.

[13] Standards Australia, **"AS 3600:2018 : Concrete Structures"**, 1-264, Sydney, 2018.

[14] CEN, **"EN 1992-1-1: Design of concrete structures - Part 1-1: General rules and rules for buildings, bridges and civil engineering structures"**, 405, Brussels, Belgium, 2023.

[15] Yu, Q., Fernández Ruiz, M. & Muttoni A., **"Considerations on the partial safety factor format for reinforced concrete structures accounting for multiple failure modes"**, Engineering Structures, 264, 114442, 2022.

[16] Goyet, J. & Bureau, A., **"Probabilistic safety of structures - evaluation of partial safety factors for new codes (In French: Sécurité probabiliste des structures - évaluation de coefficients partiels de sécurité pour l'élaboration des nouveaux règlements)"**, Construction Metallique, 27(1), 3-31, 1990.

[17] Yu, Q., Simões, J. T. & Muttoni, A., **"Model uncertainties and partial safety factors of strain-based approaches for structural concrete: example of punching shear"**, Engineering Structures, 2023.

[18] Muttoni, A., Simões, J. T., Faria, D. M. V. & Fernández Ruiz, M., **"A mechanical approach for the punching shear provisions in the second generation of Eurocode 2"**, Hormigón y acero, Spanish, 2023.

[19] Muttoni, A., **"Punching shear strength of reinforced concrete slabs without transverse reinforcement"**, ACI Structural Journal, V. 105, N° 4, pp. 440-450, USA, 2008.

[20] Sagaseta, J., Chryssanthopoulos, M., Muttoni, A., Fernández Ruiz, M. & Yu Q., **"Derivation of design values of punching shear resistance based on Eurocode Annex D"**, presentation at the 14th meeting of CEN/TC250/SC2/WG1/TG4, 23 slides, 2019.

[21] Yang, Y., Slobbe, A. & Rózsás, A., **"Calibration of shear expression on members without shear reinforcement"**, presentation at the 14th meeting of CEN/TC250/SC2/WG1/TG4, 26 slides, 2019.

[22] Muttoni, A. & Simões, J. T., **"Shear and punching shear according to the Critical Shear Crack Theory: background, recent developments and integration in codes"**, Revista IBRACON de estruturas e materiais, 16(3), 2023.

[23] European Concrete Platform, **"Eurocode 2 Commentary"**, European Committee for Standardization (CEN), Brussels, 2008.

[24] Beeby, A. & Jackson, P., **"Partial safety factor for reinforcement"**, Structures, 5, pp. 101-111, 2016.

[25] CEN, **"EN10080:2005 Steel for the reinforcement of concrete. Weldable reinforcing steel - General"**, Brussels, Belgium, 2005.

[26] Kreis, A &, Rosli, A., **"Statistische Auswertung Von Spannstahlversuchen Der EMPA Aus Jahren 1968 - 1979"**, EMPA 10820, 25703/4, p. 40, German, 1979.

[27] Ellingwood, B., **"Development of a probability based load criterion for American national standard A58 : building code requirements for minimum design loads in buildings and other structures"**, NBS SPECIAL PUBLICATION 577, 222, Washington, 1980.

[28] JCSS, **"Probalistic Model Code"**, Part III, 2001.

[29] CEN, **"EN 13670:2009 Execution of concrete structures"**, 1-66, 2010.

[30] Foster, S. J., Stewart, M. G., Loo, M., Ahammed, M. & Sirivivatnonon, V., **"Calibration of Australian Standard AS3600 Concrete Structures: part I statistical analysis of material properties and model error"**, Australian journal of structural engineering, Taylor & Francis, 17, 242-253, 2016.

[31] Stewart, M. G., Foster, S. J., Ahammed, M. & Sirivivatnonon, V., **"Calibration of Australian Standard AS3600 concrete structures part II: reliability indices and changes to capacity reduction factors"**, Australian journal of structural engineering, 4, 17, 254-266, 2016.

[32] CEN, **"EN 12390-3:2019 Testing hardened concrete - Part 3: Compressive strength of test specimens"**, 1-20, 2019.

[33] CEN, **"EN 13791:2019 Assessment of in-situ compressive strength in structures and precast concrete components"**, 2019.

[34] Moccia, F., Kubski, X., Fernández Ruiz, M. & Muttoni, A., **"The influence of casting position and disturbance induced by reinforcement on the structural concrete strength"**, Structural Concrete, 1, 28 p., 2020.

[35] Bartlett, F. M. & MacGregor, J. G., **"Effect of core diameter on concrete core strengths"**, ACI Materials Journal, 91(5), 460-470, 1994.

[36] Weibull, W., **"A statistical theory of the strength of materials"**, Stockholm: Generalstabens Litografiska Anstalts Förlag, 1939.

[37] Tucker, J. J., **"Effect of Dimensions of Specimens upon the Precision of Strength Date"**, Proceedings of the ASTM, 45, 952–9, 1945.

[38] McIntyre, M. & Scanlon, A., **"Interpretation and application of core test data in strength evaluation of existing concrete bridge structures"**, Canadian Journal of Civil Engineering, 17, 471–80, 1990.

[39] Haavisto, J., Husso, A. & Laaksonen, A., **"Compressive strength of core specimens drilled from concrete test cylinders"**, Structural Concrete, 22, E683–95, 2021.

[40] Neville, A., **"Properties of concrete"**, Adison Wesley Longman Limited, fourth edition, UK, 1995.

[41] Wittmann, F., **"Surface tension skrinkage and strength of hardened cement paste"**, Matériaux et Construction, 1(6), 547–52, 1968.

[42] Popovics, S., **"Effect of curing method and final moisture condition on compressive strength of concrete"**, Journal of the American Concrete Institute, 83, 650-7, 1986.

[43] Rüsch, H., Sell, R. & Rackwitz, R., **"Statistical analysis of concrete strength (in German: Statistische Analyse der Betonfestigkeit)"**, Berlin: Ernst, German, 1969.

[44] Bartlett, F. M. & MacGregor, J. G., **"Statistical Analysis of the Compressive Strength of Concrete in Structures"**, ACI Materials Journal, 93, 1994.

[45] Torrenti, J. M., **"On the relation between the mean compressive strength and the characteristic one"**, FIB 2018 - Proceedings for the 2018 fib Congress: Better, Smarter, Stronger, 543–7, 2019.

[46] Torrenti, J. M. & Dehn F., **"On the relation between the mean compressive strength and the characteristic one"**, Structural Concrete, 21, pp. 409-412, 2019.

[47] Giaccio, G. & Giovambattista, A., **"Bleeding: Evaluation of its effects on concrete behaviour"**, Materials and Structures, 265-271, 1986.

[48] Bartlett, F. M. & MacGregor J. G., **"Assessment of concrete strength in existing structures"**, Doctoral Thesis, University of Alberta, 1-297, 1994.

[49] Bartlett, F. M. & MacGregor, J. G., **"Statistical analysis of the compressive strength of concrete in structures"**, ACI materials journal, 93(2), 158-168, 1996.

[50] Bartlett F. M. & MacGregor J. G., **"Variation of in-place concrete strength in structures"**, ACI Materials Journal, 96, 261-70, 1999.

[51] Bartlett, F. M., **"Canadian Standards Association standard A23.3-04 resistance factor for concrete in compression"**, Canadian Journal of Civil Engineering, 34, 1029-37, 2007.

[52] ACI, **"ACI 214.4R-10(16): Guide for Obtaining Cores and Interpreting Compressive Strength Results"**, 2010.

[53] König, G., Soukhov, D. & Jungwirth, F., **"Safe concrete production for reinforced concrete structures (in German: Sichere Betonproduktion für Stahlbetontragewerke)"**, Universität Leipzig, German, 1998.

[54] CEN, **"ENV 1992-1-1:1992 Design of concrete structures - Part 1-1: General rules and rules for buildings",** 252 p., Brussels, Belgium, 1992.

[55] Foster, S. J., Stewart, M. G., Sirivivatnonon, V., Loo, K. Y., Ahammed M., Ng, T. S. & Valipour H., **"A Re-evaluation of the Safety and Reliability Indices for Reinforced Concrete Structures Designed to AS3600, UNICIV Report R-464"**, School of Civil and Environmental Engineering, UNSW, 201, 2015.

[56] Pham, L., **"Reliability analyses of reinforced concrete and composite column sections under concentric loads"**, Institution of Engineers, Australia, Civil Engineering Transactions, 27, 68–72, 1985.

[57] Muttoni, A., **"Background document to clause 4.3.3 and Annex A Partial safety factors for materials, Background Document for EN 1992-1-1:2023"**, CEN/TC 250/SC 2 N2087, 2023.

[58] Moccia, F., Yu, Q., Fernández Ruiz, M. & Muttoni, A., **"Concrete compressive strength: From material characterization to a structural value"**, Structural Concrete, 21 p., 2020.

[59] Beeby, A. W., **"Partial safety factors for reinforcement"**, Structural Engineer, 73, 262-8, 1995.

[60] Muttoni, A., Fernández Ruiz, M., Simões, J. T., Hernández Fraile, D., Hegger, J., Siburg, C. & Kueres, D., **"Background document to Clause 8.4 Punching, Background Document for EN 1992-1-1 :2023, CEN/TC 250/SC 2 N2087"**, 338-357, 2023.

[61] Muttoni, A., **"Die Anwendbarkeit der Plastizitätstheorie in der Bemessung von Stahlbeton"**, Dissertation ETHZ, 159 p., Zürich, Switzerland, German, 1989.

[62] JCSS, **"Probabilistic Model Code"**, Part III, 2001.

[63] CEN, **"EN 1990:2002: Basis of Structural Design"**, Brussels, Anglais, 2002.

[64] CEB, **"Bulletin 19: Technical conclusions of the 5th CEB meeting in Vienna"**, Comité Européen du Béton Bulletin: Section on Structural Safety, 94, Paris, France, 1959.

[65] Yu, Q., Valeri, P., Fernández Ruiz, M. & Muttoni, A., **"A consistent safety format and design approach for brittle systems and application to textile reinforced concrete structures"**, Engineering Structures, 249, 2021.

[66] Hirt, M. A., Bez, R. & Nussbaumer, A., **"Construction métallique: Notions fondamentales et méthodes de dimensionnement, 3rd ed"**, Traité de génie civil de l'École polytechnique fédérale de Lausanne, TGC 10, Lausanne: Presses polytechniques et universitaires romandes, 2015.

[67] SIA, **"SIA 263:2013 Steel structures"**, SIA, Zurich, 2013.

[68] SIA, **"SIA 269:2011 Existing Structures - Basis for examination and interventions"**, SIA, Zurich, 2011.

[69] CEN, **"EN 1990:2023 Basis of structural and geotechnical design"**, CEN European committee for standardization, Draft E, 171, Brussels, 2023.

[70] CEN, **"EN 1993-1-1: 2022 Design of steel structures - Part 1-1: General rules and rules for buildings "**, Brussels, Belgium, 2022.

[71] Knobloch, M., Bureau, A., Kuhlmann, U., Silva, L. S., Snijder, H. H., Taras, A., Bours, A.-L. & Jörg, F., **"Structural member stability verification in the new Part 1-1 of the second generation of Eurocode 3: Part 1: Evolution of Eurocodes, background to partial factors, cross-section classification and structural analysis"**, Steel Construction, vol. 13, no. 2, 98–113, 2020.

[72] CECA, **"Euronorm 25/72 - Structural steel for general use - Quality requirements"**, Publications Office of the EU, Brussels, 1972.

[73] Da Silva, L. S., **"Standardization of Safety Assessment Procedures across Brittle to Ductile Failure Modes (SAFE-BRICTILE)"**, European Commission, Research fund for coal and steel, Brussels, Belgium, RFSR-CT-2013-00023, 2017.

[74] Taras, A., **"Nationaler Anhang zu SN EN 1993-1-1, Hintergrunddokument, Draft from ETH Zurich for SIA NK 263"**, in publication, 2024.

[75] Klok, J., **"master thesis: Development of models for assessing corroded steel girder web panels in bridges (ex-tract from §9.5 Updating of the yield strength)"**, EPFL-RESSLab, 2024.

[76] Bosco, C. & Debernadi, G., **"Influence of some basic parameters on the plastic rotation of reinforced concrete elements"**, CEB Bulletin d'Information, 218, 25-44, 1993.

[77] Hughes, G. & Speirs, D. M., **"An investigation of the beam impact problem"**, Cement and Concrete Association, 42.546, 117, 1982.

[78] Bigaj, A. & Walraven, J. C., **"Size effect on rotational capacity of plastic hinges in reinforced concrete beams"**, CEB Bulletin d'Information, 218, 7-23, 1993.

[79] Shin, S.-W., Lee, K.-S. & Moon, J.-I., **"Shear Strength of Reinforced High-Strength Concrete Beams with Shear Span-to-Depth Ratios between 1.5 and 2.5"**, ACI, Structural Journal, 96, pp. 549-556, Farmington Hills, USA, 1999.

[80] Angelakos, D., **"The Influence of Concrete Strength and Longitudinal Reinforcement Ratio on the Shear Strength of Large-Size Reinforced Concrete Beams With and Without Transverse Reinforcement"**, MSc thesis, Department of Civil Engineering, University of Toronto, 181 pp., 1999.

[81] Yoshida, Y., **"Shear reinforcement for large lightly reinforced concrete members"**, Master thesis, University of Toronto, 160 p., Toronto, Canada, 2000.

[82] Vecchio, F. J. & Shim W., **"Experimental and Analytical Reexamination of Classic Concrete Beam Tests"**, ASCE Journal of Structural Engineering, Vol.130, pp. 460-469, USA, Anglais, 2004.

[83] Saatci, S. & Vecchio, F. J., **"Effects of shear mechanisms on impact behavior of reinforced concrete beams"**, ACI Structural Journal, 106.09, 2009.

[84] Fujikake, K., Li, B. & Soeun, S., **"Impact response of reinforced concrete beam and its analytical evaluation"**, Journal of Structural Engineering, 135.8, 938-950, 2009.

[85] Lau, D. & Pam, H. J., **"Experimental study of hybrid FRP reinforced concrete beams"**, Engineering Structures, 32.12, 3857-3865, 2010.

[86] Lee, J.-Y., Kim, S. W. & Mansour, M. Y., **"Nonlinear analysis of shear-critical reinforced concrete beams using fixed angle theory"**, Journal of Structural Engineering, 137.10, 1017-1029, 2011.

[87] Fujikake, K., Adhikary, S. D. & Li, B., **"Effects of high loading rate on reinforced concrete beams"**, ACI Structural Journal, 111.3, 651-660, 2014.

[88] Cavagnis, F., Fernández Ruiz, M. & Muttoni, A., **"Shear failures in reinforced concrete members without transverse reinforcement: An analysis of the critical shear crack development on the basis of test results"**, Engineering structures, Vol. 103, pp. 157-173, UK, 2015.

[89] Adhikary, S. D., Li, B. & Fujikake, K., **"Residual resistance of impact-damaged reinforced concrete beams"**, Magazine of Concrete Research, 67 (7), 364-378, 2015.

[90] Zhao, D. B., Yi, W.-J. & Kunnath S. K, **"Shear Mechanisms in Reinforced Concrete Beams under Impact Loading"**, Journal of Structural Engineering, 143 (9), 2017.

[91] Sheikh, S. A. & Uzumeri, S. M., **"Strength and ductility of tied concrete columns"**, ASCE Journal of the Structural Division, Vol. 106, pp. 1079-1102, USA, 1980.

[92] Li, D., Jin, L., Fu, J. & Lu, A., **"Size effect tests of normal-strength and high-strength RC columns subjected to axial compressive loading"**, Engineering Structures, 109, 43-60, 2016.

[93] Du, M., Du, X. & Li, D., **"Size effect tests of stocky reinforced concrete columns confined by stirrups"**, Structural Concrete, 18, 454-465, 2017.

[94] Jin, L., Du, M., Li, D., Du, X. & Xu, H., **"Effects of cross section size and transverse rebar on the behavior of short squared RC columns under axial compression"**, Engineering Structures, 142, 223-239, 2017.

[95] CEN, **"EN 1992-1-1:2023 Design of concrete structures - Part 1-1: General rules and rules for buildings, bridges and civil engineering structures"**, European Committee for Standardization, 405 p., Brussels, Belgium, 2023.

[96] Muttoni, A. & Fernández Ruiz, M., **"Shear strength of members without transverse reinforcement as function of critical shear crack width"**, ACI Structural Journal, V. 105, No 2, pp. 163-172, Farmington Hills, USA, 2008.

[97] Cantone, R., Setiawan, A., Fernández Ruiz, M. & Muttoni, A., **"Characterization of shear deformations in reinforced concrete members without shear reinforcement"**, Engineering Structures, Vol. 257, 113910, 16 p., 2022.

[98] Collins, M. P., **"Towards a Rational Theory for RC Members in Shear"**, ASCE, Journal of the Structural Division, Vol.104, No 4, pp. 219-231, Reston, USA, 1978.

[99] Guidotti, R., Fernández Ruiz, M. & Muttoni, A., **"Crushing and Flexural Strength of Slab-Column Joints"**, Engineering structures, Vol. 33 n° 3, pp. 855-867, 2011.

[100] Fernández Ruiz, M., Muttoni, A. & Gambarova, P., **"Relationship between nonlinear creep and cracking of concrete under uniaxial compression"**, Journal of Advanced Concrete Technology, Vol. 5, No 3, pp. 383-393, Japan, 2007.

[101] Ditlevsen, O., **"Distribution arbitrariness in structural reliability"**, Structural Safety and Reliability, Schuëller, Shinozuka and Yao (eds), 1241-1247, Rotterdam, 1994.

[102] CEN, **"EN 1991 :2002 Actions on structures - Part 1-1: General actions"**, Brussels, 2002.

[103] Muttoni, A., **"Background document to clause 4.3.3 and Annex A Partial safety factors for materials, Background Document for EN 1992-1-1:2023"**, CEN/TC 250/SC 2 N2087, 2023.

[104] Pejatovic, M., Fernández Ruiz, M. & Muttoni, A., **"Design of slender and squat reinforced concrete members with shear reinforcement"**, Structural Concrete, 17 p., 2022.

[105] Schneider, J. & Vrouwenvelder, T., **"Introduction to Safety and Reliability of Structures"**, IABSE Structural Engineering Documents, 5, 164 p., Zürich, Switzerland, 2017.

[106] Yu, Q., Valeri, P., Fernández Ruiz, M. & Muttoni, A., **"A consistent safety format and design approach for brittle systems and application to textile reinforced concrete structures"**, Engineering Structures, 249, 2021.

[107] Malja, X. & Muttoni, A., **"Evaluation of the model uncertainty of action effects in statically indeterminate systems"**, 14th fib International PhD Symposium in Civil Engineering, pp. 895-902, Rome, Italy, 2022.

[108] CEN, **"EN 1994-1-1:2004 Eurocode 4: Design of composite steel and concrete structures - Part 1-1: General rules and rules for buildings"**, Brussels, 2004.

[109] Barbato, M., Zona, A. & Conte, J. P., **"Probabilistic Nonlinear Response Analysis of Steel-Concrete Composite Beams"**, Journal of Structural Engineering, 140(1), 04013034, 2014.

[110] Wang, A. J. & Chung K. F., **"Integrated analysis and design of composite beams with flexible shear connectors under sagging and hogging moments"**, Steel and Composite Structures, 6 (6), 459–477, 2006.

[111] Toprac, A. A., **"Strength of three new types of composite beams"**, Center for Cold-Formed Steel Structures Library, 83, 1965.

[112] Gattesco, N., **"Analytical modeling of nonlinear behavior of composite beams with deformable connection"**, Journal of constructional steel research, 52, pp. 195-218, 1999.

[113] Nie, J. G., Fan, J. S. & Cai, C. S., **"Experimental study of partially shear-connected composite beams with profiled sheeting"**, Engineering Structures, 30(1), 1-12, 2007.

[114] Nie, J. G., Xiao, Y. & Chen, L., **"Experimental studies on shear strength of steel-concrete composite beams"**, Journal of structural Engineering, 130(8), 1206-1213, 2004.

[115] Fabbrocino, G., Manfredi, G. &, Cosenza, E., **"Non-linear analysis of composite beams under positive bending"**, 70(1), 77-89, 1998.

[116] Fabbrocino, G. & Pecce, M., **"Experimental tests on steel-concrete composite beams under negative bending"**, Third structural specialty conference of the Canadian society for civil engineering, 2000.

[117] Zhao, H. L., Yuan, Y. & Ye, Z. M., **"Simplified nonlinear simulation of steel–concrete composite beams"**, Journal of Constructional Steel Research, 71, 83-91, 2011.

[118] Yan, J. B., Li, Z. X. & Xie, J., **"Numerical and parametric studies on steel-elastic concrete composite structures"**, Journal of Constructional Steel Research, 133, 84-96, 2017.

[119] Zhang, J., Hu, X. M., Fu, W. J., Du, H., Sun, Q. M. & Zhang, Q., **"Experimental and theoretical study on longitudinal shear behavior of steel-concrete composite beams"**, Journal of Constructional Steel Research, 171, 106144, 2020.

[120] Zhou, X .H., Men, P. F., Di, J. &, Qin, F. J., **"Experimental investigation of the vertical shear performance of steel–concrete composite girders under negative moment"**, Engineering Structures, 228, 111487, 2020.

[121] Men, P. F., Zhou, X. H., Zhang, Z. X., Di, J. & Qin, F. J., **"Behaviour of steel-concrete composite girders under combined negative moment and shear"**, Journal of Constructional Steel Research, 179, 106508, 2020.

[122] Men, P. F., Di, J., Jiang, H. Y., Zhou, X. H. & Qin, F. J., **"Web shear buckling of steel-concrete composite girders in negative-moment regions"**, Engineering Structures, 112210, 2021.

[123] Men, P. F., Zhou, X. H., Ye, J. T., Di, J. & Qin, F. J., **"Shear capacity investigation of steel-concrete composite girders in hogging moment regions"**, Journal of Constructional Steel Research, 194, 107341, 2022.

[124] Ban, H. & Bradford, M. A, **"Flexural behaviour of composite beams with high strength steel"**, Engineering Structures, 56, 1130-1141, 2013.

[125] Zhao, H. L. & Yuan, Y., **"Experimental studies on composite beams with high-strength steel and concrete"**, Steel and Composite Structures, 10(5), 373-383, 2010.

[126] Chapman, J. C. & Balakrishnan, S., **"Experiments on composite beams"**, The Structural Engineer, 42, pp. 369-383, 1964.

[127] Hoffmeister, B., **"Plastische Bemessung von Verbundkonstruktionen unter Verwendung realitätsnaher Last-Verformungsansätze"**, Shaker, German, 1997.

[128] Gómez Navarro, M., **"Experimental study of the behaviour of composite beams under negative bending moments"**, EPFL, ICOM - Construction métallique, 2001.

[129] Baldwin, J. W., **"Composite Bridge Stringers"**, Missouri State Highway Department, p. 68, 1973.

[130] CEN, **"EN 1993-1-1:2005: Design of steel structures - Part 1-1: General rules and rules for buildings"**, Brussels, 2005.

[131] Hirt, M. A. & Lebet, J.-P., **"PONTS EN ACIER (TGC VOLUME 12) Conception et dimensionnement des ponts métalliques et mixtes acier-béton",** EPFL Press, 584, 2009.

[132] Ducret, J.-M., **"Etude du comportement réel des ponts mixtes et modélisation pour le dimensionnement"**, Thèse EPFL, No. 1738, 185 p., Lausanne, Switzerland, 1997.

[133] Lääne, A., **"Post-critical behaviour of composite bridges under negative moment and shear"**, EPFL thesis No. 2889, Lausanne, 2003.

[134] CEN, **"EN 1992-1-1:2004 Design of concrete structures - Part 1-1: General rules and rules for buildings"**, Brussels, 2004.

[135] CEN, **"EN 1990:2023 Basis of structural and geotechnical design"**, Brussels, Belgium, 2023.

[136] JCSS, **"Probalistic Model Code"**, Part III, 2001.

[137] Yu, Q., Valeri, P, Fernández Ruiz, M. & Muttoni, A., **"A consistent safety format and design approach for brittle systems and application to textile reinforced concrete structures"**, Engineering Structures, 249, 2021.

[138] CEN, **" EN 1991-1-1:2023 Actions on structures - Part 1-1: General actions - Specific weight of materials, self-weight of construction works and imposed loads for buildings"**, European Committee for Standardization (CEN), Brussels, Belgium, 2023.

[139] CIB, **"Publication 115, Actions On Structures - Self-weight Loads"**, CIB Commission W81, 1989.

[140] Ellingwood, B., **"Development of a probability based load criterion for American national standard A58 : building code requirements for minimum design loads in buildings and other structures"**, NBS SPECIAL PUBLICATION 577, 222, Washington, 1980.

[141] Menn, C., **"Comparison of costs and material quantities for some new highway bridges in Switzerland"**, Prestressed Concrete of Switzerland, pp. 41-48, Wildegg, Switzerland, German/English, 1982.

[142] ISO, **"EN 13670 Execution of concrete structures"**, International Organization for Standardization, 72 p., 2013.

[143] SIA 261, **"Actions sur les structures porteuses"**, 136, 2020.

[144] Huang, Y. H. & Sharpe, G. W., **"Thickness Design of Concrete Pavements by Probabilistic Method"**, Proceedings, Fourth International Conference on Concrete Pavement Design and Rehabilitation, 1989.

[145] Lytton, R. L. & Zollinger, D. G., **"Modeling Reliability in Pavements"**, 72nd Annual Meeting of the Transportation Research Board, p. 88, Washington D.C., 1993.

[146] Dalla Valle, P. & Thom, N., **"Variability In Pavement Design"**, The International Journal of Pavement Engineering and Asphalt Technology, 16, 50-67, 2015.

[147] Hugenschmidt, J. & Mastrangelo, R., **"GPR inspection of concrete bridges"**, Concrete and Cement Research, 28, 384-392, 2006.

[148] Hugenschmidt, J., Kalogeropoulos, A., Soldovieri, F. & Prisco, G., **"Processing strategies for high-resolution GPR concrete inspections"**, NDT & E International, 43, pp. 334-342, 2010.

[149] Kalogeropoulos, A., Van Der Kruk, J., Hugenschmidt, J., Bikowski, J. & Brühwiler, E., **"Full-waveform GPR inversion to assess chloride gradients in concrete"**, NDT & e International, pp. 74-84, 2013.

[150] Schneider, J. & Vrouwenvelder, T., **"Introduction to Safety and Reliability of Structures"**, IABSE Structural Engineering Documents, 5, 164 p., Zürich, Switzerland, 2017.

[151] Kenel, A., Stussi, U. & Ebschner, P., **"Central documentation of mechanical properties of existing reinforcements"**, Rapport OFROU, 669, p. 183, Suisse, German, 2015.

[152] SIA, **"SIA 162:1968 Norme pour le calcul, la construction et l'exécution des ouvrages en béton, en béton armé et en béton précontraint"**, 84 p., Zürich, Switzerland, 1968.

[153] CEN, **"EN 1992-1-1:2023 Design of concrete structures - Part 1-1: General rules and rules for buildings, bridges and civil engineering structures"**, 405 p., Brussels, Belgium, 2023.

[154] Nowak, A. S. & Szerszen, M. M., **"Calibration of design code for buildings (ACI 318): Part 1 - Statistical models for resistance"**, ACI structural journal, 3, 100, 377-382, 2003.

[155] Beeby, A. & Jackson, P., **"Partial safety factor for reinforcement"**, Structures, 5, pp. 101-111, 2016.

[156] Mirza, S. A. & MacGregor, J. G., **"Variability of mechanical properties of reinforcing bars"**, Journal of the Structural Division, American Society of Civil Engineers, 105, pp. 921-937, 1979.

[157] Kreis, A. & Rosli, A., **"Statistische Auswertung von Spannstahlversuchen der EMPA aus Jahren 1968–1979"**, EMPA 10820, 25703/4, p. 40, 1979.

[158] Mirza, S. A., Kikuchi, D. K. & MacGregor, J. G., **"Flexural Strength Reduction Factor for Bonded Prestressed Concrete Beams"**, Journal Proceedings, 77, pp. 237-246, 1980.

[159] Bassetti, A., Bailey, S. F. & Banz, A., **"Lastfaktoren für Eigenlast und Auflast zur Beurteilung der Tragsicherheit bestehender Strassenbrücken"**, Rapport OFROU, 530, 63 p., Zürich, Switzerland, German, 1998.

[160] Foster, S. J., Stewart, M. G., Loo, M., Ahammed, M. & Sirivivatnonon V., **"Calibration of Australian Standard AS3600 Concrete Structures: part I statistical analysis of material properties and model error"**, Australian journal of structural engineering, Taylor & Francis, 17, 242-253, 2016.

[161] SIA, **"SIA 262.051+A2 - Béton - Spécification, performances, production et conformité"**, Société Suisse des Ingénieurs et des Architectes, Norme suisse SN EN 206+A2:2021, pp. 148, 2021.

[162] Torrenti, J. M. & Dehn, F., **"On the relation between the mean compressive strength and the characteristic one"**, Structural Concrete, 21, pp. 409-412, 2019.

[163] Sjaarda, M., Meystre T., Nussbaumer A. & Hirt M. A., **"A systematic approach to estimating traffic load effects on bridges using weigh-in-motion data"**, Structural Concrete, 89, pp. 585-598, 2020.

[164] CEN, **"EN 1991-2 :2003 Actions on structures – Part 2: Traffic loads on bridges"**, 2003.

[165] Rice, J. A., **"Mathematical statistics and data analysis"**, Cengage Learning, 2006.

[166] Pejatovic, M., Fernández Ruiz, M. & Muttoni, A., **"Design of slender and squat reinforced concrete members with shear reinforcement"**, Structural Concrete, 17 p., 2022.

[167] Eurocode 1, **"Actions on structures - Part 1-1: General actions"**, CEN, 47, Brussels, 2002.

[168] SIA, **"SIA 269/1 :2011 - Existing structures - Actions"**, Société Suisse des Ingénieurs et des Architectes, 2011.

[169] Melchers, R. E. & Beck, A. T., **"Structural reliability analysis and prediction"**, John Wiley & Sons, 2018.

[170] Papastergiou, D., Nussbaumer, A., Sjaarda, M., Mathevet, L. L. L., Miglietta, P., Brühwiler, E. & Bertola, N., **"Évaluation De Ponts Routiers Existants Avec Un Modèle De Charge De Trafic Actualisé"**, Office fédéral des routes, 2024.

[171] OFROU, **"Updated normative bridge load models to account for actual traffic effects and reliability demands across structure types"**, Office fédéral des routes, 2025.

Projektabschluss

Schweizerische Eidgenossenschaft
Confédération suisse
Confederazione Svizzera
Confederaziun svizra

Département fédéral de l'environnement, des transports, de l'énergie et de la communication DETEC
Office fédéral des routes OFROU

RECHERCHE DANS LE DOMAINE ROUTIER DU DETEC

Version du 09.10.2013

Formulaire N° 3 : Clôture du projet

établi / modifié le : 31.07.2024

Données de base

Projet N° : BGT-20-02B

Titre du projet : Recalibration of partial safety factors for actions and resistances for new and existing bridges

Echéance effective : 30.09.2024

Textes :

Résumé des résultats du projet :

Despite advancements in standard probability modeling, the specific uncertainties each partial factor covers remain debated and are not clearly defined in codes. As statistical data evolves, partial safety factors must be updated to maintain appropriate safety levels, preventing either insufficient safety or excessive costs. This project clarifies the uncertainties each partial factor addresses and updates them based on new statistical data, focusing on road bridges and assessing variabilities in both resistance and action factors. While the semi-probabilistic approach and the corresponding Partial Safety Factor Format (PSFF) is mostly used, comparison with full probabilistic reliability calculation using Monte Carlo method is made. A database of selected WIM is validated and used for the extrapolation of action effects of 50-year maxima distribution of traffic load. It is found to depend significantly on the tail fitting accuracy, the best compromise and stable results being obtained using weekly maxima events.
Regarding materials and resistance, new statistical data were collected, analyzed and used to re-evaluate the material partial safety factors for concrete and steel (reinforcement, prestressing strands and structural), as well as the resistance factors. A focus is made on the uncertainties in reinforced concrete resistance and corresponding partial safety factors were evaluated using new statistical data and exponent sensitivity analysis. It confirms the suitability of a material factor approach for a wide range of typical resistance models (axial tension and compression, bending, shear in the presence of sufficient shear reinforcement), while a resistance factor approach is found more adequate for specific models like shear without reinforcement and punching shear. For typical resistance models, it confirmed the current partial safety factors for steel yield strength and for concrete compressive strength. Also for steel-concrete structures, the partial safety factors currently used in the standards are generally confirmed. For both new structures design and assessment of existing structures (depending on the available information), the information and calculation procedure needed for possible adjustments of the partial factors is given. The most illustrative is the positive effect of using design effective depth of slabs for specific models to achieve a more constant safety level and reduce the resistance model partial factor. For assessment, the partial factors that may be assumed in an initial analysis are given as well.
Regarding model uncertainties in calculating (in statically indeterminate systems) action effects and load-bearing capacity of structures, a sufficient amount of data is required to perform statistical analyses. To achieve this, the experimental response of statically indeterminate systems is obtained by adopting a simple and effective technique which allows using experimental results available in literature. A large database of reinforced concrete and steel-concrete component experiments, validated, is created and now available. The analyses are performed considering various mechanical models and failure modes. Findings indicate that while simple linear models with uncracked sectional stiffness lead to higher uncertainty in load-bearing capacity calculations, they offer similar safety margins as more refined models (i.e. non-linear). The study also shows section deformation capacity (linked to failure mode) influences model uncertainties; the over-design ratio of the members does as well. The partial factor covering the model uncertainties in the action effects calculation lies within 1.05 - 1.15 depending on the other uncertainties. It is implicitly accounted for in the permanent and variable action effects partial factors, while the influence of the failure mode type for specific cases is covered by the relevant partial resistance factors.
Regarding the recalibration of partial safety factors for permanent loads, it is found that structural self weight variability in bridges is mainly caused by geometrical, reinforcement content and concrete specific weight variability. As for the other permanent loads, a focus is put on the thickness and weight distribution of pavement. With respect to the default value of 1.35, the study show that the partial safety factor for the self-weight of reinforced concrete may be reduced under some conditions (modelling by experienced engineer, or of statically determined structures), but must be increased for self-weight of non-structural elements.

Schweizerische Eidgenossenschaft
Confédération suisse
Confederazione Svizzera
Confederaziun svizra

Département fédéral de l'environnement, des transports, de l'énergie et de la communication DETEC
Office fédéral des routes OFROU

Atteinte des objectifs :

The research objectives of the project were attained. At the end of the report, based on the investigations carried out and for a target value of the reliability index of 3.8 (CC2) for a 50 years reference period, a summary of the proposed partial factors for persistent and transient design situations as well as for resistances is given. Since the report provides the detailed background, the basis for recalibrating partial safety factors, as well as the information (databases, typical CoV's,. etc.), the procedures followed in this work can be reused for different resistance models, for different required target reliability indexes, for dimensioning of new as well as assessment of existing structures, etc. Regarding new structures, most of the results of this work have been implemented in the second generation of the European standard for the design of concrete structures (Eurocode 2 of 2023) and its background document. Most of the results have been already published in international scientific journals as well. The study on statically indeterminate systems model uncertainties in calculating action effects and load-bearing capacity of structures is unique.
Among the topics that could not be addressed within this project, it should be mentioned that structural system changes during construction and significant differences between modelling of complex structures and actual behaviour are not accounted for in the partial safety factors given (more relevant for brittle failure modes). Also, for steel-concrete bridges, further differentiation with respect to the section classification was not addressed.

Déductions et recommandations :

Since most of the results have been implemented in Eurocode 2 of 2023 (2nd generation), this work will serve as a reference for the next revision of structural code for concrete, and as well for the one dealing with steel-concrete structures.
The partial safety factors for strength currently in the codes can be used, though specific design adjustments can optimize safety.
The model uncertainties in statically indeterminate structures are implicitly accounted for in the permanent and variables action effects partial factors, while the influence of the failure mode type for specific cases is covered by the relevant resistance partial factors. For both reinforced concrete and steel-concrete structures, when using models based on limit analysis, it is recommended to either set limits on the deformation capacity, or verify that ductility requirements are fulfilled. For permanent loads, unlike current practice, one should differentiate the partial safety factor for structural self-weight from those for non-structural self-weights; while the first can be lowered to 1.2, the others should be increased up to 1.5 to ensure sufficient safety for both new designs and existing structures.
For reinforced concrete bridges, additional uncertainties, which depend on the complexity of the structure, the construction method, the tools used and the experience of the designer deserve to be investigated more in detail. All the same for steel-concrete bridges, further differentiation with respect to the section classification would need to be analyzed by performing a large parametric study.
If relevant for the structural system, depending on its complexity and particularly in case of governing brittle failure modes, if the behaviour cannot be improved with sound detailing during the design process, the structure should be modelled in a reasonably conservative manner and the results interpreted accordingly.

Publications :

Yu Q., Fernández Ruiz M., Muttoni A., "Considerations on the partial safety factor format for reinforced concrete structures accounting for multiple failure modes", Engineering Structures, 264, 114442, 2022.
Yu Q., Simões J. T., Muttoni A., "Model uncertainties and partial safety factors of strain-based approaches for structural concrete: example of punching shear", Engineering Structures, 2023.
Muttoni A., "Background document to clause 4.3.3 and Annex A Partial safety factors for materials, Background Document for EN 1992-1-1:2023", CEN/TC 250/SC 2 N2087, 2023.
Muttoni A., Fernández Ruiz M., Simões J. T., Hernández Fraile D., Hegger J., Siburg C., Kueres D., "Background document to Clause 8.4 Punching, Background Document for EN 1992-1-1 :2023, CEN/TC 250/SC 2 N2087", 338-357, 2023.
Malja X., Muttoni A., "Evaluation of the model uncertainty of action effects in statically indeterminate systems", 14th fib International PhD Symposium in Civil Engineering, pp. 895-902, Rome, Italy, 2022.
Malja, X., 'Influence of model uncertainty and long term deformations in action effects calculation in reinforced concrete structures', EPFL n° 10574, EPFL, Lausanne, 2024. [Online]. Available: https://doi.org/10.5075/epfl-thesis-10574
Malja, X., Nussbaumer, A. and Muttoni, A. 'Model uncertainties in action effects and load bearing capacity calculation in statically indeterminate reinforced concrete structures', Structural Concrete, p. suco.202400087, Apr. 2024, doi: 10.1002/suco.202400087.

Chef/cheffe de projet :

Nom : Muttoni Prénom : Aurélio

Service, entreprise, institut : EPFL-ENAC-IBETON

Signature du chef/de la cheffe de projet :

Schweizerische Eidgenossenschaft
Confédération suisse
Confederazione Svizzera
Confederaziun svizra

Département fédéral de l'environnement, des transports, de l'énergie et de la communication DETEC
Office fédéral des routes OFROU

RECHERCHE DANS LE DOMAINE ROUTIER DU DETEC

Formulaire N° 3 : Clôture du projet

Appréciation de la commission de suivi :

Evaluation :

The accompanying committee assesses the research project, the data and conclusions it contains as very positive. The report makes a significant contribution to understanding the sources of uncertainties, the statistical distribution of random variables, the coefficient of variation and the bias factor, which are used to determine partial safety factors in current codes and in typical verifications of structural safety made in engineering offices. For the first time, the value of model uncertainties in the calculation of internal forces and load-bearing capacity in statically indeterminate concrete and steel-concrete composite structures is also analysed in detail.

Mise en oeuvre :

The report provides a detailed background for the partial safety factors used in the structural codes and thus contributes to a better understanding of the uncertainties in modelling, the calculation of internal forces and the ultimate limit state design. This is particularly relevant for all those involved in the assessment of existing structures.

Besoin supplémentaire en matière de recherche :

The influence of system changes during the construction of a structure or the structural modelling of complex structures on the model uncertainties was not investigated in this work and should be further clarified.

Influence sur les normes :

The partial safety factors currently used in the codes are generally confirmed. However, the report makes several recommendations for a possible adjustment of the partial safety factors if a design value of the static height of concrete components is taken into account, if quality control is improved and if measured values of dimensions and concrete strength in existing components are available. The report also provides the basis for recalibrating partial safety factors as a function of the required target reliability.

Président/Présidente de la commission de suivi :

Nom : Ganz Prénom : Hans Rudolf

Service, entreprise, institut : GANZ Consulting

Signature du président/ de la présidente de la commission de suivi :